CALIFORNIA INSTITUTE OF TECHNOLOGY

EARTHQUAKE ENGINEERING RESEARCH LABORATORY

SEMI-ACTIVE CONTROL OF DYNAMICALLY EXCITED STRUCTURES USING ACTIVE INTERACTION CONTROL

BY

YUNFENG ZHANG

REPORT NO. EERL 2001-01

A REPORT ON RESEARCH PARTIALLY SUPPORTED BY
KAJIMA CORPORATION AND THE EARTHQUAKE RESEARCH AFFILIATES
PROGRAM OF THE CALIFORNIA INSTITUTE OF TECHNOLOGY

PASADENA, CALIFORNIA

MAY 2001

A REPORT ON RESEARCH PARTIALLY SUPPORTED BY KAJIMA CORPORATION AND THE EARTHQUAKE RESEARCH AFFILIATES PROGRAM OF THE CALIFORNIA INSTITUTE OF TECHNOLOGY UNDER THE SUPERVISION OF W. D. IWAN

Semi-Active Control of Dynamically Excited Structures Using Active Interaction Control

Thesis by

Yunfeng Zhang

In Partial Fulfillment of the Requirements

for the Degree of

Doctor of Philosophy

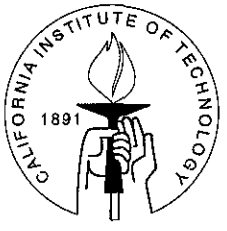

California Institute of Technology

Pasadena, California

2001

(Submitted May 21, 2001)

Acknowledgements

I would like to express my sincere appreciation to my advisor, Professor W. D. Iwan, for his guidance and encouragement during the course of my graduate study at Caltech. I consider myself fortunate for having the opportunity to share some of his knowledge and experience. My sincere gratitude also goes to other faculty members in Thomas Building for their helpful suggestions on this research. In particular, I wish to thank Professor James L. Beck and Professor John F. Hall for their encouragement and assistance in my graduate study at Caltech.

I am also grateful to Caltech for the excellent education and financial assistance which I received during my graduate study. I also express my gratitude to the Kobori Research Complex of the Kajima Corporation which has provided partial support for this investigation.

I also want to extend my thanks and best wishes to all my fellow students and friends in Thomas Building. With their presence and companionship, my graduate study at Caltech has been made most enjoyable.

Finally, I want to express my deep gratitude and love to my wife, Hongmei, for her endless patience and encouragement throughout the years of my graduate study.

Abstract

This thesis presents a family of semi-active control algorithms termed Active Interaction Control (AIC) used for response control of dynamically excited structures. The AIC approach has been developed as a semi-active means of protecting building structures against large earthquakes. The AIC algorithms include the Active Interface Damping (AID), Optimal Connection Strategy (OCS), and newly developed Tuned Interaction Damping (TID) algorithms. All of the AIC algorithms are founded upon the same basic instantaneous optimal control strategy that involves minimization of an energy-based performance index at every time instant.

A typical AIC system consists of a primary structure targeted for vibration control, a number of auxiliary structures, and interaction elements that connect the auxiliary structures to the primary structure. Through actively modulating the operating states of the interaction elements according to pre-specified control logic, control forces favorable to the control strategy are reactively developed within the interaction elements and the vibration of the primary structure is thus restrained. The merits of this structural control approach include both high control performance and minimal external power requirement for the operation of the control devices. The latter is important during large earthquakes when power blackouts are likely to occur. Most encouraging is that with currently available technology this control approach can be readily implemented in real structures.

In this thesis, the cause for an over-attachment problem in the original OCS system is clarified and corresponding counter-measures are proposed. The OCS algorithm is reformulated within an energy framework and therefore all of the AIC control algorithms are unified under the same instantaneous optimal control strategy.

To implement the AIC algorithms into multi-degree-of-freedom systems, two approaches are formulated in this thesis: the Modal Control and Nodal Control approaches. The Modal Control approach directs the control effort to certain dominant response modes, and the Nodal Control approach directly controls the response quantities in physical space. It is found that the Modal Control approach is more efficient than the Nodal Control approach. The effectiveness of the AIC control algorithms is verified through numerical simulation

results for three-story, nine-story and twenty-story steel-framed buildings. The statistical behavior of the AIC system is evaluated based on a Monte Carlo simulation.

Contents

List of Figures

List of Tables

Nomenclature

α	:	Stiffness Ratio between AS and PS
β	:	Mass Ratio between AS and PS
ψ	:	Frequency Ratio between AS and PS
γ	:	Fractional Damping Ratio between AS and PS
$\ddot{x}_g$	:	Earthquake Ground Motion Acceleration
AIC	:	Active Interaction Control
AID	:	Active Interface Damping
AS	:	Auxiliary Structure
AVD	:	Active Variable Damping
AVS	:	Active Variable Stiffness
DOF	:	Degree-of-Freedom
ELC	:	El Centro Record from the 1940 Imperial Valley Earthquake
HAC	:	Hachinohe Record from the 1968 Tokachi-oki Earthquake
IE	:	Interaction Element
KOB	:	Kobe Record from the 1995 Hyogo-ken Nanbu Earthquake
MC	:	Modal Control
MDOF	:	Multi-Degree-of-Freedom
NC	:	Nodal Control
OCS	:	Optimal Connection Strategy
PS	:	Primary Structure
SCH	:	Sylmar County Hospital Record from the *1994 Northridge Earthquake*
SDOF	:	Single-Degree-of-Freedom
TID	:	Tuned Interaction Damping
VDU	:	Variable Damping Unit
VSD	:	Variable Stiffness Device

Chapter 1 Introduction

1.1 Background and Motivation

In recent years, considerable attention has been given to research and development of structural control techniques. Successful application of structural control techniques will not only greatly improve the comfort of residents in a building, but more importantly, enhance the safety and prevent property loss when large earthquakes occur. For example, recent destructive seismic events in Northridge, California, in 1994 and Kobe, Japan, in 1995 have demonstrated the effectiveness of mitigating these hazards by use of structural control techniques [9].

Since the early conceptual study of structural control by Yao [45] in 1972, remarkable progress has been made in this field. To date, numerous methods of structural control have been proposed and some have even been implemented successfully in full-scale structures [9, 35, 36, 3].

Consideration of energy will illustrate the working mechanisms of structural control techniques [39, 34]. In conventionally designed structures, the vibrational energy of the structure induced by earthquake ground motion or wind loading is dissipated through linear viscous-like damping mechanisms in the structure. However, the linear viscous-like damping of many structures in the elastic range is insufficient to dissipate the large amount of energy associated with strong seismic excitation. Therefore, in a major earthquake event, a large portion of the seismic input energy must be dissipated through associated hysteresis by cracking and inelastic deformation of structural components. Hence damage to the structural elements and architectural components is likely to occur. Because of economic loss and life safety concerns, this mechanism for energy dissipation is undesirable. With the advent of innovative concepts of structural control, it is possible to dissipate much of the vibrational energy through external damping provided by control actions.

In the simplest case, the response of a structure can be modeled by a linear SDOF

oscillator which has its equation of motion expressed as follows.

$$m\ddot{x} + c\dot{x} + kx = -m\ddot{x}_g \tag{1.1}$$

By multiplying Eqn. (1.1) by $\dot{x}$ and integrating, the equation is transformed into an energy equation as follows.

$$\underbrace{\int m\ddot{x}\dot{x}\mathrm{d}t}_{E_K} + \underbrace{\int c\dot{x}^2\mathrm{d}t}_{E_D} + \underbrace{\int kx\dot{x}\mathrm{d}t}_{E_S} = \underbrace{\int(-m\ddot{x}_g)\dot{x}\mathrm{d}t}_{E_I} \tag{1.2}$$

where E_K, E_D, and E_S are the relative kinetic energy of the mass, the energy dissipation from linear viscous damping in the structure, and the elastic strain energy, respectively. The sum of these energies must equal the input energy E_I due to external disturbance.

For conventionally designed structures subjected to strong ground motion, it is difficult to maintain the energy balance between the input E_I and the elastic capacity of the structure E_K, E_D, E_S. Generally, some structural components will yield or crack and the linear spring force in Eqn. (1.1) will be replaced by a nonlinear term $f(x, \dot{x})$ typically involving hysteretic damping effects which increase the energy dissipation capacity of the structure.

For controlled structures, a control force term u is introduced into Eqn. (1.1). The energy dissipated by this control force may then be written as

$$E_u = \int u\dot{x}\mathrm{d}t \tag{1.3}$$

The amount of hysteretic energy dissipated by yielding or cracking of the structure can be reduced by providing the additional energy dissipation mechanism, E_u. Typically, structural control devices are installed in places where workers have access for regular inspection and replacement of damaged devices. Therefore, vibrational control by robust and stable structural control approaches is obviously more attractive than the conventional means.

The control of structural vibrations produced by external loadings can be accomplished by various means such as modifying stiffness, mass, damping, or configuration, and by providing passive or active control forces. In general, structural control methods can be classified into the following four categories [9]:

Active Control An active control system is one in which an external source powers control

actuators that apply forces to the structure in a prescribed manner. These forces can be used to both add and dissipate energy in the structure. In an active feedback control system, the signals sent to the control actuators are a function of the response of the system measured with physical sensors.

Passive Control *A passive control system does not require an external power source.* Passive control devices impart forces that are developed in response to the motion of the structure.

Hybrid Control A hybrid control system is typically defined as one which employs a combined use of active and passive devices. For example, a structure equipped with distributed viscoelastic damping supplemented by an active mass damper on or near the top of the structure, or a base-isolated structure with actuators actively controlled to enhance its performance.

Semi-active Control Semi-active control systems are a class of active control systems for which the external energy requirements are orders of magnitudes smaller than typical active control systems. Typically, semi-active control devices do not add mechanical energy to the structural system, therefore bounded-input bounded-output stability is guaranteed. Semi-active control devices are often viewed as controllable passive devices.

Besides the ability of reducing selected maximum response quantities, simplicity, reliability, and minimal power requirement are also highly desirable for structural control approaches. Semi-active control systems appear to combine the best features of both passive and active control systems and to offer the greatest likelihood for near-term acceptance of control technology as a viable means of protecting civil structures against earthquake and wind loading [35]. *A semi-active control system can produce a large control force simply* by actively changing parameters such as control device damping coefficient and stiffness. Therefore, it has the advantage that it can control the response of a large-scale structure in a large earthquake with smaller energy in comparison with a conventional active control system utilizing an actuator.

Recently, researchers at Kajima Corporation in Japan have conducted considerable research on two semi-active control systems called Active Variable Damping System (AVD)

[5, 25, 26] and Active Variable Stiffness System [22, 23, 24, 43]. The Active Variable Damping system is a seismic response control system that uses a variable damping unit (VDU) to control the damping force. The variable damping unit, which consists of a variable hydraulic damper and a damping force controller, can control a large damping force, although it consumes only a small amount of electric power [25]. Both a shaking table test performed on a three-story steel-framed structure with a mini-scale VDU (maximum force is 2 tf) and a simulation analysis of a semi-actively controlled high-rise building confirmed the effectiveness of the AVD approach in large earthquakes. Subsequently, semi-active hydraulic dampers (SHD) which can produce a maximum damping force of 1000 kN with an electric power of 70 watts were applied to a five-story office building located in Shizuoka City, Japan [26]. The hydraulic dampers are compact so that a large number of them can be installed in a single building. It is thus possible to control the building's response during a large earthquake, since a large control force is obtained in comparison with a conventional active control system.

The Active Variable Stiffness seismic response control system has been developed to preserve the safety of the building and important equipment contained therein against earthquakes of large intensities [24]. The AVS system has been implemented in an actual three-story building (KaTRI No. 21 Building) in Japan, as shown in Fig. 1.1. With this system, the building reduces its response by establishing non-resonance against earthquake motions. The non-resonant state is realized by altering the structure's stiffness with a mechanical system. The AVS system can be driven by only a small amount of power. Since the completion of the building, it has experienced three earthquakes and the observed response confirms the effectiveness of the AVS system.

In a recent joint study with Kajima Corporation, researchers at the California Institute of Technology have carried out a series of exploratory investigations on an innovative structural control approach, referred to as Active Interaction Control (AIC) [6, 7, 14, 41]. AIC is developed as a semi-active means of suppressing the vibrations of structures subjected to seismic excitation. It incorporates some important features of the AVS control approach [7]. A typical AIC system is comprised of a primary structure targeted for control, a number of auxiliary structures and interaction elements that connect the auxiliary structures to the primary structure. Through actively modulating the operating states of the interaction elements according to pre-specified control logic, control forces favorable to the control

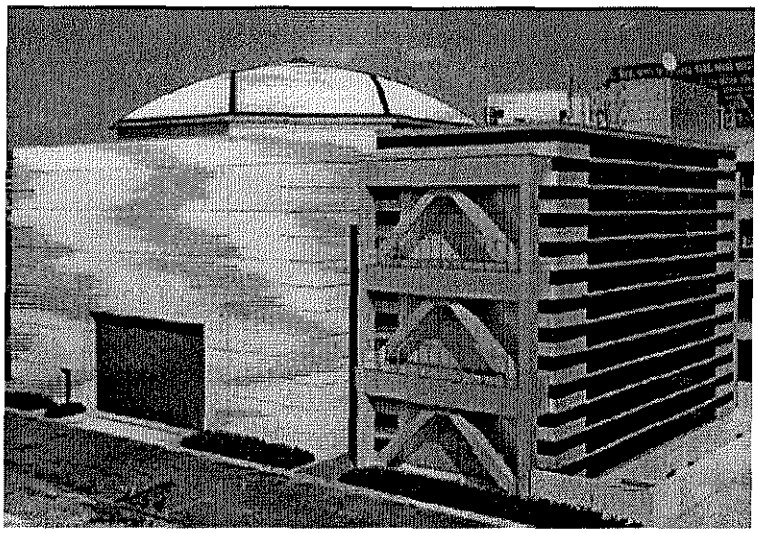

Figure 1.1: A Building with AVS Control Device

strategy are reactively developed within the interaction elements and the vibration of the primary structure is thus restrained. Minimal external power is required for the operation of interaction elements even during large earthquakes.

The first generation of AIC – the Active Interface Damping (AID) control algorithm was developed by Hayen and Iwan [6, 8]. This control approach utilizes controlled interactions between two distinct structural systems, or different components of the same structure to suppress the resonance buildup that develops in the primary structure during an external excitation. The AID control algorithm is implemented by minimizing the rate of change in the vibrational energy of the primary structure for each control-sampling period. Linear single- and multi-degree-of-freedom models have been considered to examine the performance of the AID algorithm.

The next generation of AIC, Optimal Connection Strategy (OCS), was developed by Wang and Iwan [14, 41]. Their OCS control algorithm is based on a set of three simultaneous conditions for an attachment between the primary structure and auxiliary structure. If at some representative time point, all of the three conditions are satisfied, a "Locked" state will be applied to the interaction element in the next control-sampling period and interaction between the primary structure and auxiliary structure are thus activated. An "Unlocked" state is applied to the interaction element if any of these three conditions is not met. Because of the rule-based nature of this control algorithm, it is rather difficult to implement this control algorithm to suppress the dominant response modes in structures.

Although the OCS control algorithm generally exhibits better control performance than the AID control algorithm when time delays are ignored, the excessively large number of interaction cycles associated with this algorithm presents a problem. If the duration of the "Locked" state is too short, the interaction element may not react fast enough to produce the desired effect due to its mechanical limitations. Large accelerations are also observed in the OCS-controlled primary structure. These problems partially motivate the investigation described in this thesis. Another incentive for this study is to test the AIC control algorithms within the framework of more realistic structural models.

1.2 Scope and Organization of the Thesis

This thesis summarizes the result of a follow-on study on the AIC control algorithm. The mechanism associated with the over-attachment problem in the original OCS system is clarified and corresponding counter-measures are proposed. The OCS algorithm is reformulated within an energy framework and therefore all of the AIC control algorithms are unified under the same instantaneous optimal control strategy. The effectiveness of the AIC control algorithms is verified through numerical simulation results for 3-story, 9-story and 20-story steel-framed buildings. The statistical behavior of the AIC system is evaluated based on a Monte Carlo simulation.

In Chapter 2, the working mechanism and associated control strategy underlying the AIC control algorithms are illustrated using a single-degree-of-freedom (SDOF) structure model. Founded upon the same instantaneous optimal control strategy, three sub-AIC algorithms, namely, the Active Interface Damping (AID), Optimal Connection Strategy (OCS) and newly developed Tuned Interaction Damping (TID) algorithms are discussed. A typical SDOF AIC system consists of a primary structure, an auxiliary structure and an interaction element linking the primary structure and auxiliary structure together. To simplify the subsequent analysis, assumptions are made regarding the primary structure and auxiliary structure at the beginning of this chapter. Two models are considered for the interaction element. The stability of an unforced AIC system is shown using the Lyapunov direct method. The effectiveness of AIC control algorithms is then demonstrated by numerical simulations of SDOF AIC systems subjected to various types of excitation. Next, two practical constraints which are expected to have a significant impact on control

effectiveness in an actual implementation of the AIC approach are considered. Specifically, the following two constraints are addressed for the AIC systems: control-sampling period and presence of time delays.

Eventually, any structural control approach needs to be implemented in more realistic multi-degree-of-freedom (MDOF) structural models. In Chapter 3, the AIC algorithm is reformulated within the framework of linear MDOF systems. Two approaches, the Modal Control and Nodal Control approaches, are developed to implement the AIC control algorithms in MDOF systems. The Modal Control approach directs the control effort to certain dominant response modes of the primary structure, while the Nodal Control approach tries to restrain the individual inter-story drift of the structure directly. Three structures, a 3-story building, a 9- and a 20-story steel-framed building controlled with the AIC algorithms are analyzed for several historical earthquake records.

Chapter 4 describes the statistical behavior of SDOF AIC systems. A large ensemble of artificial earthquake ground motions is generated from modified Kanai-Tajimi filtered gaussian white-noise process. Using this ensemble of artificial earthquake ground motions, a Monte Carlo simulation is carried out to assess the performance of SDOF AIC systems in a statistical sense. The parameters which have significant effects on the performance of AIC systems are the stiffness ratio α, frequency ratio ψ, AS damping ratio ζ_2 and control force limit u_{max}. The optimal values of these important parameters are determined based on the same ensemble of artificial seismic ground motions.

Chapter 5 contains the main conclusions of the work presented in this thesis and some suggestions about future research directions.

Chapter 2 Active Interaction Control of Linear SDOF Systems

2.1 Introduction

The AIC control approach has been proposed as a semi-active means of protecting structures against large earthquakes. In this chapter, a simple Active Interaction Control (AIC) system model involving two interacting SDOF systems is investigated. One of the SDOF systems is the primary structure targeted for vibration control while the other is the auxiliary structure for delivering the control force needed. Although this is a highly idealized model of complex building systems, it is fundamental to the understanding of the essential dynamic behavior of more complicated AIC systems.

In an AIC system, an interaction element which links the primary structure and auxiliary structure together is employed to facilitate the interactions between the primary structure and auxiliary structure. The objective of the control strategy under investigation is to reduce the motion of the primary structure as much as possible. Through actively controlled interactions, control force favorable to this control strategy can be generated within the interaction element. This control force plays the role of removing vibrational energy from the primary structure to the auxiliary structure. When the interaction is activated, part of the vibrational energy of the primary structure is transmitted into the auxiliary structure where it will be dissipated in the following cycles when the interaction is deactivated.

The AIC algorithms include the Active Interface Damping (AID) [6, 7], the Optimal Connection Strategy (OCS) [41, 14, 15], and newly developed Tuned Interaction Damping (TID) algorithms. All of these AIC algorithms may be founded upon the same instantaneous optimal control strategy that involves minimization of an energy-based performance index at every time instant. The effectiveness of AIC algorithms is demonstrated by numerical simulations of SDOF AIC systems subjected to various types of excitations. Finally, two practical constraints which are expected to have a significant impact on control effectiveness in an actual implementation of the AIC approach will be considered. Specifically, the

following two constraints are addressed for the AIC systems: control-sampling period and presence of time delays.

2.2 Assumptions and Formulation

For convenience and simplicity, the following acronyms are defined and will be used in the following discussion.

PS: Primary Structure; AS: Auxiliary Structure; IE: Interaction Element

The following assumptions are made in this study:

- Only response in the horizontal direction is considered.
- All system parameters are known in advance and do not change during the excitation duration. The PS and AS remain within the linear elastic range.
- The mass of IE is negligible compared to that of PS and AS and therefore the dynamics of IE is neglected. It is further assumed that an IE can respond instantaneously to control signals except for the cases with time delay.
- The system states are completely observable. Only present and past values of base acceleration and system state variables are available to determine the control input.

Under these conditions, the equations of motion for the PS and AS subjected to base excitation $\ddot{x}_g$ are expressed as

$$M\ddot{\mathbf{x}}(t) + C\dot{\mathbf{x}}(t) + K\mathbf{x}(t) = -ML\ddot{x}_g(t) + \Gamma u(t) \tag{2.1}$$

where

$\mathbf{x}(t) = \{x_1(t) \quad x_2(t)\}^T$ is the relative displacement vector,

$M = \begin{bmatrix} m_1 & 0 \\ 0 & m_2 \end{bmatrix}$ is the mass matrix, $C = \begin{bmatrix} c_1 & 0 \\ 0 & c_2 \end{bmatrix}$ is the damping matrix,

$K = \begin{bmatrix} k_1 & 0 \\ 0 & k_2 \end{bmatrix}$ is the stiffness matrix,

$L = \{1 \quad 1\}^T$, $\Gamma = \{-1 \quad 1\}^T$,

and m_1, m_2, c_1, c_2, k_1, k_2, and x_1, x_2 represent the mass, stiffness, damping factor, and relative displacement of the PS and AS respectively, as shown in Fig. 2.1. The subscripts 1 and 2 are used to denote the PS and AS respectively. $\ddot{x}_g$ is the ground acceleration. $u(t)$ is the control force developed within the IE; the sign of $u(t)$ is defined such that $u(t)$ is positive whenever the IE is in tension.

Rewriting the above equations of motion in the state-space form yields

$$\dot{X}(t) = AX(t) + B_u u(t) + B_w w(t) \tag{2.2}$$

where

$X(t) = \{\mathbf{x}(t) \quad \dot{\mathbf{x}}(t)\}^T$ is the state vector,

$$A = \begin{bmatrix} \emptyset & I \\ -M^{-1}K & -M^{-1}C \end{bmatrix}, \quad B_u = \begin{Bmatrix} \emptyset_v \\ M^{-1}\Gamma \end{Bmatrix}, \quad B_w = \begin{Bmatrix} \emptyset_v \\ -L \end{Bmatrix},$$

$w(t) = \ddot{x}_g(t)$ represents the external excitation,

and $\emptyset_v$, $\emptyset$ and I denote the null vector, null matrix and identity matrix, respectively.

In structures, the displacements and velocities of the system masses are commonly used as state variables. The above linear state equation is widely used in conventional optimal control problems and will form the basis for the formulation and solution of system dynamics in this study. By using the state equations, the well-known second-order differential equations characterizing the motion of a structural system can be rewritten as a set of first-order differential equations. Current techniques for the high-speed solution of first-order differential equations make the state-space approach particularly attractive.

To compute the dynamics of an AIC system subjected to external disturbance, a numerical scheme in discrete time has to be employed because of the nonlinearity and history dependence associated with the AIC system. The state variable, $X(t_{k+1})$ at time t_{k+1} for the given initial condition $X(t_k)$ at time t_k, is given by the following convolution integral:

$$X(t_{k+1}) = e^{A\Delta t}X(t_k) + \int_{t_k}^{t_{k+1}} e^{A(t_{k+1}-\tau)}[B_u u(\tau) + B_w w(\tau)]\mathrm{d}\tau \tag{2.3}$$

where $\Delta t = t_{k+1} - t_k$.

A partitioned predictor-corrector (PPC) method [13] is employed for computing the integral in Eqn. (2.3). A brief description of the PPC method is given in Appendix A. Using this numerical scheme, $X(t_{k+1})$ can be expressed as

$$X(t_{k+1}) = \Phi X(t_k) + B_{u1}u(t_k) + B_{u2}\hat{u}(t_{k+1}) + B_{w1}w(t_k) + B_{w2}w(t_{k+1}) \tag{2.4}$$

where

$$\begin{aligned}
\Phi &= e^{A\Delta t} \\
B_{u1} &= A^{-1}[\Phi - \frac{A^{-1}(I-\Phi)}{\Delta t}]B_u \\
B_{u2} &= A^{-1}[\frac{A^{-1}(\Phi - I)}{\Delta t} - I]B_u \\
B_{w1} &= A^{-1}[\Phi - \frac{A^{-1}(I-\Phi)}{\Delta t}]B_w \\
B_{w2} &= A^{-1}[\frac{A^{-1}(\Phi - I)}{\Delta t} - I]B_w
\end{aligned} \tag{2.5}$$

and $\hat{u}(t_{k+1})$ is the estimated value of the control force vector as described in Appendix A.

2.3 Interaction Elements

Two types of IEs are considered in this study. These are depicted in Fig. 2.2. The first type, Type A IE, consists only of an On/Off locking device which has two operating states: *locked* or *unlocked*. In its locked state, a rigid connection is provided between the PS and AS, while in its unlocked state, the force developed within the IE is equal to zero and it is further assumed that the transition from the locked state to unlocked state or the converse is accomplished instantaneously. A Type B IE is comprised of a fuse device and an On/Off locking device described above which are placed in series with each other. The mechanical properties of Type B IE is the same as that of Type A IE except that control force in a Type A IE is not allowed to exceed a pre-specified maximum value which depends on the property of the fuse device. Examples of the fuse device could be a Coulomb frictional damper or a hydraulic pressure-limiting device. It is noteworthy that recently developed magneto-rheological damper can also be used for this purpose.

The expression for the force reactively developed within the IE is given below for each type of IE.

- Type A: On/Off locking device

$$u = \begin{cases} (\frac{m_1 k_2 x_2 - m_2 k_1 x_1}{m_1 + m_2}) + (\frac{m_1 c_2 - m_2 c_1}{m_1 + m_2})\dot{x}_1 & \text{, locked} \\ 0 & \text{, unlocked} \end{cases} \tag{2.6}$$

(Note that in the locked state, it is assumed that $\ddot{x}_1 = \ddot{x}_2$, and $\dot{x}_1 = \dot{x}_2$.)

- Type B: On/Off locking device placed in series with a fuse device

$$u = \begin{cases} \begin{cases} (\frac{m_1 k_2 x_2 - m_2 k_1 x_1}{m_1 + m_2}) + (\frac{m_1 c_2 - m_2 c_1}{m_1 + m_2})\dot{x}_1 & , |u| \leq u_{max} \\ u_{max}\text{Sgn}(\dot{x}_1 - \dot{x}_2) & , |u| > u_{max} \end{cases} & \text{, locked} \\ 0 & \text{, unlocked} \end{cases} \tag{2.7}$$

where u_{max} is the control force limit associated with the fuse device and Sgn$(\cdot)$ is the signum function.

2.4 Control Strategy and Stability

Vibration control for seismically excited structures presents a unique problem since the excitation input, the earthquake ground motion, is generally unknown a priori. Also, it is usually unrealistic to provide the large power source necessary to apply the control force determined from an active control law during significant seismic events. Therefore, new optimal control strategies suitable for controlling earthquake-excited structures is highly desired. In this section, one such type of instantaneous optimal control algorithm is discussed. This algorithm was originally developed by Hayen and Iwan [6, 8].

The aim of the AIC control strategy is to reduce the motion of the PS as much as possible. This objective can be achieved by minimizing the time derivative of the relative vibrational energy of the PS at each time instant during external excitations. The relative vibrational energy of the PS is defined as

$$E_1 \equiv \frac{1}{2} m_1 \dot{x}_1^2 + \frac{1}{2} k_1 x_1^2 \tag{2.8}$$

Differentiating Eqn. (2.8) and substituting Eqn. (2.1), the time derivative of the relative

vibrational energy of the PS is expressed as

$$\dot{E}_1 = (m_1\ddot{x}_1 + k_1 x_1)\dot{x}_1 = [-u(t) - m_1\ddot{x}_g - c_1\dot{x}_1]\dot{x}_1 \tag{2.9}$$

In practice, any control algorithm has to be implemented in discrete time. Consider some time interval $[t_0, t_1]$ during which vibration control for the PS is to be accomplished. Let $[t_0, t_1]$ be uniformly partitioned into a set of appropriately short time intervals, each of duration Δt and referred to as a control-sampling period. Now, consider a representative time interval, the k^{th} control-sampling period, defined by $t \in [t_k, t_{k+1})$. As noted above, effort is directed toward minimizing the change in E_1 for the control-sampling period, denoted by ΔE_1^k, or causing this change to be as negative as possible.

$$\begin{aligned} \Delta E_1^k &= \int_{t_k}^{t_{k+1}} [-u(t) - m_1\ddot{x}_g - c_1\dot{x}_1]\dot{x}_1 \mathrm{d}t \\ &\approx -[u(t)\dot{x}_1]\Big|_{t=t_k} \Delta t - [m_1\ddot{x}_g\dot{x}_1 + c_1\dot{x}_1^2]\Big|_{t=t_k} \Delta t + O(\Delta t^2) \end{aligned} \tag{2.10}$$

If the sampling period is small enough, the higher order term $O(\Delta t^2)$ can be neglected. In addition, the second term in Eqn. (2.10) is uncontrollable in the sense that it is constant regardless of the operating state selected for the IE. Hence, to the degree of approximation considered, the difference in values of ΔE_1^k for different IE operating states depends solely on the first term in Eqn. (2.10).

The control strategy can now be described as follows: at the beginning of each control-sampling period, the state variables $X(t)$ of the PS and AS are measured and thus fully known. A control processor then uses this information to determine an appropriate operating state for the IE: *locked* or *unlocked*. In the locked state, interactions between the PS and AS are activated, while interactions are deactivated in the unlocked state. Finally, the control signal made at the beginning of each control-sampling period is sent to the control valve of the IE to switch or maintain the operating state of the IE. The system then responds to the values of $u(t)$ resulting from these interactions until the beginning of next control-sampling period, when another appropriate operating state is determined for the IE. This procedure is then repeated for each consecutive control-sampling period [6].

It is seen that the control strategy developed above is essentially the same as an instan-

taneous optimal control strategy with its performance index defined by

$$J(t) = \frac{1}{2} z_1^T(t) P z_1(t) \tag{2.11}$$

where

$$P = \begin{bmatrix} k_1 & 0 \\ 0 & m_1 \end{bmatrix}, \quad z_1 = \begin{Bmatrix} x_1 \\ \dot{x}_1 \end{Bmatrix} \tag{2.12}$$

By minimizing $\dot{E}_1$, the performance index $J(t)$ is kept as low as possible at each time instant $t \in [t_0, t_1]$. Unlike the active control case in which any desired control force can be applied, a constraint is imposed on the available control force in an AIC system because of its inherent interaction characteristics. That is, the control force $u(t)$ in the next control-sampling period is described by Eqns. (2.6) or (2.7). Therefore, minimization of the performance index $J(t)$ is done by substituting the control force value in one of the two distinct states: locked or unlocked. If $\dot{J}(t_k)_{locked}$ is less than $\dot{J}(t_k)_{unlocked}$ at discrete time instant t_k, an interaction will be activated between the PS and AS in the next sampling period, and vice versa. Because minimization is done only at discrete time instant and for very limited number of (two for the the IE considered in this study) IE operating states, the AIC algorithms are only sub-optimal [6].

A heuristic control law for the AIC control strategy can be expressed by the attachment conditions summarized in Table 2.1 for each AIC algorithm. When the attachment conditions for a particular AIC algorithm are satisfied simultaneously at the beginning of a control-sampling period, a locked state is selected for the IE, while the IE is unlocked if one of the attachment conditions is not satisfied. It is seen that one condition which drives the first term at the right-hand side of Eqn. (2.10) as negative as possible is employed by all AIC algorithms which include the AID, OCS and TID algorithms. This condition is derived from the above-formulated instantaneous optimal control strategy. It is also observed that the physical meaning of this condition ensures that no mechanical energy will be put in to the PS from the AS since $\dot{x}_1(t)$ actually represents the energy dissipation rate of PS.

When the PS and AS are attached with dissimilar velocities, the induced impact may cause damage to either or both the PS and AS. This detrimental impact effect can be eliminated if an additional attachment condition is introduced. This new attachment condition requires equal PS and AS velocities in order to initiate an interaction between the PS and

Table 2.1: Characteristics of the AIC Control Algorithms

Control Algorithms	Attachment Conditions	AS Dynamics	IE Type and Operating States
AID	$u^a(t) \cdot \dot{x}_1(t) \geq 0$	Considered	Type A, Free/Rigid
OCS	$\begin{cases} u^a(t) \cdot \dot{x}_1(t) \geq 0 \\ \dot{x}_1(t) = \dot{x}_2(t) \end{cases}$	Considered	Type A, Free/Rigid
TID	$\begin{cases} u^a(t) \cdot \dot{x}_1(t) \geq 0 \\ \dot{x}_1(t) = \dot{x}_2(t) \end{cases}$	Considered	Type B, Free/Rigid/Slip, $\lvert u^a(t) \rvert \leq u_{max}$

Note: AIC control algorithms include the Active Interface Damping (AID), Optimal Connection Strategy (OCS), and Tuned Interaction Damping (TID) algorithms. $u^a(t)$ represents the control force value calculated from the assumption that the PS is attached to the AS at time t (i.e., the IE is assumed to be locked).

AS.

However, other important reasons exist for the adoption of this additional attachment condition besides eliminating the impact effect. In an AIC system, the function of the AS can be regarded as an actuator delivering a control force to the PS. The value of the control force delivered by the AS is approximately equal to the elastic spring restoring force in the AS. Therefore, the larger the AS displacement, the larger the control force will be. It is found that the PS and AS usually achieve equal velocities at the time instant when the AS is close to its maximum displacement position. A large control force will then be generated and more energy will be dissipated from the PS if the attachment between the PS and AS is delayed until the PS and AS have equal velocities. This study shows that doing this not only will many interaction opportunities not be missed, but this new algorithm has an improved response reduction capability.

Stability is an important concern for any control system. An unstable system is not only useless in practice but can also be dangerous. For AIC algorithms, it is guaranteed that no mechanical energy will be put to the PS because of its energy dissipative characteristics. Next, we will examine the stability of unforced AIC systems by Lyapunov's direct method

[33, 27]. The PS's equation of motion may be expressed in state-space form as

$$\dot{z}_1(t) = \hat{A}z_1(t) + \hat{B}u(t) \tag{2.13}$$

where

$$\hat{A} = \begin{bmatrix} 0 & 1 \\ -\frac{k_1}{m_1} & -\frac{c_1}{m_1} \end{bmatrix}, \quad \hat{B} = \begin{Bmatrix} 0 \\ -\frac{1}{m_1} \end{Bmatrix} \tag{2.14}$$

in which the excitation term is dropped because it is not relevant to the stability of the structure [44].

A possible Lyapunov function is given by

$$V(t) = z_1^T Q z_1 \geq 0 \tag{2.15}$$

from which

$$\dot{V}(t) = \dot{z}_1^T Q z_1 + z_1^T Q \dot{z}_1 = z_1^T (Q\hat{A} + \hat{A}^T Q) z_1 + 2 z_1^T Q \hat{B} u \tag{2.16}$$

Clearly, the PS without control is stable. This means that for any given symmetric positive semi-definite matrix I_0, we can always obtain a symmetric positive semi-definite matrix Q by solving

$$Q\hat{A} + \hat{A}^T Q = -I_0 \tag{2.17}$$

Therefore, the first term in Eqn. (2.16) becomes $-z_1^T I_0 z_1 \leq 0$ because I_0 is positive semi-definite. If it can also be shown that the second term in Eqn. (2.16) is less than or equal to zero, it is clear that $\dot{V}(t)$ is negative semi-definite and by Lyapunov direct method, the PS with control is stable.

We can choose the Q matrix in Eqn. (2.17) to be the same as the P matrix in Eqn. (2.11). Then

$$I_0 = -(Q\hat{A} + \hat{A}^T Q) = \begin{bmatrix} 0 & 0 \\ 0 & 2c_1 \end{bmatrix} \tag{2.18}$$

Obviously, Q and I_0 are symmetric, positive semi-definite.

Now, the second term in Eqn. (2.16) becomes

$$z_1^T Q \hat{B} u = -m_1 u \dot{x}_1 \tag{2.19}$$

Recall that for AIC control algorithms, the control force is determined at each time instant such that $u\dot{x}_1 \geq 0$. Thus, it has been shown $\dot{V}(t)$ is negative semi-definite for the control algorithm under consideration and thus the AIC system is stable.

2.5 Idealized AID and OCS Models

Two idealized models for single-degree-of-freedom AID and OCS systems are considered herein to examine the damping effect of the AIC algorithms. The control action on the PS are modeled by a nonlinear restoring force which provides hysteretic damping to the PS.

2.5.1 Idealized SDOF AID Model

In this idealized model, the dynamics of the AS are neglected. The equation of motion of the idealized system is expressed as

$$m_1\ddot{x}_1 + c_1\dot{x}_1 + k_1x_1 + k_2[x_1 - x_1(t_c)] = -m\ddot{x}_g \tag{2.20}$$

where

$$t_c = \max(\tau; \tau \in [0, t], \dot{x}_1(\tau) = 0). \tag{2.21}$$

That is, t_c is the most recent time when the velocity of the PS reaches zero. The feedback control algorithm for this model may be defined as follows:

- The state of the IE is always set to "locked" except when $\dot{x} = 0$. At the moment when $\dot{x} = 0$, the IE is first switched to the "unlocked" state, and then immediately switched backed to the "locked" state;
- It is once again assumed that upon unlocking, the AS instantaneously returns to its zero position.

This control algorithm was first studied by Hayen and Iwan [6, 14].

Assuming c_1 to be zero, the equation of motion of the idealized system in free oscillation may be written as

$$m_1\ddot{x}_1 + k_1x_1 + k_2[x_1 - x_1(t_c)] = 0 \tag{2.22}$$

Solving the above equation with an initial condition $x_1(0) = x_0$ and $\dot{x}_1 = 0$, the equivalent viscous damping ratio may be defined as

$$\zeta = \frac{|\delta|}{\sqrt{4\pi^2 + \delta^2}} \tag{2.23}$$

where the logarithmic decrement, δ, is given by

$$\delta = 2 \ln \frac{|1 - \alpha|}{1 + \alpha}, \quad \alpha = \frac{k_2}{k_1} \tag{2.24}$$

2.5.2 Idealized SDOF OCS Model

In this model the dynamics of the AS is idealized as that upon unlocking of the IE, the AS immediately swings to its opposite maximum deformation position (i.e., $x_2(t_1^+) = -x_2(t_1)$), where t_1 is the time instant when unlocking occurs. Under such idealization, the equation of motion of the idealized OCS system is expressed as

$$m_1\ddot{x}_1 + c_1\dot{x}_1 + k_1x_1 + k_2[x_1 - x_1(t_c) - x_2(t_c)] = -m\ddot{x}_g \tag{2.25}$$

where t_c is defined by Eqn. (2.21).

This model can be realized with its heuristic control algorithm defined as

- The state of the IE is always set to "locked" except when $\dot{x} = 0$ and $x_2(t)\dot{x}_1(t) < 0$. A "locked" state for the IE is allowed only when $x_2(t)\dot{x}_1(t) \geq 0$; otherwise, the IE is immediately unlocked. At the time instant when $\dot{x} = 0$, the IE is first switched to the "unlocked" state, and then immediately switched backed to the "locked" state;
- As indicated before, it is assumed that upon unlocking, the AS immediately swings to the opposite maximum deformation position.

Similarly, assuming c_1 to be zero, the equation of motion of the idealized OCS system in free vibration can be expressed as

$$m_1\ddot{x}_1 + k_1x_1 + k_2[x_1 - x_1(t_c) - x_2(t_c)] = 0 \tag{2.26}$$

Again, solving the above equation with an initial condition $x_1(0) = x_0$ and $\dot{x}_1 = 0$ yields

the equivalent viscous damping ratio defined as

$$\zeta = \frac{|\delta|}{\sqrt{4\pi^2 + \delta^2}} \tag{2.27}$$

where the logarithmic decrement, δ, is given by

$$\delta = \ln \frac{|\alpha^2 - 6\alpha + 1|}{(\alpha + 1)^2} \tag{2.28}$$

Values of the equivalent viscous damping ratio as a function of stiffness ratio, α, are calculated for the two models and given in Table 2.2. It is observed that the OCS algorithm is much more efficient than the AID algorithm in terms of damping effect.

Table 2.2: Variations of Equivalent Damping Ratio ζ for the AID and OCS System

α		0.1	0.15	3-2$\sqrt{2}$	0.2	0.3	0.5	0.7	0.9	1.0
ζ %	AID	6.4	9.6	11.0	12.8	19.3	33.0	48.3	68.4	$\geq$ 100
	OCS	17.0	35.4	$\geq$ 100						

2.6 Optimal Connection Strategy and Tuned Interaction Damping

As mentioned before, AIC control algorithms include the Active Interface Damping (AID), Optimal Connection Strategy (OCS), and newly developed Tuned Interaction Damping (TID) algorithms. All of the AIC control algorithms are founded upon the same instantaneous optimal control strategy that involves minimization of an energy-based performance index at each time instant.

The original OCS algorithm was proposed as a set of rule-based attachment conditions consisting of three simultaneous conditions [41] which is quite different from its current form. At the beginning of a control-sampling period, if all of these three attachment conditions are satisfied simultaneously, a locked state will be applied to the IE in the next control-sampling period while an unlocked state will be applied if any one of these three conditions is not met.

In this study, the OCS algorithm has been reformulated and it is found that the old rule-based OCS algorithm can be replaced by a new energy-based OCS algorithm which has a much more rigorous theoretical base and this energy-based formulation is especially attractive when dealing with multi-degree-of-freedom systems. This new OCS algorithm is derived from the same instantaneous optimal control strategy as the AID algorithm. As stated in the preceding section, an additional attachment condition which requires equal PS and AS velocities in order to initiate an interaction is also included in the OCS algorithm besides the single attachment condition $u\dot{x}_1 \geq 0$ for the AID algorithm. Fig. 2.3 shows the response time histories of the PS controlled by the old OCS and new OCS algorithms respectively. Clearly, these two versions of OCS algorithm generate very close responses.

A distinctive characteristics of the OCS algorithm is that an interaction between the PS and AS is deliberately delayed until equal PS and AS velocities are achieved to generate a large control force within the IE. By having a large control force during interaction, the instantaneous energy dissipation rate for the PS $\dot{E}_D(t) = u(t)\dot{x}_1(t)$ is also increased by a large amount.

Although the OCS algorithm generally exhibits a better control performance than the AID algorithm if time delays are not considered, an excessively large number of Lock/unlock cycles between the PS and AS poses a new problem for the OCS algorithm. The cause of this annoying effect can be explained as follows: when a locked state is going to be initiated for the IE, the velocity of the PS and AS is generally very small as inherent in the OCS algorithm. This implies that both the PS and AS are close to their respective maximum displacement position when an interaction is initiated. As indicated by Eqn. (2.6), the control force can be approximated by the elastic spring restoring force in the AS. Therefore, if attached to the AS, the PS can only move for a very short distance from its current position before it is pushed back by the large spring restoring force present in the AS. When the PS is pushed back and thus the velocity of the PS changes sign, the PS and AS are then detached according to the OCS algorithm. After a half cycle of free oscillation of the AS, this short-duration lock/unlock cycle is repeated again. A great number of high-frequency small-amplitude oscillations are observed in the PS displacement response time history in the OCS system. To illustrate this, the steady-state part of the displacement response and lock/unlock indicator time histories for the PS and AS subjected to harmonic excitation are plotted in Fig. 2.4.

If the AS motion is attenuated during its free oscillation, the over-attachment problem is anticipated to be at least partially alleviated. Furthermore, if an interaction is initiated at the time instant when the amplitude of the AS motion is zero, the behavior of the OCS system will be quite similar to that of an AID system, while the undesirable impact effect due to the PS and AS velocity dissimilarity is eliminated.

The most straightforward way of reducing the amplitude of the AS motion is to add damping to the AS to damp out its free oscillation motion when an interaction is deactivated. In the present study, linear viscous damping is added to AS for this purpose. Numerical study has been carried out to examine this approach.The result for a harmonic excitation case is shown in Fig. 2.5. The normalized displacement is defined as the ratio of the maximum displacement response of the PS with OCS control and that without control. The following parameter values are used:

- Mass ratio of the AS and PS: $\beta = m_2/m_1 = 0.02$, 0.1, and 0.5.
- Forcing period of harmonical excitation: $T_{exc} = 0.5$ and 2 second.

Based on the numerical simulation results, the following conclusions are drawn:

1. With the AS damping ratio increasing, a general trend is observed that the attachment number decreases while usually maintaining a comparable PS displacement response. However, this observation is valid only for the cases in which the mass ratio β is less than 0.1 and the AS damping ratio ζ_2 is less than 30%. An optimal value for ζ_2 is determined approximately as 15% for the harmonically excited OCS system with the PS's natural period equal to 1 second. It is practically feasible to achieve an AS damping ratio of 15% by installing external damping devices with the AS.

2. As the AS's damping and mass values further increase, the performance of an OCS system deteriorates and in some cases is even worse than the uncontrolled PS. Fig. 2.6 shows both the PS and AS displacement response time history of a harmonically excited OCS system with the following parameter values: $\zeta_2 = 60\%$, $\beta = 0.1$. Clearly, in this particular case, the performance of this OCS system is poorer than that of the uncontrolled PS. It is also seen that the PS displacement response of this OCS system exhibits a chaotic behavior. The cause for this can be explained as follows: with a high mass ratio β and high AS damping ratio ζ_2, the AS now moves very slowly

because of its relatively small natural frequency and the AS motion is damped out quickly by its high damping. Therefore, lots of interaction opportunities are missed and the timing for the attachment between the PS and AS becomes chaotic. This causes the performance of this OCS system to deteriorate. This also confirms that an efficient OCS system requires an AS with a high natural frequency.

Careful study of the problem of excessive attachment motivated the concept of Tuned Interaction Damping (TID) control algorithm. A longer duration in the locked state is also expected by using the Type B IE previously discussed. The maximum control force level (e.g., slip force level for a Coulomb damper) which can be developed in the IE can be tuned for the optimal control performance of a TID system.

Suppression of peak displacement and absolute acceleration in seismic events is equally important in structural control of building structures. Although the OCS algorithm is generally more efficient than the AID algorithm in terms of suppression of PS displacement and velocity response, large PS acceleration response also occurs in the OCS system. This large PS acceleration response is caused by the fact that at the time of unlock-to-lock switch, a large control force is suddenly applied to the PS and therefore the PS acceleration is immediately increased by a large value. In a TID system, because of its bounded control force level, the PS acceleration is also bounded by a certain level. Fig. 2.7 shows the displacement response time histories of the AID ($\zeta_2 = 0$), OCS with undamped AS ($\zeta_2 = 0$), OCS with damped AS ($\zeta_2 = 15\%$), and TID ($\zeta_2 = 15\%$) systems. It is seen in Table 2.3 that while the TID system has a comparable displacement response with the AID and OCS systems under harmonic excitation, the PS absolute acceleration in the TID system is also reduced from that of the OCS system. This beneficial characteristic of the TID system will be further observed in the next section. From Fig. 2.8, it is verified that the attachment number is reduced in the OCS system with a damped AS, and the TID system. In Fig. 2.9, it is observed the TID system exhibits a much more favorable continuous hysteresis loop shape in contrast to a narrow-striped hysteresis loop shape for the OCS system.

It is expected that a TID system will also perform better than AID or OCS systems when subjected to near-field seismic excitations. Near-field earthquake ground motion involves large velocity pulses. Non-isolated rectangular (or trapezoidal if the maximum control force level is tuned to be high) hysteresis loops are anticipated for the TID system subjected to

Table 2.3: Maximum Value of the PS Acceleration, Velocity, and Displacement Response Under Harmonical Excitation, Type 1 Configuration

Algorithms	Displacement (cm)	Acceleration (cm/s/s)	Attachment Number
Uncontrolled (A/U)	3.7	146.6	NA
AID	*2.0*	*193.5*	*60*
OCS (1)	1.6	195.5	156
OCS (2)	1.9	176.2	48
TID	2.2	131.1	30

Note: A/U = Always unlocked; OCS (1) = OCS with undamped AS; OCS (2) = OCS with damped AS.

an impulsive near-field excitation while many isolated stripe-like hysteresis loops exist with the AID and OCS systems. This will be further discussed in the next section.

To effectively implement the TID algorithm, the following recommendations are given.

1. To obtain an optimal value of maximum control force u_{max}, numerical experiments needs to be done over the possible seismic events on the site of the building structure in consideration. Currently, no analytical approach is available for this because of the nonlinearity and timing sensitivity associated with the AIC algorithms. An optimal value for the harmonic excitation cases generally will not be the optimal value for random-like seismic excitations. The final optimal value will be a compromise between all control performance indices, such as peak displacement, peak absolute acceleration of the PS, attachment number, and hardware cost.

2. To achieve better control performance, an appropriate AS damping ratio value needs to be used in combination with an optimal maximum control force level in the TID system. In this section, TID systems with an AS of 15% damping ratio are considered. Note that 15% AS damping ratio is only optimal for the harmonic excitation cases and may not be optimal for seismic excitations.

The TID system is more advantageous than a purely passive system with a frictional damper. A passive frictional damping device may be modeled as an elastic spring with a stiffness k_2 placed in series with a Coulomb damper. To fully utilize the friction mechanism as an energy dissipation means, the amplitude of the PS motion must be sufficiently large to activate the Coulomb damper. However, under most seismic events which are minor to medium events, it is usually difficult to activate the hysteresis damper which is pre-set

to a high frictional force level with the purpose of dissipating more energy under major seismic events. Therefore, a compromise has to be made between the performance levels under all types of seismic events. For a TID system, this problem no longer exists, since the AS motion is usually large enough to activate the fuse device. To protect structures from near-field seismic excitations, a high maximum control force level needs to be implemented. The control philosophy for the TID algorithm is that during minor to medium seismic occurrences, the OCS algorithm will be implemented, while a more efficient TID control algorithm will be activated under large seismic events.

2.7 Numerical Study and Discussion

Two configurations of AIC systems are considered in this study, as shown in Fig. 2.10. A Type 1 Configuration AIC system consists of a PS and AS both fixed to the ground and an IE linking the PS and AS together to facilitate the interaction between them. In a Type 2 Configuration AIC system, the PS is fixed to the ground and the AS is mounted on the PS, while the IE is connecting the AS and the ground. It is thought that the Type 2 Configuration AIC system may represent much closely the situation in a realistic AIC system.

In this study, nondimensional unity mass is considered for the PS ($m_1 = 1$); the natural period and damping ratio of the PS are set to 1 second, and 2% respectively. The PS natural period ranges between 0.1 and 10 seconds when constructing response spectra. The dynamics of the AS is fully determined by the following nondimensional parameters,

$$\alpha = \frac{k_2}{k_1}, \qquad \psi = \frac{\omega_2}{\omega_1}, \qquad \gamma = \frac{\zeta_2}{\zeta_1} \tag{2.29}$$

In the present study, the values of α, ψ and γ are taken to be 2, 20 and 1 unless otherwise specified.

The value of the control-sampling period is set to 0.004 second in this study. With currently available technology, this value is believed to be achievable. However, to achieve further improved control performance, smaller control-sampling periods need to be utilized. For accuracy of numerical integration, the control-sampling period is subdivided into many integration-sampling periods. In this study, each control-sampling period is uniformly di-

vided into eight integration-sampling periods.

2.7.1 Idealized Case: Free Oscillation

Consider a PS initially at rest, released from its initial position $x_0 = 1$, and an AS at rest at its zero position at the start. The damping factor of the PS is set to zero to study the damping effect provided by the AIC algorithms. Fig. 2.11 plots the PS displacement response time history of the AIC system in free oscillation. The damping effect from the AIC algorithm is clearly observed. The PS motion is quickly damped out due to the damping from actively controlled interaction. It is seen that an AIC system with larger stiffness ratio $\alpha = 2$ has larger damping effect than one with $\alpha = 0.5$. Also observed is that both Type 1 and 2 configurations yield very similar response.

Hysteresis loops provide a good measure of energy dissipation capacity. In Fig. 2.12, hysteresis diagrams describing the relationship between the control force and PS displacement are plotted for each of the AIC algorithms. For the OCS algorithm with $\zeta_2 = 2\%$, a large control force still persists even when the PS motion has been greatly attenuated. This large control force is caused by the unattenuated motion of the AS. High-frequency lock/unlock cycles with the OCS system are observed from a great number of narrow stripes present in its hysteresis diagram. For the TID algorithm with $\zeta_2 = 15\%$ and $u_{max} = 15$ (for $\alpha = 0.5$) or 20 (for $\alpha = 2$), the problem of high-frequency lock/unlock cycles is clearly lessened.

2.7.2 Seismic Excitation

Four historical records are selected to evaluate the proposed control algorithms. They include: (1) the N-S component of El Centro (ELC) record from the 1940 Imperial Valley earthquake. (2) The N-S component of Hachinohe (HAC) from the 1968 Tokachi-oki earthquake. (3) The N-S component of Sylmar County Hospital (SCH) from the 1994 Northridge earthquake. (4) The N-S component of Kobe (KOB) from the 1995 Hyogo-ken Nanbu earthquake. Among them, ELC and HAC are far-field records, while SCH and KOB are near-field records. These earthquake records are shown in Fig. 2.13.

The various responses, including the displacement, velocity, acceleration, and attachment time history, hysteresis loops of the AID, OCS and TID systems are plotted in Figs. 2.14 to 2.41. In Tables 2.4 to 2.7, the peak and root-mean-square (RMS) values of some

Table 2.4: Acceleration, Velocity, and Displacement of the PS and AS Under ELC Ground Motion

Algorithms			Displ. (cm)		Velocity (cm/s)		Accel. (cm/s/s)	
			Peak	RMS	Peak	RMS	Peak	RMS
Uncontrolled		A/U	16.8	4.0	117.7	25.6	664.2	157.0
		A/L	*8.8*	*3.6*	*98.9*	*39.1*	*1045.0*	*425.5*
Hysteresis Damper			6.8	1.4	61.8	14.2	439.6	145.7
Type 1	AID	PS	2.2	0.5	20.6	3.7	378.5	60.1
		AS	4.2	0.7	508.0	24.9	67.0G	3.3G
	OCS	PS	1.4	0.3	12.1	2.2	308.1	62.4
		AS	3.8	0.9	468.0	52.5	61.6G	7.1G
	TID	PS	2.3	0.5	25.1	3.6	259.9	56.7
		AS	2.3	0.7	221.2	23.8	35.0G	3.4G
Type 2	AID	PS	2.2	0.5	20.2	3.7	375.6	63.0
	OCS	PS	1.4	0.3	13.5	2.2	309.2	71.0
	TID	PS	2.2	0.5	24.3	3.6	260.7	60.0

Note: A/U = IE always unlocked; A/L = IE always locked; 1G = 981.5 cm/s/s; Hysteresis Damper refers to the case in which the only difference with the TID system is that the IE is always locked.

significant response quantities are listed for both Type 1 and 2 configurations of the AIC systems.

It is observed that the response of the AIC system with Type 1 configuration is very close to that of Type 2 configuration. It is concluded that the difference in AS location between Type 1 configuration and Type 2 configuration has negligible effect on the performance of *the AIC system.*

It is seen that the displacements and velocity responses of the PS controlled by the AID, OCS and TID algorithms are greatly reduced from the uncontrolled responses. For ELC, HAC, KOB ground motions, the peak values of the controlled PS displacements are less than 20% of the corresponding uncontrolled responses with IE always unlocked. This is very encouraging for the AIC algorithms. The acceleration responses of the PS controlled by the TID algorithm are much smaller than that of the AID and OCS algorithms while maintaining a comparable displacement response. In general, the PS motion reduction capacity of the TID system is very close to that of the AID system, while the OCS system is slightly better than the TID system in terms of the PS motion reduction.

However, the TID algorithm appears more attractive in regard to the AS response. It is observed that all the response quantities of the AS in the TID system are much smaller

Table 2.5: Acceleration, Velocity, and Displacement of the PS and AS Under HAC Ground Motion

Algorithms			Displ. (cm)		Velocity (cm/s)		Accel. (cm/s/s)	
			Peak	RMS	Peak	RMS	Peak	RMS
Uncontrolled		A/U	13.0	5.2	79.4	32.9	514.6	206.7
		A/L	5.4	1.8	58.5	19.3	642.0	211.1
Hysteresis Damper			3.5	0.9	31.0	8.8	251.9	94.1
Type 1	AID	PS	2.1	0.5	16.8	2.8	294.2	46.8
		AS	2.7	0.5	329.7	18.2	43.6G	2.4G
	OCS	PS	1.2	0.3	14.2	1.7	290.1	47.2
		AS	3.1	0.7	375.6	40.2	49.6G	5.5G
	TID	PS	2.4	0.5	15.8	2.6	208.3	44.8
		AS	1.5	0.5	145.6	18.4	23.1G	2.6G
Type 2	AID	PS	2.1	0.5	16.9	2.8	297.4	48.8
	OCS	PS	1.2	0.3	12.5	1.6	278.7	53.0
	TID	PS	2.4	0.5	15.6	2.6	208.2	46.8

Note: A/U = IE always unlocked; A/L = IE always locked; 1G = 981.5 cm/s/s; Hysteresis Damper refers to the case in which the only difference with the TID system is that the IE is always locked.

Table 2.6: Acceleration, Velocity, and Displacement of the PS and AS Under SCH Ground Motion

Algorithms			Displ. (cm)		Velocity (cm/s)		Accel. (cm/s/s)	
			Peak	RMS	Peak	RMS	Peak	RMS
Uncontrolled		A/U	23.8	5.5	168.3	33.3	940.8	215.9
		A/L	12.6	4.3	151.7	47.0	1491.8	508.7
Hysteresis Damper			13.1	2.6	110.5	26.2	1096.0	280.9
Type 1	AID	PS	7.1	1.1	70.8	6.8	1076.2	109.4
		AS	11.2	1.2	1368.7	42.7	180.3G	5.6G
	OCS	PS	5.7	0.7	42.4	3.9	866.3	112.4
		AS	*10.7*	*1.6*	*1304.4*	*92.1*	*171.8G*	*12.6G*
	TID	PS	6.4	1.1	64.5	6.1	833.2	103.6
		AS	7.8	1.2	749.3	42.1	118.8G	6.0G
Type 2	AID	PS	6.9	1.1	69.6	6.7	1063.2	114.5
	OCS	PS	5.7	0.7	42.4	4.1	869.6	129.4
	TID	PS	6.3	1.0	64.6	6.1	827.1	108.4

Note: A/U = IE always unlocked; A/L = IE always locked; 1G = 981.5 cm/s/s; Hysteresis Damper refers to the case in which the only difference with the TID system is that the IE is always locked.

Table 2.7: Acceleration, Velocity, and Displacement of the PS and AS Under KOB Ground Motion

Algorithms			Displ. (cm)		Velocity (cm/s)		Accel. (cm/s/s)	
			Peak	RMS	Peak	RMS	Peak	RMS
Uncontrolled		A/U	42.7	13.9	269.4	88.3	1688.3	550.5
		A/L	17.5	4.1	202.4	44.5	2078.2	485.7
Hysteresis Damper			13.5	3.0	105.9	27.0	1025.4	292.3
Type 1	AID	PS	6.3	1.2	56.0	9.1	1080.2	151.9
		AS	11.4	1.9	1385.5	61.0	183.2G	8.0G
	OCS	PS	5.0	0.8	46.8	5.4	846.9	148.0
		AS	9.3	2.2	1133.3	132.8	149.7G	17.9G
	TID	PS	6.1	1.1	52.2	8.3	730.2	138.6
		AS	6.6	1.7	633.9	56.4	100.7G	8.0g
Type 2	AID	PS	6.3	1.2	56.0	9.4	1056.1	159.7
	OCS	PS	5.0	0.8	45.5	5.5	849.5	171.5
	TID	PS	6.1	1.1	52.1	8.3	739.7	144.6

Note: A/U = IE always unlocked; A/L = IE always locked; 1G = 981.5 cm/s/s; Hysteresis Damper refers to the case in which the only difference with the TID system is that the IE is always locked.

than those of the AID and OCS systems. This favorable AS performance of the TID system may extend the life-time of the AS and reduce the repair cost and prevent disturbance to building functions after a major earthquake occurs.

Figs. 2.19, 2.26, 2.33, and 2.40 show the attachment time histories of the AIC systems under ELC, HAC, SCH, and KOB ground motions respectively. Table 2.8 lists the number of attachments between the PS and AS in the entire duration (30 seconds) of the input ground motions. It is observed that the attachment number in the TID system is much smaller than that of the OCS system. In practice, it is likely that short-duration attachment cycles may not be executed because of the limitation of mechanical devices. For the OCS system, such short-duration attachment cycles account for a large portion of attachment cycles and this is reflected by many narrow-striped hysteresis loops in its hysteresis diagram. For the TID system, however, narrow-striped hysteresis loops only account for a limited portion of total dissipated energy because of its bounded control force. Therefore, more robust performance is expected for the TID system in real practice.

Control force vs. PS displacement are shown in Figs. 2.20, 2.27, 2.34, and 2.41 for the AID, OCS and TID systems under ELC, HAC, SCH and KOB ground motions respectively. It is seen that for the AID sytem, the hysteresis loops are comprised of many triangular

Table 2.8: Number of Attachments Between the PS and AS in the Entire 30-second Duration of Input Ground Motion ELC, HAC, SCH, and KOB for the AID, OCS and TID Algorithms

Algorithms		Earthquake Record			
		ELC	HAC	SCH	KOB
Type 1	AID	191	192	210	192
	OCS	283	261	285	270
	TID	195	177	195	185
Type 2	AID	188	193	204	194
	OCS	264	256	276	272
	TID	190	180	195	184

shapes, while many narrow-striped shapes form the hysteresis loops of the OCS system and more favorable continuous trapezoidal shapes occur in the hysteresis loops of the TID system.

2.8 Effects of Sampling Period and Time Delay

Since the first introduction of active and semi-active control in civil structures, intensive research efforts have been made in the area of theoretical study or numerical simulation while little experimental work has been carried out. However, these experiments did shed some light on the importance of some practical aspects of structural control techniques. Among the constraints which are expected to have a significant impact on control effectiveness, two important practical issues, sampling period and time delay, are examined herein.

2.8.1 Control-Sampling Period

The control-sampling period is defined as the uniform elapsed time between discrete time instants at which control decisions are made. The length of the control-sampling period directly affects the control performance of the AIC systems. Clearly, if the control-sampling period is set too long, the original instantaneous optimal condition may not be optimal any more during the following sampling period and the performance of the control system may thus degrade. In the meanwhile, an over-refined sampling period will impose infeasible requirements on costly information processing equipment and will not improve control performance due to mechanical limitations of the control devices. Therefore, a practical value of control-sampling period needs to be determined by addressing all of these concerns.

Figs. 2.42 to 2.45 plot the displacement time histories of the PS controlled by the AID, OCS and TID algorithms under ELC, HAC, SCH and KOB ground motions respectively. Figs. 2.46 to 2.49 show the response spectra of the AIC systems under ELC, HAC, SCH and KOB ground motions respectively. It is seen that the AID system is much less sensitive to the sampling period changes than the OCS system. For the OCS system, reducing the sampling period doesn't guarantee a decreasing trend in the response spectra. This observation further verifies the high sensitivity to the timing in the OCS system. For the TID system, a decreasing trend is observed in the response spectra as the control sampling period decreases. Again, the response spectra verify that the TID system is more robust to the sampling period than the OCS system. For the TID system, dt = 0.001 second gives a response spectrum close to that of dt = 0.005 second.

2.8.2 Time Delay

Presence of time delays in the AIC system can arise from data acquisition and decision processes, and mechanical limitations of the IE (e.g., the transition from one operating state to the other is not instantaneous).

In this study, time delay is defined to be a constant time interval between time instants when the control decision is made and the IE achieves the desired control state. For simplicity, the length of time delay is assumed to be a multiple of the control-sampling period.

It is important to note that presence of time delay will not pose a stability problem to the AIC systems because the energy input to the overall system is bounded. Because of the high AS natural frequency, the AS response if uninteracted with the PS is generally very small since its frequency does not fall within the predominant frequency range of most seismic excitations. Although in a delayed time instant, because of the presence of time delay, vibrational energy will flow from the AS into the PS instead of in the favorable opposite direction (namely, vibrational energy is transmitted from the PS to the AS), the PS response is bounded because the overall input energy is bounded.

The effect of time delay on the performance of the AIC systems is investigated by computing the displacement and response spectra of the PS subjected to various values of time delay. These results are shown in Figs. 2.50 to 2.57.

From these figures, it is seen that the system performance gradually deteriorates as time

delay increases. As concluded above, instability in the AIC systems is not observed in the presence of selected time delay values. It is noticed that the performance of AIC systems with a large time delay value (0.2 second) is still better than that of the uncontrolled systems. Also observed is that the OCS algorithm is slightly more sensitive to the time delay than the AID and TID algorithms. For the AID and OCS system, a mixed trend in response spectra is observed as time delay increases, that is, the increase of time delay may increase the response spectra in some frequency range while reducing the response spectra in other frequency range. In the TID system, a clear trend of increase is observed with increasing time delay values.

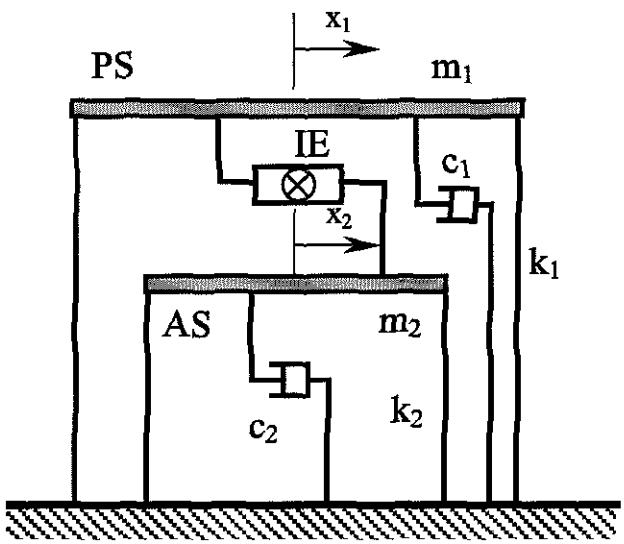

Figure 2.1: Schematic of an AIC System Model

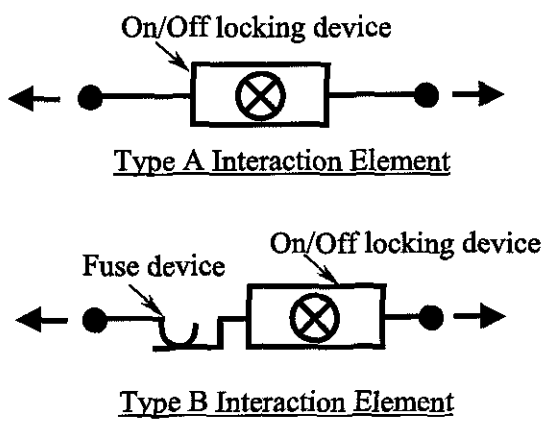

Figure 2.2: Schematic of Interaction Elements

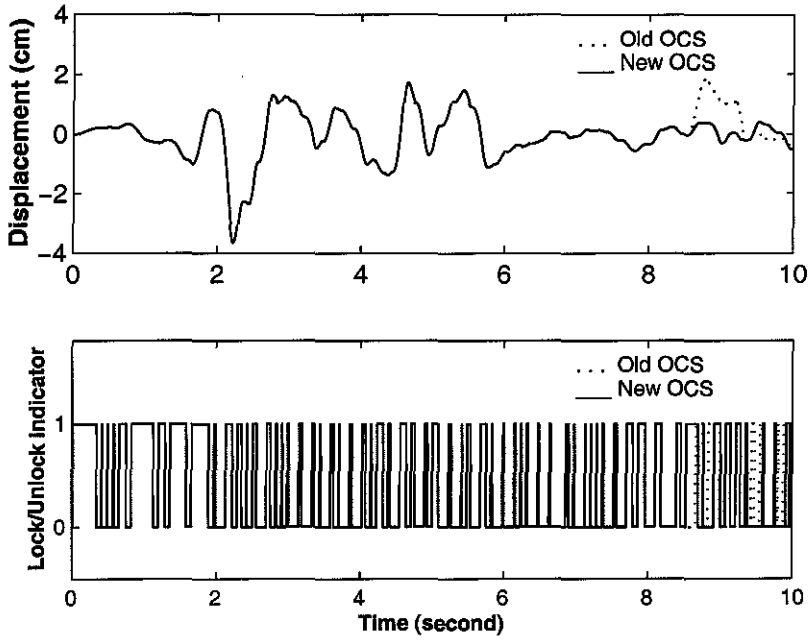

Figure 2.3: Response Time Histories of the PS Controlled by the Two OCS Algorithms Under ELC Ground Motion

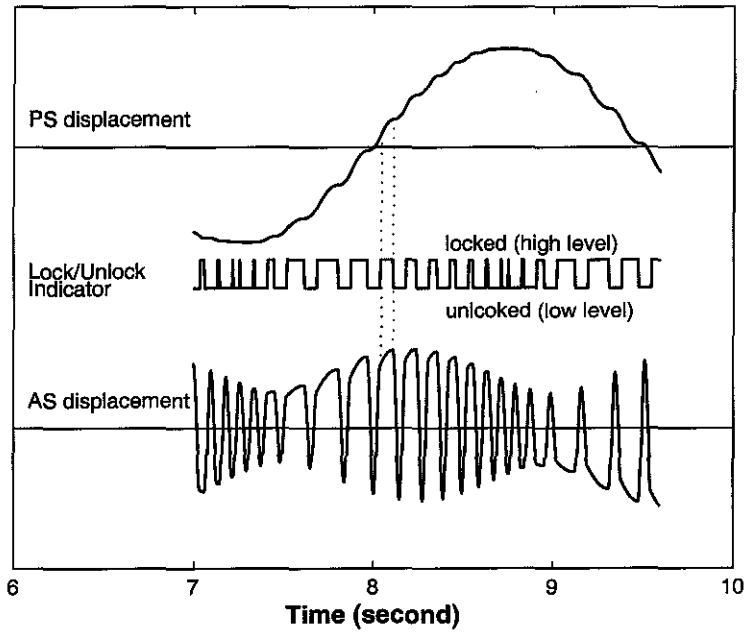

Figure 2.4: Response Time Histories of the PS and AS Controlled by the OCS Algorithm Under Harmonic Excitation

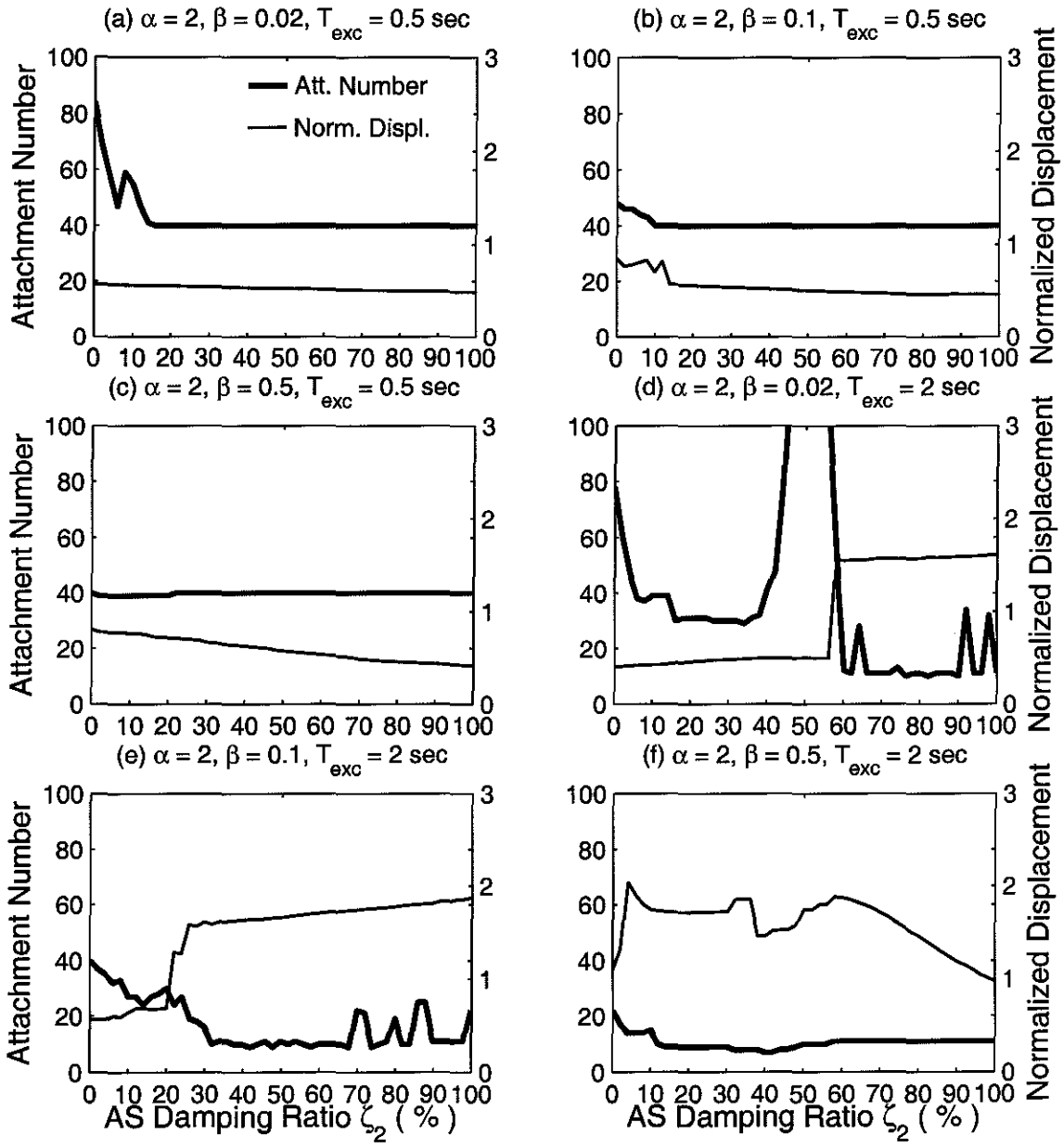

Figure 2.5: Attachment Number and Normalized Displacement vs. AS Damping Ratio of the OCS System Under Harmonic Excitation (thick line = Attachment Number, thin line = Normalized Displacement Response of the PS, α = Stiffness Ratio, β = Mass Ratio, T_{exc} = Forcing Frequency)

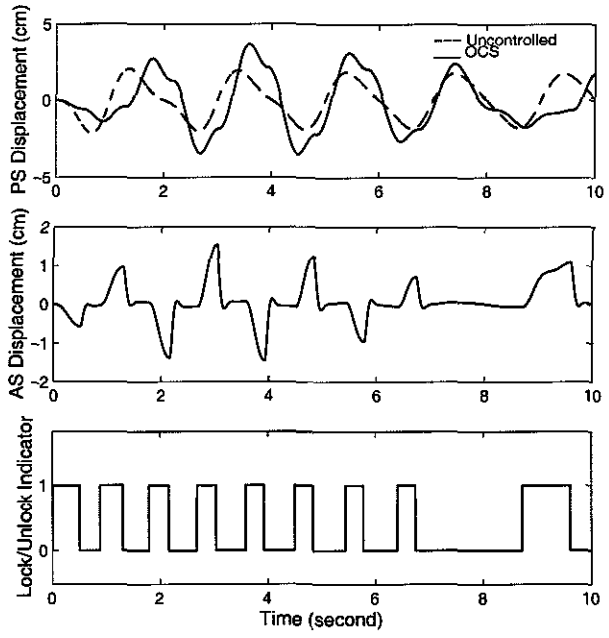

Figure 2.6: Response Time History of a Harmonically Excited OCS System with AS Parameters: $\zeta_2 = 60\%$, $\beta = m_2/m_1 = 0.1$

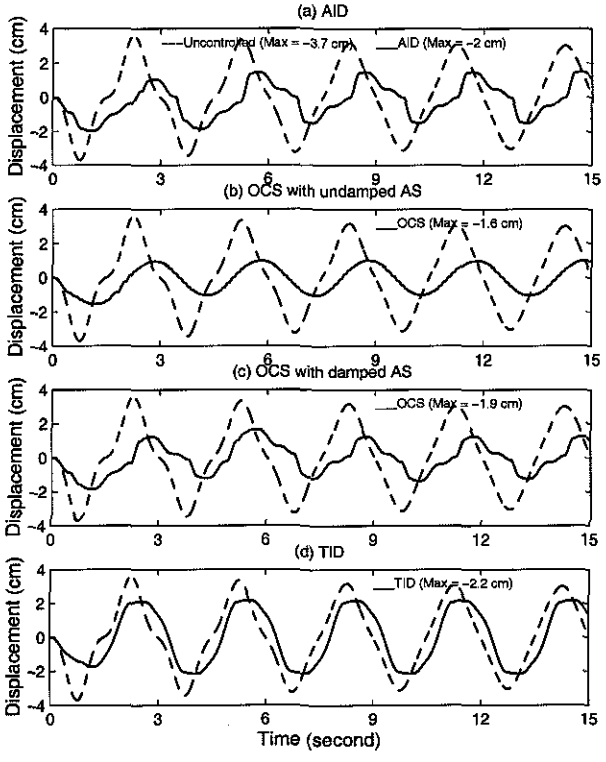

Figure 2.7: Response Time History of the AID, OCS with Undamped AS, OCS with Damped AS, and TID Systems Under Harmonic Excitation

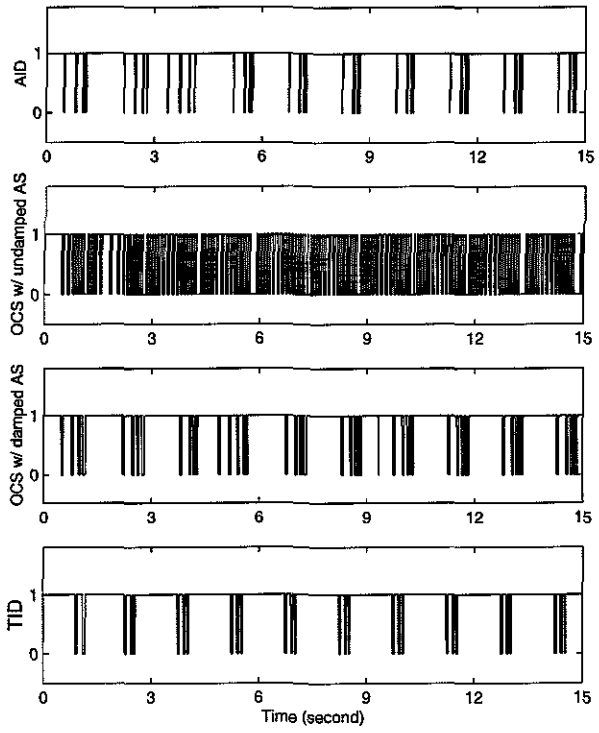

Figure 2.8: Attachment Number Time History of the *AID*, *OCS* with *Undamped AS*, *OCS* with Damped AS, and TID Systems Under Harmonic Excitation

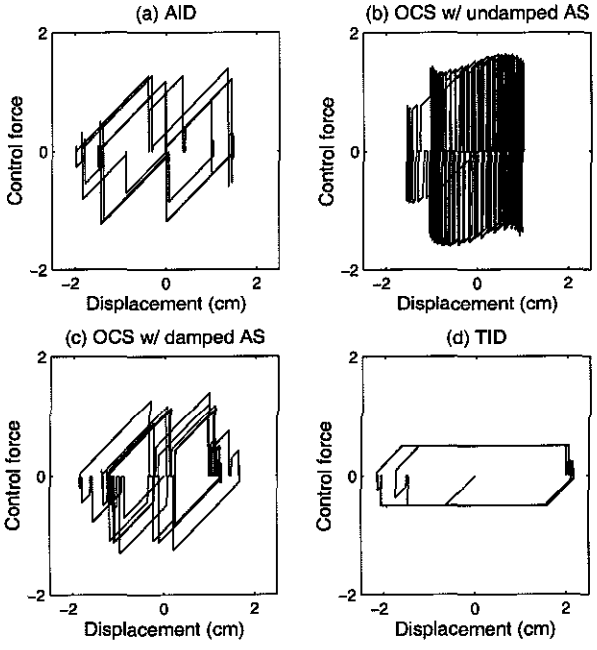

Figure 2.9: Hysteresis Diagrams of the AID, OCS with Undamped AS, OCS with Damped AS, and TID Systems Under Harmonic Excitation

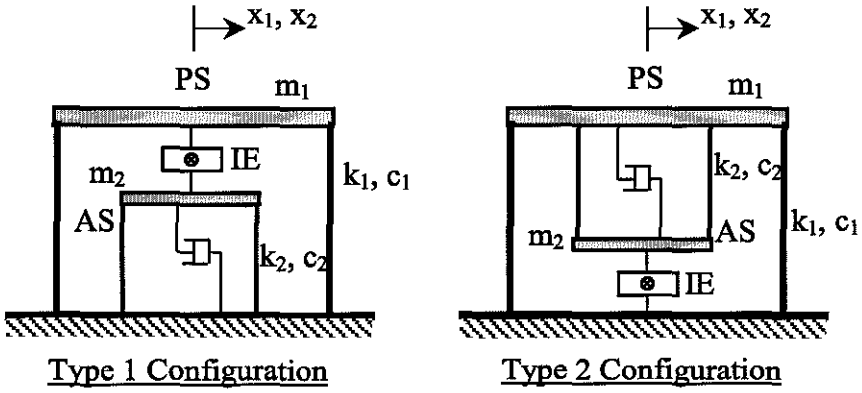

Figure 2.10: Schematic of Two Configurations of AIC Systems

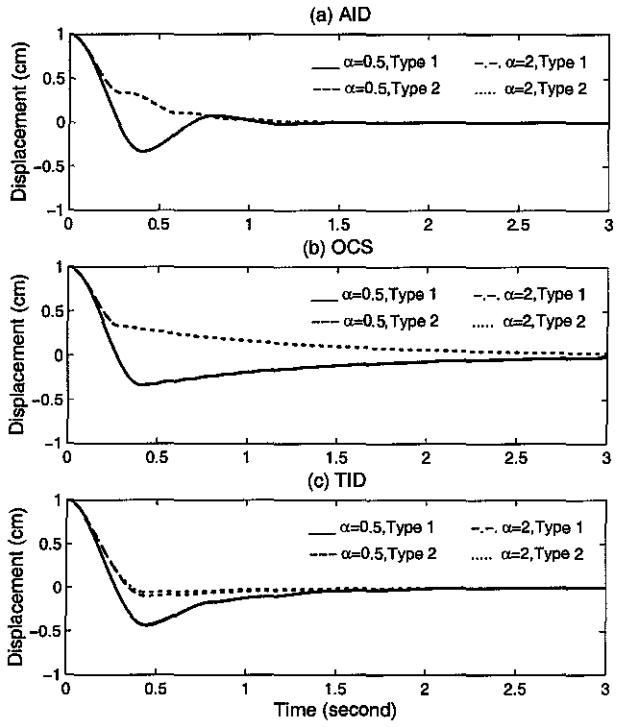

Figure 2.11: Displacement Time History of AIC System in Free Vibration

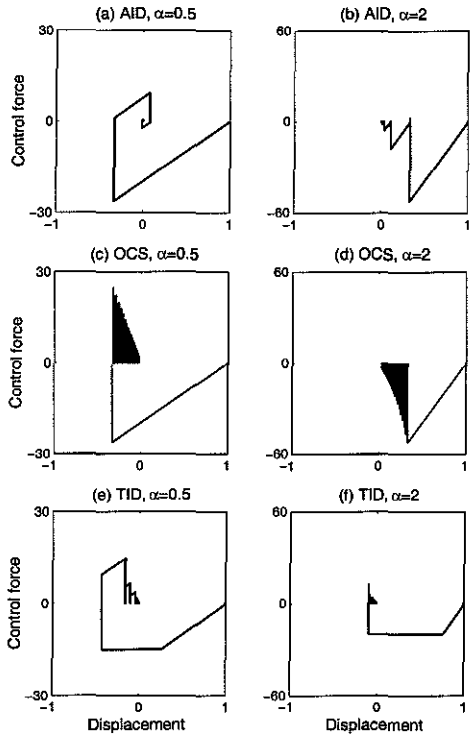

Figure 2.12: Hysteresis Diagram of AIC System in Free Vibration, Type 1 Configuration

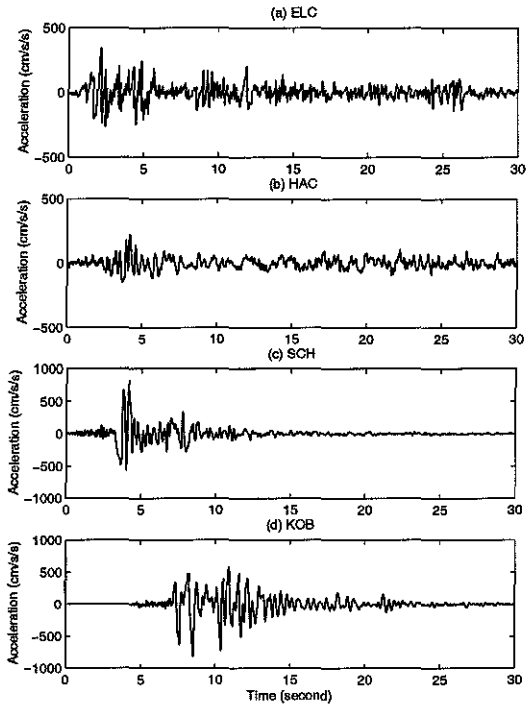

Figure 2.13: Accelerograms of Four Historical Earthquakes: (a) El Centro (b) Hachinohe (c) Northridge (d) Kobe

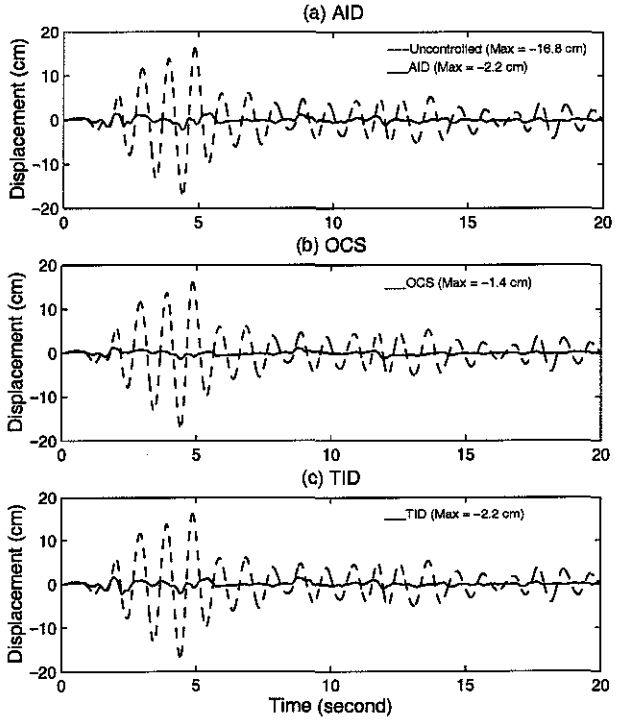

Figure 2.14: Displacement Time Histories of the Controlled PS Excited by the ELC Ground Motion, Type 1 Configuration

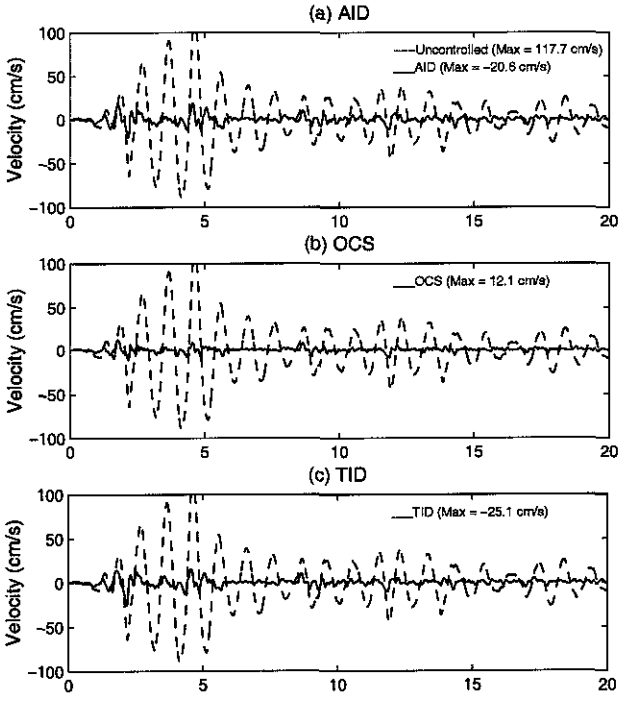

Figure 2.15: Velocity Time Histories of the Controlled PS Excited by the ELC Ground Motion, Type 1 Configuration

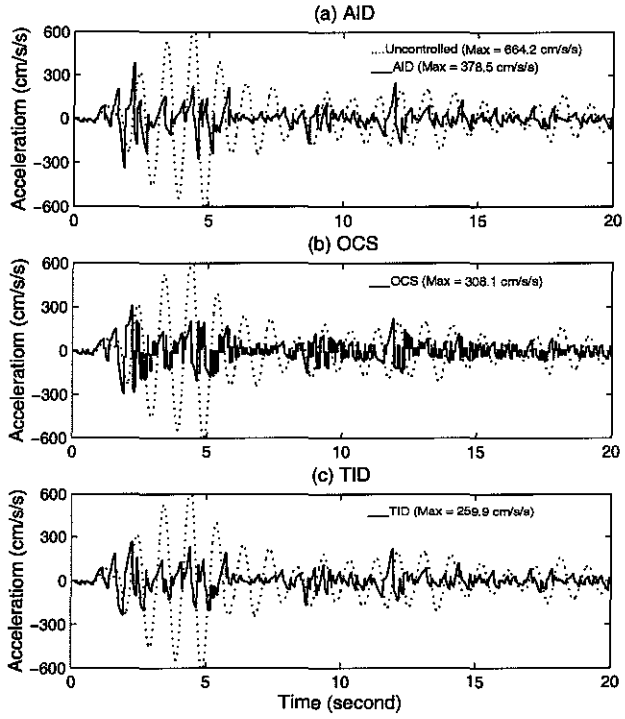

Figure 2.16: Acceleration Time Histories of the Controlled PS Excited by the ELC Ground Motion, Type 1 Configuration

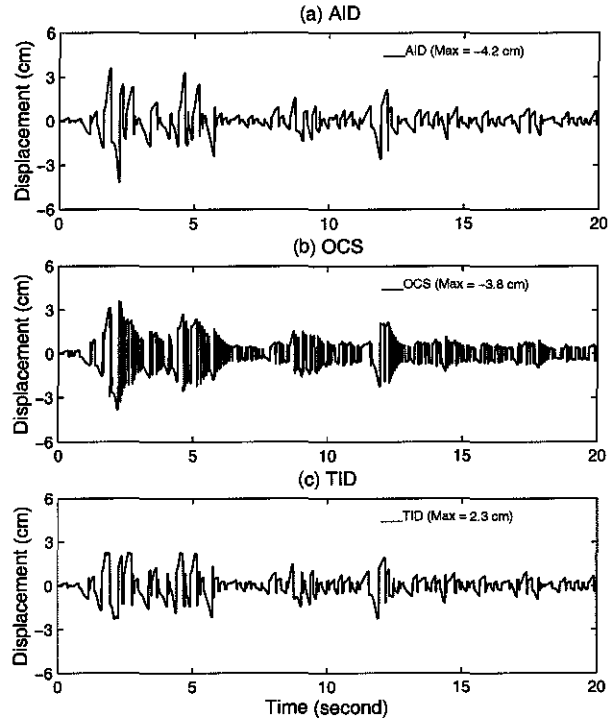

Figure 2.17: Displacement Time Histories of the AS Excited by the ELC Ground Motion, Type 1 Configuration

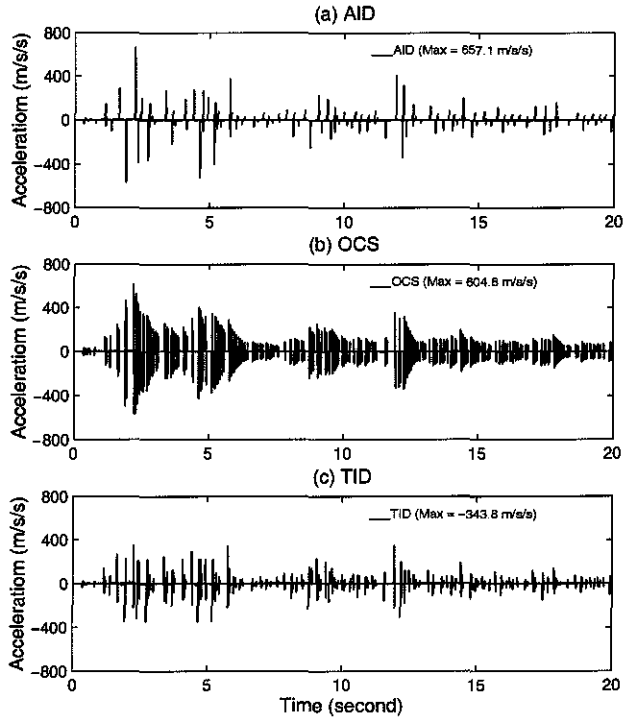

Figure 2.18: Acceleration Time Histories of the AS Excited by the ELC Ground Motion, Type 1 Configuration

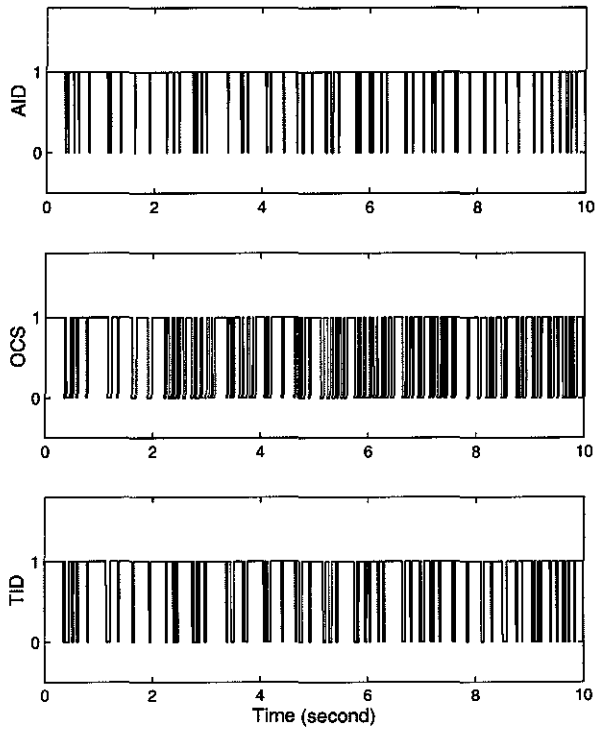

Figure 2.19: Attachment Time Histories of the AID, OCS, and TID Systems Excited by the ELC Ground Motion, Type 1 Configuration

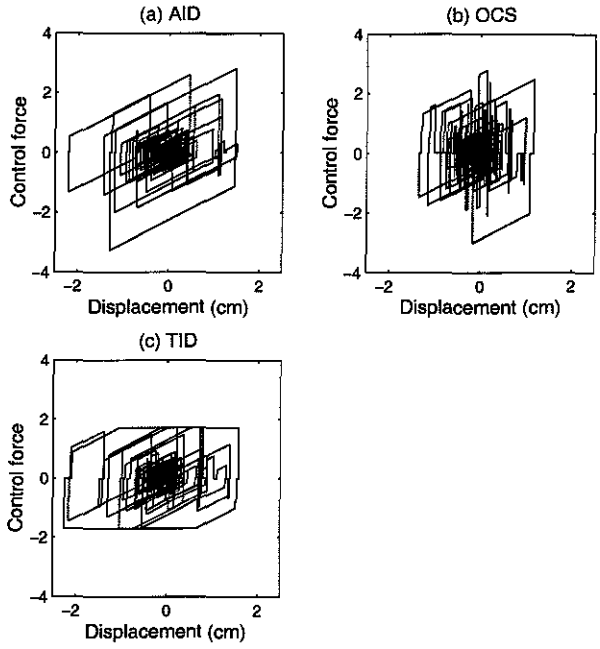

Figure 2.20: Hysteresis Diagram of the AID, OCS, and TID Systems Excited by the ELC Ground Motion, Type 1 Configuration

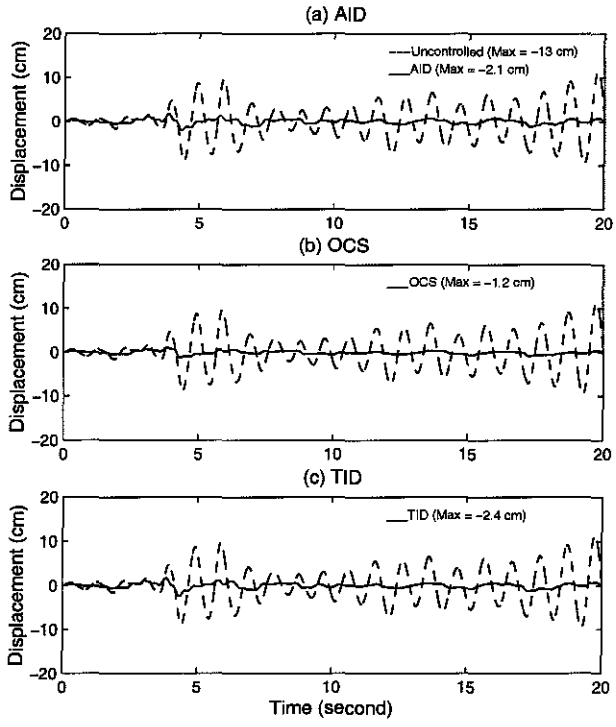

Figure 2.21: Displacement Time Histories of the PS Controlled by the AID, OCS, and TID Algorithms Excited by the HAC Ground Motion, Type 1 Configuration

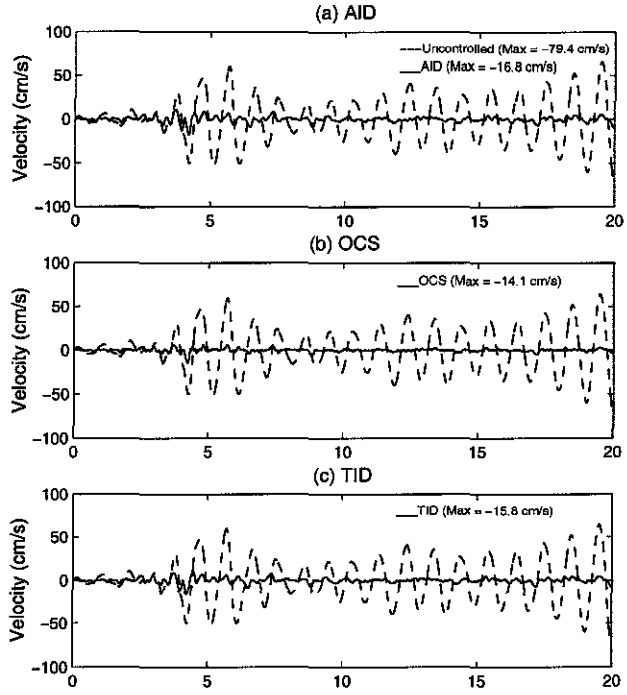

Figure 2.22: Velocity Time Histories of the PS Controlled by the AID, OCS, and TID Algorithms Excited by the HAC Ground Motion, Type 1 Configuration

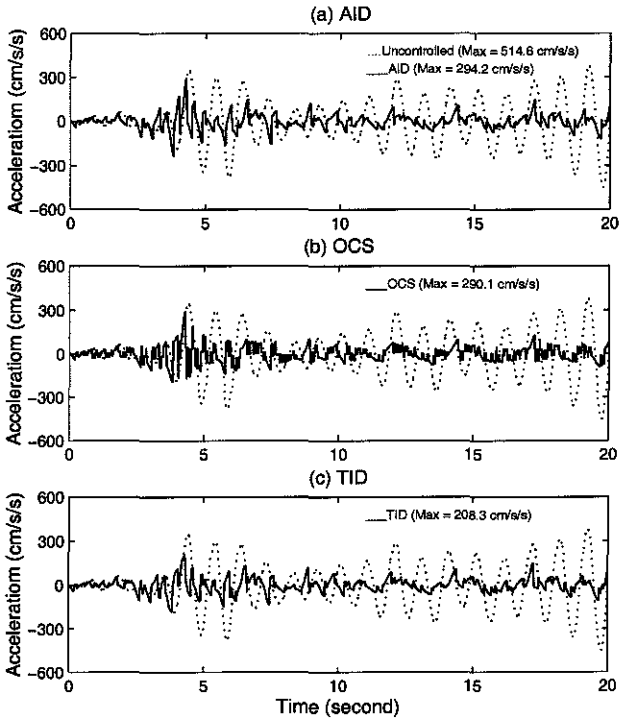

Figure 2.23: Acceleration Time Histories of the PS Controlled by the AID, OCS, and TID Algorithms Excited by the HAC Ground Motion, Type 1 Configuration

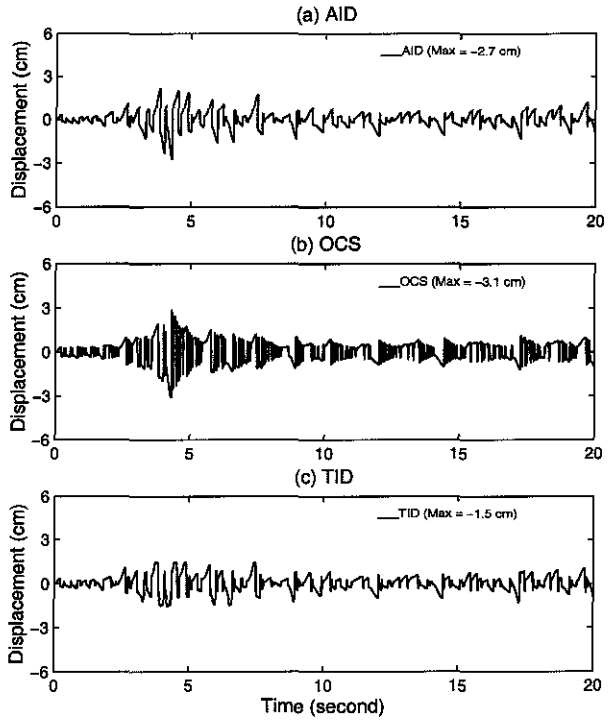

Figure 2.24: Displacement Time Histories of the AS Controlled by the AID, OCS, and TID Algorithms Excited by the HAC Ground Motion, Type 1 Configuration

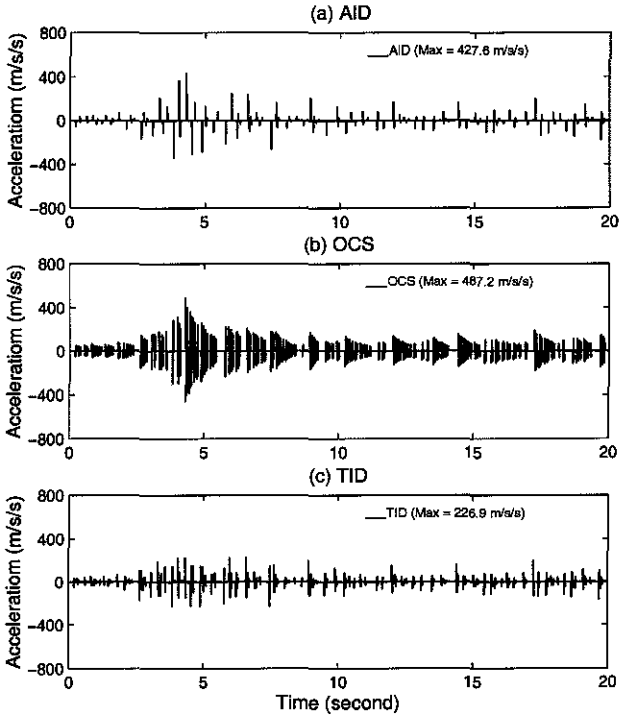

Figure 2.25: Acceleration Time Histories of the AS in the AID, OCS, and TID Systems Excited by the HAC Ground Motion, Type 1 Configuration

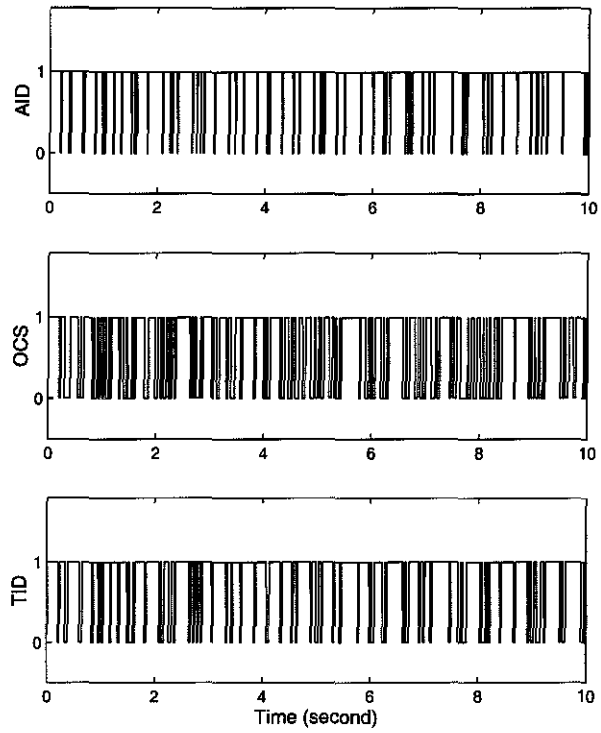

Figure 2.26: Attachment Time Histories of the AID, OCS, and TID Systems Excited by the HAC Ground Motion, Type 1 Configuration

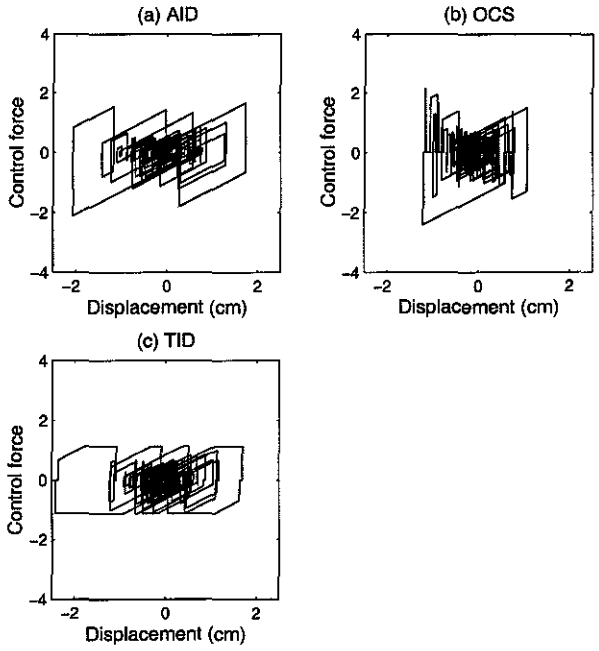

Figure 2.27: Hysteresis Diagram (Control Force vs. PS Displacement) of the AID, OCS, and TID Systems Excited by the HAC Ground Motion, Type 1 Configuration

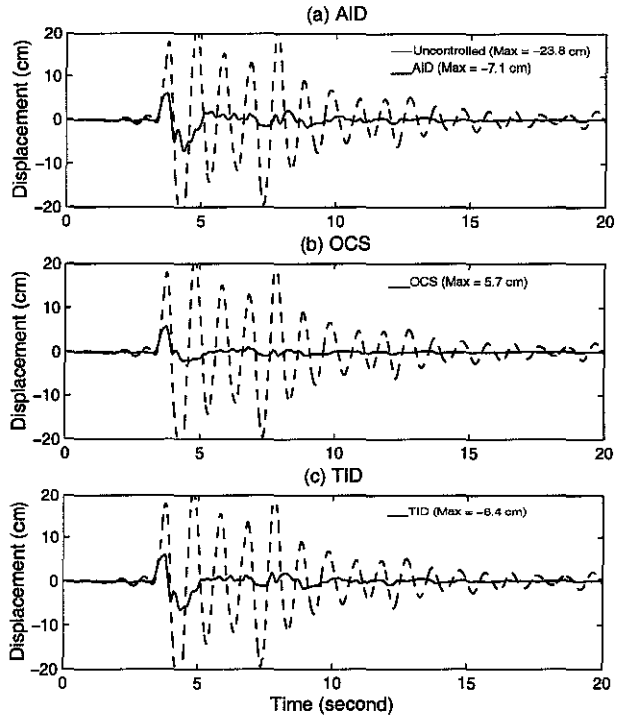

Figure 2.28: Displacement Time Histories of the PS Controlled by the AID, OCS, and TID Algorithms Excited by the SCH Ground Motion, Type 1 Configuration

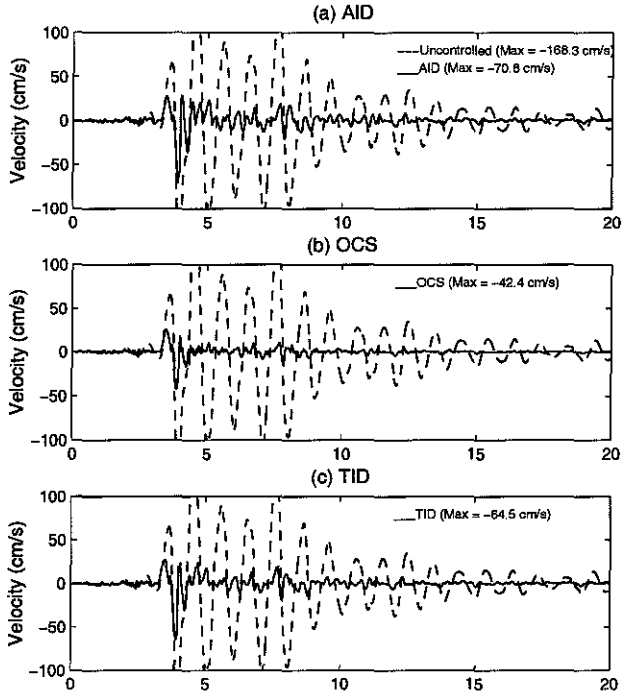

Figure 2.29: Velocity Time Histories of the PS Controlled by the AID, OCS, and TID Algorithms Excited by the SCH Ground Motion, Type 1 Configuration

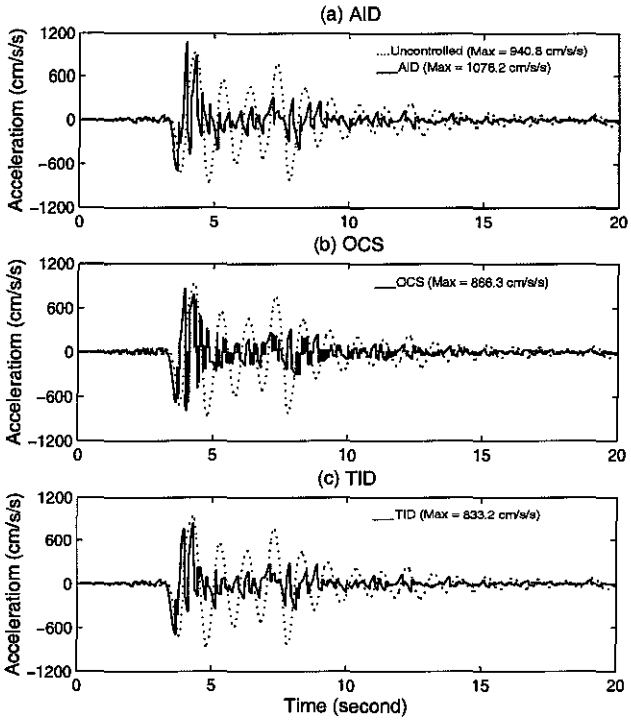

Figure 2.30: Acceleration Time Histories of the PS Controlled by the AID, OCS, and TID Algorithms Excited by the SCH Ground Motion, Type 1 Configuration

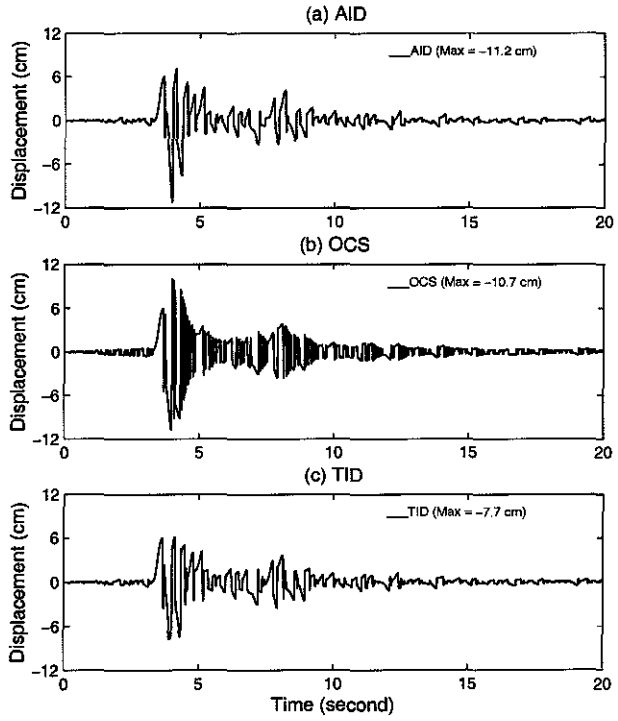

Figure 2.31: Displacement Time Histories of the AS Controlled by the AID, OCS, and TID Algorithms Excited by the SCH Ground Motion, Type 1 Configuration

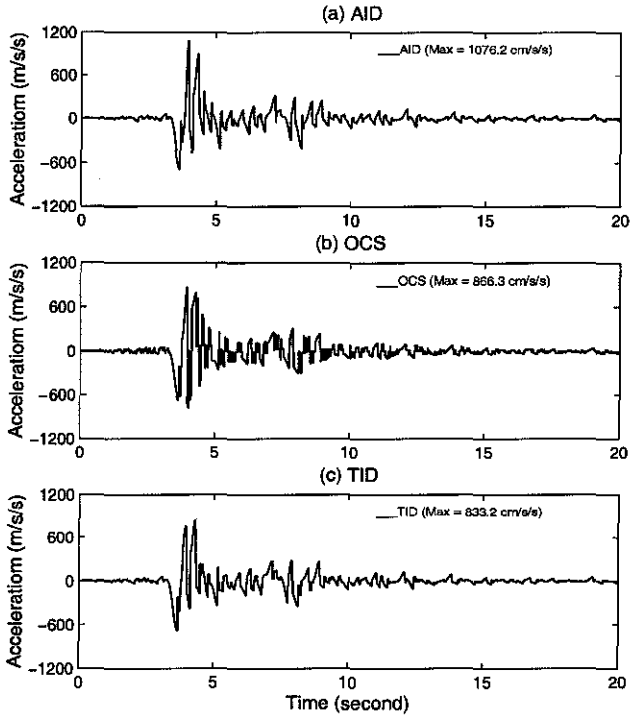

Figure 2.32: Acceleration Time Histories of the AS in the AID, OCS, and TID Systems Excited by the SCH Ground Motion, Type 1 Configuration

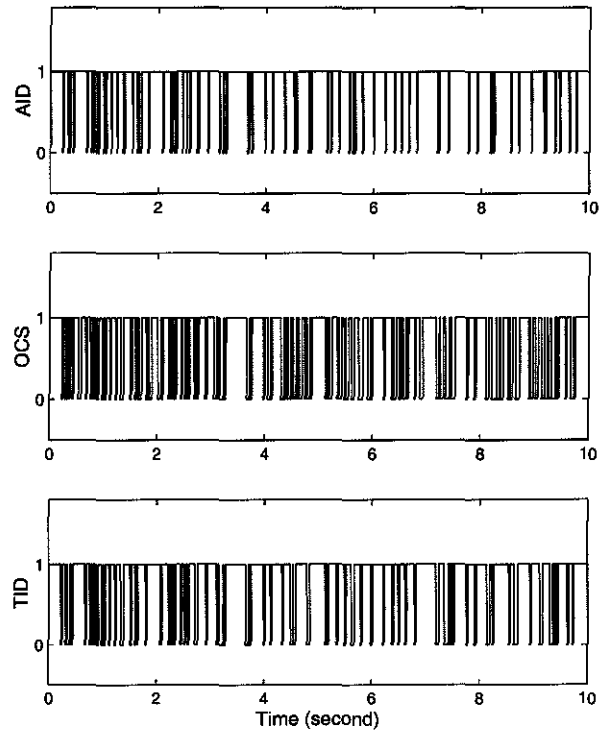

Figure 2.33: Attachment Time Histories of the AID, OCS, and TID Systems Excited by the SCH Ground Motion, Type 1 Configuration

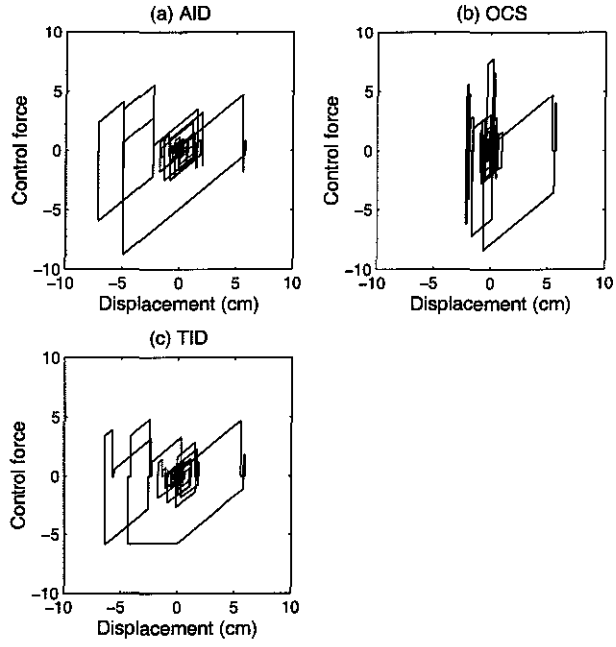

Figure 2.34: Hysteresis Diagram (Control Force vs. PS Displacement) of the AID, OCS, and TID Systems Excited by the SCH Ground Motion, Type 1 Configuration

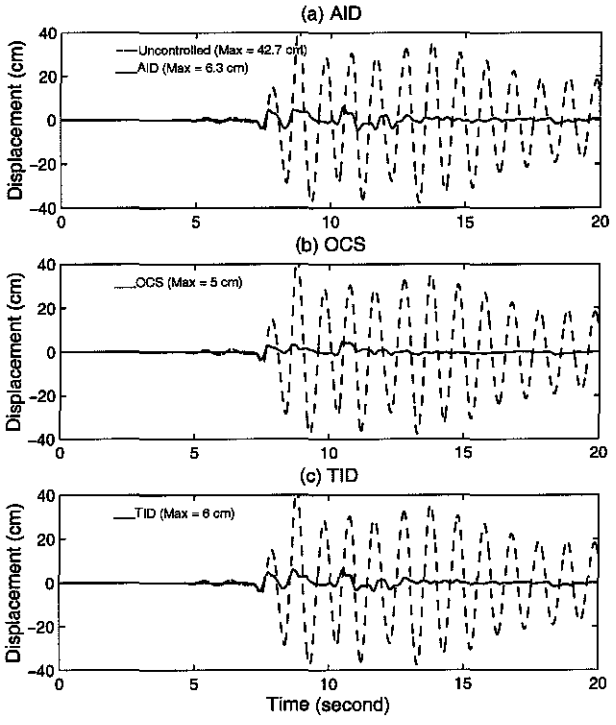

Figure 2.35: Displacement Time Histories of the PS Controlled by the AID, OCS, and TID Algorithms Excited by the KOB Ground Motion, Type 1 Configuration

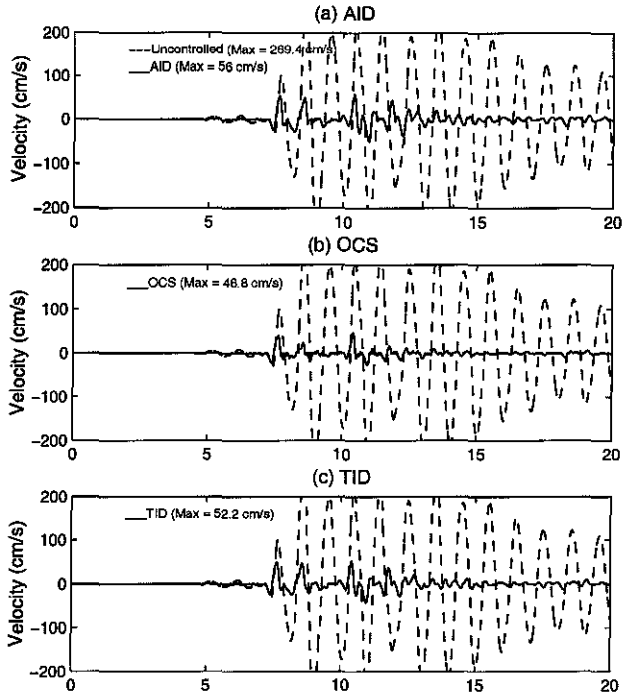

Figure 2.36: Velocity Time Histories of the PS Controlled by the AID, OCS, and TID Algorithms Excited by the KOB Ground Motion, Type 1 Configuration

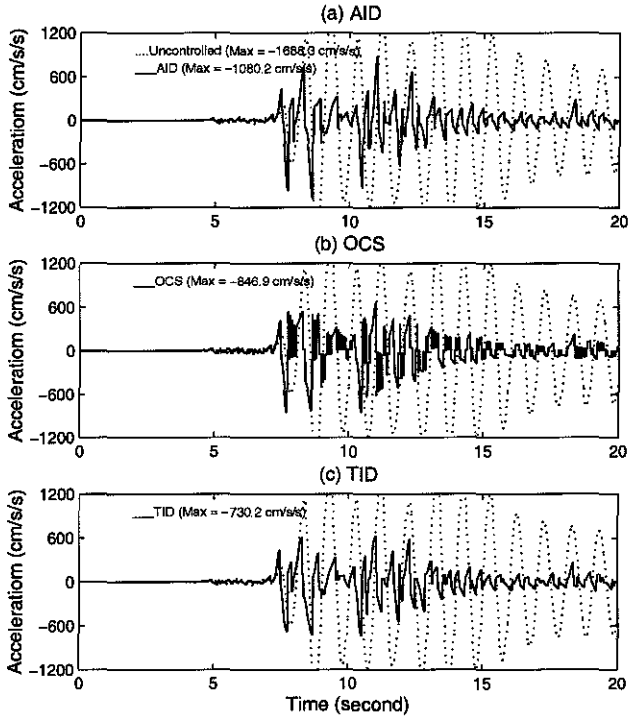

Figure 2.37: Acceleration Time Histories of the PS Controlled by the AID, OCS, and TID Algorithms Excited by the KOB Ground Motion, Type 1 Configuration

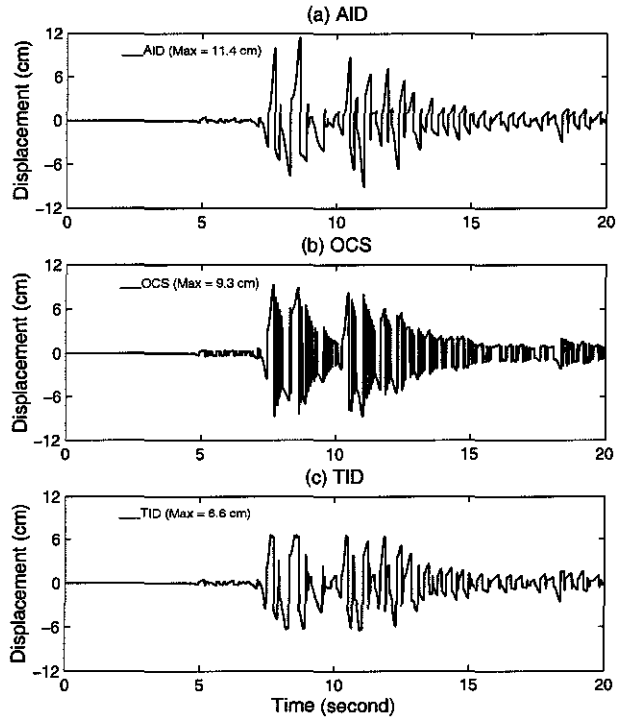

Figure 2.38: Displacement Time Histories of the AS Controlled by the AID, OCS, and TID Algorithms Excited by the KOB Ground Motion, Type 1 Configuration

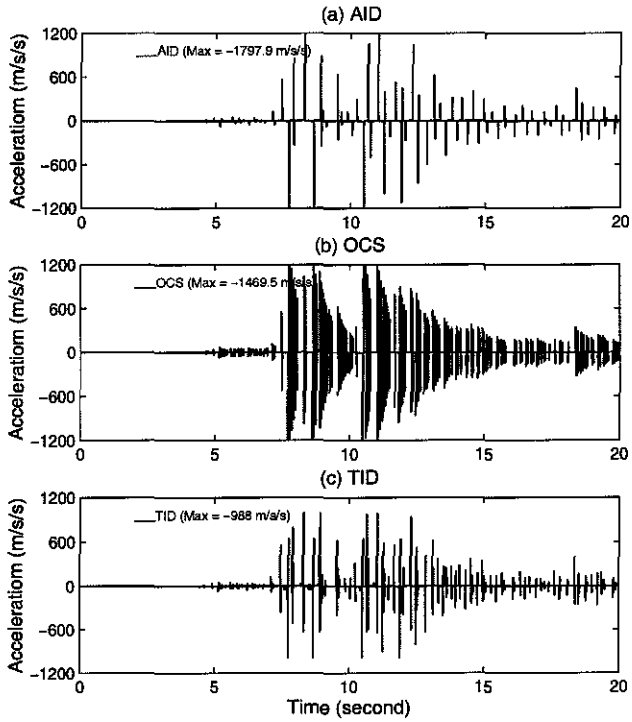

Figure 2.39: Acceleration Time Histories of the AS in the AID, OCS, and TID Systems Excited by the KOB Ground Motion, Type 1 Configuration

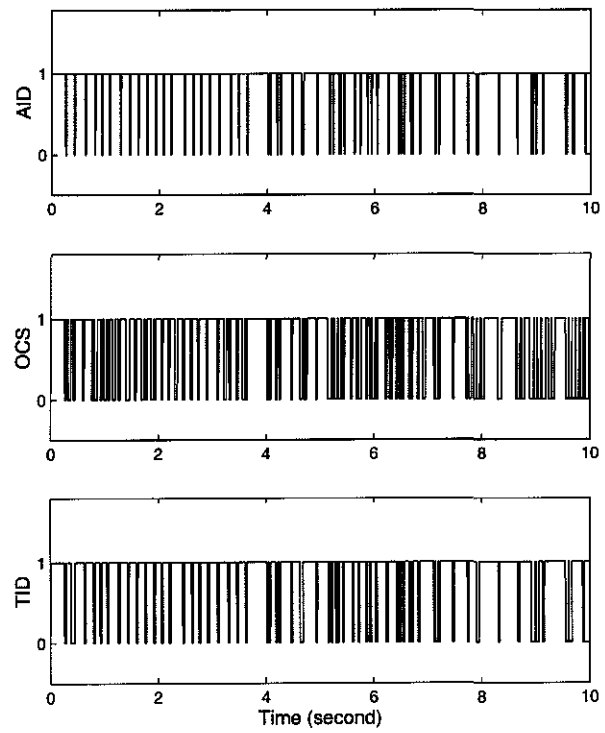

Figure 2.40: Attachment Time Histories of the AID, OCS, and TID Systems Excited by the KOB Ground Motion, Type 1 Configuration

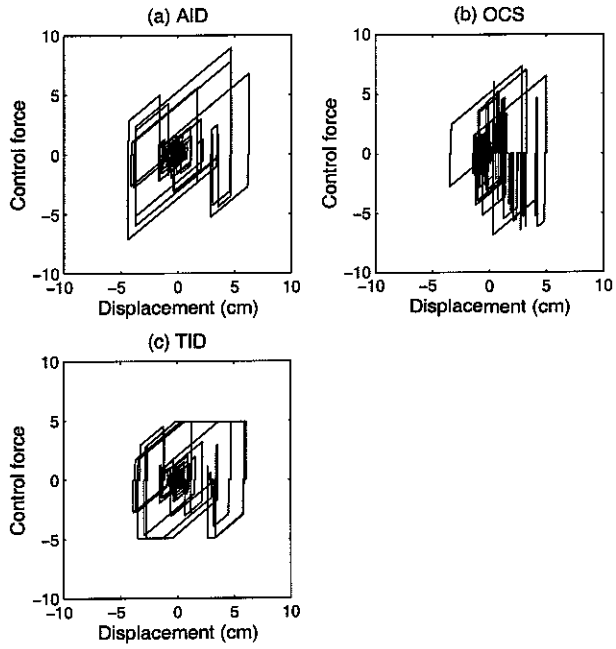

Figure 2.41: Hysteresis Diagram (Control Force vs. PS Displacement) of the AID, OCS, and TID Systems Excited by the KOB Ground Motion, Type 1 Configuration

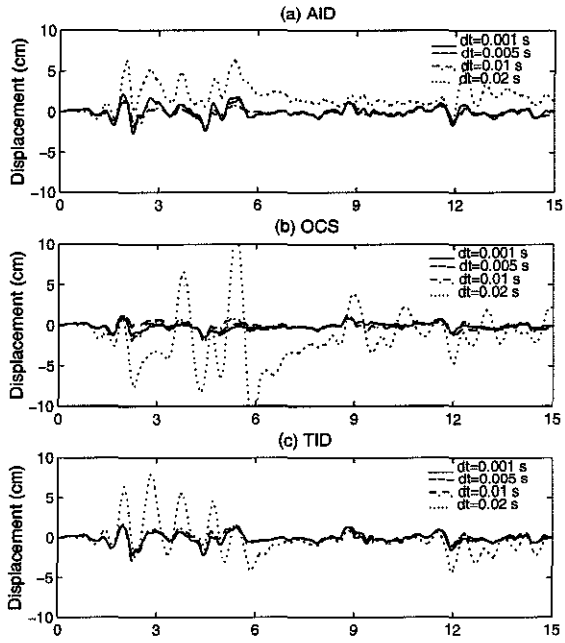

Figure 2.42: Effect of Control-Sampling Period – Displacement Time Histories of the PS Controlled by the AIC Algorithms Under the ELC Ground Motion, Type 1 Configuration

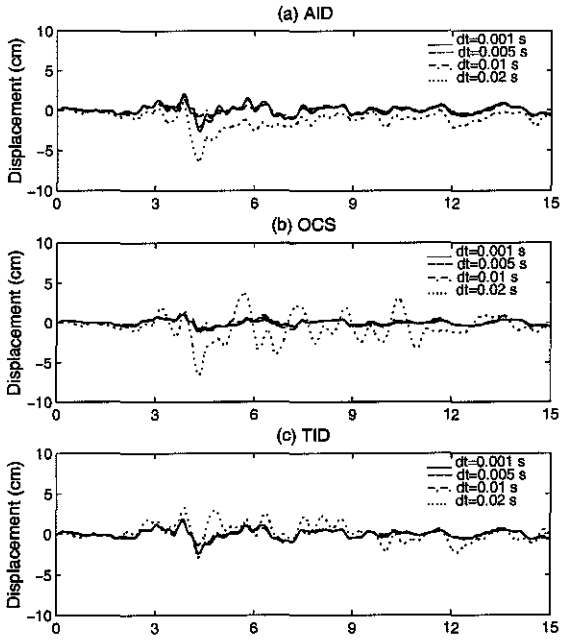

Figure 2.43: Effect of Control-Sampling Period – Displacement Time Histories of the PS Controlled by the AIC Algorithms Under the HAC Ground Motion, Type 1 Configuration

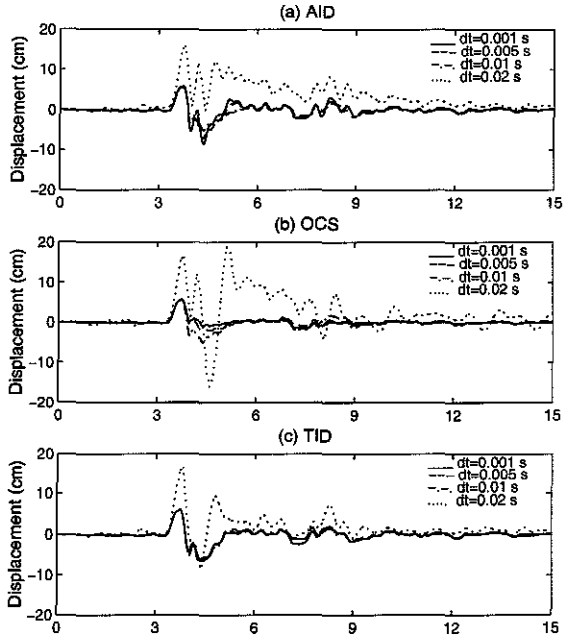

Figure 2.44: Effect of Control-Sampling Period – Displacement Time Histories of the PS Controlled by the AIC Algorithms Under the SCH Ground Motion, Type 1 Configuration

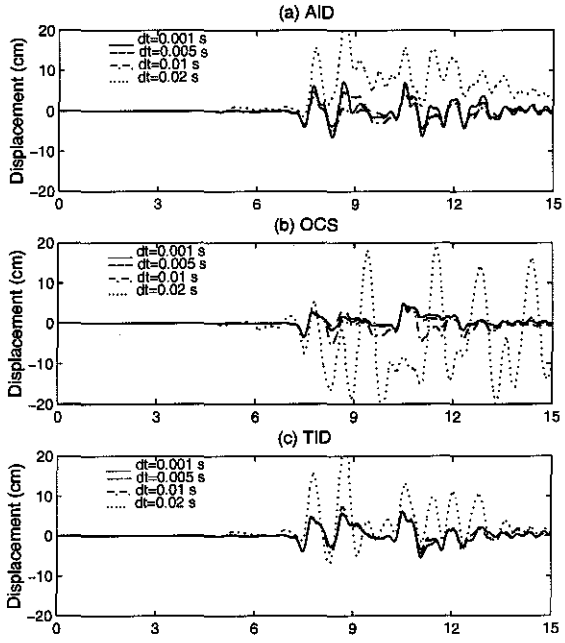

Figure 2.45: Effect of Control-Sampling Period – Displacement Time Histories of the PS Controlled by the AIC Algorithms Under the KOB Ground Motion, Type 1 Configuration

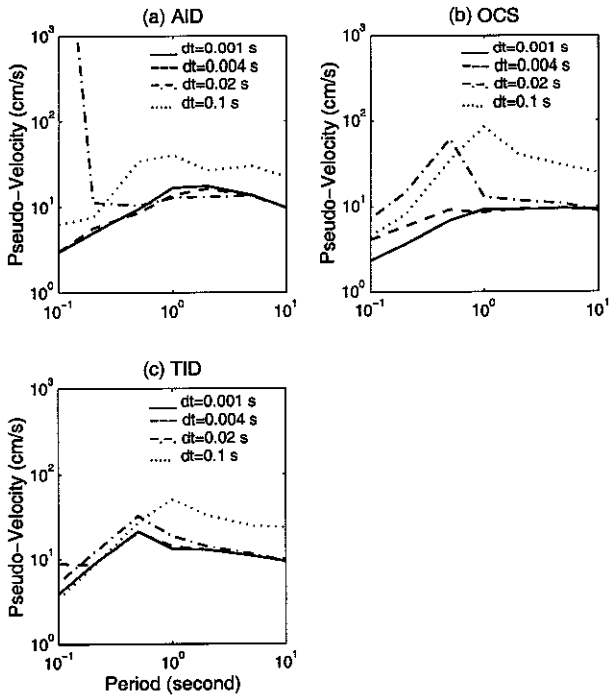

Figure 2.46: Effect of Control-Sampling Period – Response Spectra of the PS Controlled by the AIC Algorithms Under the ELC Ground Motion, Type 1 Configuration

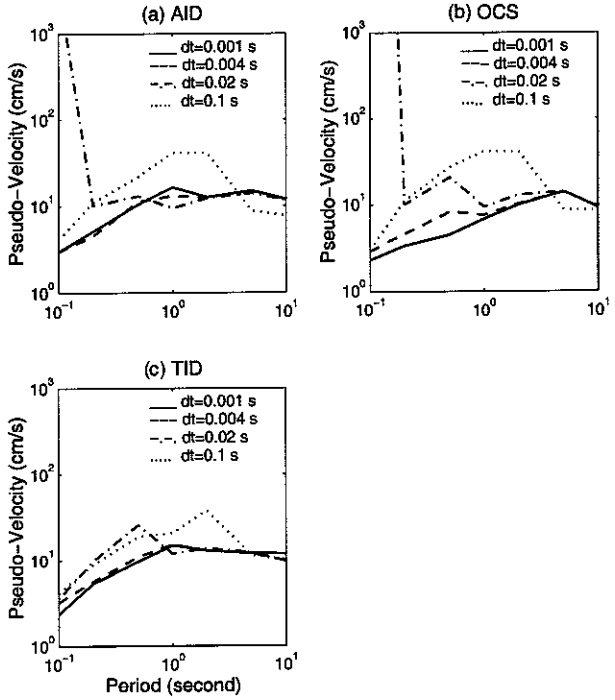

Figure 2.47: Effect of Control-Sampling Period – Response Spectra of the PS Controlled by the AIC Algorithms Under the HAC Ground Motion, Type 1 Configuration

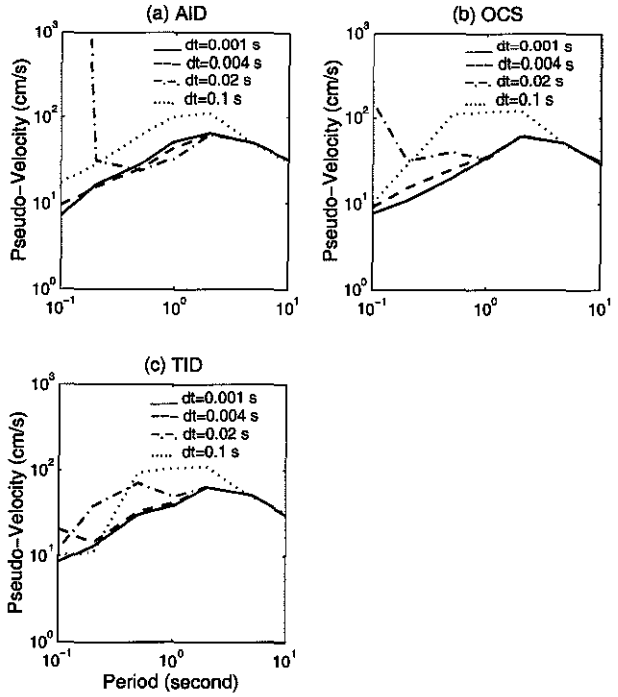

Figure 2.48: Effect of Control-Sampling Period – Response Spectra of the PS Controlled by the AIC Algorithms Under the SCH Ground Motion, Type 1 Configuration

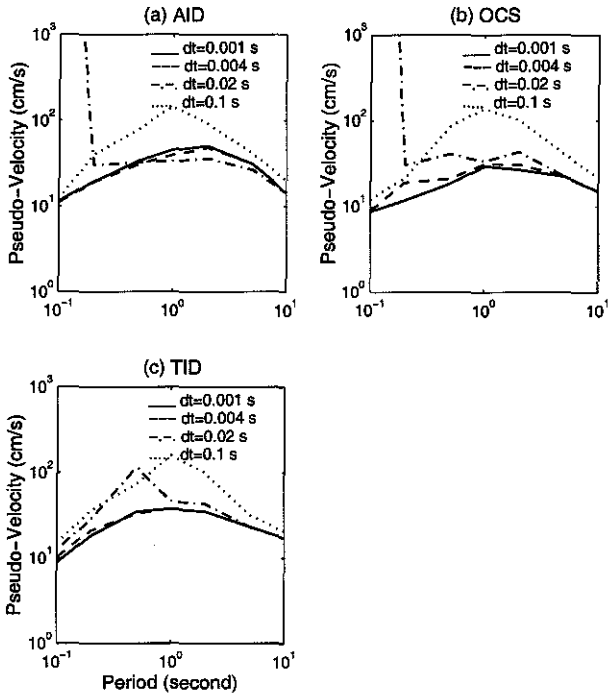

Figure 2.49: Effect of Control-Sampling Period – Response Spectra of the PS Controlled by the AIC Algorithms Under the KOB Ground Motion, Type 1 Configuration

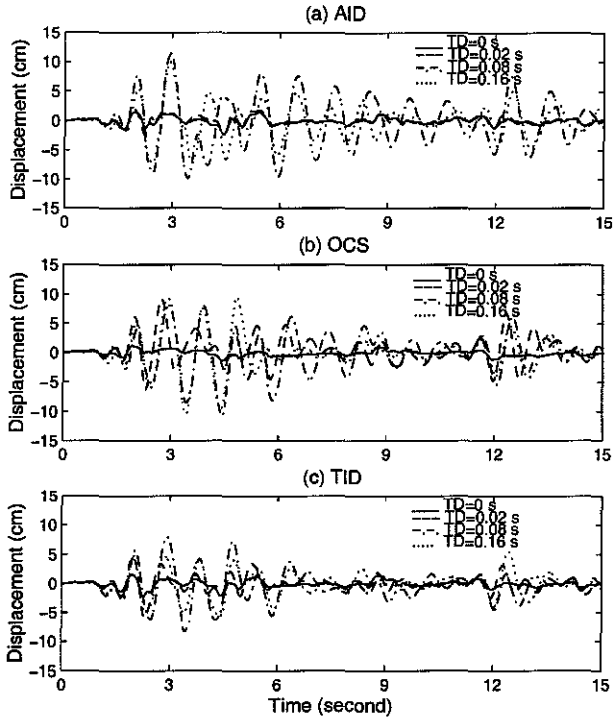

Figure 2.50: Effect of Time Delay – Displacement Time Histories of the PS Controlled by the AIC Algorithms Under the ELC Ground Motion (TD = Time Delay), Type 1 Configuration

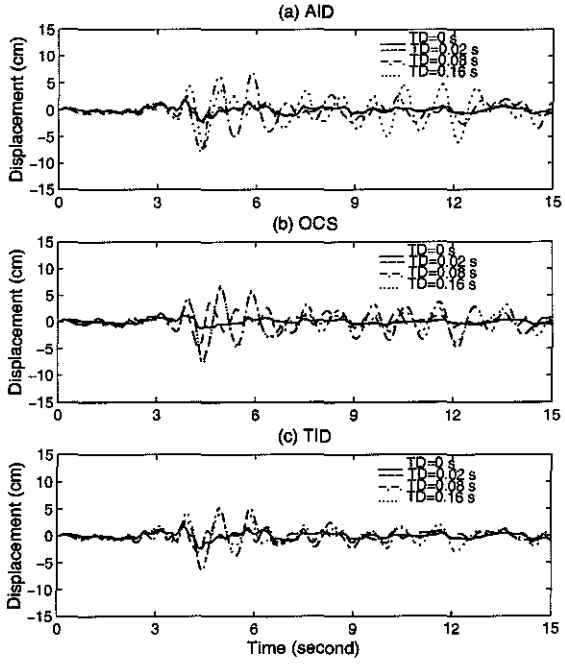

Figure 2.51: Effect of Time Delay – Displacement Time Histories of the PS Controlled by the AIC Algorithms Under the HAC Ground Motion (TD = Time Delay), Type 1 Configuration

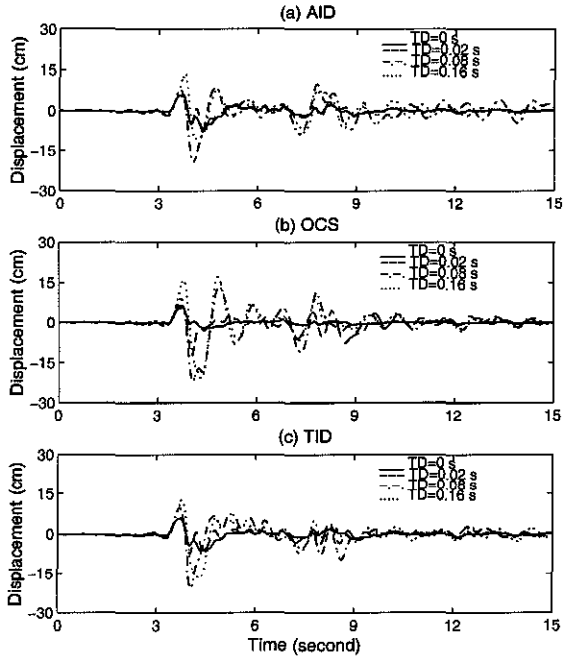

Figure 2.52: Effect of Time Delay – Displacement Time Histories of the PS Controlled by the AIC Algorithms Under the SCH Ground Motion (TD = Time Delay), Type 1 Configuration

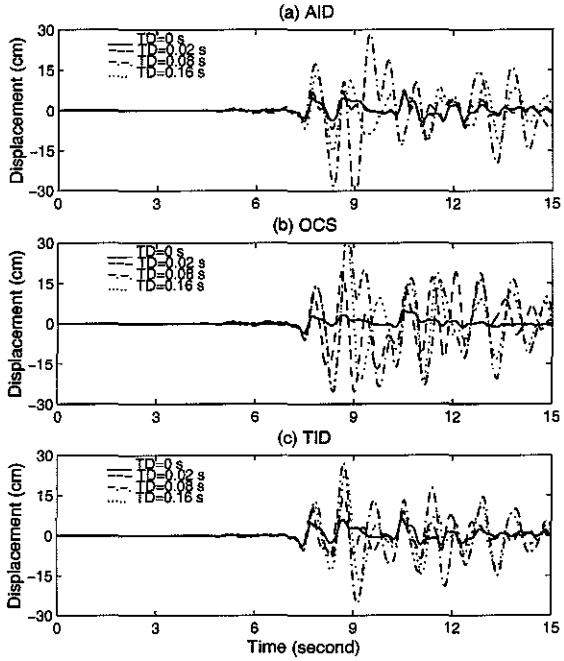

Figure 2.53: Effect of Time Delay – Displacement Time Histories of the PS Controlled by the AIC Algorithms Under the KOB Ground Motion (TD = Time Delay), Type 1 Configuration

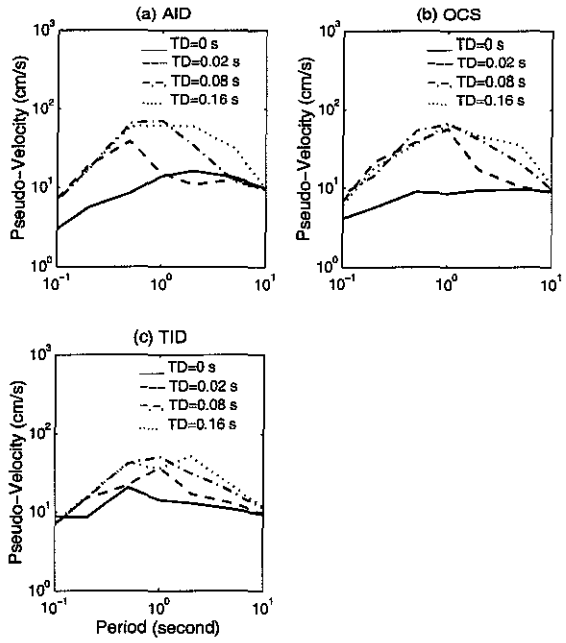

Figure 2.54: Effect of Time Delay – Response Spectra of the PS Controlled by the AIC Algorithms Under the ELC Ground Motion (TD = Time Delay), Type 1 Configuration

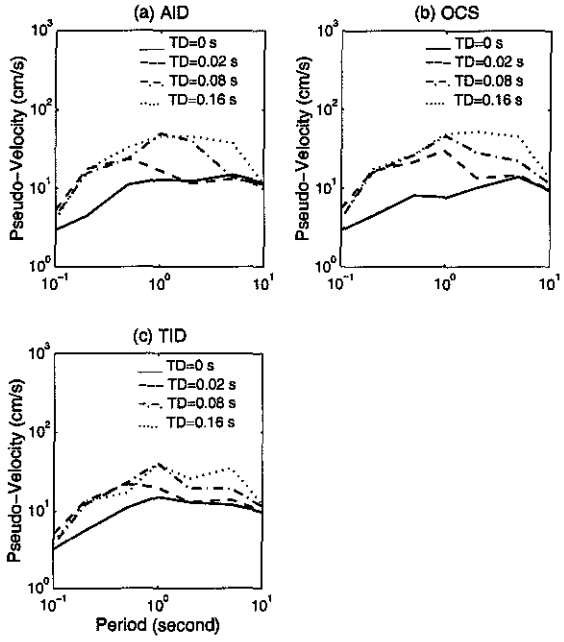

Figure 2.55: Effect of Time Delay – Response Spectra of the PS Controlled by the AIC Algorithms Under the HAC Ground Motion (TD = Time Delay), Type 1 Configuration

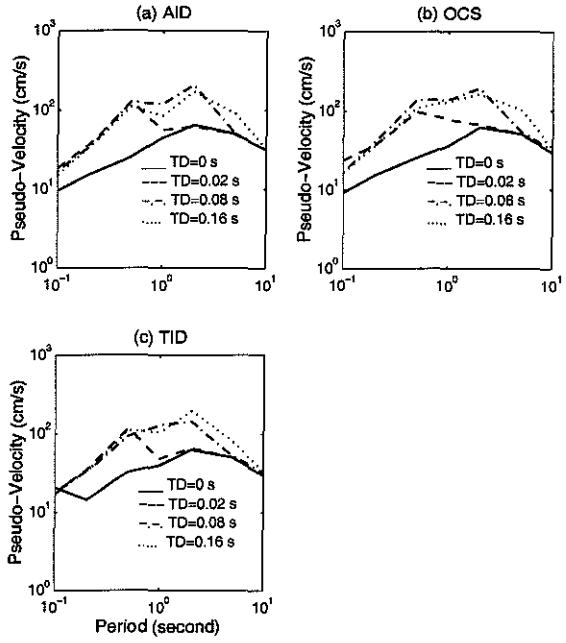

Figure 2.56: Effect of Time Delay – Response Spectra of the PS Controlled by the AIC Algorithms Under the SCH Ground Motion (TD = Time Delay), Type 1 Configuration

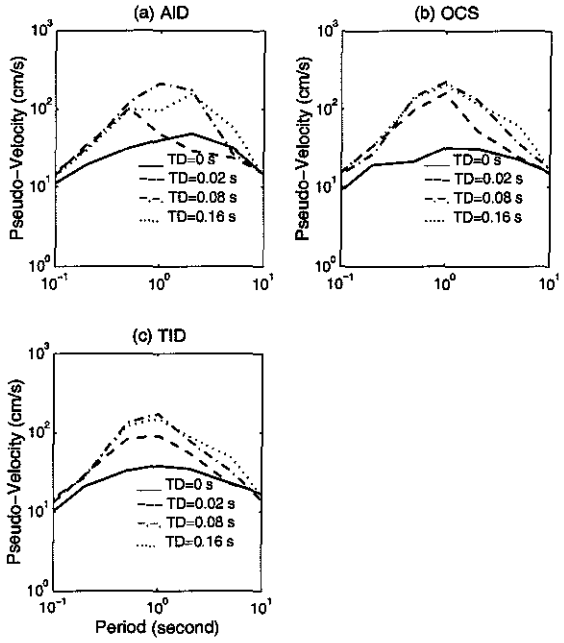

Figure 2.57: Effect of Time Delay – Response Spectra of the PS Controlled by the AIC Algorithms Under the KOB Ground Motion (TD = Time Delay), Type 1 Configuration

Chapter 3 Active Interaction Control of Linear MDOF Systems

3.1 Introduction

Eventually, any structural control approach needs to be implemented in real structures and therefore its effectiveness should be checked for more realistic MDOF structural models. In this chapter, the AIC algorithm is reformulated within the framework of linear *MDOF* systems. Two approaches, the Modal Control (MC) and Nodal Control (NC) approaches are developed to implement the AIC control algorithms in MDOF systems. The Modal Control approach directs the control effort to certain dominant response modes of the primary structure, while the Nodal Control approach tries to restrain the individual inter-story drift of the structure directly. *Three structures, a 3-story, a 9- and a 20-story steel-framed* buildings controlled with the AIC algorithms are analyzed for several historical earthquake records.

AIC incorporates some important aspects of the Active Variable Stiffness (AVS) control approach developed and implemented by the Kajima Corporation and the Kobori Research Complex *[24]. The AVS system is also proposed as a semi-active seismic response control* system. It actively controls structural characteristics, such as stiffness of a building, to establish a non-resonant state against earthquake excitations, thus suppressing the building's response. A 3-story steel building (The KaTRI No. 21 Building, Kajima Corporation) equipped with an AVS system was constructed in 1990 to accumulate practical data and investigate *this structural control approach. This structure is* utilized here as one of the three models to test the AIC algorithms.

Another two MDOF structural models, a 9- and a 20-story steel-framed benchmark building designed for the Los Angeles, California region from SAC project, are also employed in this study. The SAC Joint Venture was formed in mid-1994 with the specific goal of investigating the damage to welded steel moment frame buildings in the 1994 Northridge earthquake and developing repair techniques and new design approaches to minimize dam-

age to steel moment frame buildings in future earthquakes. The three Joint Venture partners are the Structural Engineers Association of California (SEAOC), the Applied Technology Council (ATC), and California Universities for Research in Earthquake Engineering (CUREe) [31].

3.2 Model Formulation

A typical MDOF AIC system consists of a primary structure (PS) targeted for control, a number of auxiliary structures (AS) and interaction elements (IE) which link the PS and AS together. As shown in Fig. 3.1, the AS is typically installed between two adjacent floors of the primary structure. The dynamics of an AS can be modeled as a SDOF oscillator mounted on its support floor of the PS. When the PS is excited by an external disturbance, the AS is excited by the motion of its support floor. Through actively modulating the operating states of the IE connecting the AS to PS, control force favorable to the control strategy is reactively developed within the IE and the vibration of the PS is thus restrained.

Without loss of generality, the following assumptions are made in this chapter:

- Planar models of the PS and AS are considered in this study. Only the response in the horizontal direction is considered for the PS and AS.
- All system parameters are known a priori and do not change during the excitation duration. The PS and AS remain within the linear elastic range.
- The mass of the IE is negligible compared to that of the PS and AS and therefore the dynamics of the IE are neglected.
- Only present and past values of base acceleration and system state variables are available to determine the control input.

A typical AIC system is shown in Fig. 3.1. The equations of motion for the PS subjected to base excitation $\ddot{x}_g$ are expressed as

$$M_1\ddot{\boldsymbol{x}}(t) + C_1\dot{\boldsymbol{x}}(t) + K_1\boldsymbol{x}(t) = -M_1L\ddot{x}_g(t) + H_1\boldsymbol{u}(t) + H_2\boldsymbol{u}_2(t) \tag{3.1}$$

where M_1, C_1, K_1 are the mass, damping and stiffness matrices of the PS respectively. L is the identity vector with all its components equal to one. H_1 and H_2 are the location

matrices of control forces $\boldsymbol{u}(t)$ and $\boldsymbol{u}_2(t)$, respectively. $\boldsymbol{u}(t) = \{u_n \cdots u_1\}^T \in \mathcal{R}^n$ is the control force vector developed within the IEs; the sign of the control force $u_i(t)$ is defined such that $u_i(t)$ is positive when the ith IE is in tension. $\boldsymbol{u}_2(t) = \{u_{2,n} \cdots u_{2,2}\}^T \in \mathcal{R}^{n-1}$ is the force vector applied on the support floors by the corresponding AS. The position and positive directions of u_i and $u_{2,i}$ are illustrated in Fig. 3.2. $\boldsymbol{x}(t) \in \mathcal{R}^n$ is the displacement vector of the PS relative to a datum line fixed to the ground. $\ddot{x}_g$ is the ground motion acceleration.

$$M_1 = \begin{bmatrix} m_{1,n} & & 0 \\ & \ddots & \\ 0 & & m_{1,1} \end{bmatrix}, \quad K_1 = \begin{bmatrix} k_{1,n} & -k_{1,n} & & 0 \\ -k_{1,n} & k_{1,n}+k_{1,n-1} & -k_{1,n-1} & \\ & & \ddots & \\ 0 & & -k_{1,2} & k_{1,2}+k_{1,1} \end{bmatrix} \tag{3.2}$$

$$H_1 = \begin{bmatrix} -\varrho_n & & 0 \\ & \ddots & \\ 0 & & -\varrho_1 \end{bmatrix}, \quad H_2 = \begin{bmatrix} 0 & & 0 \\ \varrho_n & \ddots & \\ & \ddots & 0 \\ 0 & & \varrho_2 \end{bmatrix} \tag{3.3}$$

where ϱ_i is an indicator defined by

$$\varrho_i = \begin{cases} 1 & : \quad \text{if } i\text{th story AS is installed} \\ 0 & : \quad \text{if } i\text{th story AS is not installed} \end{cases} \tag{3.4}$$

Each AS is modeled as a SDOF oscillator excited by the motion of its support floor of the PS. The equation of motion for a typical AS mounted on the ith floor can be expressed as

$$m_{2,i}\ddot{y}_i(t) + c_{2,i}(\dot{y}_i(t) - \dot{x}_i(t)) + k_{2,i}(y_i(t) - x_i(t)) = -m_{2,i}\ddot{x}_g(t) + u_i(t) \tag{3.5}$$

where $m_{2,i}$, $c_{2,i}$, $k_{2,i}$ are the mass, damping factor and stiffness of the ith AS, respectively. y_i represents the displacement of the ith AS relative to a datum line fixed to the ground. x_i is the relative displacement of the ith floor of the PS on which the ith AS is mounted.

3.3 Control Force

As stated before, the control force in an AIC system is generated reactively within the IE by the interactions between the PS and AS. The values of the control forces produced in this way are computed below under various conditions. Type A IEs are assumed to be used here for simplicity in presenting the equations of motion. The modifications required for the Type B IEs are readily derived.

3.3.1 Top (N^{th}) Floor

Considering the free body diagram shown in Fig. 3.3, the equations of motion for the top floor mass and the Nth story AS if interactions are activated are expressed as

$$\begin{cases} m_{1,N}\ddot{x}_N + k_{1,N}(x_N - x_{N-1}) = -m_{1,N}\ddot{x}_g - u_N \\ m_{2,N}\ddot{y}_N + c_{2,N}(\dot{y}_N - \dot{x}_{N-1}) + k_{2,N}(y_N - x_{N-1}) = -m_{2,N}\ddot{x}_g + u_N \end{cases} \tag{3.6}$$

Solving the above equations with the equal velocity and acceleration condition (i.e., $\ddot{x}_N = \ddot{y}_N$ and $\dot{x}_N = \dot{y}_N$) yields

$$u_N = \begin{cases} \frac{1}{m_{1,N}+m_{2,N}}\{[m_{1,N}k_{2,N}(y_N - x_{N-1}) - m_{2,N}k_{1,N}(x_N - x_{N-1})] \\ \quad +m_{1,N}c_{2,N}(\dot{x}_N - \dot{x}_{N-1})\} & , N\text{th IE locked} \\ 0 & , N\text{th IE unlocked} \end{cases} \tag{3.7}$$

where locked means the Nth IE is locked and unlocked means the Nth IE is unlocked.

We can also write out

$$u_{2,N} = \begin{cases} u_N & , N\text{th IE locked} \\ k_{2,N}(y_N - x_{N-1}) + c_{2,N}(\dot{y}_N - \dot{x}_{N-1}) & , N\text{th IE unlocked} \end{cases} \tag{3.8}$$

3.3.2 Other (i^{th}) Floors (i = 1, ... , N-1)

In this section, two cases need to be distinguished. Consider first the case in which no AS is installed in the $(i+1)$st story. The equations of motion for the ith floor mass and the

ith story AS (i=1, ... , N-1) if interaction is activated are expressed as

$$\begin{cases} m_{1,i}\ddot{x}_i - k_{1,i+1}(x_{i+1} - x_i) + k_{1,i}(x_i - x_{i-1}) = -m_{1,i}\ddot{x}_g - u_i \\ m_{2,i}\ddot{y}_i + c_{2,i}(\dot{y}_i - \dot{x}_{i-1}) + k_{2,i}(y_i - x_{i-1}) = -m_{2,i}\ddot{x}_g + u_i \end{cases} \tag{3.9}$$

Solving the above equations with the equal velocity and acceleration condition (i.e., $\ddot{x}_i = \ddot{y}_i$ and $\dot{x}_i = \dot{y}_i$) yields

$$u_i = \begin{cases} \frac{1}{m_{1,i}+m_{2,i}}\{[m_{1,i}k_{2,i}(y_i - x_{i-1}) - m_{2,i}k_{1,i}(x_i - x_{i-1})] \\ \quad +m_{1,i}c_{2,i}(\dot{x}_i - \dot{x}_{i-1}) + m_{2,i}k_{1,i+1}(x_{i+1} - x_i)\} & , i\text{th IE locked} \\ 0 & , i\text{th IE unlocked} \end{cases} \tag{3.10}$$

Next, consider the second case in which AS is present in the $(i+1)$st story. The equations of motion for the ith floor mass and the ith story AS (i=1, ... , N-1) if interaction is activated are now expressed as

$$\begin{cases} m_{1,i}\ddot{x}_i - k_{1,i+1}(x_{i+1} - x_i) + k_{1,i}(x_i - x_{i-1}) = -m_{1,i}\ddot{x}_g + u_{2,i+1} - u_i \\ m_{2,i}\ddot{y}_i + c_{2,i}(\dot{y}_i - \dot{x}_{i-1}) + k_{2,i}(y_i - x_{i-1}) = -m_{2,i}\ddot{x}_g + u_i \end{cases} \tag{3.11}$$

Similarly,

$$u_i = \begin{cases} \frac{1}{m_{1,i}+m_{2,i}}\{[m_{1,i}k_{2,i}(y_i - x_{i-1}) - m_{2,i}k_{1,i}(x_i - x_{i-1})] \\ \quad +m_{1,i}c_{2,i}(\dot{x}_i - \dot{x}_{i-1}) + m_{2,i}k_{1,i+1}(x_{i+1} - x_i) + m_{2,i}u_{2,i+1}\} & , i\text{th IE locked} \\ 0 & , i\text{th IE unlocked} \end{cases} \tag{3.12}$$

Furthermore, we also have

$$u_{2,i} = \begin{cases} u_i & , i\text{th IE locked} \\ k_{2,i}(y_i - x_{i-1}) + c_{2,i}(\dot{y}_i - \dot{x}_{i-1}) & , i\text{th IE unlocked} \end{cases} \tag{3.13}$$

3.4 Modal Control

The Modal Control approach is formulated below to implement the AIC control algorithms in linear MDOF systems. Another discussion of Modal Control approach in reduced modal space can be found in references [6, 7].

The motion of discrete systems is governed by a set of simultaneous second-order ordi-

nary differential equations. Specifically, the equations of motion of the undamped primary structure can be expressed as

$$M_1\ddot{\boldsymbol{x}}(t) + K_1\boldsymbol{x}(t) = \boldsymbol{f} \tag{3.14}$$

where $\boldsymbol{f}$ is the external loading acted on the structure.

The response of an n-DOF system can be represented by a superposition of modal vectors multiplied by generalized coordinates, namely,

$$\boldsymbol{x}(t) = \Phi\boldsymbol{q} \tag{3.15}$$

where Φ is an n×n modal matrix with the modal vectors as its columns and $\boldsymbol{q}$ is the modal coordinate vector denoting the contribution from each mode, i.e.,

$$\Phi = [\phi_1\ \phi_2\ \cdots\ \phi_{n-1}\ \phi_n], \quad \boldsymbol{q} = \{q_1\ q_2\ \cdots\ q_{n-1}\ q_n\}^T \tag{3.16}$$

The modal vectors can be found by solving the eigenvalue problem

$$(K_1 - \omega^2 M_1)\phi = 0$$

The orthogonality of natural modes implies that the following square matrices are diagonal:

$$D_M \equiv \Phi^T M_1 \Phi = \begin{bmatrix} d_M^1 & & 0 \\ & \ddots & \\ 0 & & d_M^n \end{bmatrix}, \quad D_K \equiv \Phi^T K_1 \Phi = \begin{bmatrix} d_M^1\omega_1^2 & & 0 \\ & \ddots & \\ 0 & & d_M^n\omega_n^2 \end{bmatrix} \tag{3.17}$$

where ω_r is the natural circular frequency of the rth mode and Φ^T denotes the transpose of Φ. *If modal damping is assigned to the PS, then*

$$D_C \equiv \Phi^T C_1 \Phi = \begin{bmatrix} 2d_M^1\zeta_1\omega_1 & & 0 \\ & \ddots & \\ 0 & & 2d_M^n\zeta_n\omega_n \end{bmatrix} \tag{3.18}$$

where d_M^r and ζ_r are referred to as the modal inertias and modal damping ratios, respectively.

Pre-multiplying Eqn. (3.1) by Φ^T gives

$$D_M\ddot{\boldsymbol{q}}(t) + D_C\dot{\boldsymbol{q}}(t) + D_K\boldsymbol{q}(t) = -\Phi^T M_1 L\ddot{x}_g(t) + \Phi^T H_1\boldsymbol{u}(t) + \Phi^T H_2\boldsymbol{u}_2(t) \tag{3.19}$$

It is a well-known fact that the response for building structures is usually concentrated in the first several modes when subjected to earthquake excitations. Therefore, we can choose these predominant response modes as the controlled modes. Denote the controlled modes by c_1, c_2, ... , c_k and the remaining uncontrolled modes by u_1, u_2, ... , u_j, with $k + j = n$, which is the total number of degrees of freedom of the MDOF system.

The relative vibrational energy of the PS for the controlled modes is defined as

$$E_c = \frac{1}{2}\boldsymbol{q}_c^T D_k^c \boldsymbol{q}_c + \frac{1}{2}\dot{\boldsymbol{q}}_c^T D_M^c \dot{\boldsymbol{q}}_c \tag{3.20}$$

where

$$D_K^c = \Phi_c^T K_1 \Phi_c, \quad D_M^c = \Phi_c^T M_1 \Phi_c \tag{3.21}$$

and $\boldsymbol{q}_c = \{q_{c1}\, q_{c2} \cdots q_{ck}\}^T$ is a vector containing only the modal coordinates corresponding to the controlled modes. $\Phi_c = [\phi_{c1}\, \phi_{c2} \cdots \phi_{ck}]$ is an n×k matrix containing only the modal vectors of the controlled modes. k is the total number of the controlled modes.

For convenience in the following formulation process, we introduce a k×n transformation matrix Ω_c which is defined such that the elements in the rth row are zeros except for the unity element in the cr^{th} column (counting from left) of the same row. For example, if n=4, and the controlled modes are the 1st and 3rd modes, i.e., k=2, c1=1, c2=3, then

$$\Omega_c = \begin{bmatrix} 1 & 0 & 0 & 0 \\ 0 & 0 & 1 & 0 \end{bmatrix}$$

Using this notation,

$$\Phi_c = \Phi\Omega_c^T, \quad \boldsymbol{q}_c = \Omega_c\boldsymbol{q} \tag{3.22}$$

and

$$D_M^c = \Omega_c D_M \Omega_c^T, \quad D_K^c = \Omega_c D_K \Omega_c^T, \quad D_C^c = \Omega_c D_C \Omega_c^T \tag{3.23}$$

The equations of motion in the reduced modal space that contain only the controlled

modes can be expressed as

$$\begin{aligned} D_M^c \ddot{\boldsymbol{q}}_c(t) + D_C^c \dot{\boldsymbol{q}}_c(t) + D_K^c \boldsymbol{q}_c(t) &= -\Omega_c \Phi^T M_1 L \ddot{x}_g(t) + \Omega_c \Phi^T H_1 \boldsymbol{u}(t) \\ &\quad + \Omega_c \Phi^T H_2 \boldsymbol{u}_2(t) \end{aligned} \tag{3.24}$$

In order to formulate the control algorithm for the proposed control approach, the derivative of E_c with respect to time, t, must be considered. Taking the time derivative of Eqn. (3.20) yields

$$\dot{E}_c = \boldsymbol{q}_c^T D_k^c \dot{\boldsymbol{q}}_c + \dot{\boldsymbol{q}}_c^T D_M^c \ddot{\boldsymbol{q}}_c \tag{3.25}$$

Substituting Eqn. (3.24) into Eqn. (3.25) gives

$$\begin{aligned} \dot{E}_c &= \boldsymbol{q}_c^T D_k^c \dot{\boldsymbol{q}}_c + \dot{\boldsymbol{q}}_c^T (-D_C^c \dot{\boldsymbol{q}}_c(t) - D_K^c \boldsymbol{q}_c(t) - \Omega_c \Phi^T M_1 L \ddot{x}_g(t) \\ &\quad + \Omega_c \Phi^T H_1 \boldsymbol{u}(t) + \Omega_c \Phi^T H_2 \boldsymbol{u}_2(t)) \\ &= -\dot{\boldsymbol{q}}_c^T D_C^c \dot{\boldsymbol{q}}_c(t) - \dot{\boldsymbol{q}}_c^T \Omega_c \Phi^T M_1 L \ddot{x}_g(t) + \dot{\boldsymbol{q}}_c^T \Omega_c \Phi^T H_1 \boldsymbol{u}(t) \\ &\quad + \dot{\boldsymbol{q}}_c^T \Omega_c \Phi^T H_2 \boldsymbol{u}_2(t) \end{aligned} \tag{3.26}$$

Consider some time interval $[t_0, t_1]$ during which control of the PS is to be accomplished (e.g., the duration of external disturbances). The objective of this control strategy is to reduce the motion of the PS as much as possible. This objective can be achieved if an effort is made to drive $\dot{E}_c$ to be as negative as possible, and as often as possible (ideally, a continuous effort would be made for an optimal effect). The control signal for the operation of the IEs is therefore determined such that the time rate of change in the relative vibrational energy of the PS is minimized at every time instant. The first and second terms in Eqn. (3.26) are uncontrollable in the sense that these quantities are constant regardless of the operating states selected for the IEs. However, the third and fourth terms in Eqn. (3.26) are controllable by selecting appropriate operating states for the IEs such that the values of $\boldsymbol{u}(t)$ and $\boldsymbol{u}_2(t)$ associated with the selected operating states of the IEs will minimize $\dot{E}_c$.

It is noteworthy that the third and fourth terms in Eqn. (3.26) can be decomposed as

follows:

$$\dot{\boldsymbol{q}}_c^T \Omega_c \Phi^T H_1 \boldsymbol{u}(t) = \boldsymbol{S}_1^T(t)\boldsymbol{u}(t) = \sum_{i=1}^{n_c} s_{1,i}(t) \cdot u_i(t) \tag{3.27}$$

$$\dot{\boldsymbol{q}}_c^T \Omega_c \Phi^T H_2 \boldsymbol{u}_2(t) = \boldsymbol{S}_2^T(t)\boldsymbol{u}(t) = \sum_{i=1}^{n_c} s_{2,i}(t) \cdot u_{2,i}(t)$$

where n_c denotes the number of the AS installed in an AIC system.

In Eqn. (3.27), $s_{1,i}(t)$ and $s_{2,i}(t)$ are fixed at time t regardless of the operating states selected for the IEs at this moment. Furthermore, contribution from each control force term to $\dot{E}_c$ is isolated from others. Therefore, selecting the operating state for one IE can be done independent of the selection of other IE operating states. The total number of possible structural configurations needed to examine at each time instant is thus reduced to $2n_c$ for the modal control approach considered.

In practice, the control algorithm has to be implemented in discrete time. First, the duration $[t_0, t_1]$ of external disturbance is uniformly partitioned into a set of appropriate short time intervals, each of duration δt and referred to as a control-sampling period. Consider a representative short time interval, the k-th sampling period, defined by $t \in [t_k, t_{k+1}]$. At time point t_k, the state variables of the PS and AS are measured; a control processor then uses this information to determine an appropriate operating state for each IE: locked or unlocked. In the locked state, interactions between the PS and AS are activated, while in the unlocked state, interactions between the PS and AS are deactivated. Interactions are permitted in the k-th control sampling period only when their anticipated effect is favorable to the control strategy. The control signal made at the beginning of each sampling period is then sent to the controller valve of the IE to switch or maintain the operating state of the IE. This procedure is repeated for each consecutive sampling period.

If different weights need to be assigned to each of the controlled modes, a k×k scaling matrix, Λ_s, with the weights as its diagonal elements is introduced.

$$\Lambda_s = \begin{bmatrix} \lambda_{c1} & & 0 \\ & \ddots & \\ 0 & & \lambda_{ck} \end{bmatrix} \tag{3.28}$$

With this scaling matrix, the relative vibrational energy is rewritten as

$$E_{c,s} = \frac{1}{2}\boldsymbol{q}_c^T \Lambda_s D_k^c \boldsymbol{q}_c + \frac{1}{2}\dot{\boldsymbol{q}}_c^T \Lambda_s D_M^c \dot{\boldsymbol{q}}_c \tag{3.29}$$

Taking the time derivative of Eqn. (3.29) and substituting Eqn. (3.24) yields

$$\begin{aligned}
\dot{E}_{c,s} &= \boldsymbol{q}_c^T \Lambda_s D_k^c \dot{\boldsymbol{q}}_c + \dot{\boldsymbol{q}}_c^T \Lambda_s (-D_C^c \dot{\boldsymbol{q}}_c(t) - D_K^c \boldsymbol{q}_c(t) \\
&\quad -\Omega_c \Phi^T M_1 L \ddot{x}_g(t) + \Omega_c \Phi^T H_1 \boldsymbol{u}(t) + \Omega_c \Phi^T H_2 \boldsymbol{u}_2(t)) \\
&= -\dot{\boldsymbol{q}}_c^T \Lambda_s D_C^c \dot{\boldsymbol{q}}_c(t) - \dot{\boldsymbol{q}}_c^T \Lambda_s \Omega_c \Phi^T M_1 L \ddot{x}_g(t) \\
&\quad +\dot{\boldsymbol{q}}_c^T \Lambda_s \Omega_c \Phi^T H_1 \boldsymbol{u}(t) + \dot{\boldsymbol{q}}_c^T \Lambda_s \Omega_c \Phi^T H_2 \boldsymbol{u}_2(t)
\end{aligned} \tag{3.30}$$

The third and fourth terms in the above equation can be used for control purpose as discussed before.

As in the SDOF case, a heuristic control law for our control strategy can be expressed by the attachment conditions summarized in Table 3.1 for each AIC algorithm. When the attachment conditions for a particular AIC algorithm are satisfied simultaneously at the beginning of a control-sampling period, a locked state is selected for the IE in consideration, while the IE is unlocked if one of the attachment conditions is not satisfied. It is again observed that one condition which drives the time derivative of the relative vibrational energy as negative as possible are employed by all AIC algorithms which include the AID, OCS and TID algorithms. This condition is derived from the instantaneous optimal control strategy with the relative vibration energy for the controlled modes as its performance index.

3.5 Nodal Control

Unlike the Modal Control approach which tries to minimize the responses of several dominant modes in the structure, the Nodal Control approach directs its control effort to restraining the individual inter-story drift of the structure directly. Namely, for the Nodal Control approach, the control algorithm is formulated directly in physical space.

The Nodal Control approach for Active Interaction Control of MDOF structures is very similar to the AIC algorithms for SDOF systems described in Chapter 2 except that relative

Table 3.1: Characteristics of the AIC Control Algorithms (Modal Control)

Control Algorithms	Attachment Conditions for the ith AS	AS Dynamics	IE Type and Operating States
AID	$s_{1,i}(t) \cdot u_i^a(t) + s_{2,i}(t) \cdot u_{2,i}^a(t) \leq 0$	Considered	Type A, Free/Rigid
OCS	$\begin{cases} s_{1,i}(t) \cdot u_i^a(t) + s_{2,i}(t) \cdot u_{2,i}^a(t) \leq 0 \\ \dot{x}_i(t) = \dot{y}_i(t) \end{cases}$	Considered	Type A, Free/Rigid
TID	$\begin{cases} s_{1,i}(t) \cdot u_i^a(t) + s_{2,i}(t) \cdot u_{2,i}^a(t) \leq 0 \\ \dot{x}_i(t) = \dot{y}_i(t) \end{cases}$	Considered	Type B, Free/Rigid/Slip, $\lvert u_i^a(t) \rvert \leq u_{max}^i$

Note: AIC control algorithms include the Active Interface Damping (AID), Optimal Connection Strategy (OCS), and Tuned Interaction Damping (TID) algorithms. The definitions for the functions $s_{1,i}(t)$ and $s_{2,i}(t)$ are given in Eqn. (3.27). $u_i^a(t)$ and $u_{2,i}^a(t)$ represent the control force values calculated from the assumption that the PS is attached to the ith AS at time t (i.e., the ith IE is assumed to be locked).

inter-story drift is now used. More rigorously, the control effort of Nodal Control is directed to minimizing the time derivative of relative vibrational energy E_i for each individual story defined by

$$E_{1,i} \equiv \frac{1}{2} m_{1,i} (\dot{x}_i - \dot{x}_{i-1})^2 + \frac{1}{2} k_{1,i} (x_i - x_{i-1})^2 \tag{3.31}$$

If a lumped mass model is employed to represent a MDOF structure, the equation of motion for the ith floor mass (node) is expressed as

$$m_{1,i} \ddot{x}_i - k_{1,i+1}(x_{i+1} - x_i) + k_{1,i}(x_i - x_{i-1}) = -m_{1,i} \ddot{x}_g + u_{2,i+1} - u_i \tag{3.32}$$

Differentiating Eqn. (3.31) and substituting Eqn. (3.32), the time derivative of the relative vibrational energy of the ith story is expressed as

$$\begin{aligned} \dot{E}_{1,i}(t) &= [m_{1,i}(\ddot{x}_i - \ddot{x}_{i-1}) + k_{1,i}(x_i - x_{i-1})](\dot{x}_i - \dot{x}_{i-1}) \\ &= [-u_i(t) + k_{1,i+1}(x_{i+1} - x_i) - m_{1,i}(\ddot{x}_{i-1} + \ddot{x}_g) \\ &\quad + u_{2,i+1}](\dot{x}_i - \dot{x}_{i-1}) \end{aligned} \tag{3.33}$$

The difference in values of $\dot{E}_{1,i}$ for different operating states of the ith story IE depends

Table 3.2: Characteristics of the AIC Control Algorithms (Nodal Control)

Control Algorithms	Attachment Conditions for the ith AS	AS Dynamics	IE Type and Operating States
AID	$u_i^a(t) \cdot (\dot{x}_i(t) - \dot{x}_{i-1}(t)) \geq 0$	Considered	Type A, Free/Rigid
OCS	$\begin{cases} u_i^a(t) \cdot (\dot{x}_i(t) - \dot{x}_{i-1}(t)) \geq 0 \\ \dot{x}_i(t) = \dot{y}_i(t) \end{cases}$	*Considered*	*Type A*, Free/Rigid
TID	$\begin{cases} u_i^a(t) \cdot (\dot{x}_i(t) - \dot{x}_{i-1}(t)) \geq 0 \\ \dot{x}_i(t) = \dot{y}_i(t) \end{cases}$	Considered	Type B, Free/Rigid/Slip $\lvert u_i^a(t) \rvert \leq u_{max}^i$

Note: AIC control algorithms include the Active Interface Damping (AID), Optimal Connection Strategy (OCS), and Tuned Interaction Damping (TID) algorithms. $u_i^a(t)$ represents the control force value calculated from the assumption that the PS is attached to the ith AS at time t (i.e., the ith IE is assumed to be locked).

solely on the first term in Eqn. (3.33). Other terms in Eqn. (3.33) are unchanged regardless of the operating state selected for the ith story IE. Therefore, to minimize the time derivative of relative vibrational energy for the ith story, the first term at the right-hand side of Eqn. (3.33) should be driven as negative as possible at each time instant. From Eqn. (3.33), it is seen that the control decision for each story IE can be made independent of the IEs in *other stories.*

The Nodal Control approach implemented in discrete time can now be described as follows. At the beginning of a representative control-sampling period $[t_k,\ t_{k+1}]$, or time instant t_k, the state variables of the PS and AS are measured and thus fully known. Control forces corresponding to the locked and unlocked states of the ith story IE are computed by a control processor. Then, an appropriate operating state for the IE is determined according to the attachment conditions described in Table 3.2. Finally, the control signal made at the beginning of each sampling period is sent to the control valve of the IE to switch or maintain the operating state of the ith story IE. This process is done simultaneously for all the IEs. Then, the system responds to the values of $\boldsymbol{u}(t)$ resulting from these interactions until the beginning of the next control-sampling period, when another appropriate operating state is determined. This procedure is then repeated for each consecutive control-sampling period.

From Eqn. (3.33), we can see that the ith story $\dot{E}_{1,i}(t)$ may not be minimized in the whole state space $\boldsymbol{u}(t)$ due to the presence of $u_{2,i+1}(t)$ in this equation. Stated in another way, the operating states selected for the (i+1)st IE may lead to a value of $u_{2,i+1}(t)$ which increases the value of $\dot{E}_{1,i}(t)$.

The advantage of the Nodal Control approach is that only limited state information is needed in order to control the AS installed in a particular story. For example, in order to control the ith story IE, we only need to know the state variables of the (i-1)st, ith and (i+1)st floors. For the Modal Control approach described in the preceding section, complete information of the state variables is required to accurately evaluate the modal coordinates of the PS. In the case of reduced state information, although the modal coordinates of the controlled modes can be approximately evaluated by means of an estimator algorithm [7], some degree of accuracy is lost in this approximation process.

3.6 Building Models and Design Procedure

Three steel-framed building models are utilized herein to verify the practicality and effectiveness of the proposed AIC control approach through numerical simulation. These include a three-story building located in Japan and two benchmark steel-framed buildings designed for the Los Angeles, California region, as described below. These building models are selected to represent typical low-, middle- and high-rise buildings.

A general procedure for the design of an AIC system used in this study is described first.

3.6.1 General Design Procedure for AIC System

It is believed that with currently available technology, the AIC control approach can be readily implemented in real structures. The following describes the general procedure for the design of an AIC system.

Suppose the primary structure intended for AIC control is given. We will focus our discussion on planar, linear models of framed structures in this study. The models will consist of interconnected beam and column elements in which the mass and stiffness properties are taken to be uniformly distributed. The elements will be of the two-node type, each node having vertical, horizontal, and rotational displacements associated with it. In this study, a

rigid floor assumption is made to simplify the analysis. A numerical model for the primary structure under consideration is finally derived using finite element method (FEM).

Once a model for the primary structure (PS) is obtained, we can set out to design the auxiliary structures (AS) and interaction elements (IE) in the AIC system.

To keep the mode shapes of the PS unaffected as much as possible in the presence of interactions between the PS and AS, the total stiffness of all ASs installed in one story is chosen to be proportional to the corresponding story stiffness of the PS. In addition, this proportional factor is kept constant for any story in the PS except where there is no AS in the story. If a high value is chosen for the AS stiffness, this high AS stiffness value generally corresponds to a cost increase because of increased material use and detailing requirement. This will also lead to an increase in the AS mass which increases the project cost. However, an overly low value of the AS stiffness will decrease the performance of the AIC system which is also undesirable. Therefore, choosing an optimal value for the proportional factor is very important in the design of AS for an AIC system.

Through a parametric study, quite often we have an optimal value for the AS natural frequency and this optimal frequency value will be used for all ASs installed. We recommend a value around 0.05 second for the AS natural period. If the AS natural frequency is known, then the AS mass can be easily determined from its stiffness and natural frequency. For practicality consideration, we need to distribute a large AS mass among the ASs in the same story if a large AS mass value is obtained from the last step. Therefore, this results in several identical ASs in one story so that the mass of each AS is reasonably small (e.g., each AS mass is kept less than 3000 kg). The damping factor of the AS is then determined by using $c_{2,i} = 2\zeta_{2,i} m_{2,i} \omega_{2,i}$ and the damping coefficient $\zeta_{2,i}$ is generally known from parametric study described in Chapter 2.

3.6.2 Outline of a 3-story Building Model

The outline of this three-story steel-framed building (the KaTRI No. 21 Building, Kajima Corporation, Japan) equipped with an AVS control system [24], is shown in Fig. 3.4. Steel braces placed in the transverse direction (gable side), and the variable stiffness device (VSD) installed between the respective brace tops and the lateral beams are utilized to facilitate the change of structural stiffness in the transverse direction. The VSD switches over the locked and unlocked states and is the physical prototype of the Type A IE in an AIC system.

Table 3.3: Characteristics of the Auxiliary Structures in the Three-story Building

Story	Stiffness $k_{2,i}$ of i^{th} AS (kN/mm)	Mass $m_{2,i}$ of i^{th} AS (kg)	Damping coeff. $c_{2,i}$ of i^{th} AS (10^3 kg/sec)	Natural Period (second)
3	104.922	437	8.6 (64.3)	0.013
2	104.726	436	8.6 (64.2)	0.013
1	122.393	510	10.0 (75.0)	0.013

Note: In the column for the damping coefficients of the AS, the number outside the bracket refers to the values used for the AID, OCS system, while the number in the bracket represents the value used for the TID system.

The same control system already installed in this building can be used for the AIC system with only slight modification. For this reason, this structure is utilized as one of the three models here to test the AIC algorithm.

The numerical simulation is based on a planar, linear model of the transverse structural frame in the original building. A lumped mass model of this controlled structure is shown in Fig. 3.5. The mass of the building is concentrated at each floor level. The stiffness of the structural steel frame (PS) and AS was evaluated based on the cross-sections of the members [24]. The characteristics of the AS installed in each story is given in Table 3.3. It should be noted that the parameters of the AS is not optimized for the AIC system. The original parameter values of the AVS system are employed again for the AIC system with only the control logic part being changed.

The natural periods for this linear lumped mass model with IE always being unlocked are 1.21, 0.33, and 0.22 second, respectively. Two-percent modal damping ratio is assigned to each mode of the PS.

3.6.3 Outline of a 9-story Building Model

This nine-story steel-framed structure was designed by Brandow & Johnston Associates for the SAC Phase II steel Project. Although not actually constructed, this structure meets seismic code and represents a typical medium-rise building designed for the Los Angeles, California, region. This building also serves as a benchmark structure for both the SAC studies and a benchmark control problem for seismically excited buildings [29].

The nine-story structure is 45.73 m (150 ft) by 45.73 m (150 ft) in plan, and 37.19 m (122 ft) in elevation. The bays are 9.15 m (30 ft) on center, in both directions, with five

Table 3.4: Characteristics of the Auxiliary Structures in the Nine-story Building

Story	Stiffness $k_{2,i}$ of i^{th} AS (kN/mm)	Mass $m_{2,i}$ of i^{th} AS (kg)	Damping coeff. $c_{2,i}$ of i^{th} AS (10^3 kg/sec)	Natural Period (second)
9	28.428×1	2296×1	10.2×1 (76.6×1)	0.056
8	28.720×2	2319×2	10.3×2 (77.4×2)	0.056
7	22.692×3	1833×3	8.2×3 (61.2×3)	0.056
6	25.840×3	2087×3	9.3×3 (69.7×3)	0.056
5	22.262×4	1798×4	8.0×4 (60.0×4)	0.056
4	25.285×4	2042×4	9.1×4 (68.2×4)	0.056
3	29.047×4	2346×4	10.4×4 (78.3×4)	0.056
2	30.316×4	2448×4	10.9×4 (81.7×4)	0.056
1	20.038×3	1618×3	21.6×3 (54.0×3)	0.056

Note: In the column for the damping coefficients of the AS, the number outside the bracket refers to the values used for the AID, OCS system, while the number in the bracket represents the value used for the TID system.

bays each in the north-south (N-S) and east-west (E-W) directions. The building's lateral load-resisting system is comprised of steel perimeter moment-resisting frames (MRFs) with simple framing on the furthest south E-W frame. The interior bays of the structure contain simple framing with composite floors [29]. The columns are 345 MPa (50 ksi) steel. The columns of the MRF are wide-flange. The levels of the nine-story building are numbered with respect to the ground level in Fig. 3.6. The building has a basement level denoted B-1. Typical floor-to-floor heights (for analysis purposes measured from center-of-beam to center-of-beam) are 3.96 m (13 ft). The floor-to-floor height of the basement level is 3.65 m (12 ft) and for the first floor is 5.49 m (18 ft).

The column lines employ two-tier construction, i.e., monolithic column pieces are connected every two levels beginning with the first level. Column splices, which are seismic (tension) splices to carry bending and uplift forces, are located on the first, third, fifth and seventh levels at 1.83 m (6 ft) above the center-line of the beam to column joint. The column bases are modeled as pinned and secured to the ground (at the B-1 level). Concrete foundation walls and surrounding soil are assumed to restrain the structure at the ground level from horizontal displacement.

The floor system is comprised of 248 MPa (36 ksi) steel wide-flange beams acting compositely with the floor slab. Each frame resists one half of the seismic mass associated with the entire structure.

The seismic mass of the structure is due to various components of the structure, including the steel framing, floor slabs, ceiling/flooring, mechanical/electrical, partitions, roofing and a penthouse located on the roof. The seismic mass of the ground level is 9.65×10^5 kg (66.0 kips-sec^2/ft), for the first level is 1.01×10^6 kg (69.0 kips-sec^2/ft), for the second through eighth levels is 9.89×10^5 kg (67.7 kips-sec^2/ft) and for the ninth level is 1.07×10^6 kg (73.2 kips-sec^2/ft). The seismic mass of the above ground levels of the entire structure is 9.00×10^6 kg (616 kips-sec^2/ft). The nine-story N-S MRF is depicted in Fig. 3.6.

The numerical study will focus on an in-plane analysis of this nine-story structure. The frames considered in the development of the evaluation model are the N-S MRFs in the short direction of the building. The finite element model for this linear planar structure is obtained using the code listed in Appendix C. The ASs and IEs for AIC control purpose are assumed to be installed in the same N-S frames. To keep the PS vibrating in its first mode as much as possible during the control process, the stiffness of the AS is chosen as one-fourth of the approximate story stiffness of the PS in this study. The AS mass is determined in such a way that the natural frequency of each AS is equal to 40 times the fundamental frequency of the PS. In this case, the natural period of the AS is 0.056 second. The characteristics of the AS installed on each floor are given in Table 3.4. The AS's properties were selected for the optimal control effect of this nine-story building. To distribute the large mass demand on the AS on each floor, several identical AS's are provided on one floor so that the mass of each AS is varying between 1,500 kg and 3,000 kg. The arrangement of the AS in the N-S frame of this nine-story building is illustrated in Fig. 3.8.

To minimize computational costs, a static condensation technique is used to eliminate all rotational and vertical DOFs from the dynamic analysis. It is assumed that the inertias associated with the rotational and vertical DOFs are negligible. Also, a rigid floor assumption is made, and therefore only the horizontal DOF corresponding to each floor of this nine-story structure is retained. To justify this reduced-DOF model, comparison is made with the results given in Ref. [29]. The results from both models agree very well within the linear elastic range. The first five natural periods of this nine-story structure without the AS are 2.26, 0.85, 0.49, 0.32, and 0.23 second, respectively. Again, two-percent modal damping ratio is assigned to each mode of this linear model.

3.6.4 Outline of a 20-story Building Model

This 20-story steel-framed structure was also designed by Brandow & Johnston Associates for the same purpose as that of the 9-story building discussed above [29].

This 20-story structure is 30.48 m (100 ft) by 36.58 m (120 ft) in plan, and 80.77 (265 ft) m in elevation. The bays are 6.10 m (20 ft) on center, in both directions, with five bays in the north-south (N-S) direction and six bays in the east-west (E-W) direction. The building's lateral load-resisting system is comprised of steel perimeter moment-resisting frames (MRFs). The interior bays of the structure contain simple framing with composite floors.

The columns are 345 MPa (50 ksi) steel. The interior columns of the MRF are wide-flange. The corner columns are box columns. The levels of the 20-story building are numbered with respect to the ground level. The building has two basement levels. The level directly below the ground level is the second basement (B-1). The level below B-1 is the second basement (B-2). Typical floor-to-floor heights (for analysis purposes measured from center-of-beam to center-of-beam) are 3.96 m (13 ft). The floor-to-floor heights for the two basement levels are 3.65 m (12 ft) and for the ground level is 5.49 m (18 ft).

The column lines employ three-tier construction, i.e., monolithic column pieces are connected every three levels beginning with the first level. Column splices, which are seismic (tension) splices to carry bending and uplift forces, are located on the first, fourth, seventh, tenth, thirteenth, sixteenth and eighteenth levels at 1.83 m (6 ft) above the center-line of the beam to column joint. The column bases are modeled as pinned and secured to the ground (at the B-2 level). Concrete foundation walls and surrounding soil are assumed to restrain the structure at the ground level from horizontal displacement.

The floor system is comprised of 248 MPa (36 ksi) steel wide-flange beams acting compositely with the floor slab. Similar to the nine-story building, each frame resists one half of the seismic mass associated with the entire structure.

The seismic mass of the structure is due to various components of the structure, including the steel framing, floor slabs, ceiling/flooring, mechanical/electrical, partitions, roofing and a penthouse located on the roof. The seismic mass, including both N-S MRFs, of the ground level is 5.32×10^5 kg (36.4 kips-sec^2/ft), for the first level is 5.63×10^5 kg (38.6 kips-sec^2/ft), for the second level to nineteenth level is 5.52×10^5 kg (37.8 kips-sec^2/ft) and for the 20th

Table 3.5: Characteristics of the Auxiliary Structures in the 20-story Building

Story	Stiffness $k_{2,i}$ of i^{th} AS (kN/mm)	Mass $m_{2,i}$ of i^{th} AS (kg)	Damping coeff. $c_{2,i}$ of i^{th} AS (10^3 kg/sec)	Natural Period (second)
20	21.530×1	1613×1	7.5×1 (55.9×1)	0.054
19	21.103×2	1581×2	7.3×2 (54.8×2)	0.054
18	25.818×2	1934×2	8.9×2 (67.0×2)	0.054
17	29.000×2	2173×2	10.0×2 (75.3×2)	0.054
16	30.423×2	2280×2	10.5×2 (79.0×2)	0.054
15	31.253×2	2342×2	10.8×2 (81.2×2)	0.054
14	24.130×3	1809×3	8.4×3 (62.7×3)	0.054
13	28.307×3	2121×3	9.8×3 (73.5×3)	0.054
12	29.698×3	2225×3	10.3×3 (77.1×3)	0.054
11	31.817×3	2384×3	11.0×3 (82.6×3)	0.054
10	34.120×3	2556×3	11.8×3 (88.6×3)	0.054
9	34.877×3	2613×3	12.1×3 (90.6×3)	0.054
8	34.918×3	2616×3	12.1×3 (90.7×3)	0.054
7	34.937×3	2618×3	12.1×3 (90.7×3)	0.054
6	35.552×3	2664×3	12.3×3 (92.3×3)	0.054
5	30.322×4	2272×4	10.5×4 (78.7×4)	0.054
4	35.245×4	2641×4	12.2×4 (91.5×4)	0.054
3	37.009×4	2773×4	12.8×4 (96.1×4)	0.054
2	36.357×4	2724×4	12.6×4 (94.4×4)	0.054
1	24.539×3	1839×3	8.5×3 (63.7×3)	0.054

Note: In the column for the damping coefficients of the AS, the number outside the bracket refers to the values used for the AID, OCS system, while the number in the bracket represents the value used for the TID system.

level is 5.84×10^5 kg (40.0 kips-sec^2/ft). The seismic mass of the above ground levels of the entire structure is 1.11×10^7 kg (760 kips-sec^2/ft). The 20-story building N-S MRF is depicted in Fig. 3.7.

The numerical study will focus on an in-plane analysis of this 20-story structure. The frames considered in the development of the planar, linear model are the N-S MRFs in the short direction of the building. The finite element model for this linear planar structure is obtained using the code listed in Appendix C. The ASs and IEs for AIC control purpose are assumed to be installed in the same N-S frames. To keep the PS vibrating in its original modes as much as possible during the control process, the stiffness of the AS in each story is modulated to be proportional to the corresponding story stiffness of the PS. In this study, the total spring stiffness of the AS in one story is chosen as one-fourth of the

approximate stiffness of the story in which the AS is installed. The AS mass is determined in a way such that the natural period of the AS is 0.054 second. It is worth noting that all these parameters are optimized for this particular 20-story building based on numerical experiments. The details of the AS installed on each floor are given in Table 3.5. The AIC system described above is feasible with consideration of currently available technology. To distribute the large mass demand on AS in one story, several identical ASs are provided in one story so that each AS mass is ranging from 1500 kg to 3000 kg. The arrangement of the AS in the N-S frame of this 20-story building is illustrated in Fig. 3.8.

For computational cost considerations, a static condensation is employed to eliminate all rotational and vertical DOFs from dynamic analysis. It is assumed that the inertias associated with the rotational and vertical DOFs are negligible. Also, a rigid floor assumption is made and therefore only the horizontal DOF corresponding to each floor of the 20-story structure is retained. The accuracy of this reduced-order model has been confirmed by comparing with the elastic results for El Centro ground motion given in Ref. [29].

The first five natural periods of this 20-story structure without AS are 3.83, 1.33, 0.77, 0.55, and 0.42 second, respectively. These values agree quite well with the results from the full-order model. Finally, two-percent modal damping ratios are again assigned to each mode of the linear model.

3.7 Numerical Study and Discussion

In order to evaluate the proposed control algorithms based on numerical simulations, four historical earthquake records are selected: (1) The N-S component of El Centro (ELC) record from the 1940 Imperial Valley earthquake; (2) The N-S component of Hachinohe (HAC) from the 1968 Tokachi-oki earthquake; (3) The N-S component of Sylmar County Hospital (SCH) from the 1994 Northridge earthquake; (4) The N-S component of Kobe (KOB) from the 1995 Hyogo-ken Nanbu earthquake. Among them, ELC and HAC are far-field records, whereas SCH and KOB are near-field records.

In this study, the two Japanese records HAC and KOB are used for the simulation of the 3-story building model which is located in Japan, while the U.S. records ELC and SCH are used for the 9-story and 20-story buildings designed for the Los Angeles, California, region.

In implementing the Modal Control approach, only the first mode is selected as the controlled mode for the 3-story and 9-story buildings. However, to achieve the best control performance, the first four modes are selected as the controlled modes for the 20-story building. All of the higher modes other than the selected controlled modes are neglected in the control algorithms which determine the appropriate operating states for the IEs.

The partitioned predictor-corrector numerical scheme is again used here for numerically integrating the coupled equations of motion of a MDOF AIC system. The control-sampling period is taken to be 0.004 second in this study. With currently available technology, this value is believed to be achievable. However, to achieve further improved control performance, smaller control-sampling periods might be utilized. For accuracy of numerical integration, the control-sampling period is subdivided into many integration-sampling periods. In this study, each control-sampling period is uniformly divided into eight integration-sampling periods except for the three-story model, where a much smaller value is selected for the integration-sampling period because of its small AS natural period. In the simulation of the three-story building model, each control-sampling period is uniformly divided into 40 integration-sampling periods.

To evaluate the proposed control algorithms, the following quantities related to the building responses are defined.

1. Peak inter-story drift ratio:

$$J_1 = \frac{\max_{t,i} \frac{|d_i(t)|}{h_i}}{\delta^{\max}} \tag{3.34}$$

where $d_i(t)$ is the inter-story drift of the ith story over the time history of each earthquake, h_i is the height of each of the associated stories, $\delta_{\max}$ is the maximum inter-story drift ratio of the uncontrolled structure calculated by equation of $\max_{t,i} |d_i(t)/h_i|$.

2. Peak acceleration level:

$$J_2 = \frac{\max_{t,i} |\ddot{x}_{ai}(t)|}{\ddot{x}_a^{\max}} \tag{3.35}$$

where $\ddot{x}_{ai}(t)$ and $\ddot{x}_a^{\max}$ are absolute acceleration of the ith level with and without control devices respectively.

3. Normed inter-story drift ratio:

$$J_3 = \frac{\max_i \frac{\|d_i(t)\|}{h_i}}{\|\delta^{\max}\|} \tag{3.36}$$

where the normed value for $\|\delta^{\max}\| \equiv \max_i \|d_i(t)/h_i\|$ is the maximum normed inter-story drift ratio corresponding to the uncontrolled structure excited by each respective earthquake.

4. Normed acceleration level:

$$J_4 = \frac{\max_i \|\ddot{x}_{ai}(t)\|}{\|\ddot{x}_a^{\max}\|} \tag{3.37}$$

where $\|\ddot{x}_a^{\max}\|$ are the maximum normed absolute acceleration corresponding to the uncontrolled structure excited by each respective earthquake.

The index i in the above expressions falls within the range $i = [1,3]$, $i = [1,9]$, $i = [1,20]$ for the 3-, 9- and 20-story buildings respectively (includes only above ground levels).

The norm, $\|\cdot\|$, is computed using the following equation:

$$\|\cdot\| \equiv \sqrt{\frac{1}{t_f}\int_0^{t_f} [\cdot]^2 \mathrm{d}t} \tag{3.38}$$

and t_f is the duration of the external excitation. The definition for this norm is seen to be the same as the root-mean-square.

3.7.1 The 3-story Building Model

The simulation results for this model are presented in Figs. 3.9 to 3.14 for the Modal Control case. The results for the Nodal Control case are presented in Figs. 3.33 to 3.36. Tables 3.6 and 3.7 list some of the important response quantities of this three-story building model for the Modal Control and Nodal Control case respectively.

CASE 1: Modal Control

In Figs. 3.11 and 3.15, distributions of maximum inter-story drift ratio and absolute acceleration along the building height are plotted. It is observed that the AIC control algorithms in general are capable of greatly reducing the inter-story drift in the PS. However, undesirable large acceleration values are observed to accompany this drift reduction in the AID

Table 3.6: Response of the Three-story Building, Modal Control

		Uncontrolled A/L	Hysteresis Damper	AID	OCS	TID	25% Damping
HAC	J_1	0.3273	0.2123	0.1066	0.2059	0.1719	0.3297
	J_2	1.6202	0.4445	1.0349	1.2037	0.5461	0.3604
	J_3	0.3279	0.1271	0.0735	0.0796	0.0919	0.2173
	J_4	1.6888	0.4080	0.2506	0.3186	0.2810	0.2308
KOB	J_1	0.5012	0.5275	0.1057	0.5014	0.3825	0.4664
	J_2	2.2808	0.7034	1.5344	2.4278	0.5904	0.4842
	J_3	0.4286	0.2066	0.0577	0.1690	0.1510	0.2190
	J_4	2.1889	0.4086	0.2874	0.5118	0.2649	0.2428

Note: A/L = IE always locked; Hysteresis Damper refers to the case in which the only difference with the TID system is that the IE is always locked. 25% Damping refers to the high damping system described in Section 3.7.4.

and OCS systems. Inherent with the AIC control strategy is the fact that by minimizing the relative vibration energy of the PS at each time instant, only displacement and velocity of the PS are directly minimized. However, suppression of inter-story drift and absolute acceleration in seismic events is equally important in the structural control of building structures. The maximum values of the absolute acceleration of the PS in the TID system are clearly reduced, even compared with the uncontrolled response because of its bounded control force level. Also observed is that in the AID and OCS systems, large acceleration values usually occur at the lower floors.

The first story drift time histories of the PS are shown in Figs. 3.9 and 3.13. The effectiveness of the AIC algorithms is once again confirmed. It is also observed that the first story drift value in the OCS system is much larger than those in the AID and TID systems under the KOB ground motion. This can be attributed to the fact that the parameters of the AS in this three-story building is not optimized in order to be consistent with the *actual values of the auxiliary braces in the same building.* The absolute acceleration time histories of the PS at the roof level are shown in Figs. 3.10 and 3.14.

The advantage of the TID system over the other AIC systems is clear from Figs. 3.12 and 3.16, which show the distributions of attachment number, control force, AS displacement relative to its support floor, and AS absolute acceleration along the building height. When additional damping is added to the AS and an upper bound is imposed on the control force level, as is the case in the TID system, the number of attachments for the TID system

Table 3.7: Response of the Three-story Building, Nodal Control

		Uncontrolled A/L	Hysteresis Damper	AID	OCS	TID
HAC	J_1	0.3273	0.2123	0.1233	0.1252	0.2319
	J_2	1.6202	0.4445	1.5395	1.5084	0.7239
	J_3	0.3279	0.1271	0.0807	0.0926	0.1113
	J_4	1.6888	0.4080	0.3201	0.3262	0.2711

Note: A/L = IE always locked; Hysteresis Damper refers to the case in which the only difference with the TID system is that the IE is always locked.

is reduced compared to that of the AID and OCS system. The relatively small value of the control force, AS relative displacement and AS absolute acceleration observed in the TID system are important in practice, which implies less damage to the AS and PS during seismic events and thus less cost in repair and maintenance of the AIC system.

From Figs. 3.11 and 3.15, it is observed that a passive system with Hysteresis Damper is less effective than the AIC systems in reducing the inter-story drift of this building. However, unlike the uncontrolled case with IE always locked, the peak acceleration value at each floor level of this passive system with Hysteresis Damper is very close to that of the TID system and is much smaller than that of the uncontrolled systems. For this particular building, the AID system is most efficient in reducing the inter-story drifts. These observations are also consistent with the data given in Table 3.6.

CASE 2: Nodal Control

The Nodal Control approach has a performance comparable to that of the Modal Control approach. From Fig. 3.35, it is observed that the maximum inter-story drift ratio for the OCS system is further reduced from those in the case of Modal Control approach. However, with this approach also arises the side effect that the attachment number increases by a large amount and absolute accelerations both for the PS and AS are larger than those for the Modal Control approach.

It is observed from both Fig. 3.35 and Table 3.7 that the AID system has a response level similar to that of the OCS system for the Nodal Control case. Also observed is that the peak values of both inter-story drift and acceleration of the passive system with Hysteresis Damper is smaller than those of the TID system under Nodal Control while the normed

responses for the Hysteresis Damper case are larger than those of the TID system.

3.7.2 The 9-story Building Model

It should be noted that the parameters of the ASs considered in this study are optimally selected for this building. The simulation results for this model are presented in Figs. 3.17 to 3.24 for the Modal Control case. The results for the Nodal Control case are presented in Figs. 3.37 to 3.40. Tables 3.8 and 3.9 list some of the important response quantities of this nine-story building model for the Modal Control and Nodal Control case respectively.

CASE 1: Modal Control

From Figs. 3.19 and 3.23, it is seen that the AIC control approaches in general are very effective in controlling the PS's inter-story drift. As in the three-story building model, excessively large acceleration values are also observed here in the AID and OCS systems. This is especially evident in the OCS system. With bounded control force levels, the absolute acceleration values of the PS in the TID system are apparently much smaller than the other AIC systems. It is also observed that in the AID and OCS systems, large acceleration values generally occur at the lower floors of the PS.

The first story drift time histories for the PS are shown in Figs. 3.17 and 3.21. The AIC control algorithms are seen to be more effective in the far-field ground motion (ELC) case than in the near-field ground motion (SCH) case. The absolute acceleration time histories of the PS at the roof level are shown in Figs. 3.10 and 3.14. It is observed that the high-frequency components in the time history waveform for the three-story building model is much weaker in the waveform for this nine-story building model. The relatively large value of the fundamental natural period of this nine-story building model and that only the first mode are targeted for control could be the cause for this effect. It is observed from Table 3.8 that the TID system is very effective in controlling both inter-story drift and acceleration of this nine-story building.

In Figs. 3.20 and 3.24, distributions of attachment number, control force, AS displacement relative to its support floor, and AS absolute acceleration along the building height are plotted. From these figures, we see the advantage of the TID system over the other AIC systems again.

Table 3.8: Response of the Nine-story Building, Modal Control

		Uncontrolled A/L	Hysteresis Damper	AID	OCS	TID	25% Damping
ELC	J_1	0.7540	0.5450	0.4718	0.4284	0.3889	0.3360
	J_2	1.2458	0.7441	0.9856	2.8934	0.7879	0.3839
	J_3	0.7753	0.5079	0.3732	0.2792	0.3223	0.2787
	J_4	1.2781	0.7474	0.5752	1.1440	0.4003	0.2106
SCH	J_1	0.9223	0.8390	0.6281	0.5865	0.6136	0.4594
	J_2	1.3114	0.9541	1.9479	3.2226	0.9157	0.4015
	J_3	0.5910	0.4720	0.2281	0.2003	0.2649	0.2934
	J_4	0.9618	0.6487	0.4664	0.9244	0.3781	0.2606

Note: A/L = IE always locked; Hysteresis Damper refers to the case in which the only difference with the TID system is that the IE is always locked. 25% Damping refers to the high damping system described in Section 3.7.4.

From Table 3.8, it is again observed that a passive system with Hysteresis Damper is better than the uncontrolled system with IE always locked. However, this passive system with Hysteresis Damper is less effective in controlling inter-story drift than the AIC systems. Although the peak acceleration values of this passive system with Hysteresis Damper are close to those of the TID system, its normed acceleration values are much larger than those of the TID system.

CASE 2: Nodal Control

The results for the Nodal Control case are presented in Figs. 3.37 to 3.40 and Table 3.9. In this nine-story building model, the Nodal Control approach has a slightly lower performance than the Modal Control approach. It is also observed that more high-frequency components emerge in the wave form with the Nodal Control approach. This can also be verified by large value of the attachment number with this approach.

3.7.3 The 20-story Building Model

It should be noted that the parameters of the AS considered in this study are optimally selected for this building. The simulation results for this model are presented in Figs. 3.25 to 3.32 for the modal control case. The results for the nodal control case are presented in Figs. 3.41 to 3.44. Tables 3.10 and 3.11 list some of the important response quantities of this 20-story building model for the Modal Control and Nodal Control case respectively.

Table 3.9: Response of the Nine-story Building, Nodal Control

		Uncontrolled A/L	Hysteresis Damper	AID	OCS	TID
ELC	J_1	0.7540	0.5450	0.4548	0.4824	0.5001
	J_2	1.2458	0.7441	1.5212	1.7247	1.3058
	J_3	0.7753	0.5079	0.3312	0.3880	0.3859
	J_4	1.2781	0.7474	0.4109	0.9368	0.4277

Note: A/L = IE always locked; Hysteresis Damper refers to the case in which the only difference with the TID system is that the IE is always locked.

Table 3.10: Response of the 20-story Building, Modal Control

		Uncontrolled A/L	Hysteresis Damper	AID	OCS	TID	25% Damping
ELC	J_1	1.3826	0.8859	0.6180	0.5341	0.5882	0.3513
	J_2	1.4061	0.9415	3.2273	3.7344	1.3826	0.5433
	J_3	2.2006	0.8693	0.4827	0.4194	0.5018	0.3905
	J_4	1.8140	1.0447	1.3460	2.2461	0.8780	0.4227
SCH	J_1	1.1407	0.7378	1.0333	0.8740	0.8066	0.4455
	J_2	1.3580	0.8970	3.0492	4.7471	1.2237	0.5225
	J_3	1.3515	0.5396	0.3992	0.3926	0.5068	0.3077
	J_4	1.3788	0.6398	1.1396	1.7684	0.5854	0.3223

Note: A/L = IE always locked; Hysteresis Damper refers to the case in which the only difference with the TID system is that the IE is always locked. 25% Damping refers to the high damping system described in Section 3.7.4.

CASE 1: Modal Control

Because of the substantial contribution to the inter-story drift from the higher modes in this 20-story building model, a control scheme based on controlling only the first mode would not yield satisfactory results. Even with wave propagation behavior complicating the response of this tall structure (pulse-like response is pronounced in the first-mode displacement time history for the first eight seconds), the modal response still concentrates in the first four modes. The Modal Control approach should be capable of controlling the inter-story drift values of the PS if the first four modes are selected as the controlled modes.

From Figs. 3.27 and 3.31, we see that the AIC control algorithms are generally effective in suppressing the inter-story drift of the PS subjected to both far-field and near-field ground motions. However, undesirable large accelerations are observed to occur in the PS of the AID and OCS systems, while the maximum absolute acceleration values of the PS in the

TID system are slightly larger than that in the uncontrolled system.

As mentioned before, the TID system differs from the AID and OCS systems by the fact that in the TID system, additional viscous damping is added to the ASs and an upper bound is imposed on the control force developed within the IEs. The advantage of the TID system over the other AIC algorithms is once again corroborated in view of the maximum control force and number of attachments. The number of attachments is defined as the number of attachments between the PS and AS during the excitation duration. An excessively high number of attachments may cause infeasible mechanical requirements and may deteriorate the control performance. The relatively small value of the control force observed in the TID system is also important in practical application, as it means less damage to the AS and PS during seismic events and thus less cost in repair and maintenance of the AIC system.

It is observed from Table 3.10 that although for the ELC ground motion case the peak inter-story drift value of the passive system with Hysteresis Damper is larger than that of the TID system, an opposite behavior is observed for the SCH ground motion case. The peak acceleration values of the passive system with Hysteresis Damper are smaller than those of the TID system for both ground motion cases although its normed acceleration values are larger than those of the TID system.

CASE 2: Nodal Control

The Nodal Control approach has a performance worse than that of the Modal Control approach in terms of inter-story drift reduction capability. However, it is also observed that the acceleration responses for the Nodal Control case is smaller than those for the corresponding Modal Control case. With this approach also arises the bad effect of high-frequency lock/unlock cycles with the control devices. The attachment number increases by a large amount for the AID and OCS systems. Large absolute accelerations also occur both in the PS and AS.

It is observed from Table 3.11 that except for the peak acceleration level J_2, all other response quantities for the passive system with Hysteresis Damper are larger than those of the TID system.

Table 3.11: Response of the 20-story Building, Nodal Control

		Uncontrolled A/L	Hysteresis Damper	AID	OCS	TID
ELC	J_1	1.3826	0.8859	0.5632	0.7414	0.6003
	J_2	1.4061	0.9415	1.8986	2.1923	1.2975
	J_3	*2.2006*	*0.8693*	*0.5611*	*0.6516*	*0.5936*
	J_4	1.8140	1.0447	0.9330	1.7232	0.7569

Note: A/L = IE always locked; Hysteresis Damper refers to the case in which the only difference with the TID system is that the IE is always locked.

3.7.4 The High Viscous Damping System

A series of viscous dampers are placed at each story along the building height. Therefore, the damping matrix is tri-diagonal. It is further assumed that the damping matrix is proportional to the stiffness matrix so the damping is of Rayleigh type. The constant of proportionality is determined such that the first modal damping ratio, ζ_1, is equal to 25%. This damping ratio is calibrated through free vibration test.

The results of the numerical study are presented in Tables 3.6, 3.8, 3.10, and Figs. 3.11, 3.12, 3.15, 3.16, 3.19, 3.20, 3.23, 3.24, 3.27, 3.28, 3.31, 3.32 for three building cases (in thick solid lines).

Three conclusions can be drawn from the tables and figures:

1. The system with high viscous damping ($\zeta_1 = 25\%$) performs better in the tall building case than in the low-rise building case. In the three-story building case, both peak and normed values of the inter-story drift ratio are much higher than those for the AIC systems; However, the acceleration response of the system with high viscous damping are the smallest among all passive and semi-active systems.

2. *The performance of the system with high viscous damping are better when subjected* to earthquake ground motion of large ampiltude (e.g., KOB and SCH).

3. In the 20-story building case, the forces developed within the viscous dampers are much higher than the control forces in the TID system. However, in the three-story building case, their peak values are similar.

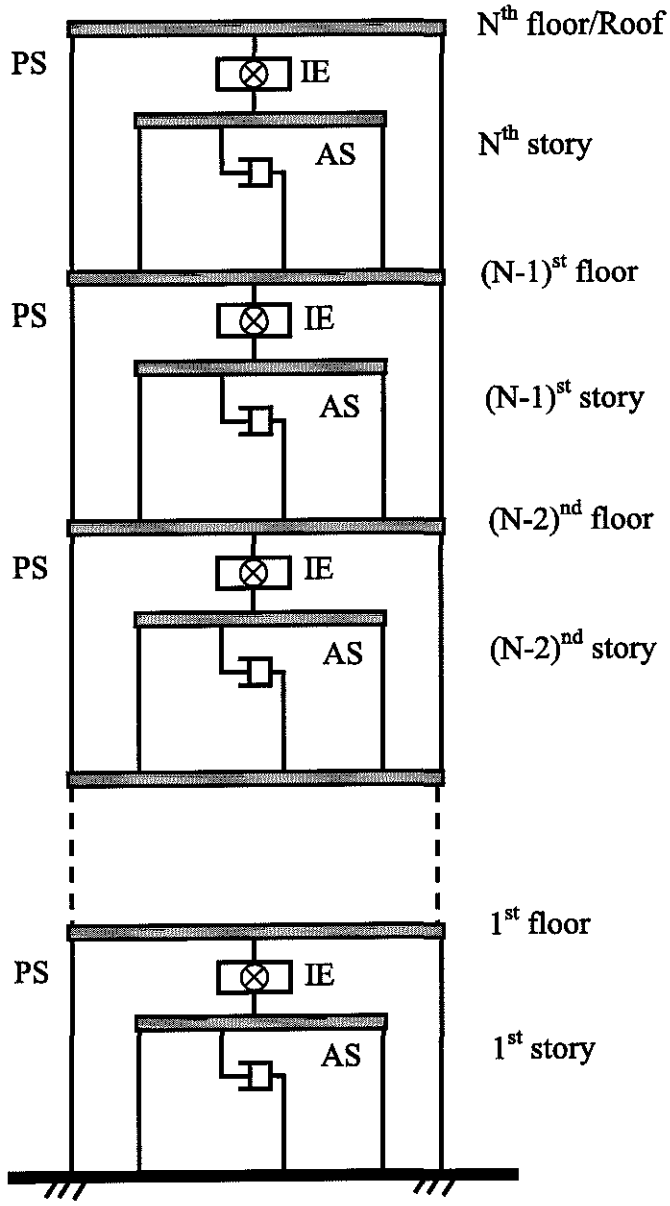

Figure 3.1: Schematic of a MDOF AIC System Model

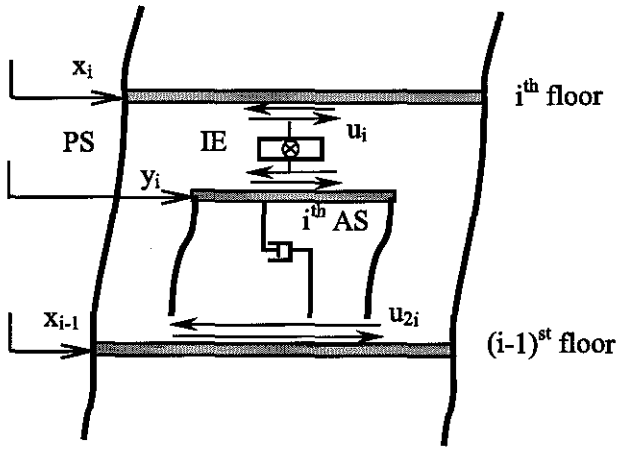

Figure 3.2: Location and Positive Directions of Control Forces $u_i(t)$ and $u_{2,i}(t)$

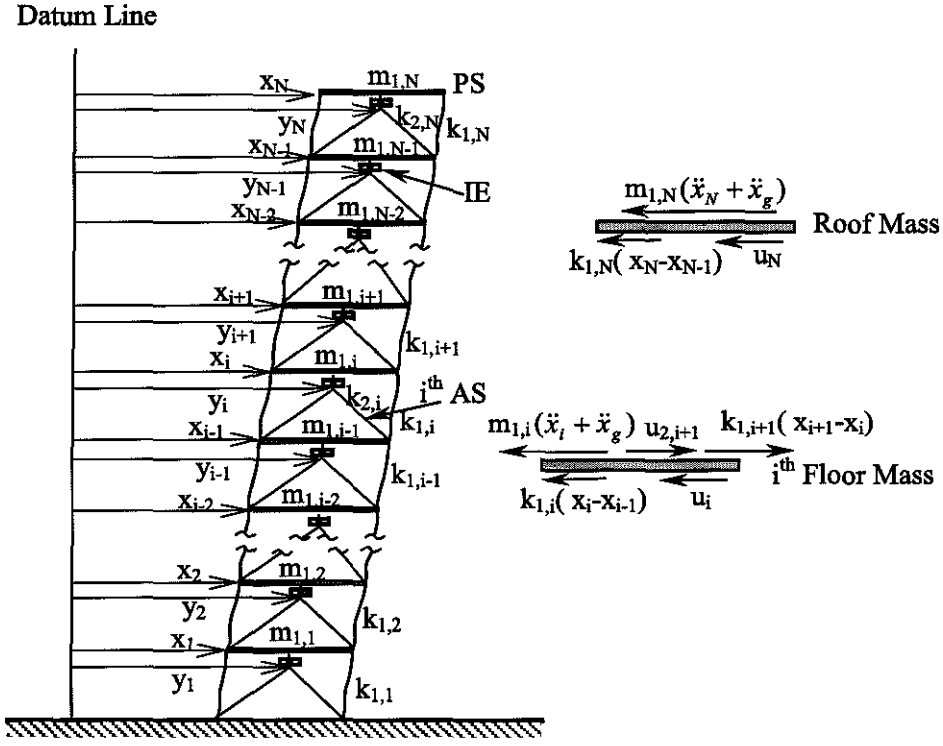

Figure 3.3: Free Body Diagrams of Lumped Mass Nodes in a MDOF Structure

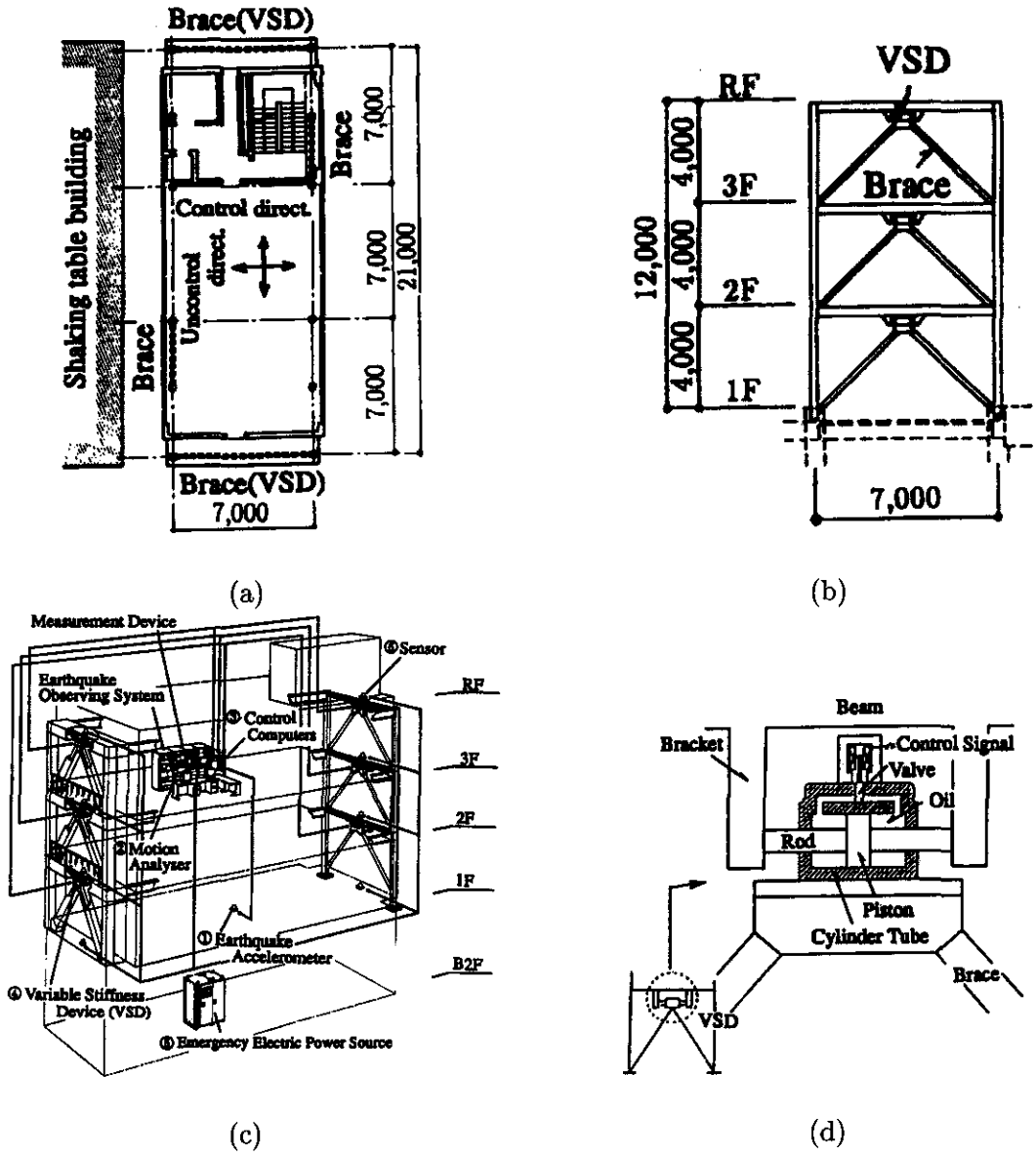

Figure 3.4: Outline of the Three-story Control Building: (a) Typical Floor Plan; (b) Transverse Section; (c) Control System Layout; (d) Variable Stiffness Device (VSD) (reprinted from reference [24])

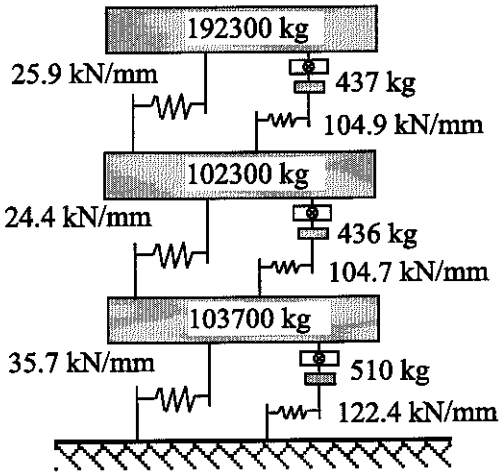

Figure 3.5: Analytical Model of the Three-story Building Model

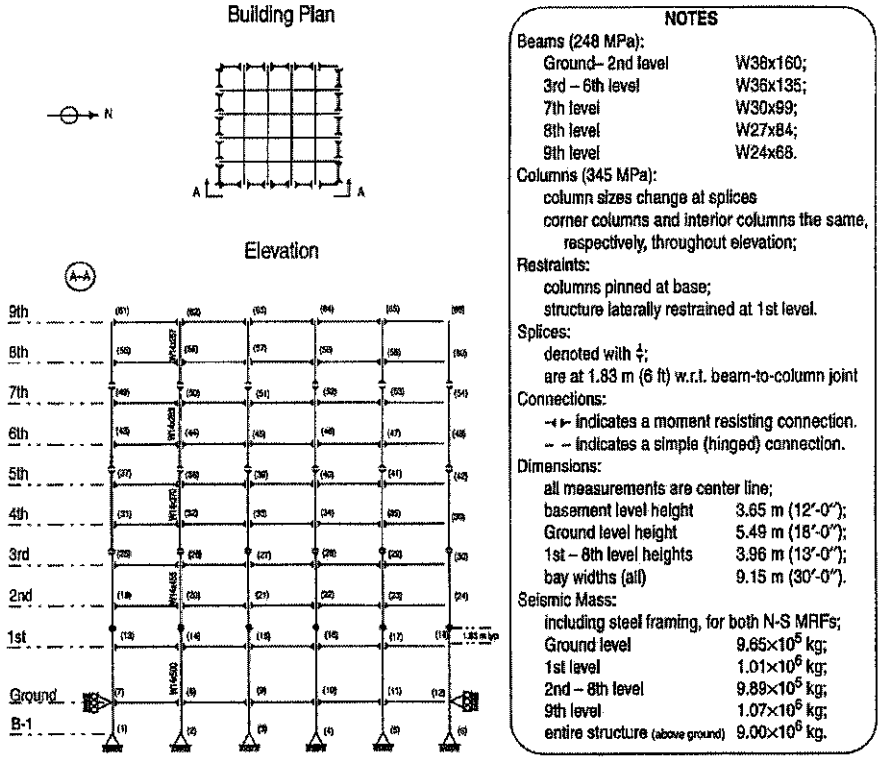

Figure 3.6: Outline of the Nine-story Control Benchmark Building Model (reprinted from Ref. [29])

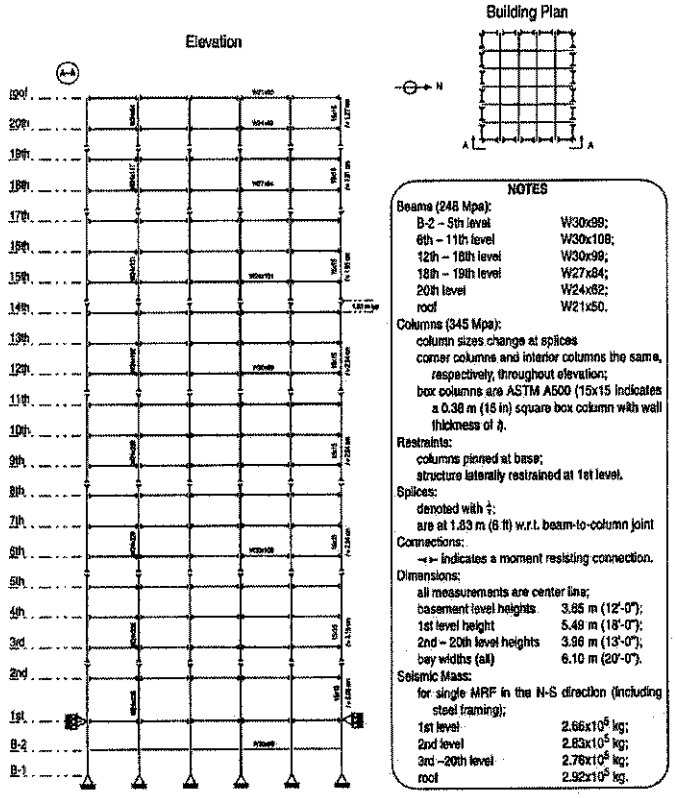

Figure 3.7: Outline of the 20-story Control Benchmark Building Model (reprinted from Ref. [29])

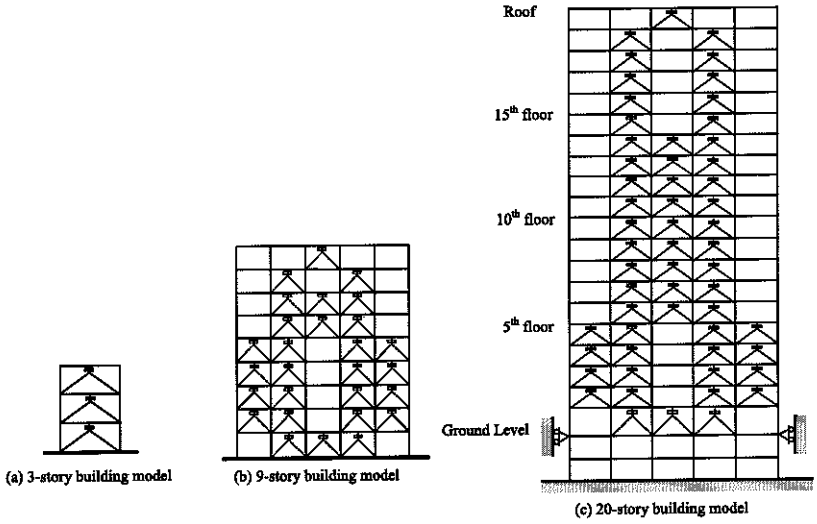

Figure 3.8: Schematics of the Arrangement of the AS in the Building Models

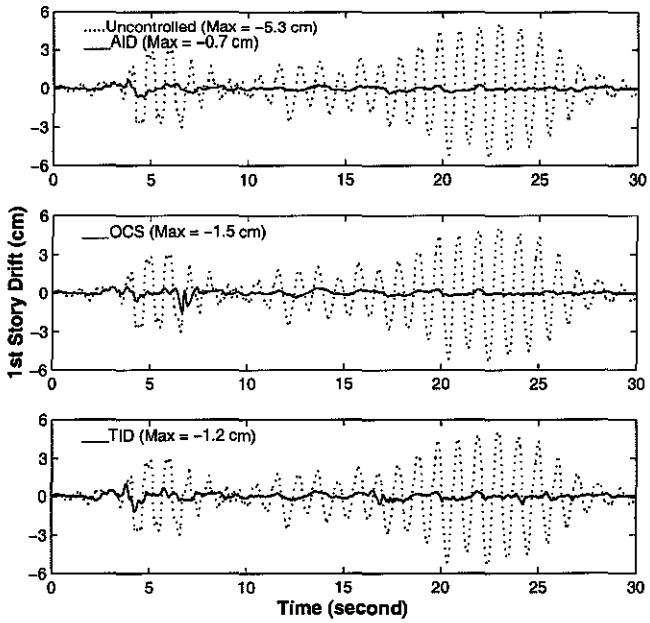

Figure 3.9: First Story Drift Time Histories of the Three-story Building Controlled by the AID, OCS and TID Algorithms Respectively, Under the HAC Ground Motion, Modal Control

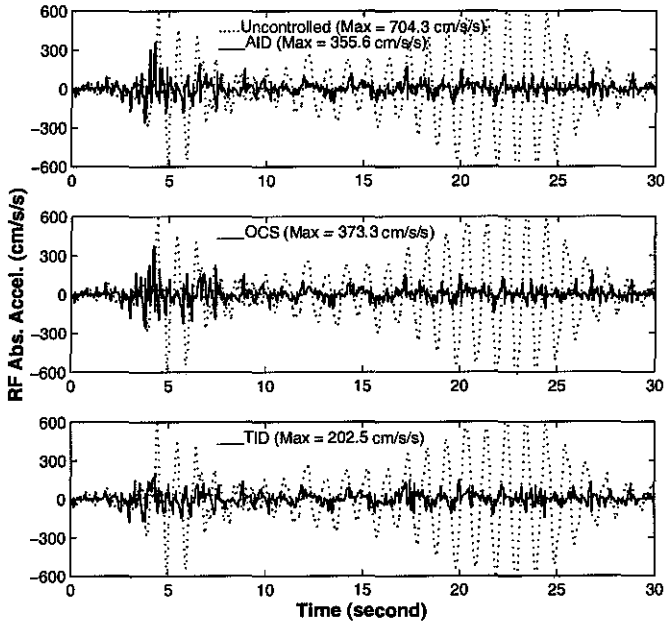

Figure 3.10: Roof Level Absolute Acceleration Time Histories of the Three-story Building Controlled by the AID, OCS and TID Algorithms Respectively, Under the HAC Ground Motion, Modal Control

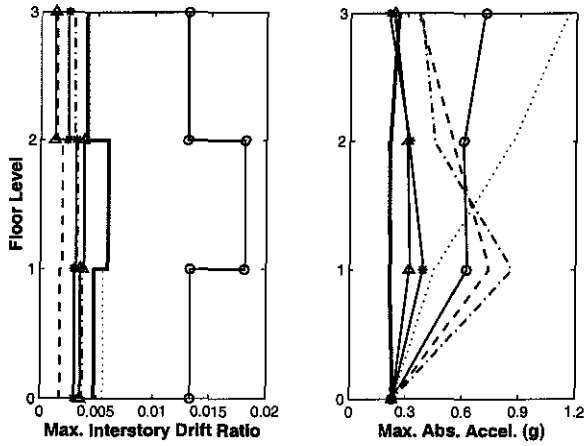

Figure 3.11: Distribution of (a) Maximum Interstory Drift Ratio, (b) Maximum Absolute Acceleration in the Three-story Building Under the HAC Ground Motion, Modal Control (–o– uncontrolled with IE always unlocked, ··· uncontrolled with IE always locked, - - - AID, - · - · OCS, -*- TID, -△- Hysteresis Damper, thick — 25% Damping)

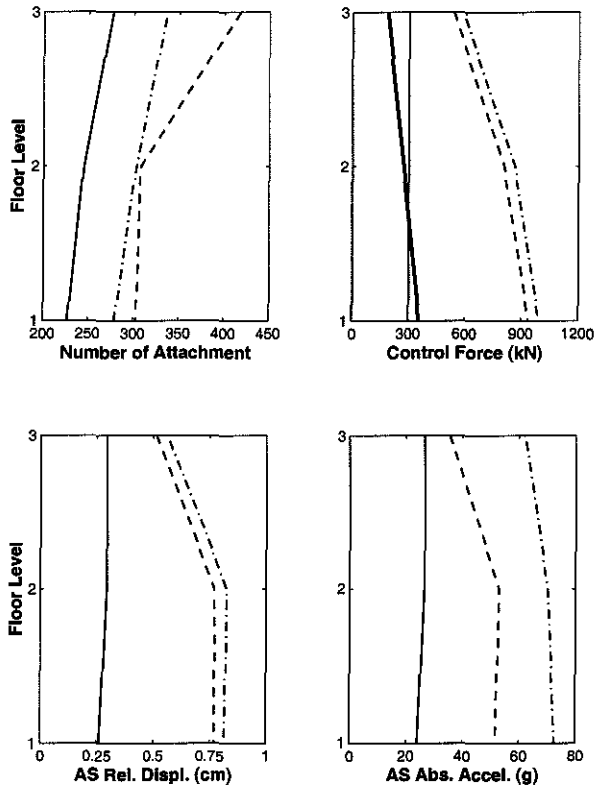

Figure 3.12: Distribution of (a) Number of Attachment, (b) Control Force, (c) AS Displacement Relative to the Support Floor, (d) AS Absolute Acceleration in the Three-story Building Under the HAC Ground Motion, Modal Control (- - - AID, - · - · OCS, — TID, thick — 25% Damping)

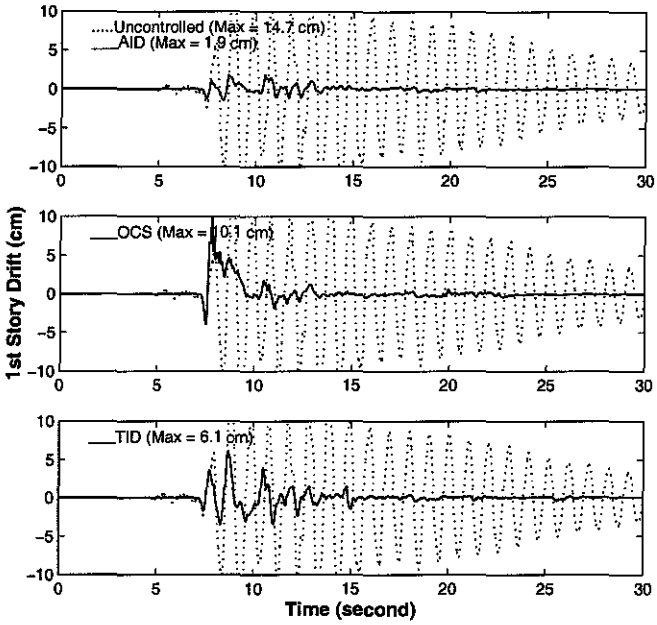

Figure 3.13: First Story Drift Time Histories of the Three-story Building Controlled by the AID, OCS and TID Algorithms Respectively, Under the KOB Ground Motion, Modal Control

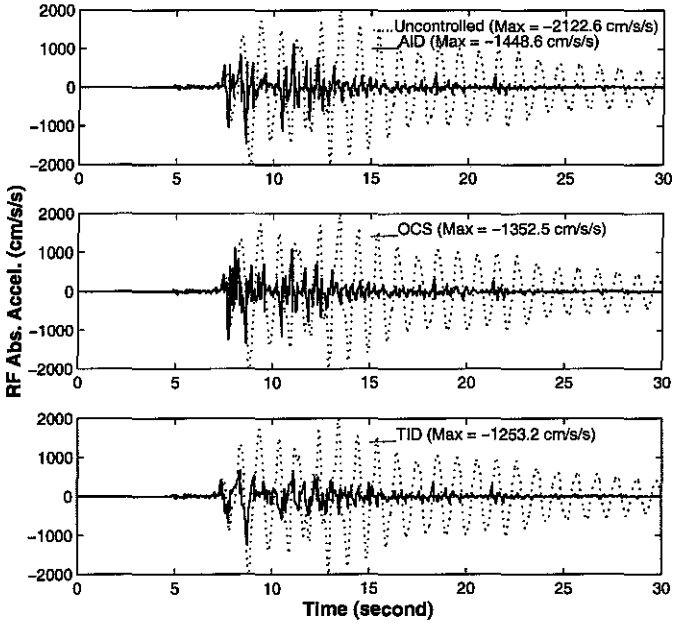

Figure 3.14: Roof Level Absolute Acceleration Time Histories of the Three-story Building Controlled by the AID, OCS and TID Algorithms Respectively, Under the KOB Ground Motion, Modal Control

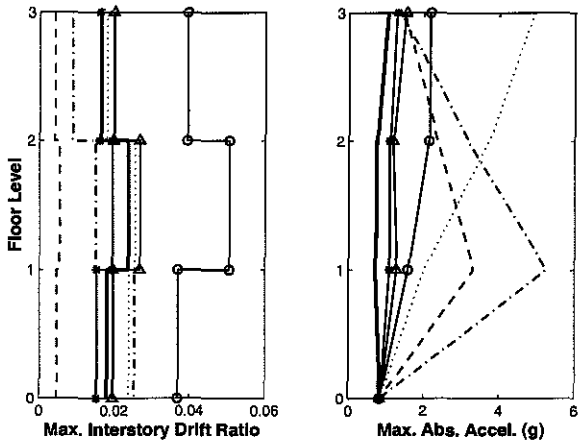

Figure 3.15: Distribution of (a) Maximum Interstory Drift Ratio, (b) Maximum Absolute Acceleration in the Three-story Building Under the KOB Ground Motion, Modal Control (–o– uncontrolled with IE always unlocked, ··· uncontrolled with IE always locked, - - - AID, - · - · OCS, -∗- TID, -△- Hysteresis Damper, thick — 25% Damping)

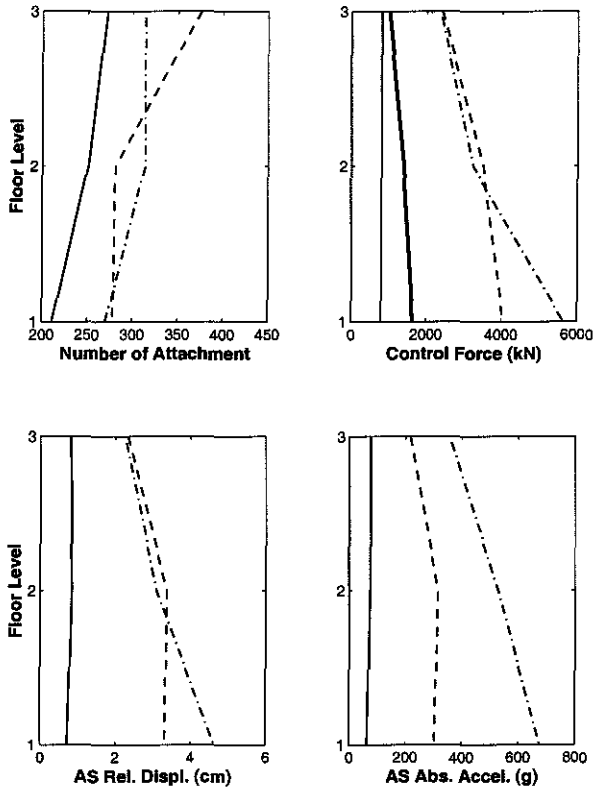

Figure 3.16: Distribution of (a) Number of Attachment, (b) Control Force, (c) AS Displacement Relative to the Support Floor, (d) AS Absolute Acceleration in the Three-story Building Under the KOB Ground Motion, Modal Control (- - - AID, - · - · OCS, — TID, thick — 25% Damping)

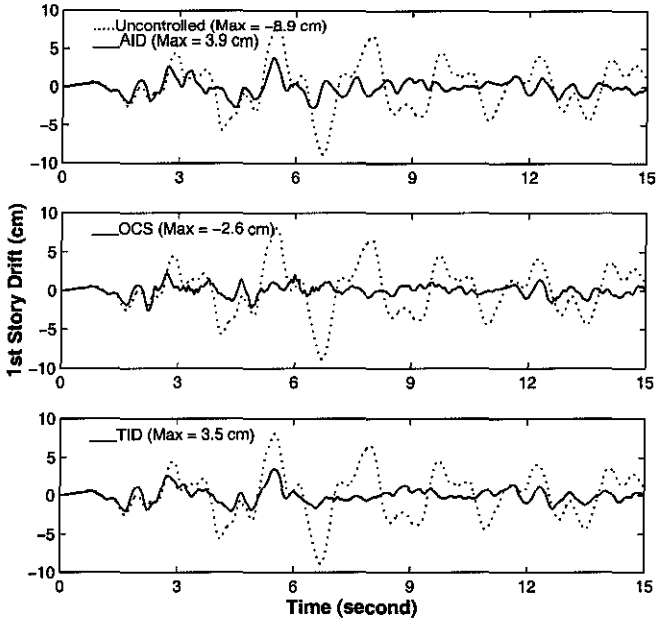

Figure 3.17: First Story Drift Time Histories of the Nine-story Building Controlled by the AID, OCS and TID Algorithms Respectively, Under the ELC Ground Motion, Modal Control

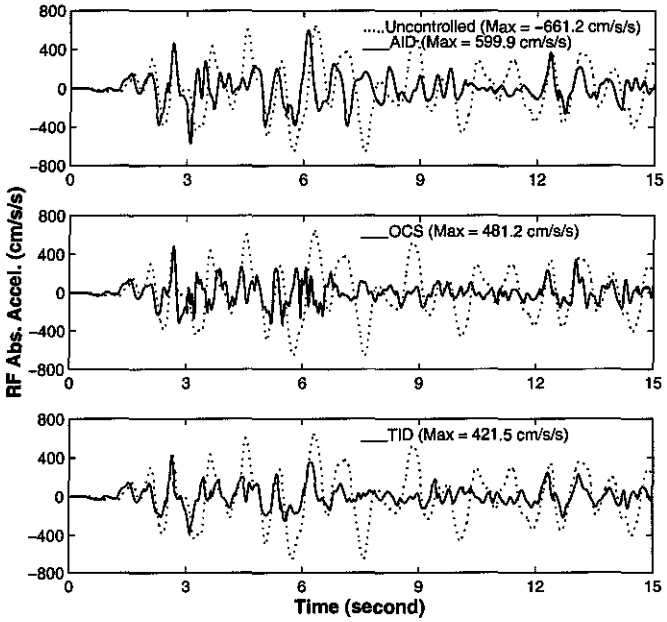

Figure 3.18: Roof Level Absolute Acceleration Time Histories of the Nine-story Building Controlled by the AID, OCS and TID Algorithms Respectively, Under the ELC Ground Motion, Modal Control

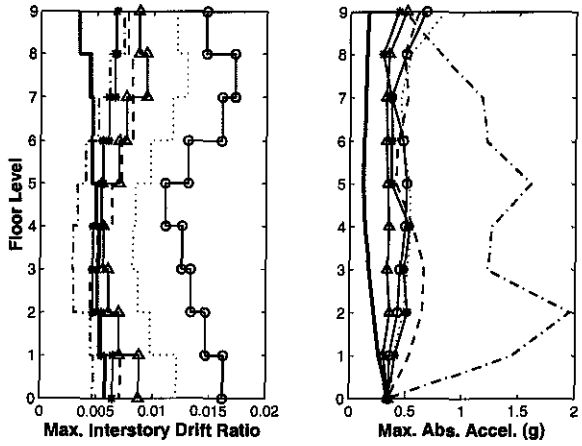

Figure 3.19: Distribution of (a) Maximum Interstory Drift Ratio, (b) Maximum Absolute Acceleration in the Nine-story Building Under the ELC Ground Motion, Modal Control (–o– uncontrolled with IE always unlocked, ··· uncontrolled with IE always locked, - - - AID, - · - · OCS, -∗- TID, -△- Hysteresis Damper, thick — 25% Damping)

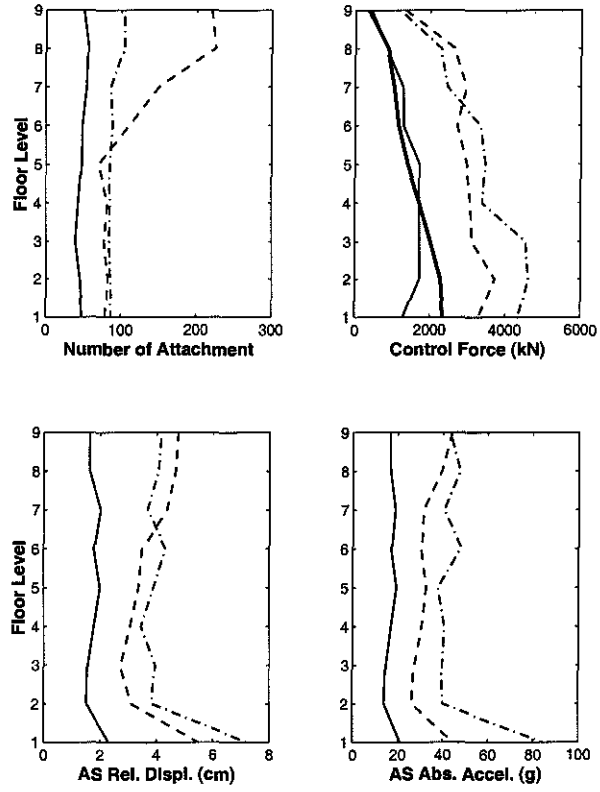

Figure 3.20: Distribution of (a) Number of Attachment, (b) Control Force, (c) AS Displacement Relative to the Support Floor, (d) AS Absolute Acceleration in the Nine-story Building Under the ELC Ground Motion, Modal Control (- - - AID, - · - · OCS, — TID, thick — 25% Damping)

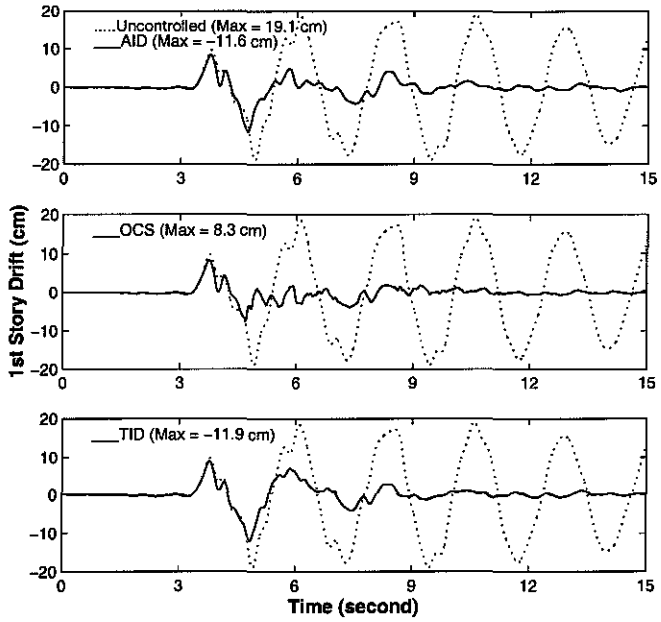

Figure 3.21: First Story Drift Time Histories of the Nine-story Building Controlled by the AID, OCS and TID Algorithms Respectively, Under the SCH Ground Motion, Modal Control

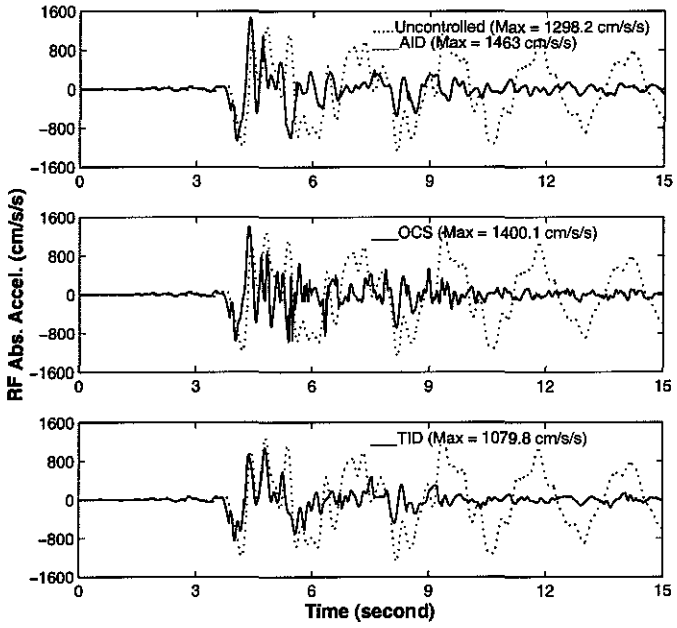

Figure 3.22: Roof Level Absolute Acceleration Time Histories of the Nine-story Building Controlled by the AID, OCS and TID Algorithms Respectively, Under the SCH Ground Motion, Modal Control

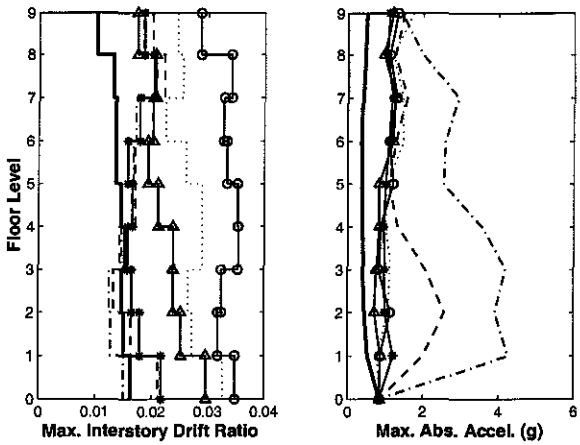

Figure 3.23: Distribution of (a) Maximum Interstory Drift Ratio, (b) Maximum Absolute Acceleration in the Nine-story Building Under the SCH Ground Motion, Modal Control (–o– uncontrolled with IE always unlocked, ··· uncontrolled with IE always locked, - - - AID, - · - · OCS, -*- TID, -△- Hysteresis Damper, thick — 25% Damping)

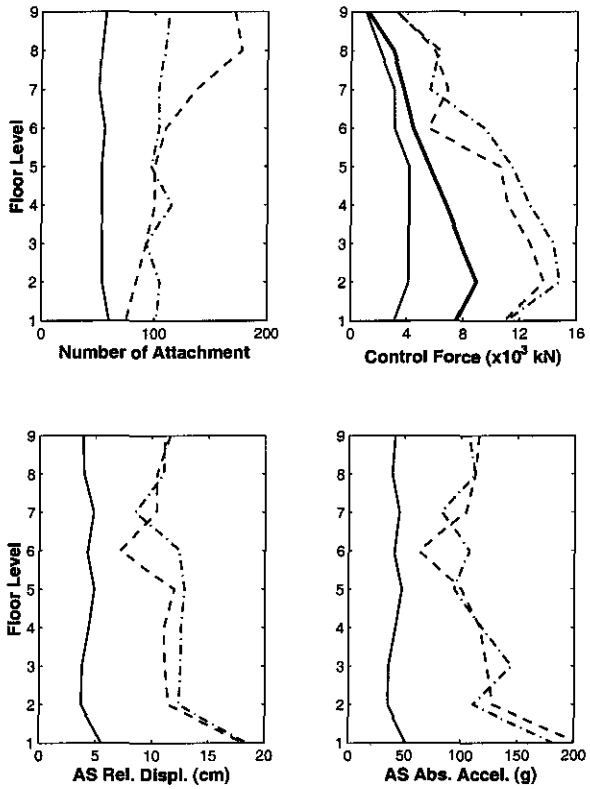

Figure 3.24: Distribution of (a) Number of Attachment, (b) Control Force, (c) AS Displacement Relative to the Support Floor, (d) AS Absolute Acceleration in the Nine-story Building Under the SCH Ground Motion, Modal Control (- - - AID, - · - · OCS, — TID, thick — 25% Damping)

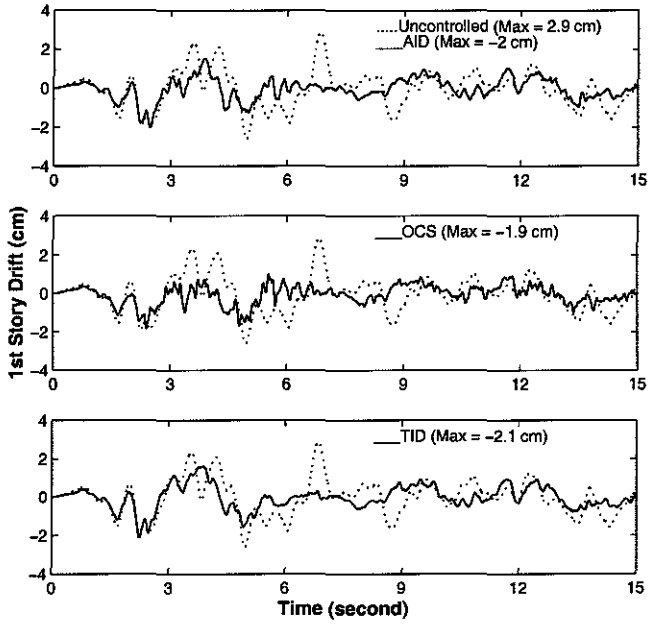

Figure 3.25: First Story Drift Time Histories of the 20-story Building Controlled by the AID, OCS and TID Algorithms Respectively, Under the ELC Ground Motion, Modal Control

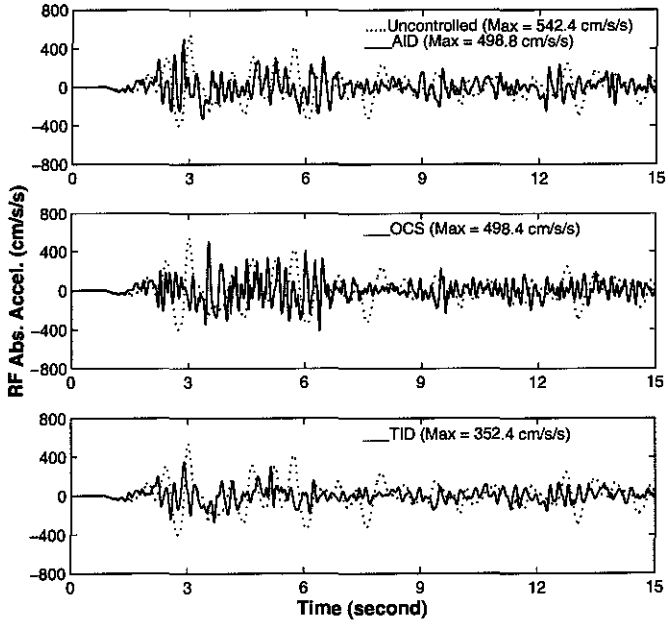

Figure 3.26: Roof Level Absolute Acceleration Time Histories of the 20-story Building Controlled by the AID, OCS and TID Algorithms Respectively, Under the ELC Ground Motion, Modal Control

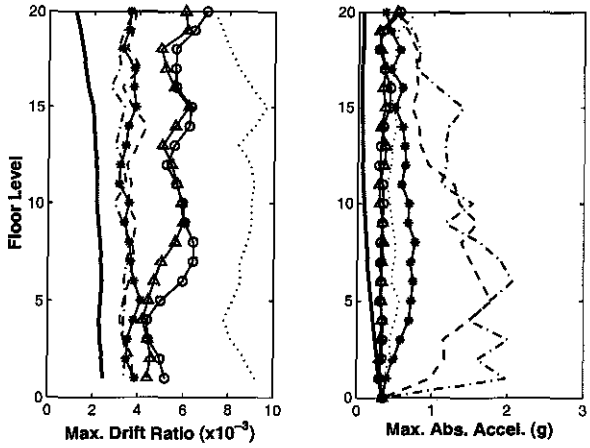

Figure 3.27: Distribution of (a) Maximum Interstory Drift Ratio, (b) Maximum Absolute Acceleration in the 20-story Building Under the ELC Ground Motion, Modal Control (–o– uncontrolled with IE always unlocked, ··· uncontrolled with IE always locked, - - - AID, - · - · OCS, -∗- TID, -△- Hysteresis Damper, thick — 25% Damping)

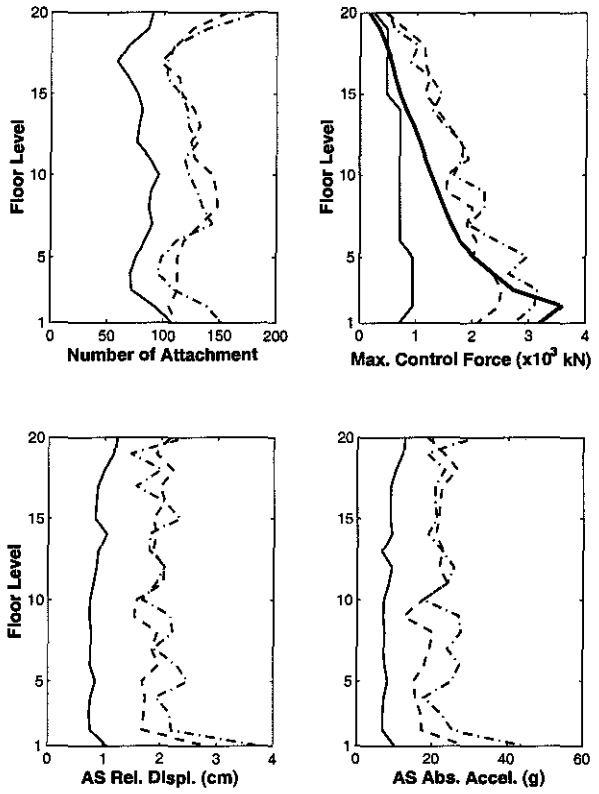

Figure 3.28: Distribution of (a) Number of Attachment, (b) Control Force, (c) AS Displacement Relative to the Support Floor, (d) AS Absolute Acceleration in the 20-story Building Under the ELC Ground Motion, Modal Control (- - - AID, - · - · OCS, — TID, thick — 25% Damping)

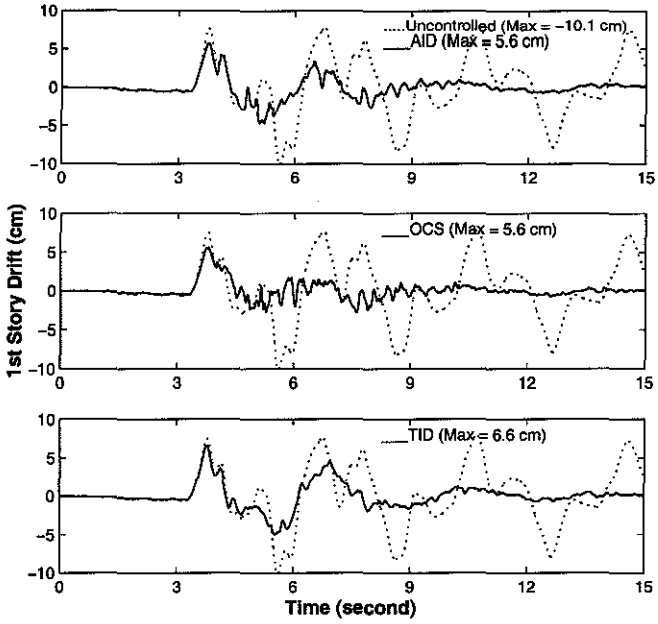

Figure 3.29: First Story Drift Time Histories of the 20-story Building Controlled by the AID, OCS and TID Algorithms Respectively, Under the SCH Ground Motion, Modal Control

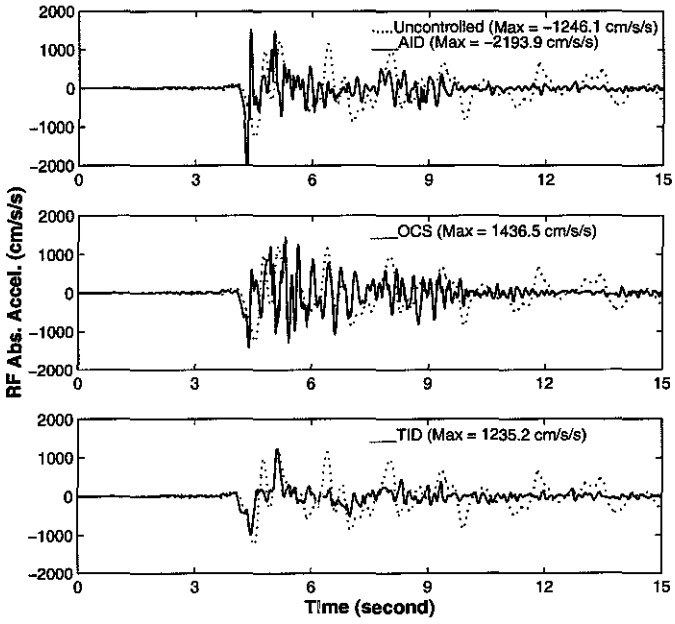

Figure 3.30: Roof Level Absolute Acceleration Time Histories of the 20-story Building Controlled by the AID, OCS and TID Algorithms Respectively, Under the SCH Ground Motion, Modal Control

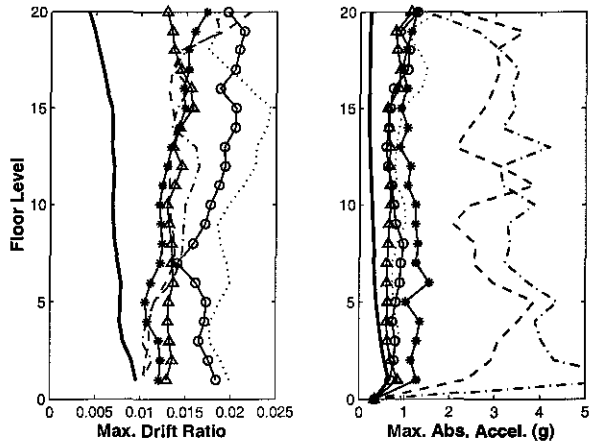

Figure 3.31: Distribution of (a) Maximum Interstory Drift Ratio, (b) Maximum Absolute Acceleration in the 20-story Building Under the SCH Ground Motion, Modal Control (–○– uncontrolled with IE always unlocked, ··· uncontrolled with IE always locked, - - - AID, - · - · OCS, -∗- TID, -△- Hysteresis Damper, thick — 25% Damping)

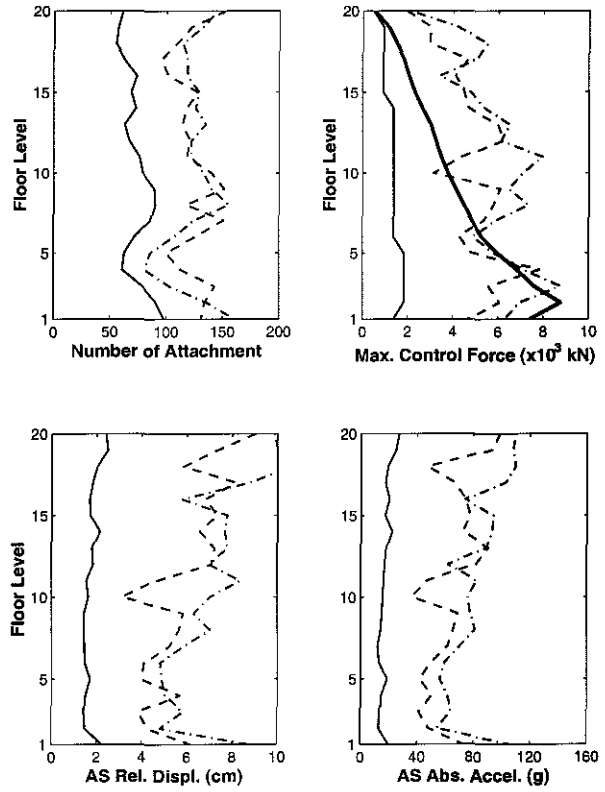

Figure 3.32: Distribution of (a) Number of Attachment, (b) Control Force, (c) AS Displacement Relative to the Support Floor, (d) AS Absolute Acceleration in the 20-story Building Under the SCH Ground Motion, Modal Control (- - - AID, - · - · OCS, — TID, thick — 25% Damping)

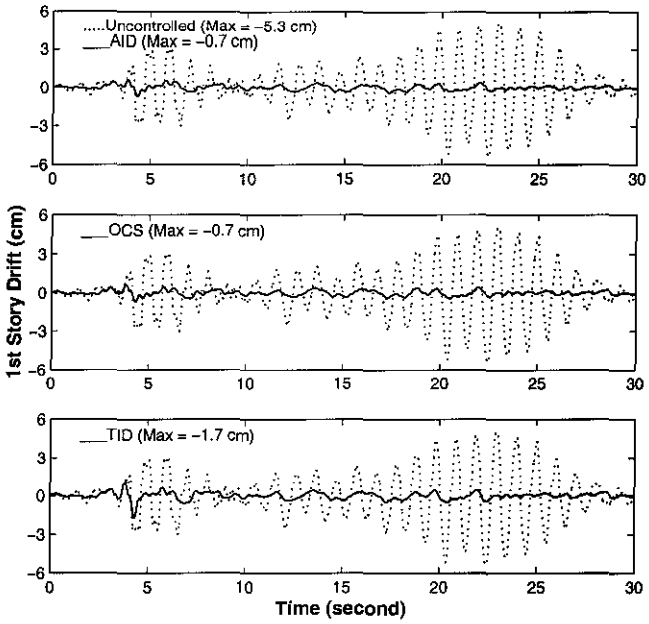

Figure 3.33: First Story Drift Time Histories of the Three-story Building Controlled by the AID, OCS and TID Algorithms Respectively, Under the HAC Ground Motion, Nodal Control

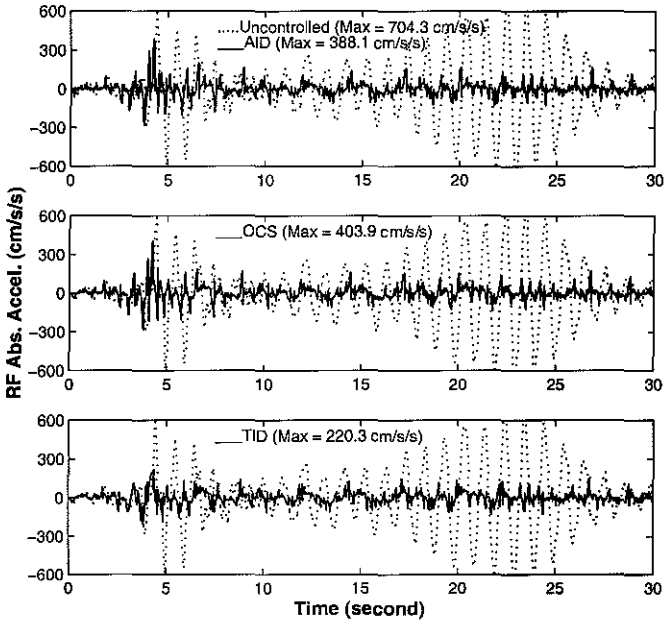

Figure 3.34: Roof Level Absolute Acceleration Time Histories of the Three-story Building Controlled by the AID, OCS and TID Algorithms Respectively, Under the HAC Ground Motion, Nodal Control

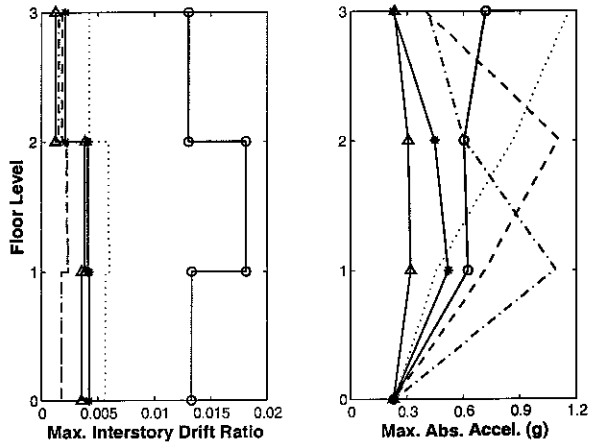

Figure 3.35: Distribution of (a) Maximum Interstory Drift Ratio, (b) Maximum Absolute Acceleration in the Three-story Building Under the HAC Ground Motion, Nodal Control (–o– uncontrolled with IE always unlocked, ··· uncontrolled with IE always locked, - - - AID, - · - · OCS, -∗- TID, -△- Hysteresis Damper)

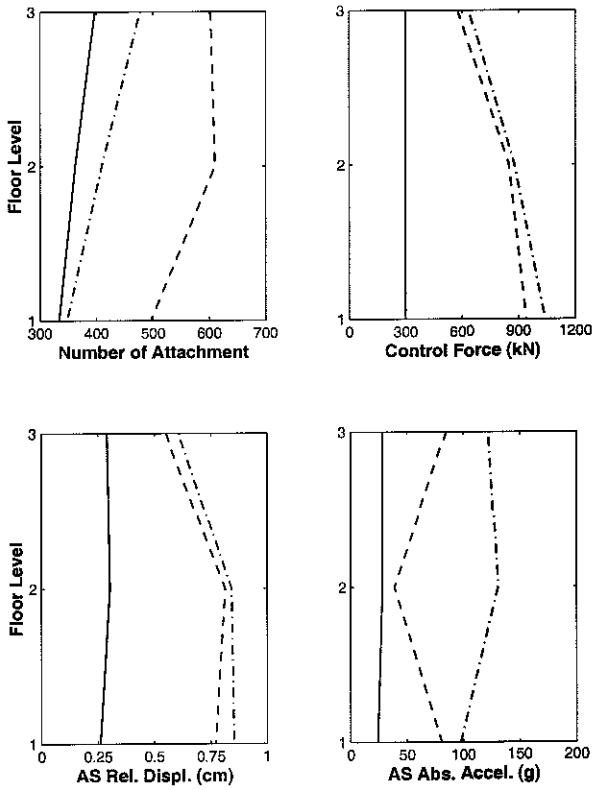

Figure 3.36: Distribution of (a) Number of Attachment, (b) Control Force, (c) AS Displacement Relative to the Support Floor, (d) AS Absolute Acceleration in the Three-story Building Under the HAC Ground Motion, Nodal Control (- - - AID, - · - · OCS, — TID)

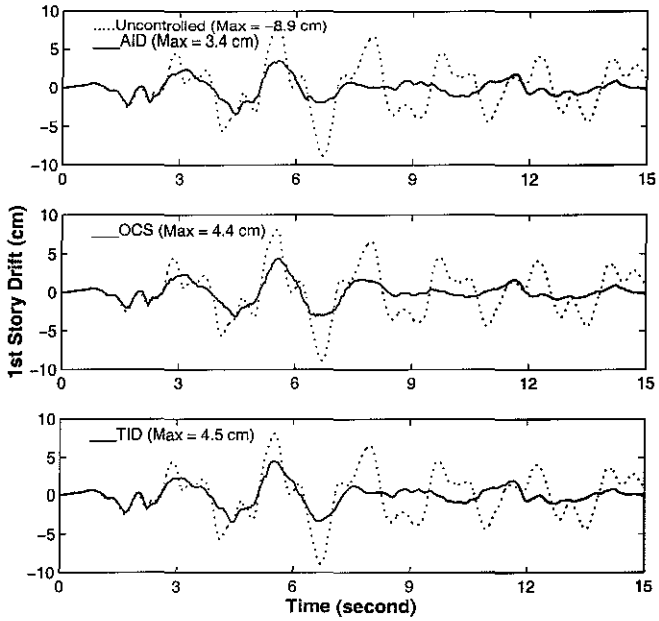

Figure 3.37: First Story Drift Time Histories of the Nine-story Building Controlled by the AID, OCS and TID Algorithms Respectively, Under the ELC Ground Motion, Nodal Control

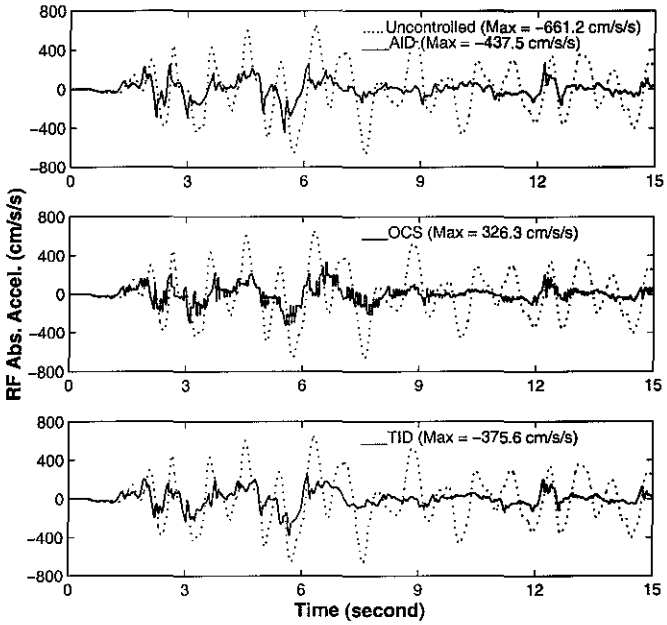

Figure 3.38: Roof Level Absolute Acceleration Time Histories of the Nine-story Building Controlled by the AID, OCS and TID Algorithms Respectively, Under the ELC Ground Motion, Nodal Control

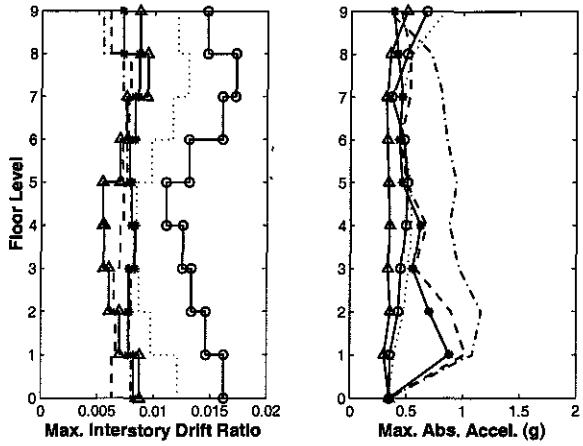

Figure 3.39: Distribution of (a) Maximum Interstory Drift Ratio, (b) Maximum Absolute Acceleration in the Nine-story Building Under the ELC Ground Motion, Nodal Control (–o– uncontrolled with IE always unlocked, ··· uncontrolled with IE always locked, - - - AID, - · - · OCS, -∗- TID, -△- Hysteresis Damper)

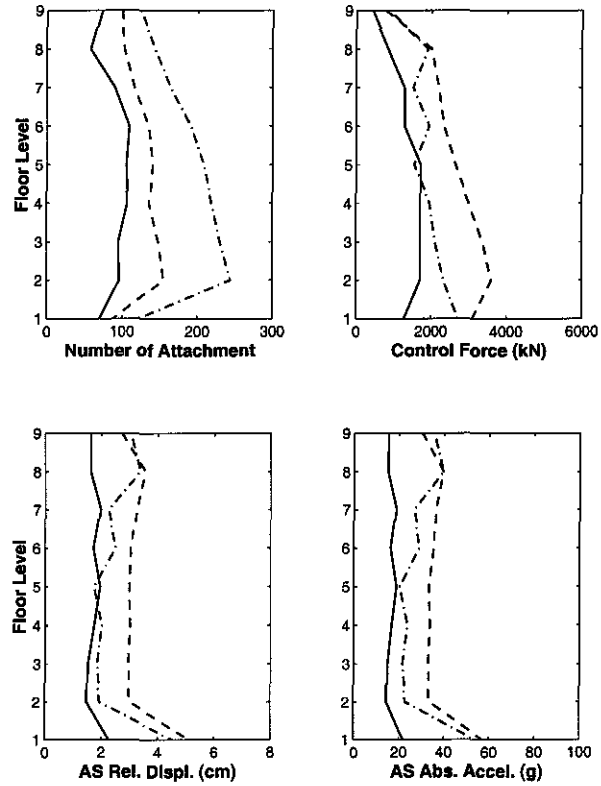

Figure 3.40: Distribution of (a) Number of Attachment, (b) Control Force, (c) AS Displacement Relative to the Support Floor, (d) AS Absolute Acceleration in the Nine-story Building Under the ELC Ground Motion, Nodal Control (- - - AID, - · - · OCS, — TID)

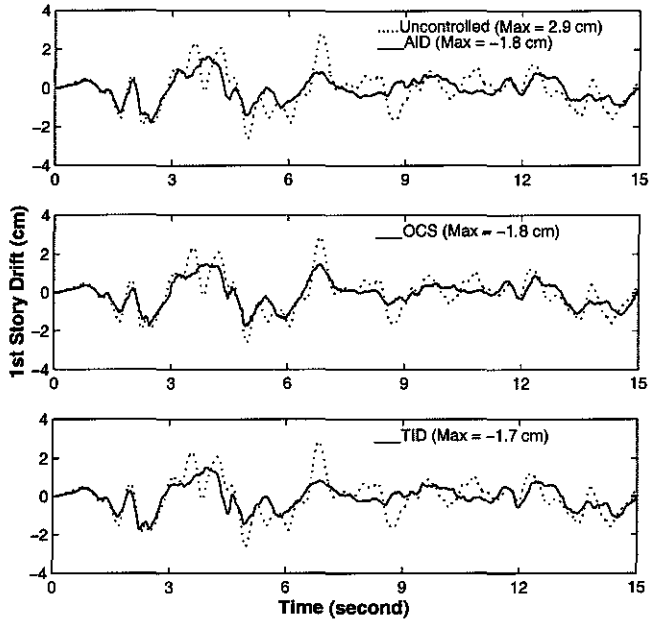

Figure 3.41: First Story Drift Time Histories of the 20-story Building Controlled by the AID, OCS and TID Algorithms Respectively, Under the ELC Ground Motion, Nodal Control

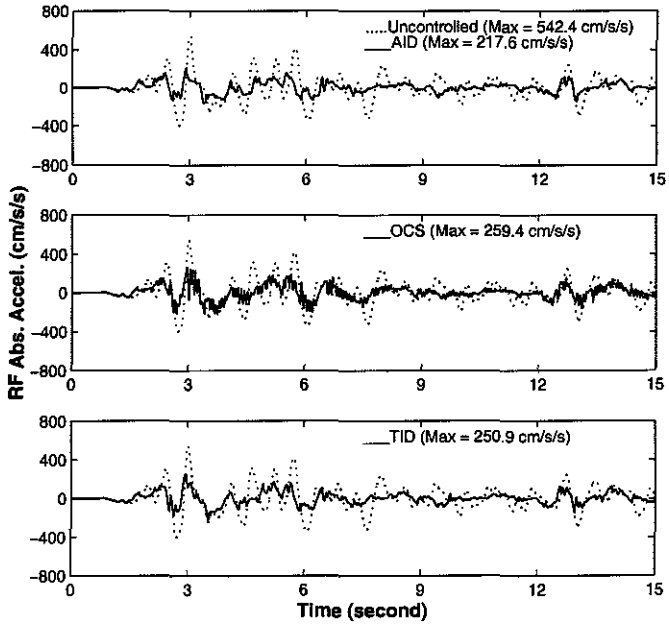

Figure 3.42: Roof Level Absolute Acceleration Time Histories of the 20-story Building Controlled by the AID, OCS and TID Algorithms Respectively, Under the ELC Ground Motion, Nodal Control

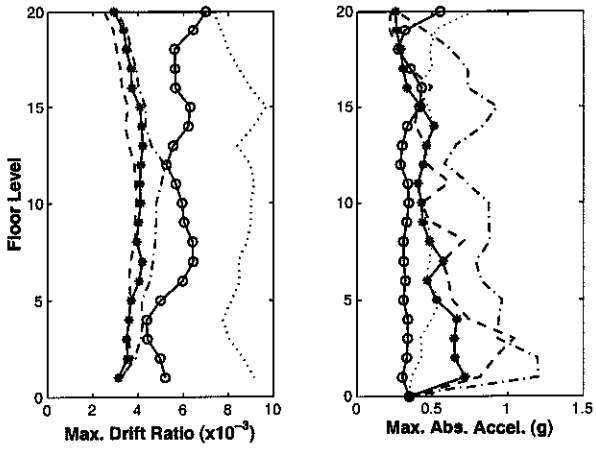

Figure 3.43: Distribution of (a) Maximum Interstory Drift Ratio, (b) Maximum Absolute Acceleration in the 20-story Building Under the ELC Ground Motion, Nodal Control (–o– uncontrolled with IE always unlocked, ··· uncontrolled with IE always locked, - - - AID, - · - · - OCS, -*- TID)

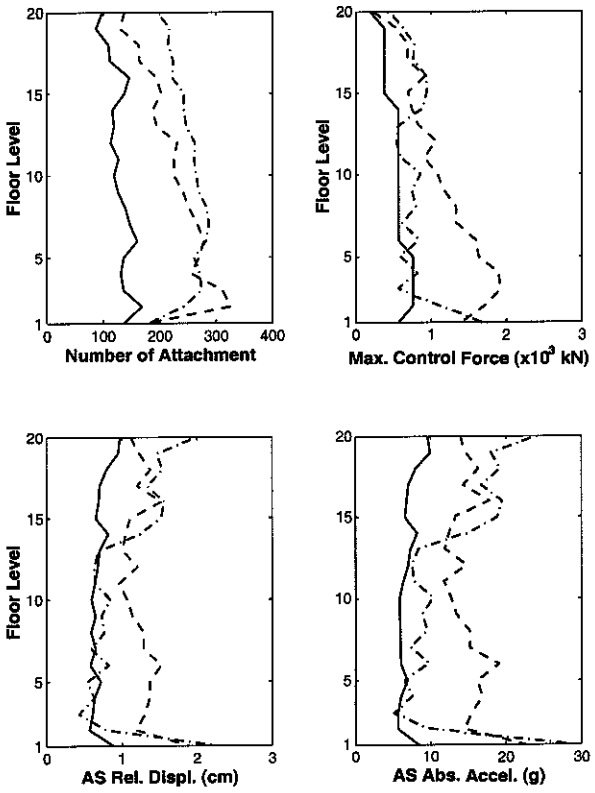

Figure 3.44: Distribution of (a) Number of Attachment, (b) Control Force, (c) AS Displacement Relative to the Support Floor, (d) AS Absolute Acceleration in the 20-story Building Under the ELC Ground Motion, Nodal Control (- - - AID, - · - · OCS, — TID)

Chapter 4 Statistical Behavior of Active Interaction Control Systems

4.1 Introduction

In this chapter, the performance of SDOF AIC systems is evaluated statistically based on a large ensemble of artificial earthquake ground motions consisting of 2,000 records. These artificial ground motions were generated from modified Kanai-Tajimi filtered gaussian white-noise process.

The effects of the AS stiffness, mass, damping factor, and control force limit of the fuse device on the performance of SDOF AIC systems are studied in terms of the following nondimensional parameters:

$$\alpha = \frac{k_2}{k_1}, \quad \psi = \frac{\omega_2}{\omega_1}, \quad \gamma = \frac{\zeta_2}{\zeta_1}, \quad \eta = \frac{u_{max}}{m_1 \max_{t\in[0,t_1]} |\ddot{x}_g(t)|}$$

where k_1, k_2 is the stiffness of the PS and AS respectively; ω_1, ω_2 is the natural frequency of the PS and AS respectively; ζ_1, ζ_2 is the fraction of critical damping for the PS and AS respectively; u_{max} is the control force limit in the fuse device; $\ddot{x}_g(t)$ is the ground motion acceleration.

The optimal values of these parameters in the statistical sense are obtained based on the same ensemble of artificial seismic ground motions.

4.2 Simulation of Earthquake Ground Motions

In this section, the algorithms and properties of artificially generated accelerograms based upon modified Kanai-Tajimi filtered gaussian white noise random process are described.

To carry out Monte Carlo simulation, a large ensemble of earthquake accelerograms are required. Individual real earthquake records are limited in the sense that they are conditional on a single realization of a set of random parameters such as magnitude, fault mechanism, wave propagation path, local site condition, etc. Only a limited number of

strong motion records have been collected at present owing to the limited historical seismic events and inadequate instrumentation arrays in the field. Thus, due to the limitations and paucity of recorded accelerograms, the capability to generating artificial accelerograms are highly desired. Many techniques have been developed to simulate artificial earthquakes [4, 17, 20, 30, 32, 21, 42].

In the recorded earthquake ground motions, the power spectral density functions are not constant but have the predominant frequencies mainly due to the resonance of subsoil layers. The representative power spectral density function [2] might be expressed in the form

$$\mathrm{S}(\omega) \equiv \mathrm{S}_0 |H_1(\omega)|^2 |H_2(\omega)|^2 \tag{4.1}$$

where S_0 is a constant and

$$H_1(\omega) = \frac{1 + 2i\xi_1(\frac{\omega}{\omega_1})}{[1 - (\frac{\omega}{\omega_1})^2] + 2i\xi_1(\frac{\omega}{\omega_1})}, \quad H_2(\omega) = \frac{(\frac{\omega}{\omega_2})^2}{[1 - (\frac{\omega}{\omega_2})^2] + 2i\xi_2(\frac{\omega}{\omega_2})} \tag{4.2}$$

The first of Eqn. (4.2) is the well-known Kanai-Tajimi filter function which amplifies the frequency content in the neighbourhood of $\omega = \omega_1$ and increasingly attenuates the frequency content above $\omega = \omega_1$ as $\omega \to \infty$ [19, 37]. The second of Eqn. (4.2) is used to attenuate the very low frequency content. Parameters ω_1 and ξ_1 appearing in $H_1(\omega)$ may be thought of as some characteristic ground frequency and characteristic damping ratio of subsoil layers, respectively. Housner and Jennings [10] have suggested 15.6 rad/sec for ω_1 and 0.64 for ξ_1 as being representative of firm soil conditions. Values for parameters ω_2 and ξ_2 have been determined as 1.2 rad/sec and 0.84 respectively by calibrating to the N-S component of 1940 El Centro record. The power spectral density function $\mathrm{S}(\omega)$ will have the general appearance shown in Fig. 4.1.

For the simulation of artificial earthquake accelerograms with specific frequency content, two methods are commonly used. One is based on the filtered gaussian white noise and in the other method accelerograms are directly synthesized by the superposition of sinusoidal waveforms. The intent herein is to focus on the second method to generate artificial ground motions. Note the well-known fact that a Gaussain process can be represented in terms of a harmonic series

$$x(t) = 2\sum_{i=1}^{n} \sqrt{\mathrm{S}(\omega_i)\Delta\omega}\,\sin(\omega_i t + \phi_i) \tag{4.3}$$

where ω_i are selected frequencies at equal spacing $\Delta\omega$, and ϕ_i are randomly generated phase angle with uniform distribution over the interval $(0, 2\pi)$. Note that unilateral power spectrum $S(\omega)$ is used herein. A sample function of the process $x(t)$ and its power spectral density are illustrated in Fig. 4.2.

The envelope of recorded earthquake accelerograms are typically composed of three parts in time domain, namely, build-up, nearly constant with high intensity level, and decaying. The simple model of a nonstationary synthetic accelerogram is expressed as

$$a(t) = e(t) \cdot x(t) \tag{4.4}$$

where $x(t)$ is a stationary random process synthesized by the method described above and $e(t)$ is a deterministic envelope function. The form of the modulating envelope function is chosen as

$$e(t) = a_1 t \exp(-a_2 t) \tag{4.5}$$

Based on the results of a regression analysis of the 1940 El Centro record [16], the value of parameter a_2 is determined as 0.255 over a duration of 30 seconds. The value of a_1 is set as $1/1.4427$ to force the maximum value of $e(t)$ to be unity over a duration of thirty seconds. The appearance of a curve $e(t)$ corresponding to these parameter values is illustrated in Fig. 4.3.

Although ground motion models which account for the time-varying nature of relative frequency content have also been proposed, time-invariant models in which $S(\omega)$ reflects the frequency content during the most intense part of the ground motion are believed to be sufficiently accurate for most studies.

To obtain an earthquake accelerogram consistent with design response spectrum in amplitude, we normalize the nonstationary accelerogram $a(t)$ by a scale factor corresponding to a specified design response spectrum. The design response spectrum described in the 1997 Uniform Building Code (UBC) [40] is used for this purpose. The parameters for the design spectrum corresponding to a near-field site of an earthquake with magnitude ≥ 7.0 are listed in Table 4.1.

The scaling factor is determined as the ratio between the design response spectrum and average value of the actual response spectrum calculated from ground motion $a(t)$ over a certain frequency range. This frequency range has been chosen to be the interval $[T_s\ T_v]$

Table 4.1: Parameters of the UBC Design Spectrum [40]

	Parameters	Value	Source
1	Seismic zone factor Z	0.40	Table 16-I, zone 4
2	Soil profile type	S_D	Table 16-J, stiff soil
3	Seismic source type	A	Table 16-U, max. moment magnitude M $\geq$ 7.0
4	Near-source factor N_a	1.0	Table 16-S, $\geq$ 10 km to fault
5	Near-source factor N_v	1.0	Table 16-T, $\geq$ 15 km to fault
6	Seismic coefficient C_a	0.44	Table 16-Q, $C_a = 0.44N_a$
7	Seismic coefficient C_v	0.64	Table 16-R, $C_v = 0.64N_v$
8	Control period T_s	0.582 sec	Figure 16-3, $T_s = C_v/2.5C_a$
9	Control period T_0	0.116 sec	Figure 16-3, $T_0 = 0.2T_s$

in which the spectral pseudo-velocity is constant for the 1997 UBC code [40]. T_v is chosen to be 3.0 second in this study. The constant spectral velocity over this frequency range is equal to $9.815C_v/2\pi$ m/s from the UBC code.

The accelerogram $a(t)$ obtained in the last step is now multiplied by the scaling factor determined above to raise or lower the entire response spectrum. A typical artificial ground motion accelerogram obtained in this way is illustrated in Fig. 4.4.

The accelerograms generated by the procedure described in this section will be used for the excitation input in the subsequent Monte Carlo simulation.

4.3 Statistical Performance of AIC Systems

In the preceding chapters, it has been shown that AIC algorithms are capable of significantly reducing the vibrations of structures subjected to external excitations. However, the performance of AIC systems varies with each of the particular seismic excitations considered. Therefore, we would be much more confident in the AIC algorithm if robust performance is demonstrated for the AIC system over a large ensemble of seismic excitations. Based on the statistical values obtained in this way, the performance of each AIC algorithm can be more accurately evaluated.

For the AIC system considered in this study, large stiffness ratio values are employed to promote good control performance. Under such a condition, significant hysteretic damping can be induced into the PS through interaction with a stiff AS. It is admittedly difficult to conduct an exact random response analysis of strongly nonlinear system. Therefore, a

Monte Carlo simulation is required to obtain the response statistics of the AIC systems subjected to random excitations. On the other hand, the control force produced by the interactions between the PS and AS is very sensitive to the time domain characteristics of the seismic excitation such that a random analysis in the frequency domain is inappropriate in this case. 2,000 records are generated for the accelerogram ensemble by the procedure described above.

The following nondimensional parameters are considered for the PS in simulations:

$$m_1 = 1, \quad k_1 = 4\pi^2, \quad \zeta_1 = 2\%, \quad T_1 = 1 \text{ sec}$$

where m_1, k_1, ζ_1 and T_1 are the mass, stiffness, critical damping ratio and natural period of the PS respectively. Meanwhile, four different cases of parametric variation are considered for the AS as described below.

1. CASE 1: Varying Stiffness Ratio α for AID and OCS
   $\alpha = 0.25, 0.5, 1.0, 1.5, 2.0, 4.0, 6.0, 8.0$ with $\psi = 10$, $\zeta_2 = 2\%$ or 15%.

2. CASE 2: Varying Frequency Ratio ψ for AID and OCS
   $\psi = 5, 10, 15, 20, 25, 30, 35, 40$ with $\alpha = 2$, $\zeta_2 = 2\%$ or 15%.

3. CASE 3: Varying AS Damping Ratio ζ_2 for AID and OCS
   $\zeta_2 = 0\%, 4\%, 8\%, 12\%, 16\%, 20\%, 40\%, 80\%$ with $\alpha = 2$, $\psi = 10$.

4. CASE 4: Varying Control Force Limit Ratio η for TID
   The nondimensional parameter η is defined as

$$\eta = \frac{u_{max}}{m_1 \max_{t\in[0,t_1]} |\ddot{x}_g(t)|} \tag{4.6}$$

   where $\ddot{x}_g(t)$ is the earthquake ground motion acceleration; m_1 is the mass of the PS.
   $\eta = 0.1, 0.2, 0.3, 0.4, 0.5, 0.6, 0.7, 0.8$ with $\alpha = 2$, $\psi = 10$, $\zeta_2 = 2\%$ or 15%.

The statistics of the simulation results are listed in Tables 4.2 to 4.14. The statistical quantities of interest and their abbreviations are defined as follows:

μ = Sample mean value;

σ = Sample standard deviation;

t_1 = Duration of excitation, being set to 15 seconds in this study.

PF = Maximum acceleration value in an accelerogram, i.e., $\max_{t\in[0,t_1]}|\ddot{x}_g(t)|$;

PDP = Maximum value of PS's displacement response, i.e., $\max_{t\in[0,t_1]}|x_1(t)|$;

PVP = Maximum value of PS's velocity response, i.e., $\max_{t\in[0,t_1]}|\dot{x}_1(t)|$;

PAP = Maximum value of PS's absolute acceleration response, i.e., $\max_{t\in[0,t_1]}|\ddot{x}_1(t)+\ddot{x}_g(t)|$;

RDP = Time average of PS's displacement response, i.e., $\int_0^{t_1}|x_1(\tau)|d\tau/t_1$;

RVP = Time average of PS's velocity response, i.e., $\int_0^{t_1}|\dot{x}_1(\tau)|d\tau/t_1$;

RAP = Time average of PS's absolute acceleration response, i.e., $\int_0^{t_1}|\ddot{x}_1(\tau)+\ddot{x}_g(\tau)|d\tau/t_1$;

PDA = Maximum value of AS's displacement response, i.e., $\max_{t\in[0,t_1]}|x_2(t)|$;

PVA = Maximum value of AS's velocity response, i.e., $\max_{t\in[0,t_1]}|\dot{x}_1(t)|$;

PAA = Maximum value of AS's absolute acceleration response, i.e., $\max_{t\in[0,t_1]}|\ddot{x}_1(t)+\ddot{x}_g(t)|$;

RDA = Time average of AS's displacement response, i.e., $\int_0^{t_1}|x_1(\tau)|d\tau/t_1$;

RVA = Time average of AS's velocity response, i.e., $\int_0^{t_1}|\dot{x}_1(\tau)|d\tau/t_1$;

RAA = Time average of AS's absolute acceleration response, i.e., $\int_0^{t_1}|\ddot{x}_1(\tau)+\ddot{x}_g(\tau)|d\tau/t_1$;

PU = Peak value of control force, i.e., $\max_{t\in[0,t_1]}|u(t)|$;

RU = Time average of control force, i.e., $\int_0^{t_1}|u(\tau)|d\tau/t_1$;

NAT = Total number of attachment cycles;

TAT = Average duration of attachment cycles;

NPD = Total number of peaks exceeding a certain level (= 0.02 m) for PS's displacement response;

NPA = Total number of peaks exceeding a certain level (= 3 m/s/s) for PS's acceleration response;

TPD = Duration with PS's displacement response exceeding a certain level (= 0.02 m).

The histograms describing the probability distributions of PDP, PAP and NAT are plotted in Figs. 4.5 to 4.7. The normalized frequency of occurrence P_i is defined as

$$P_i = \frac{N_i}{N \cdot \Delta_i} \tag{4.7}$$

where N is the ensemble size; N_i is the number of occurrence for the quantity falling within the interval $[x_i, x_i + \Delta_i)$; Δ_i is the corresponding interval length. Clearly,

$$\sum_{i=1}^{N} P_i = 1$$

Therefore, P_i also represents the probability density of the corresponding quantity in a discrete sense.

Based on the informations given in Tables 4.2 to 4.14 and Figs. 4.5 to 4.7, the following conclusions can be drawn:

1. The AIC algorithms are very effective in controlling the displacement and velocity responses of the PS, but generally not effective in suppressing the acceleration response of the PS. As shown in Fig. 4.5, the frequency of occurrence for the controlled response is distributed over a much narrower region than the uncontrolled response. It is observed in Fig. 4.5 that even the worst case of the controlled response is still better than the most favorable case of the uncontrolled response.

2. For the cases with a small AS damping ratio ($\zeta_2 = 2\%$), the performance of the OCS and TID algorithms is better than the AID algorithm in terms of PS displacement control. However, with an increased value of AS damping ratio ($\zeta_2 = 15\%$), the performance of all three AIC algorithms becomes almost identical in terms of PS displacement control.

3. As revealed in the preceding chapters, setting a control force limit by adding a fuse device to the interaction element has certain positive effect on both suppressing the PS acceleration and attachment number. However, as indicated in Fig. 4.7, adding an appropriate amount of damping to the AS is much more advantageous than setting control force limit in reducing attachment number of the OCS system. The effect of increasing AS damping is not so significant on the AID system than on the OCS system.

4. In general, the AS response of the OCS system is greater than that of the AID system in terms of AS displacement, velocity and acceleration.

5. The control force in the OCS system is greater than that in the AID system. This explains why the OCS system has a larger PS displacement reduction capability and a larger PS acceleration response than the AID system.

4.4 Parametric Study

This study has found that an optimal value does exist for each of the parameters α, ψ, ζ_2 and u_{max} under a particular earthquake ground motion. However, the optimal values determined from one particular earthquake ground motion may not be optimal for another ground motion record which has distinct time and frequency domain characteristics. This motivates the research effort described in this section to determine the optimal values for the parameters in a statistical sense based on a large ensemble of artificial earthquake ground motions.

Four cases of parametric variation are described in the preceding section and they are considered here again.

4.4.1 Stiffness Ratio α

Stiffness ratio $\alpha = k_2/k_1$ plays a very important role in the control performance of AIC systems. Since AS can be regarded as acting as an actuator delivering the control force in an AIC system, large AS stiffness will enhance the capacity of this "actuator" and hence greater reduction of the PS displacement and velocity response is achieved as a consequence of large control force present in the PS. However, side effects such as large acceleration and attachment number also come with large values of stiffness ratio α.

Tables 4.4 to 4.7 list the statistics of some important response quantities of the AID and OCS systems with varying stiffness ratio and fixed parameters ψ and ζ_2. Fig. 4.8 plot the variation of some response quantities given in these tables. From these tables and figures, the following observations can be made:

1. The PS displacement and velocity responses of the AID system decrease monotonically with increasing α values. High AS stiffness values result in high control force which implies more energy dissipated from the PS. However, with increasing α values, the PS acceleration response increases in the AID system. Changing AS damping ratio seems not to have much effect on the response of the AID system.

2. For the OCS system, the results are quite different for the two cases with different values of AS damping ratio ζ_2. For the case with small AS damping ratio ($\zeta_2 = 2\%$), the PS displacement response decreases as α increases while the PS acceleration

generally increases with increasing α values. For the case with a higher AS damping ratio value ($\zeta_2 = 15\%$), the PS displacement response decreases in the beginning and then increases after a certain value of α is reached within the range of α value considered. For the high AS damping case, the PS acceleration response is very close to that of the AID system. Increasing AS damping ratio has significant effects on the response and behavior of the OCS system. It is observed that the response of the OCS system with high AS damping is very close to the AID systems.

3. Changing AS damping ratio doesn't have much influence on the response of the AS in both AID and OCS systems.

4.4.2 Frequency Ratio ψ

In this subsection, we focus on the effect of varying parameters ψ on the control performance of the AID and OCS systems.

In the past research on AIC systems, a typical value considered for the mass ratio β is 0.02. If $\alpha = 2$ is chosen as a typical stiffness ratio value, then the corresponding frequency ratio ψ is equal to 10.

Tables 4.8 to 4.11 give the statistics of some important response quantities of the AID and OCS systems with varying frequency ratio and fixed parameters α and ζ_2. Fig. 4.9 plot the variation of some response quantities given in these tables.

Changing frequency ratio ψ seems not to have a strong effect on the response of the AID system. It is also observed that the response of the OCS system with varying ψ exhibits much more complicated behavior than the case with varying α. The effect of ψ on the PS response of the OCS system appears less significant as AS damping ratio is increased to 15%. It is again observed that the response of the OCS system with high AS damping is very close to the AID systems.

The control efficiency of the AIC algorithms depends on the fast motion of AS with high natural frequency. As the natural frequency of AS decreased, the performance of the AIC systems generally decrease. It is seen that the control performance of the OCS system with low damping ratio is more sensitive to the change of ψ values than the AID systems. Based on the information collected on the attachment number, PS displacement and acceleration response, an optimal range for the ψ value is suggested to be kept between 10 and 20.

4.4.3 AS Damping Ratio ζ_2

Tables 4.12 to 4.13 give the statistics of some important response quantities of the AID and OCS systems with varying AS damping ratio and fixed parameters α and ψ. Fig. 4.10 plot the variation of some response quantities given in these tables.

Previously, we have observed that AS damping ratio has a significant effect on the performance of the OCS system while its effect is negligible on the AID system. This phenomenon can be easily understood from the operating mechanisms of the AID and OCS algorithms as described in Chapter 2. It is again observed that changing AS damping ratio has a negligible effect on the AID system.

For the OCS system, the displacement and velocity response of the PS is seen to monotonically increase with increasing AS damping ratio ζ_2. It is also observed that increasing AS damping ratio will slightly increase the absolute acceleration response of the PS in the OCS system.

The objective of increasing AS damping ratio is to reduce the attachment number in the OCS system. However, an AS with too high damping ratio value will deteriorate the performance of the OCS system because this type of AS will move relatively slowly and lots of attachment opportunities are thus missed. An AS with an excessively large damping ratio is also likely to lead to bad timing of the interactions between the PS and AS and thus deteriorate the PS response of the OCS system. On the other hand, high damping added to AS also increases the equipment cost. Based on the information given in Tables 4.12 to 4.13 and Fig. 4.10, we recommend using an AS damping ratio ζ_2 in the range between 7% to 15%.

For both the AID and OCS system, the response of the AS is almost unaffected by the change in AS damping ratio.

4.4.4 Control Force Limit Ratio η

The control force limit u_{max} is calculated from the nondimensional parameter η using the following equation:

$$u_{max} = \eta \cdot m_1 \cdot \max_{t\in[0,t_1]} |\ddot{x}_g(t)| \tag{4.8}$$

where $\ddot{x}_g(t)$ is the earthquake ground motion acceleration; m_1 is the mass of the PS.

There is no doubt on the fact that changing the control force limit u_{max} of a TID system

has a significant effect on the performance of a TID system. Tables 4.13 to 4.14 give the statistics of some important response quantities of the TID system with varying control force limit u_{max} and fixed parameters α, ψ and ζ_2. Figs. 4.11 plots the variation of some response quantities given in these tables.

It is observed that for small u_{max} values, AS damping ratio seems not to have much effects on the response of TID system. However, for increased u_{max} values, AS damping ratio does have an effect on the response of the TID system. It is also observed that changing AS damping ratio have only slight effects on the PS acceleration response and AS displacement and acceleration responses.

As control force limit u_{max} increases, the PS displacement response will generally decrease although the decreasing rate of the PS displacement response is very small after a certain η value is exceeded. More interesting behavior is observed with the PS acceleration response with varying control force limit ratio η. With increasing η values, the PS acceleration initially decreases and then increases after a certain value of η is reached.

For this particular combination of α, ψ and ζ_2 values, an optimal value for η is recommended to be around 0.5.

Table 4.2: Statistics of the Uncontrolled Response From the Simulation Results (Unit: m, sec)

	PF	PDP	PVP	PAP	RDP	RVP	RAP
μ	6.1209	0.2151	1.4116	11.5715	0.0878	0.5563	3.8346
σ	1.1001	0.0564	0.3773	2.5705	0.0255	0.1599	0.9556

Table 4.3: Statistics of the AID-Controlled Response With Varying Stiffness Ratio α ($\zeta_2 = 2\%$, $\psi = 10$) From the Simulation Results (Unit: m, sec)

		α							
		0.25	0.5	1.0	1.5	2.0	4.0	6.0	8.0
PDP	μ	0.1006	0.0783	0.0608	0.0520	0.0461	0.0332	0.0277	0.0248
	σ	0.0197	0.0146	0.0109	0.0098	0.0082	0.0053	0.0051	0.0045
PVP	μ	0.7462	0.6316	0.5361	0.4816	0.4418	0.3521	0.3104	0.2867
	σ	0.1593	0.1310	0.1092	0.1011	0.0888	0.0711	0.0623	0.0581
PAP	μ	5.7947	5.6605	5.9740	6.3559	6.6732	7.4888	7.9822	8.3653
	σ	1.2476	1.1178	1.2019	1.3335	1.3705	1.4319	1.5076	1.5983
RDP	μ	0.0298	0.0225	0.0170	0.0144	0.0127	0.0093	0.0078	0.0069
	σ	0.0041	0.0027	0.0019	0.0016	0.0014	0.0010	0.0009	0.0008
RVP	μ	0.2145	0.1728	0.1406	0.1238	0.1124	0.0879	0.0755	0.0680
	σ	0.0328	0.0242	0.0196	0.0178	0.0162	0.0126	0.0106	0.0095
RAP	μ	1.4925	1.3557	1.3516	1.4010	1.4503	1.5872	1.6649	1.7129
	σ	0.2299	0.1873	0.1821	0.1922	0.2009	0.2152	0.2252	0.2306
PDA	μ	0.1987	0.1442	0.1017	0.0811	0.0682	0.0435	0.0329	0.0269
	σ	0.0438	0.0282	0.0197	0.0168	0.0140	0.0085	0.0064	0.0052
PVA	μ	12.1083	8.7894	6.1984	4.9493	4.1566	2.6526	2.0048	1.6306
	σ	2.6703	1.7199	1.2024	1.0304	0.8550	0.5198	0.3869	0.3173
PAA	μ	784.52	569.23	401.24	320.26	269.05	171.64	129.93	106.26
	σ	173.00	111.42	77.75	66.49	55.08	33.58	25.06	20.56
RDA	μ	0.0577	0.0394	0.0263	0.0204	0.0170	0.0105	0.0078	0.0063
	σ	0.0093	0.0056	0.0036	0.0029	0.0024	0.0015	0.0011	0.0009
RVA	μ	1.0043	0.7453	0.5505	0.4558	0.3964	0.2749	0.2180	0.1844
	σ	0.1587	0.1061	0.0771	0.0652	0.0573	0.0393	0.0304	0.0253
RAA	μ	63.95	47.22	34.59	28.46	24.65	16.94	13.38	11.30
	σ	10.12	6.70	4.83	4.05	3.55	2.41	1.86	1.54
PU	μ	1.9483	2.8200	3.9563	4.7134	5.2544	6.5738	7.3260	7.8424
	σ	0.4296	0.5521	0.7661	0.9776	1.0751	1.2856	1.4153	1.5188
RU	μ	0.5446	0.7367	0.9655	1.1133	1.2184	1.4511	1.5656	1.6339
	σ	0.0884	0.1049	0.1327	0.1557	0.1719	0.1997	0.2146	0.2216
NAT	μ	51.0	59.6	71.4	80.0	86.5	105.4	118.8	129.0
	σ	3.9	3.9	3.6	4.1	3.8	3.6	3.9	3.9
TAT	μ	0.2685	0.2254	0.1833	0.1610	0.1467	0.1157	0.0998	0.0899
	σ	0.0223	0.0163	0.0103	0.0095	0.0075	0.0048	0.0039	0.0034
NPD	μ	24.6	21.6	17.5	14.4	12.3	6.7	3.8	2.3
	σ	3.6	3.9	3.9	3.9	3.8	2.8	2.2	1.8
NPA	μ	8.1	8.1	9.7	11.6	13.3	19.2	23.8	27.5
	σ	6.1	5.5	5.5	5.7	5.9	6.5	7.0	7.5
TPD	μ	6.2509	4.6364	3.1065	2.2603	1.7391	0.7404	0.3498	0.1961
	σ	0.9403	0.8161	0.6603	0.5711	0.4894	0.2958	0.2123	0.1618

Table 4.4: Statistics of the OCS-Controlled Response With Varying Stiffness Ratio α ($\zeta_2 = 2\%$, $\psi = 10$) From the Simulation Results (Unit: m, sec)

		α							
		0.25	0.5	1.0	1.5	2.0	4.0	6.0	8.0
PDP	μ	0.0601	0.0468	0.0375	0.0344	0.0325	0.0299	0.0282	0.0276
	σ	0.0148	0.0107	0.0085	0.0078	0.0071	0.0072	0.0060	0.0077
PVP	μ	0.4738	0.3990	0.3438	0.3336	0.3262	0.3315	0.3304	0.3421
	σ	0.1071	0.0896	0.0776	0.0768	0.0711	0.0766	0.0816	0.0805
PAP	μ	4.5367	4.7509	5.2567	5.7726	6.2013	7.6700	8.7437	9.7116
	σ	0.9028	0.8946	0.9873	1.0569	1.1245	1.4430	1.7682	1.7238
RDP	μ	0.0156	0.0125	0.0103	0.0095	0.0090	0.0083	0.0080	0.0079
	σ	0.0020	0.0016	0.0015	0.0013	0.0013	0.0012	0.0011	0.0013
RVP	μ	0.1116	0.0908	0.0769	0.0715	0.0688	0.0655	0.0646	0.0651
	σ	0.0163	0.0129	0.0113	0.0109	0.0101	0.0096	0.0097	0.0100
RAP	μ	1.3110	1.4250	1.5719	1.6663	1.7358	1.9304	2.0598	2.1631
	σ	0.1740	0.1861	0.2018	0.2207	0.2341	0.2603	0.2790	0.2889
PDA	μ	0.2707	0.1736	0.1107	0.0851	0.0709	0.0468	0.0370	0.0317
	σ	0.0498	0.0324	0.0204	0.0159	0.0132	0.0087	0.0073	0.0057
PVA	μ	16.4875	10.5734	6.7410	5.1785	4.3162	2.8339	2.2433	1.9176
	σ	3.0360	1.9775	1.2443	0.9674	0.8023	0.5255	0.4459	0.3471
PAA	μ	1068.69	685.17	436.92	335.76	280.01	184.48	146.16	125.19
	σ	196.70	127.95	80.52	62.83	52.02	34.18	28.85	22.50
RDA	μ	0.1260	0.0774	0.0470	0.0352	0.0287	0.0179	0.0138	0.0115
	σ	0.0171	0.0103	0.0062	0.0048	0.0039	0.0025	0.0019	0.0016
RVA	μ	3.6610	2.5286	1.7259	1.3752	1.1726	0.8044	0.6494	0.5615
	σ	0.4997	0.3394	0.2298	0.1900	0.1639	0.1115	0.0908	0.0773
RAA	μ	236.52	162.94	110.93	88.25	75.16	51.40	41.38	35.68
	σ	32.27	21.88	14.78	12.20	10.52	7.12	5.78	4.91
PU	μ	2.6642	3.4072	4.3242	4.9592	5.4885	7.0927	8.2657	9.2666
	σ	0.4904	0.6364	0.7976	0.9292	1.0210	1.3182	1.6281	1.6677
RU	μ	1.0919	1.2859	1.4750	1.5846	1.6621	1.8681	2.0027	2.1077
	σ	0.1490	0.1726	0.1925	0.2122	0.2264	0.2543	0.2727	0.2847
NAT	μ	84.2	96.0	107.5	114.1	117.9	127.9	133.0	135.7
	σ	3.6	3.7	3.7	4.2	3.7	4.2	4.4	4.2
TAT	μ	0.1135	0.0881	0.0669	0.0567	0.0502	0.0369	0.0307	0.0271
	σ	0.0066	0.0045	0.0032	0.0028	0.0023	0.0016	0.0014	0.0011
NPD	μ	13.7	10.6	7.6	6.4	5.7	4.5	4.2	4.0
	σ	3.6	3.5	3.4	3.0	3.1	2.9	2.7	2.6
NPA	μ	6.6	11.1	22.3	32.8	41.2	65.3	79.9	89.3
	σ	5.8	7.5	10.6	12.3	13.2	13.4	13.4	12.7
TPD	μ	2.4776	1.6434	1.0118	0.7966	0.6628	0.4838	0.4184	0.3694
	σ	0.6097	0.5267	0.4680	0.3956	0.3659	0.3273	0.2930	0.2530

Table 4.5: Statistics of the AID-Controlled Response With Varying Stiffness Ratio α ($\zeta_2 = 15\%$, $\psi = 10$) From the Simulation Results (Unit: m, sec)

		α							
		0.25	0.5	1.0	1.5	2.0	4.0	6.0	8.0
PDP	μ	0.1067	0.0821	0.0623	0.0527	0.0464	0.0325	0.0264	0.0238
	σ	0.0223	0.0154	0.0111	0.0097	0.0083	0.0049	0.0047	0.0041
PVP	μ	0.7900	0.6629	0.5593	0.5007	0.4592	0.3588	0.3062	0.2751
	σ	0.1721	0.1380	0.1145	0.1054	0.0975	0.0719	0.0612	0.0536
PAP	μ	6.0165	5.8144	6.0593	6.3814	6.6744	7.4007	7.7979	8.0369
	σ	1.3462	1.1784	1.2036	1.3277	1.3868	1.4462	1.4902	1.4974
RDP	μ	0.0322	0.0238	0.0176	0.0146	0.0128	0.0091	0.0075	0.0066
	σ	0.0049	0.0030	0.0020	0.0016	0.0014	0.0009	0.0008	0.0008
RVP	μ	0.2318	0.1847	0.1486	0.1302	0.1180	0.0902	0.0758	0.0668
	σ	0.0375	0.0267	0.0212	0.0189	0.0172	0.0129	0.0108	0.0095
RAP	μ	1.6029	1.4226	1.3809	1.4119	1.4523	1.5653	1.6273	1.6636
	σ	0.2605	0.2062	0.1891	0.1945	0.2017	0.2147	0.2229	0.2272
PDA	μ	0.1907	0.1401	0.0993	0.0795	0.0671	0.0426	0.0319	0.0258
	σ	0.0432	0.0281	0.0187	0.0162	0.0139	0.0085	0.0062	0.0048
PVA	μ	9.6442	7.0884	5.0263	4.0251	3.3960	2.1560	1.6093	1.2944
	σ	2.1831	1.4205	0.9471	0.8216	0.7051	0.4293	0.3145	0.2427
PAA	μ	752.49	552.79	391.71	313.65	264.47	167.89	125.56	101.37
	σ	170.35	110.76	73.71	63.76	54.69	33.33	24.47	19.04
RDA	μ	0.0535	0.0370	0.0248	0.0193	0.0161	0.0099	0.0073	0.0059
	σ	0.0090	0.0054	0.0034	0.0027	0.0023	0.0014	0.0010	0.0008
RVA	μ	0.8481	0.6313	0.4672	0.3879	0.3380	0.2334	0.1849	0.1557
	σ	0.1403	0.0923	0.0656	0.0555	0.0488	0.0334	0.0261	0.0219
RAA	μ	55.12	40.76	29.83	24.57	21.29	14.49	11.40	9.55
	σ	9.17	5.96	4.18	3.49	3.05	2.06	1.59	1.33
PU	μ	1.8686	2.7392	3.8646	4.6209	5.1721	6.4509	7.1066	7.5191
	σ	0.4230	0.5490	0.7266	0.9387	1.0696	1.2815	1.3868	1.4126
RU	μ	0.5083	0.6984	0.9244	1.0702	1.1762	1.4054	1.5140	1.5758
	σ	0.0856	0.1027	0.1270	0.1486	0.1652	0.1950	0.2092	0.2170
NAT	μ	48.3	56.4	67.0	74.7	81.3	98.7	110.1	119.7
	σ	3.9	3.8	3.8	3.8	4.1	4.0	4.2	4.3
TAT	μ	0.2858	0.2405	0.1978	0.1748	0.1586	0.1263	0.1104	0.0994
	σ	0.0251	0.0175	0.0124	0.0099	0.0090	0.0059	0.0048	0.0042
NPD	μ	25.4	22.6	18.3	14.9	12.5	6.6	3.2	1.9
	σ	3.6	4.0	4.0	3.9	3.6	2.6	2.1	1.7
NPA	μ	8.8	8.6	9.9	11.6	13.2	18.3	22.1	24.9
	σ	6.2	5.8	5.5	5.5	5.7	6.4	6.7	6.9
TPD	μ	6.7229	4.9863	3.2842	2.3441	1.7894	0.6922	0.2878	0.1578
	σ	0.9864	0.8620	0.6857	0.5700	0.4845	0.2682	0.2074	0.1446

Table 4.6: Statistics of the OCS-Controlled Response With Varying Stiffness Ratio α ($\zeta_2 = 15\%$, $\psi = 10$) From the Simulation Results (Unit: m, sec)

		α							
		0.25	0.5	1.0	1.5	2.0	4.0	6.0	8.0
PDP	μ	0.0837	0.0679	0.0536	0.0464	0.0421	0.0379	0.0407	0.0515
	σ	0.0160	0.0137	0.0107	0.0090	0.0090	0.0192	0.0256	0.0313
PVP	μ	0.6250	0.5417	0.4535	0.4077	0.3832	0.3411	0.3348	0.3625
	σ	0.1323	0.1119	0.0938	0.0798	0.0778	0.1038	0.1214	0.1523
PAP	μ	5.1066	5.1461	5.4964	5.8227	6.1228	6.9395	7.4591	7.9460
	σ	1.0031	1.0248	1.1056	1.1472	1.2188	1.3609	1.4360	1.5970
RDP	μ	0.0237	0.0188	0.0149	0.0130	0.0117	0.0102	0.0104	0.0123
	σ	0.0029	0.0023	0.0018	0.0015	0.0014	0.0031	0.0044	0.0058
RVP	μ	0.1671	0.1375	0.1117	0.0989	0.0906	0.0763	0.0725	0.0751
	σ	0.0236	0.0192	0.0160	0.0135	0.0123	0.0149	0.0190	0.0231
RAP	μ	1.2829	1.2628	1.3299	1.3923	1.4404	1.5675	1.6332	1.6812
	σ	0.1780	0.1689	0.1767	0.1850	0.1890	0.2106	0.2181	0.2338
PDA	μ	0.2238	0.1528	0.1008	0.0778	0.0652	0.0413	0.0318	0.0268
	σ	0.0452	0.0302	0.0200	0.0155	0.0131	0.0089	0.0066	0.0061
PVA	μ	11.3203	7.7306	5.1031	3.9391	3.2955	2.0892	1.6016	1.3462
	σ	2.2839	1.5276	1.0141	0.7881	0.6629	0.4531	0.3338	0.3103
PAA	μ	883.37	603.12	397.79	307.03	256.96	162.70	125.09	105.41
	σ	178.30	119.12	78.91	61.29	51.57	35.15	26.10	24.09
RDA	μ	0.0750	0.0480	0.0301	0.0226	0.0183	0.0109	0.0080	0.0065
	σ	0.0109	0.0067	0.0041	0.0031	0.0025	0.0015	0.0011	0.0009
RVA	μ	1.4008	1.0084	0.7108	0.5726	0.4879	0.3268	0.2564	0.2176
	σ	0.1980	0.1387	0.0982	0.0781	0.0656	0.0450	0.0350	0.0316
RAA	μ	92.01	66.02	46.33	37.18	31.57	20.93	16.29	13.75
	σ	13.01	9.08	6.41	5.08	4.25	2.88	2.22	1.99
PU	μ	2.1995	2.9966	3.9341	4.5331	5.0357	6.2632	7.1019	7.8671
	σ	0.4439	0.5921	0.7811	0.9059	1.0121	1.3630	1.4948	1.8288
RU	μ	0.7043	0.8892	1.0931	1.2095	1.2889	1.4691	1.5575	1.6244
	σ	0.1029	0.1243	0.1492	0.1677	0.1761	0.2017	0.2124	0.2308
NAT	μ	57.6	66.7	77.6	84.1	89.0	100.3	105.4	108.1
	σ	3.1	3.3	3.5	3.7	3.1	4.7	5.3	6.3
TAT	μ	0.2042	0.1662	0.1327	0.1157	0.1046	0.0818	0.0711	0.0641
	σ	0.0131	0.0101	0.0075	0.0062	0.0047	0.0038	0.0030	0.0028
NPD	μ	20.8	17.7	14.2	11.7	10.1	6.4	5.5	6.4
	σ	3.8	3.9	4.0	3.6	3.3	3.1	3.1	3.8
NPA	μ	6.1	6.7	8.4	10.6	12.5	19.2	23.9	27.8
	σ	5.4	5.6	5.6	5.8	6.1	7.3	7.9	8.8
TPD	μ	4.7963	3.5646	2.4135	1.8247	1.4523	0.8742	0.8084	1.1207
	σ	0.8394	0.7363	0.6471	0.5365	0.4672	0.5233	0.6360	0.8713

Table 4.7: Statistics of the AID-Controlled Response With Varying Frequency Ratio ψ (ζ_2 = 2%, α = 2) From the Simulation Results (Unit: m, sec)

		ψ							
		5	10	15	20	25	30	35	40
PDP	μ	0.0524	0.0461	0.0440	0.0420	0.0436	0.0394	0.0450	0.0421
	σ	0.0097	0.0082	0.0073	0.0071	0.0072	0.0075	0.0076	0.0073
PVP	μ	0.5407	0.4418	0.4075	0.3891	0.4027	0.3565	0.4222	0.3869
	σ	0.1221	0.0888	0.0777	0.0750	0.0777	0.0714	0.0839	0.0752
PAP	μ	7.2348	6.6732	6.4379	6.2586	6.3863	5.9683	6.5346	6.2329
	σ	1.5695	1.3705	1.2718	1.2191	1.2581	1.1492	1.3221	1.2197
RDP	μ	0.0143	0.0127	0.0123	0.0120	0.0123	0.0115	0.0126	0.0122
	σ	0.0016	0.0014	0.0012	0.0013	0.0013	0.0014	0.0013	0.0013
RVP	μ	0.1413	0.1124	0.1010	0.0933	0.0985	0.0817	0.1043	0.0920
	σ	0.0213	0.0162	0.0139	0.0126	0.0135	0.0110	0.0146	0.0123
RAP	μ	1.5897	1.4503	1.4067	1.3844	1.3779	1.3711	1.3836	1.3565
	σ	0.2320	0.2009	0.1879	0.1825	0.1825	0.1765	0.1846	0.1771
PDA	μ	0.0772	0.0682	0.0653	0.0639	0.0645	0.0617	0.0654	0.0632
	σ	0.0167	0.0140	0.0129	0.0124	0.0127	0.0119	0.0132	0.0124
PVA	μ	2.3717	4.1566	5.9709	7.7819	9.4051	11.2725	10.9182	13.1637
	σ	0.5195	0.8550	1.1781	1.5157	1.8458	2.1757	2.1861	2.5720
PAA	μ	76.18	269.05	580.30	1008.87	1591.37	2193.06	3163.33	3993.73
	σ	16.46	55.08	114.34	196.46	312.09	423.28	636.76	780.79
RDA	μ	0.0198	0.0170	0.0165	0.0164	0.0158	0.0167	0.0153	0.0157
	σ	0.0029	0.0024	0.0023	0.0022	0.0022	0.0022	0.0021	0.0021
RVA	μ	0.3193	0.3964	0.4846	0.5797	0.5667	0.8115	0.5423	0.6922
	σ	0.0485	0.0573	0.0677	0.0792	0.0782	0.1085	0.0763	0.0941
RAA	μ	9.36	24.65	46.27	74.62	103.80	158.47	178.88	231.61
	σ	1.40	3.55	6.44	10.19	14.25	21.17	24.81	31.27
PU	μ	5.5327	5.2544	5.1044	5.0150	5.0735	4.8612	5.1548	4.9847
	σ	1.1911	1.0751	1.0052	0.9763	0.9953	0.9380	1.0378	0.9745
RU	μ	1.2548	1.2184	1.2208	1.2324	1.1983	1.2687	1.1693	1.2079
	σ	0.1870	0.1719	0.1686	0.1687	0.1636	0.1706	0.1603	0.1644
NAT	μ	73.0	86.5	96.1	106.0	101.4	130.4	96.1	113.6
	σ	3.4	3.8	4.5	4.7	4.9	5.7	4.8	5.4
TAT	μ	0.1591	0.1467	0.1365	0.1255	0.1360	0.1026	0.1484	0.1240
	σ	0.0089	0.0075	0.0072	0.0061	0.0072	0.0050	0.0079	0.0063
NPD	μ	15.7	12.3	11.2	10.8	11.2	9.8	11.6	11.1
	σ	4.1	3.8	3.5	3.4	3.6	3.7	3.5	3.6
NPA	μ	15.6	13.3	12.2	11.5	11.7	10.7	12.1	10.9
	σ	6.4	5.9	5.7	5.3	5.5	5.2	5.4	4.8
TPD	μ	2.2444	1.7391	1.6243	1.5662	1.6513	1.3951	1.7321	1.6206
	σ	0.5443	0.4894	0.4669	0.4922	0.4864	0.5133	0.4769	0.5025

Table 4.8: Statistics of the OCS-Controlled Response With Varying Frequency Ratio ψ (ζ_2 = 2%, α = 2) From the Simulation Results (Unit: m, sec)

		ψ							
		5	10	15	20	25	30	35	40
PDP	μ	0.0528	0.0325	0.0280	0.0289	0.0262	0.0337	0.0329	0.0381
	σ	0.0129	0.0071	0.0072	0.0069	0.0065	0.0068	0.0073	0.0070
PVP	μ	0.4846	0.3262	0.2740	0.2777	0.2509	0.3118	0.3054	0.3459
	σ	0.1069	0.0711	0.0644	0.0647	0.0598	0.0663	0.0669	0.0687
PAP	μ	8.0310	6.2013	5.5795	5.4373	5.2464	5.5849	5.5150	5.8596
	σ	1.4056	1.1245	1.0880	1.0777	1.0204	1.1074	1.0884	1.1342
RDP	μ	0.0140	0.0090	0.0080	0.0085	0.0077	0.0100	0.0098	0.0113
	σ	0.0020	0.0013	0.0013	0.0013	0.0013	0.0014	0.0014	0.0014
RVP	μ	0.1094	0.0688	0.0567	0.0560	0.0484	0.0650	0.0624	0.0769
	σ	0.0167	0.0101	0.0082	0.0081	0.0070	0.0090	0.0088	0.0104
RAP	μ	1.9671	1.7358	1.5895	1.4910	1.5385	1.3826	1.3863	1.3411
	σ	0.2850	0.2341	0.2104	0.1947	0.2022	0.1771	0.1781	0.1720
PDA	μ	0.0983	0.0709	0.0625	0.0596	0.0582	0.0591	0.0588	0.0605
	σ	0.0173	0.0132	0.0119	0.0112	0.0108	0.0112	0.0111	0.0116
PVA	μ	2.9886	4.3162	5.7049	7.2557	8.4845	10.7923	12.2703	13.2212
	σ	0.5282	0.8023	1.0867	1.3698	1.5755	2.0423	2.3136	2.5438
PAA	μ	96.99	280.01	554.74	940.83	1436.21	2099.65	2844.57	3822.16
	σ	17.08	52.02	105.59	177.61	266.74	397.29	536.43	735.33
RDA	μ	0.0404	0.0287	0.0240	0.0214	0.0219	0.0185	0.0185	0.0169
	σ	0.0061	0.0039	0.0032	0.0028	0.0029	0.0024	0.0024	0.0023
RVA	μ	1.0074	1.1726	1.2486	1.2795	1.6195	1.2815	1.4508	1.2637
	σ	0.1531	0.1639	0.1696	0.1720	0.2147	0.1703	0.1966	0.1771
RAA	μ	31.52	75.16	122.62	171.53	257.90	270.32	352.75	373.86
	σ	4.80	10.52	16.63	23.01	34.16	35.51	47.30	50.61
PU	μ	7.1811	5.4885	4.8863	4.6794	4.5808	4.6546	4.6361	4.7710
	σ	1.2671	1.0210	0.9311	0.8837	0.8510	0.8810	0.8745	0.9177
RU	μ	1.8088	1.6621	1.5397	1.4458	1.5153	1.3251	1.3392	1.2483
	σ	0.2680	0.2264	0.2056	0.1909	0.1997	0.1751	0.1774	0.1670
NAT	μ	77.3	117.9	138.4	146.1	185.8	140.5	156.5	125.1
	σ	3.6	3.7	4.1	4.6	7.0	4.8	6.1	4.9
TAT	μ	0.0465	0.0502	0.0558	0.0625	0.0514	0.0797	0.0734	0.0998
	σ	0.0028	0.0023	0.0023	0.0028	0.0025	0.0034	0.0034	0.0047
NPD	μ	13.6	5.7	3.7	4.6	3.6	7.7	7.4	9.4
	σ	3.9	3.1	2.8	3.2	3.2	4.0	4.1	3.8
NPA	μ	48.2	41.2	26.2	17.4	22.2	11.5	12.1	10.2
	σ	10.3	13.2	12.2	8.9	11.9	5.7	6.1	4.9
TPD	μ	2.0742	0.6628	0.4195	0.5203	0.3682	0.9674	0.8836	1.3093
	σ	0.5880	0.3659	0.3427	0.3981	0.3432	0.5051	0.4785	0.5042

Table 4.9: Statistics of the AID-Controlled Response With Varying Frequency Ratio ψ (ζ_2 = 15%, α = 2) From the Simulation Results (Unit: m, sec)

		ψ							
		5	10	15	20	25	30	35	40
PDP	μ	0.0505	0.0464	0.0451	0.0444	0.0452	0.0422	0.0462	0.0444
	σ	0.0095	0.0083	0.0078	0.0074	0.0078	0.0070	0.0079	0.0074
PVP	μ	0.5187	0.4592	0.4335	0.4143	0.4312	0.3900	0.4504	0.4143
	σ	0.1165	0.0975	0.0870	0.0816	0.0865	0.0755	0.0927	0.0820
PAP	μ	6.8164	6.6744	6.5349	6.4307	6.5467	6.2328	6.7059	6.4399
	σ	1.4578	1.3868	1.3453	1.2953	1.3398	1.2202	1.3863	1.2932
RDP	μ	0.0140	0.0128	0.0126	0.0124	0.0127	0.0122	0.0129	0.0126
	σ	0.0016	0.0014	0.0013	0.0013	0.0013	0.0013	0.0013	0.0013
RVP	μ	0.1345	0.1180	0.1089	0.1026	0.1075	0.0935	0.1136	0.1018
	σ	0.0203	0.0172	0.0155	0.0144	0.0152	0.0126	0.0163	0.0142
RAP	μ	1.5238	1.4523	1.4097	1.3853	1.3959	1.3594	1.4229	1.3710
	σ	0.2183	0.2017	0.1916	0.1851	0.1886	0.1776	0.1941	0.1818
PDA	μ	0.0715	0.0671	0.0656	0.0646	0.0654	0.0632	0.0664	0.0646
	σ	0.0151	0.0139	0.0134	0.0130	0.0132	0.0124	0.0136	0.0129
PVA	μ	1.8285	3.3960	4.9724	6.5303	8.1429	9.5767	9.9016	11.8364
	σ	0.3908	0.7051	1.0193	1.3169	1.6539	1.8764	2.0185	2.3808
PAA	μ	70.40	264.47	582.01	1019.64	1611.69	2243.84	3207.79	4079.30
	σ	14.85	54.69	118.94	205.22	326.66	439.55	659.25	816.98
RDA	μ	0.0180	0.0161	0.0156	0.0155	0.0152	0.0156	0.0150	0.0152
	σ	0.0026	0.0023	0.0022	0.0021	0.0021	0.0021	0.0021	0.0021
RVA	μ	0.2740	0.3380	0.4081	0.4776	0.4860	0.6187	0.4857	0.5871
	σ	0.0408	0.0488	0.0575	0.0665	0.0687	0.0835	0.0692	0.0813
RAA	μ	7.66	21.29	40.40	64.88	93.42	131.47	167.32	210.23
	σ	1.12	3.05	5.67	9.01	13.13	17.71	23.62	28.97
PU	μ	5.1351	5.1721	5.1248	5.0724	5.1414	4.9763	5.2296	5.0939
	σ	1.0799	1.0696	1.0471	1.0207	1.0421	0.9747	1.0750	1.0203
RU	μ	1.1930	1.1762	1.1741	1.1808	1.1628	1.2001	1.1528	1.1682
	σ	0.1729	0.1652	0.1627	0.1621	0.1603	0.1627	0.1592	0.1592
NAT	μ	71.8	81.3	87.8	93.6	91.3	105.6	88.2	98.3
	σ	3.3	4.1	4.4	4.6	4.5	5.3	4.9	5.0
TAT	μ	0.1622	0.1586	0.1514	0.1445	0.1526	0.1300	0.1624	0.1447
	σ	0.0089	0.0090	0.0086	0.0078	0.0082	0.0071	0.0095	0.0078
NPD	μ	14.7	12.5	11.7	11.4	11.7	10.9	12.2	11.4
	σ	4.0	3.6	3.6	3.4	3.5	3.6	3.5	3.5
NPA	μ	13.8	13.2	12.5	11.9	12.4	11.0	13.0	11.8
	σ	6.1	5.7	5.7	5.5	5.7	5.2	5.7	5.2
TPD	μ	2.1492	1.7894	1.7144	1.6754	1.7418	1.6168	1.8204	1.7348
	σ	0.5470	0.4845	0.4784	0.4742	0.4772	0.4990	0.4869	0.4873

Table 4.10: Statistics of the OCS-Controlled Response With Varying Frequency Ratio ψ ($\zeta_2 = 15\%$, $\alpha = 2$) From the Simulation Results (Unit: m, sec)

		ψ							
		5	10	15	20	25	30	35	40
PDP	μ	0.0686	0.0421	0.0396	0.0397	0.0400	0.0403	0.0401	0.0414
	σ	0.0297	0.0090	0.0072	0.0079	0.0072	0.0074	0.0077	0.0073
PVP	μ	0.5123	0.3832	0.3602	0.3591	0.3633	0.3680	0.3617	0.3792
	σ	0.1468	0.0778	0.0705	0.0732	0.0717	0.0736	0.0755	0.0733
PAP	μ	6.5219	6.1228	5.9876	5.9757	6.0096	6.0499	5.9912	6.1403
	σ	1.3472	1.2188	1.1503	1.1397	1.1552	1.1720	1.1799	1.1776
RDP	μ	0.0172	0.0117	0.0114	0.0115	0.0115	0.0118	0.0117	0.0121
	σ	0.0054	0.0014	0.0013	0.0013	0.0013	0.0014	0.0014	0.0013
RVP	μ	0.1254	0.0906	0.0845	0.0834	0.0845	0.0854	0.0829	0.0895
	σ	0.0284	0.0123	0.0114	0.0115	0.0115	0.0117	0.0113	0.0121
RAP	μ	1.5457	1.4404	1.3966	1.3724	1.3557	1.3507	1.3495	1.3436
	σ	0.2276	0.1890	0.1809	0.1779	0.1762	0.1747	0.1740	0.1739
PDA	μ	0.0763	0.0652	0.0625	0.0619	0.0617	0.0619	0.0617	0.0623
	σ	0.0171	0.0131	0.0123	0.0121	0.0119	0.0120	0.0120	0.0121
PVA	μ	1.9450	3.2955	4.7396	6.2614	7.6842	9.3820	10.3851	11.4293
	σ	0.4363	0.6629	0.9325	1.2235	1.4828	1.8158	2.0271	2.2131
PAA	μ	75.17	256.96	554.64	977.48	1520.74	2198.09	2981.51	3936.59
	σ	16.85	51.57	109.13	191.02	293.40	425.42	581.95	762.20
RDA	μ	0.0208	0.0183	0.0174	0.0168	0.0163	0.0162	0.0162	0.0157
	σ	0.0031	0.0025	0.0023	0.0023	0.0022	0.0022	0.0022	0.0021
RVA	μ	0.3757	0.4879	0.5736	0.6446	0.6950	0.7575	0.8344	0.8409
	σ	0.0557	0.0656	0.0765	0.0861	0.0928	0.1010	0.1113	0.1114
RAA	μ	11.41	31.57	58.00	90.08	126.53	169.52	217.29	267.22
	σ	1.69	4.25	7.76	12.07	16.99	22.71	29.01	35.71
PU	μ	5.5588	5.0357	4.8866	4.8639	4.8518	4.8748	4.8611	4.9158
	σ	1.2615	1.0121	0.9617	0.9506	0.9362	0.9432	0.9486	0.9518
RU	μ	1.2921	1.2889	1.2673	1.2496	1.2263	1.2216	1.2347	1.1964
	σ	0.1902	0.1761	0.1703	0.1679	0.1655	0.1641	0.1668	0.1615
NAT	μ	64.3	89.0	99.5	104.5	104.2	107.4	115.4	105.2
	σ	4.7	3.1	3.8	4.5	4.5	4.8	5.2	5.0
TAT	μ	0.1027	0.1046	0.1074	0.1103	0.1168	0.1166	0.1113	0.1249
	σ	0.0058	0.0047	0.0052	0.0056	0.0058	0.0060	0.0057	0.0067
NPD	μ	13.9	10.1	9.4	9.7	9.7	10.3	10.3	10.7
	σ	3.5	3.3	3.3	3.5	3.5	3.6	3.7	3.6
NPA	μ	14.8	12.5	11.1	10.7	10.5	10.5	10.3	10.6
	σ	6.8	6.1	5.6	5.4	5.1	5.2	5.0	5.1
TPD	μ	2.5705	1.4523	1.3411	1.3759	1.3994	1.4835	1.4551	1.5780
	σ	0.7380	0.4672	0.4545	0.4864	0.4799	0.5166	0.5299	0.5073

Table 4.11: Statistics of the AID-Controlled Response With Varying AS Damping Ratio ζ_2 ($\alpha = 2$, $\psi = 10$) From the Simulation Results (Unit: m, sec)

		$\zeta_2\%$							
		0	4	8	12	16	20	40	80
PDP	μ	0.0461	0.0461	0.0461	0.0463	0.0464	0.0466	0.0450	0.0435
	σ	0.0080	0.0080	0.0082	0.0083	0.0083	0.0081	0.0078	0.0077
PVP	μ	0.4404	0.4442	0.4494	0.4553	0.4603	0.4537	0.4439	0.4375
	σ	0.0870	0.0899	0.0929	0.0960	0.0977	0.0956	0.0927	0.0927
PAP	μ	6.6756	6.6579	6.6626	6.6691	6.6700	6.5712	6.3660	6.0690
	σ	1.3550	1.3682	1.3759	1.3815	1.3854	1.3684	1.3055	1.2399
RDP	μ	0.0127	0.0127	0.0127	0.0128	0.0128	0.0130	0.0126	0.0122
	σ	0.0013	0.0013	0.0013	0.0014	0.0014	0.0014	0.0013	0.0013
RVP	μ	0.1119	0.1131	0.1149	0.1167	0.1183	0.1150	0.1124	0.1111
	σ	0.0161	0.0162	0.0165	0.0170	0.0172	0.0167	0.0162	0.0162
RAP	μ	1.4533	1.4475	1.4476	1.4490	1.4527	1.4365	1.4119	1.3934
	σ	0.2012	0.1992	0.1997	0.2002	0.2010	0.1982	0.1932	0.1903
PDA	μ	0.0685	0.0679	0.0676	0.0673	0.0670	0.0661	0.0632	0.0582
	σ	0.0138	0.0139	0.0139	0.0140	0.0138	0.0136	0.0128	0.0117
PVA	μ	4.3025	4.0197	3.7759	3.5521	3.3445	3.1280	2.4015	1.5533
	σ	0.8720	0.8253	0.7793	0.7411	0.6924	0.6470	0.4904	0.3122
PAA	μ	270.28	267.98	266.72	265.49	264.00	260.55	248.87	228.62
	σ	54.56	54.70	54.76	55.12	54.48	53.67	50.52	45.76
RDA	μ	0.0171	0.0168	0.0165	0.0162	0.0160	0.0160	0.0151	0.0138
	σ	0.0024	0.0024	0.0023	0.0023	0.0022	0.0022	0.0021	0.0019
RVA	μ	0.4071	0.3856	0.3668	0.3496	0.3348	0.3381	0.2873	0.2165
	σ	0.0584	0.0549	0.0524	0.0505	0.0481	0.0485	0.0413	0.0311
RAA	μ	25.31	24.01	22.91	21.93	21.10	20.51	17.79	14.37
	σ	3.61	3.40	3.26	3.14	3.01	2.92	2.50	1.99
PU	μ	5.2774	5.2341	5.2114	5.1890	5.1638	5.1025	4.9098	4.6330
	σ	1.0649	1.0684	1.0697	1.0771	1.0651	1.0508	0.9970	0.9282
RU	μ	1.2270	1.2092	1.1949	1.1828	1.1736	1.1795	1.1485	1.1148
	σ	0.1736	0.1694	0.1677	0.1656	0.1643	0.1654	0.1592	0.1528
NAT	μ	87.4	85.4	83.8	82.1	80.4	82.4	80.3	76.0
	σ	3.8	3.9	4.1	4.0	4.1	3.9	3.9	3.9
TAT	μ	0.1451	0.1490	0.1524	0.1561	0.1607	0.1541	0.1563	0.1588
	σ	0.0074	0.0079	0.0086	0.0087	0.0092	0.0084	0.0086	0.0089
NPD	μ	12.2	12.3	12.3	12.4	12.5	12.7	11.9	11.3
	σ	3.9	3.8	3.7	3.7	3.7	3.8	3.5	3.5
NPA	μ	13.4	13.4	13.2	13.1	13.1	12.6	11.7	10.7
	σ	5.9	5.9	5.8	5.7	5.7	5.7	5.4	5.4
TPD	μ	1.7441	1.7479	1.7634	1.7737	1.7926	1.8558	1.7415	1.6051
	σ	0.4992	0.4839	0.4739	0.4850	0.4821	0.5075	0.4765	0.4603

Table 4.12: Statistics of the OCS-Controlled Response With Varying AS Damping Ratio ζ_2 ($\alpha = 2$, $\psi = 10$) From the Simulation Results (Unit: m, sec)

		ζ_2%							
		0	4	8	12	16	20	40	80
PDP	μ	0.0284	0.0344	0.0379	0.0411	0.0421	0.0454	0.0620	0.0718
	σ	0.0058	0.0073	0.0081	0.0116	0.0092	0.0153	0.0272	0.0268
PVP	μ	0.3508	0.3282	0.3522	0.3722	0.3859	0.3990	0.4597	0.4877
	σ	0.0787	0.0693	0.0761	0.0816	0.0789	0.0977	0.1295	0.1235
PAP	μ	10.2147	5.9415	5.9840	6.0822	6.1134	6.1557	6.1874	6.0505
	σ	1.4669	1.0898	1.1433	1.1569	1.2029	1.2100	1.2570	1.2895
RDP	μ	0.0079	0.0096	0.0107	0.0115	0.0118	0.0125	0.0153	0.0179
	σ	0.0010	0.0013	0.0013	0.0017	0.0014	0.0024	0.0037	0.0042
RVP	μ	0.0670	0.0731	0.0813	0.0873	0.0915	0.0963	0.1129	0.1242
	σ	0.0093	0.0106	0.0115	0.0131	0.0124	0.0159	0.0205	0.0208
RAP	μ	2.7419	1.6023	1.5017	1.4593	1.4354	1.4230	1.4013	1.3840
	σ	0.3779	0.2099	0.1970	0.1930	0.1883	0.1872	0.1929	0.1847
PDA	μ	0.1257	0.0670	0.0657	0.0653	0.0650	0.0647	0.0665	0.0659
	σ	0.0184	0.0127	0.0131	0.0135	0.0128	0.0128	0.0153	0.0155
PVA	μ	7.8764	3.9640	3.6674	3.4405	3.2456	3.0626	2.5254	1.7583
	σ	1.1494	0.7480	0.7305	0.7130	0.6390	0.6058	0.5814	0.4133
PAA	μ	496.28	264.57	259.15	257.43	256.39	255.20	261.90	258.98
	σ	72.47	50.02	51.62	53.29	50.41	50.29	60.34	60.94
RDA	μ	0.0761	0.0241	0.0207	0.0191	0.0181	0.0174	0.0155	0.0140
	σ	0.0109	0.0032	0.0028	0.0026	0.0025	0.0024	0.0022	0.0019
RVA	μ	4.1982	0.8691	0.6450	0.5391	0.4738	0.4282	0.3092	0.2178
	σ	0.6061	0.1177	0.0871	0.0730	0.0634	0.0579	0.0441	0.0305
RAA	μ	267.01	55.91	41.65	34.86	30.65	27.70	20.14	14.43
	σ	38.52	7.58	5.64	4.72	4.11	3.75	2.88	2.00
PU	μ	9.7296	5.1842	5.0762	5.0437	5.0248	5.0036	5.1757	5.2424
	σ	1.4202	0.9825	1.0127	1.0471	0.9889	0.9866	1.1952	1.2311
RU	μ	2.6931	1.5115	1.3850	1.3206	1.2797	1.2492	1.1744	1.1338
	σ	0.3730	0.2020	0.1873	0.1790	0.1745	0.1695	0.1658	0.1529
NAT	μ	138.0	108.6	97.9	92.2	88.2	84.9	72.4	57.9
	σ	4.9	3.8	3.7	3.6	3.2	3.6	4.7	5.0
TAT	μ	0.0203	0.0658	0.0852	0.0975	0.1067	0.1139	0.1390	0.1655
	σ	0.0012	0.0032	0.0043	0.0048	0.0049	0.0053	0.0081	0.0094
NPD	μ	4.2	6.6	8.3	9.6	10.2	10.7	12.3	13.9
	σ	2.6	3.2	3.2	3.5	3.2	3.2	3.6	3.8
NPA	μ	126.7	23.9	15.6	13.3	12.3	11.7	11.0	10.1
	σ	6.6	9.7	7.2	6.3	6.1	5.8	5.6	5.4
TPD	μ	0.4070	0.8229	1.1292	1.3684	1.4870	1.6266	2.1569	2.8141
	σ	0.2637	0.3962	0.4385	0.4654	0.4534	0.5089	0.6620	0.8655

Table 4.13: Statistics of the TID-Controlled Response With Varying Control Force Limit ratio η ($\alpha = 2$, $\psi = 10$, $\zeta_2 = 2\%$) From the Simulation Results (Unit: m, sec)

		u_{max}							
		0.5	1.0	1.5	2.0	2.5	3.0	4.0	5.0
PDP	μ	0.1192	0.0784	0.0564	0.0433	0.0366	0.0341	0.0330	0.0326
	σ	0.0331	0.0192	0.0147	0.0106	0.0091	0.0083	0.0079	0.0075
PVP	μ	0.8211	0.5761	0.4525	0.3734	0.3324	0.3214	0.3215	0.3210
	σ	0.2301	0.1411	0.1136	0.0826	0.0716	0.0784	0.0720	0.0726
PAP	μ	5.3535	4.3520	4.0903	4.1818	4.5074	4.9648	5.4348	5.8033
	σ	1.3851	0.9041	0.8286	0.7681	0.8074	0.8817	0.9342	0.9919
RDP	μ	0.0336	0.0195	0.0137	0.0110	0.0097	0.0093	0.0091	0.0090
	σ	0.0088	0.0037	0.0023	0.0015	0.0013	0.0014	0.0013	0.0012
RVP	μ	0.2230	0.1369	0.0998	0.0817	0.0739	0.0702	0.0693	0.0687
	σ	0.0568	0.0264	0.0182	0.0131	0.0114	0.0111	0.0104	0.0102
RAP	μ	1.4899	1.2683	1.3632	1.4889	1.5871	1.6532	1.6976	1.7176
	σ	0.3445	0.1764	0.1840	0.1999	0.2155	0.2221	0.2267	0.2291
PDA	μ	0.0204	0.0245	0.0305	0.0371	0.0442	0.0516	0.0587	0.0646
	σ	0.0041	0.0041	0.0052	0.0064	0.0077	0.0091	0.0101	0.0108
PVA	μ	0.8227	1.0800	1.5439	2.0142	2.4851	2.9517	3.4160	3.8208
	σ	0.2127	0.1878	0.2716	0.3542	0.4414	0.5232	0.5973	0.6433
PAA	μ	51.01	67.36	96.94	127.52	158.31	189.13	219.77	246.76
	σ	13.21	11.78	17.07	22.54	28.20	33.69	38.64	41.65
RDA	μ	0.0089	0.0141	0.0185	0.0220	0.0245	0.0263	0.0275	0.0281
	σ	0.0014	0.0022	0.0028	0.0032	0.0035	0.0037	0.0038	0.0038
RVA	μ	0.2287	0.3916	0.5889	0.7653	0.9090	1.0165	1.0925	1.1357
	σ	0.0392	0.0733	0.1062	0.1284	0.1417	0.1511	0.1557	0.1590
RAA	μ	14.24	24.94	37.74	49.13	58.34	65.21	70.05	72.81
	σ	2.45	4.71	6.82	8.22	9.09	9.69	9.99	10.19
PU	μ	0.6096	1.2191	1.8287	2.4383	3.0479	3.6574	4.2638	4.8105
	σ	0.1092	0.2184	0.3276	0.4367	0.5459	0.6551	0.7547	0.8179
RU	μ	0.5235	0.9129	1.1858	1.3734	1.4950	1.5723	1.6211	1.6433
	σ	0.0886	0.1425	0.1745	0.1944	0.2070	0.2131	0.2189	0.2211
NAT	μ	60.9	85.0	99.6	108.4	113.1	115.9	116.9	117.7
	σ	5.7	6.3	5.5	5.1	4.3	3.9	3.9	3.6
TAT	μ	0.1922	0.1120	0.0808	0.0657	0.0578	0.0536	0.0517	0.0507
	σ	0.0257	0.0142	0.0089	0.0060	0.0041	0.0030	0.0025	0.0022
NPD	μ	19.4	14.0	10.5	8.1	6.5	6.0	5.8	5.5
	σ	3.4	3.5	3.3	3.1	3.0	3.2	3.0	2.9
NPA	μ	6.6	4.4	5.8	12.6	23.0	32.6	37.8	39.6
	σ	6.4	5.4	6.6	11.8	14.8	14.7	14.0	13.4
TPD	μ	5.4488	3.0582	1.8518	1.1887	0.8566	0.7334	0.6760	0.6471
	σ	0.9887	0.7347	0.5713	0.4458	0.3936	0.4016	0.3773	0.3575

Table 4.14: Statistics of the TID-Controlled Response With Varying Control Force Limit ratio η ($\alpha = 2$, $\psi = 10$, $\zeta_2 = 15\%$) From the Simulation Results (Unit: m, sec)

		u_{max}							
		0.5	1.0	1.5	2.0	2.5	3.0	4.0	5.0
PDP	μ	0.1200	0.0799	0.0599	0.0503	0.0445	0.0426	0.0424	0.0421
	σ	0.0330	0.0194	0.0144	0.0123	0.0094	0.0092	0.0096	0.0092
PVP	μ	0.8243	0.5837	0.4763	0.4179	0.3918	0.3816	0.3814	0.3825
	σ	0.2295	0.1419	0.1120	0.0919	0.0825	0.0760	0.0772	0.0774
PAP	μ	5.3733	4.3936	4.2170	4.4239	4.7715	5.1938	5.6043	5.8838
	σ	1.3784	0.9110	0.8198	0.8071	0.8596	0.9211	1.0033	1.0835
RDP	μ	0.0338	0.0202	0.0151	0.0131	0.0122	0.0119	0.0118	0.0117
	σ	0.0088	0.0037	0.0022	0.0018	0.0015	0.0014	0.0014	0.0013
RVP	μ	0.2247	0.1423	0.1114	0.0990	0.0935	0.0914	0.0910	0.0906
	σ	0.0566	0.0264	0.0179	0.0146	0.0135	0.0126	0.0124	0.0122
RAP	μ	1.4934	1.2436	1.2859	1.3496	1.3914	1.4156	1.4309	1.4361
	σ	0.3439	0.1753	0.1705	0.1763	0.1823	0.1834	0.1877	0.1885
PDA	μ	0.0132	0.0210	0.0287	0.0363	0.0438	0.0509	0.0571	0.0615
	σ	0.0024	0.0036	0.0050	0.0063	0.0077	0.0088	0.0097	0.0108
PVA	μ	0.5145	0.8818	1.2692	1.6581	2.0458	2.4320	2.7835	3.0486
	σ	0.0941	0.1555	0.2226	0.2922	0.3630	0.4332	0.4809	0.5323
PAA	μ	35.38	65.04	95.44	126.20	156.97	187.75	215.87	237.14
	σ	5.86	11.25	16.81	22.36	27.84	33.43	37.22	41.22
RDA	μ	0.0072	0.0118	0.0147	0.0164	0.0174	0.0178	0.0181	0.0182
	σ	0.0012	0.0018	0.0021	0.0023	0.0023	0.0024	0.0025	0.0025
RVA	μ	0.1396	0.2474	0.3339	0.3942	0.4347	0.4593	0.4748	0.4821
	σ	0.0236	0.0416	0.0529	0.0587	0.0617	0.0629	0.0643	0.0650
RAA	μ	8.48	15.58	21.33	25.35	28.05	29.68	30.70	31.18
	σ	1.46	2.66	3.41	3.79	3.98	4.07	4.17	4.21
PU	μ	0.6096	1.2191	1.8287	2.4383	3.0479	3.6562	4.2161	4.6411
	σ	0.1092	0.2184	0.3276	0.4367	0.5459	0.6549	0.7295	0.8072
RU	μ	0.5069	0.8407	1.0449	1.1624	1.2270	1.2585	1.2767	1.2842
	σ	0.0838	0.1259	0.1502	0.1606	0.1654	0.1695	0.1739	0.1756
NAT	μ	57.7	74.4	82.5	86.3	87.9	88.5	88.8	88.9
	σ	5.0	4.8	3.9	3.7	3.5	3.4	3.3	3.1
TAT	μ	0.2073	0.1430	0.1206	0.1115	0.1076	0.1059	0.1050	0.1048
	σ	0.0235	0.0131	0.0081	0.0064	0.0056	0.0052	0.0049	0.0048
NPD	μ	19.4	14.8	12.1	10.8	10.4	10.0	10.1	9.9
	σ	3.5	3.5	3.6	3.4	3.4	3.2	3.2	3.3
NPA	μ	6.6	4.5	5.7	8.6	10.8	11.9	12.3	12.4
	σ	6.4	5.3	5.7	6.2	6.2	6.1	6.1	6.0
TPD	μ	5.4980	3.2345	2.2127	1.7764	1.5785	1.4944	1.4721	1.4432
	σ	0.9787	0.7429	0.5919	0.5377	0.4885	0.4649	0.4748	0.4661

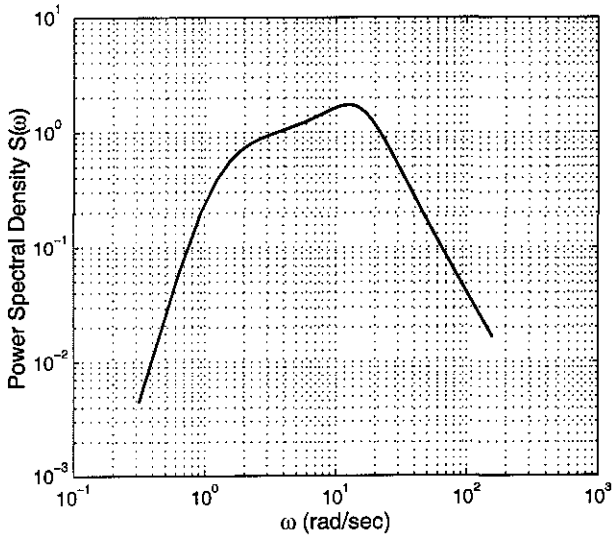

Figure 4.1: General Appearance of Power Spectral Density Function $S(\omega)$

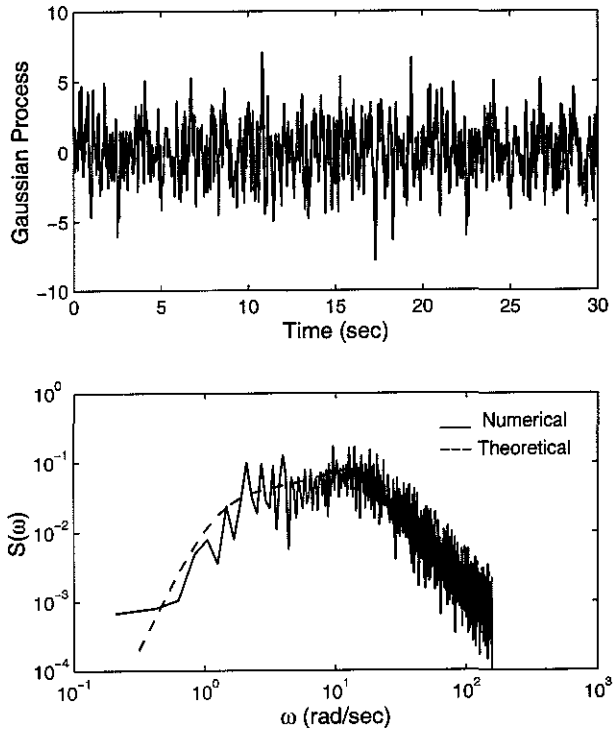

Figure 4.2: A Typical Gaussian Process and Its Power Spectral Density Function $S(\omega)$

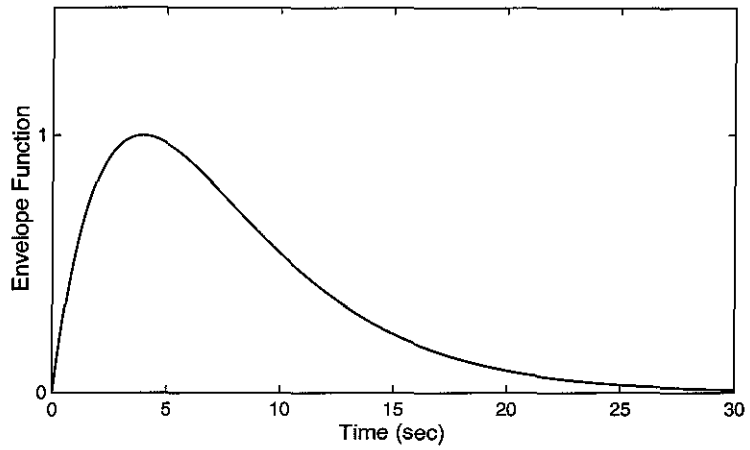

Figure 4.3: Intensity Envelope Function $e(t)$ for Nonstationary Process $a(t)$

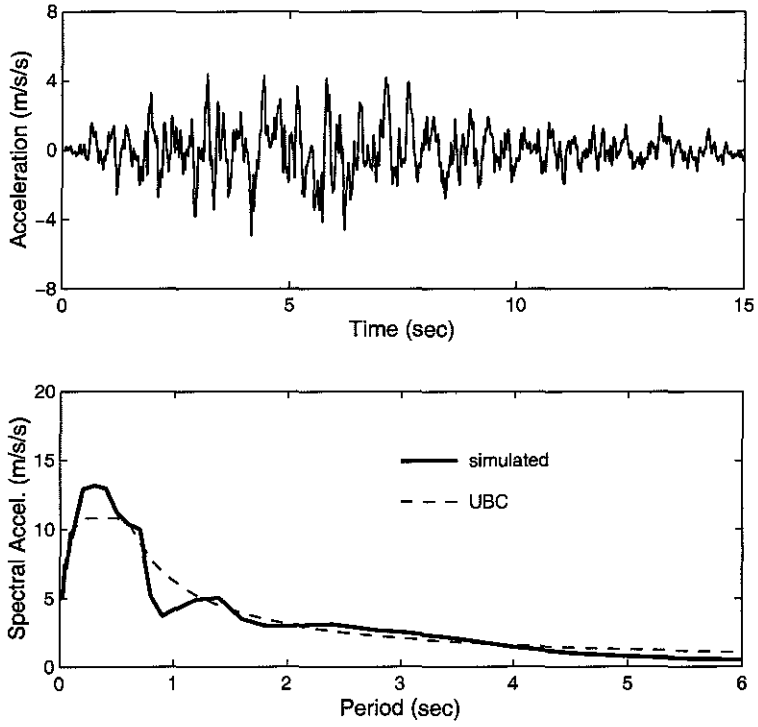

Figure 4.4: A Typical Artificial Ground Motion Accelerogram

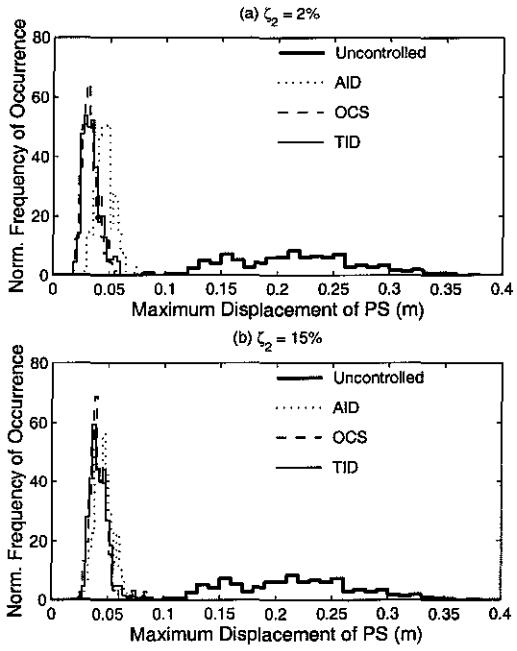

Figure 4.5: Normalized Occurrence Frequency of the Maximum Displacement of PS ($\alpha = 2$, $\psi = 10$, $\eta = 0.6$)

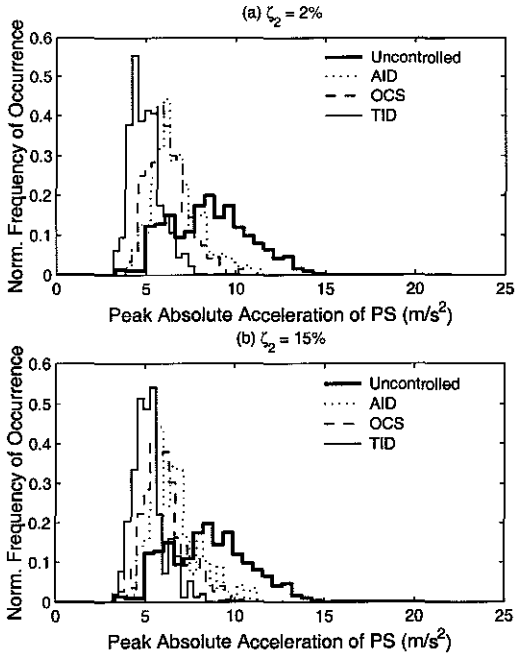

Figure 4.6: Normalized Occurrence Frequency of the Maximum Absolute Acceleration of PS ($\alpha = 2$, $\psi = 10$, $\eta = 0.6$)

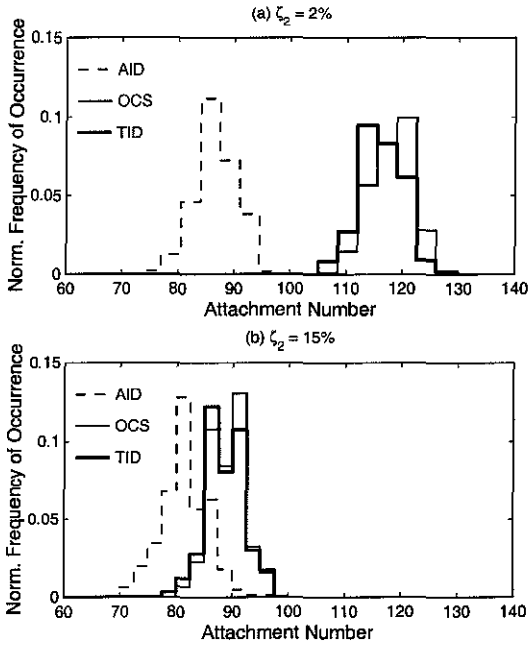

Figure 4.7: Normalized Occurrence Frequency of the Attachment Number ($\alpha = 2$, $\psi = 10$, $\eta = 0.6$)

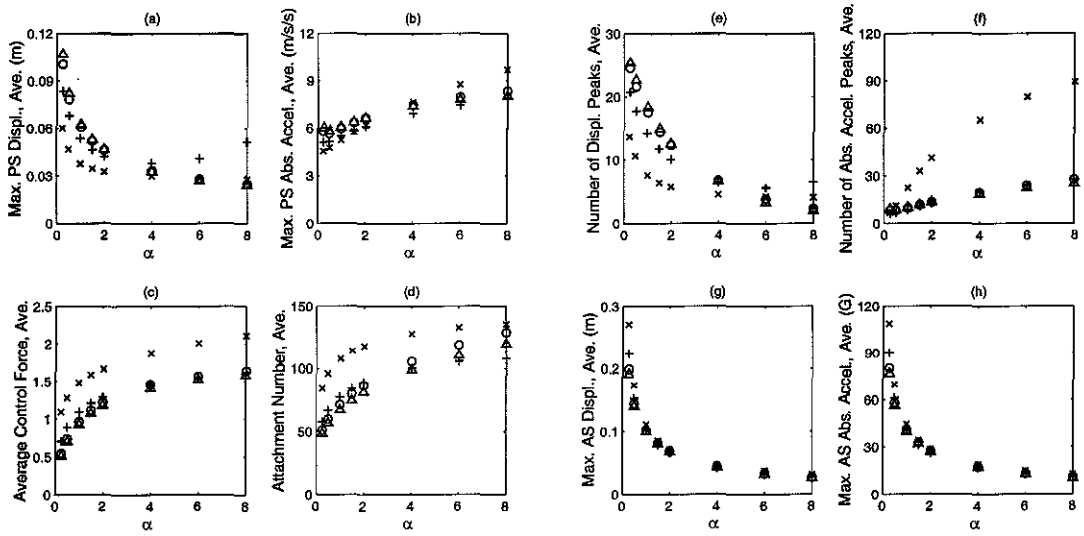

Figure 4.8: Variation of Mean Values of (a) Maximum Displacement of PS; (b) Maximum Absolute Acceleration of PS; (c) Average Control Force; (d) Attachment Number; (e) Number of Peak Displacements of PS; (f) Number of Peak Absolute Acceleration of PS; (g) Maximum Displacement of AS; (h) Maximum Absolute Acceleration of AS with Stiffness Ratio α (ψ=10, $\circ$ AID with ζ_2=2%, $\triangle$ AID with ζ_2=15%, $\times$ OCS with ζ_2=2%, + OCS with ζ_2=15%)

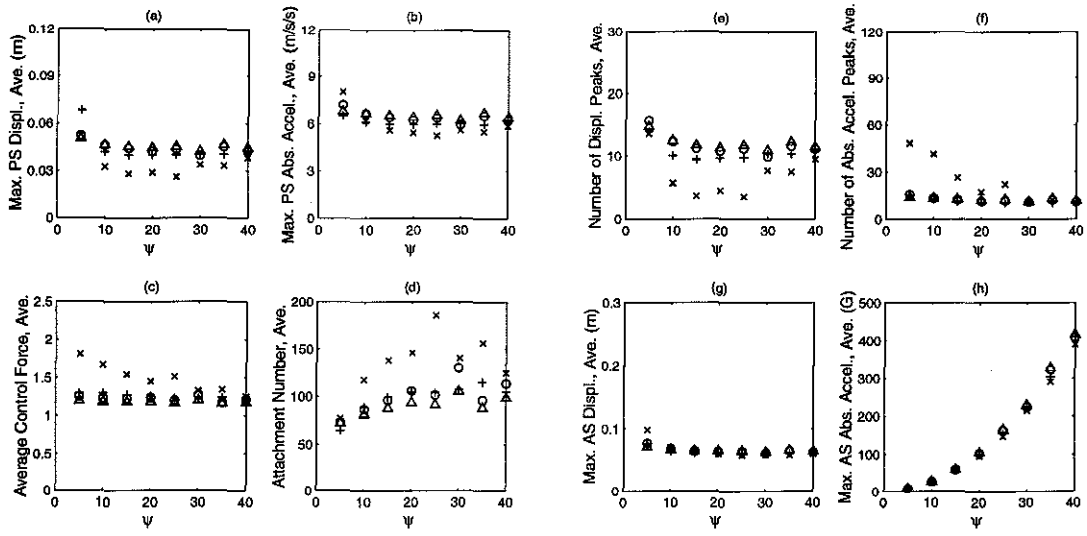

Figure 4.9: Variation of Mean Values of (a) Maximum Displacement of PS; (b) Maximum Absolute Acceleration of PS; (c) Average Control Force; (d) Attachment Number; (e) Number of Peak Displacements of PS; (f) Number of Peak Absolute Acceleration of PS; (g) Maximum Displacement of AS; (h) Maximum Absolute Acceleration with Frequency Ratio ψ (α=2, $\circ$ AID with ζ_2=2%, $\triangle$ AID with ζ_2=15%, $\times$ OCS with ζ_2=2%, + OCS with ζ_2=15%)

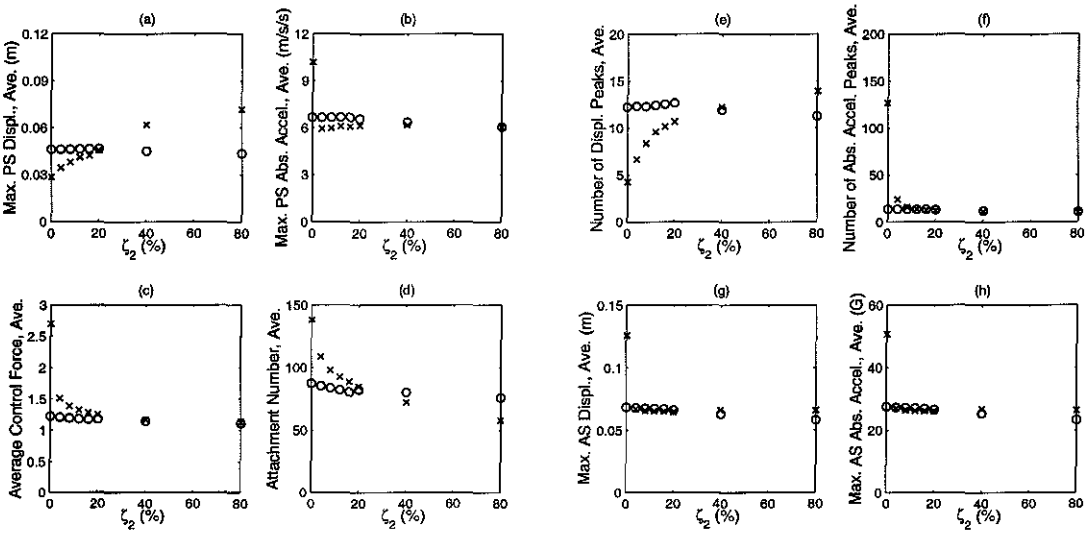

Figure 4.10: Variation of Mean Values of (a) Maximum Displacement of PS; (b) Maximum Absolute Acceleration of PS; (c) Average Control Force; (d) Attachment Number; (e) Number of Peak Displacements of PS; (f) Number of Peak Absolute Acceleration of PS; (g) Maximum Displacement of AS; (h) Maximum Absolute Acceleration of AS with AS Damping Ratio ζ_2 (α=2, ψ=10, $\circ$ AID, $\times$ OCS)

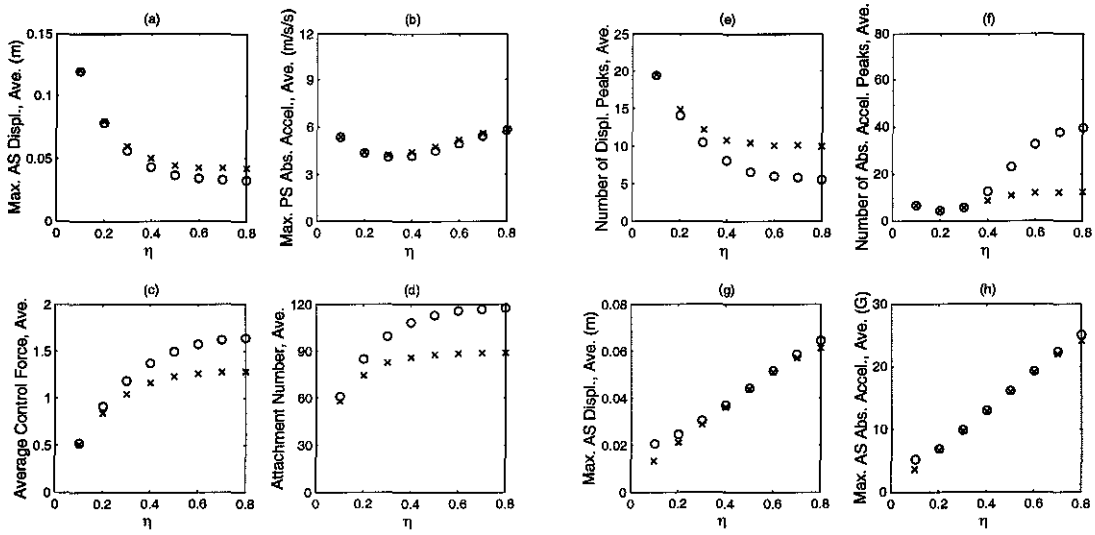

Figure 4.11: Variation of Mean Values of (a) Maximum Displacement of PS; (b) Maximum Absolute Acceleration of PS; (c) Average Control Force; (d) Attachment Number; (e) Number of Peak Displacements of PS; (f) Number of Peak Absolute Acceleration of PS; (g) Maximum Displacement of AS; (h) Maximum Absolute Acceleration of AS with Control Force Limit Ratio η (α=2, ψ=10, $\circ$ TID with ζ_2=2%, $\times$ TID with ζ_2=15%)

Chapter 5 Conclusions and Future Research Directions

5.1 Summary

AIC utilizes controlled interactions between distinct structures, or members of the same structure, to reduce the response of a primary structure subjected to environmental excitations. In this report, a family of AIC algorithms, which are all founded upon the same instantaneous optimal control strategy that involves minimization of an energy-based performance index at each time instant, are formulated and their performances are compared with each other. The AIC algorithms include the Active Interface Damping (AID) [6], Optimal Connection Strategy (OCS), and newly developed Tuned Interaction Damping (TID) algorithms.

The AIC approach has been developed as a semi-active means of protecting building structures against large earthquakes. A typical AIC system consists of a primary structure targeted for vibration control, a number of auxiliary structures, and interaction elements that connect the auxiliary structures to the primary structure. Through actively modulating the operating states of the interaction elements according to pre-specified control logic, control forces favorable to the control strategy are reactively developed within the interaction elements and the vibration of the primary structure is thus restrained. The merits of this structural control approach include both high control performance and minimal external power requirement for the operation of the control devices. The latter is important during large earthquakes when power blackouts are likely to occur. Most encouraging is that with currently available technology this control approach can be readily implemented in real structures.

The main objective of the AIC control strategy is to minimize the displacements of a primary structure. This objective is accomplished through an effort to maintain the relative vibrational energy of the primary structure as small as possible over the course of an excitation event. It has been previously shown that this energy provides an upper bound

for each of the story displacements of the primary structure.

When the primary structure (PS) and auxiliary structure (AS) are attached with dissimilar velocities, the induced impact may cause damage to either or both the PS and AS. This detrimental impact can be eliminated if an additional attachment condition is introduced. This new attachment condition requires equal PS and AS velocities in order to initiate an interaction between the PS and AS. In an AIC system, the function of the AS can be regarded as an actuator delivering a control force to the PS. The value of the control force delivered by the AS is approximately equal to the elastic spring restoring force in the AS. Therefore, the larger the AS displacement, the larger the control force will be. It is found that the PS and AS usually achieve equal velocities at the time instant when the AS is close to its maximum displacement. A large control force will then be generated and more energy will be dissipated from the PS if the attachment between the PS and AS is delayed until the PS and AS have equal velocities. However, drastically increased peak accelerations at the lower floors of the primary structure and too many attachment cycles are also observed in the AID and OCS systems. To overcome these problems, the TID algorithm with proper AS damping and bounded control force level is proposed and investigated herein.

Two approaches, the Modal Control (MC) and Nodal Control (NC) approach, are developed to implement the AIC control algorithms in multi-degree-of-freedom systems. The Modal Control approach directs the control effort to certain dominant response modes of the primary structure, while the Nodal Control approach tries to restrain the individual inter-story drift of the primary structure directly. It is found that the Modal Control approach is more efficient than the Nodal Control approach.

The results of numerical simulations verify the efficacy of the AIC control approaches in controlling vibrations of building structures during large earthquakes.

5.2 Conclusions

Based on the analytical and numerical simulation results obtained in this study, the following list summarizes the main conclusions for this study:

1. An effective AIC system utilizes the dynamics of an auxiliary structure with large stiffness and high natural frequency that implies a light mass of the auxiliary structure.

2. The AIC control algorithms are inherently stable.

3. All of the three AIC control algorithms considered herein lead to significant reduction in displacement and velocity response of the primary structure even under severe seismic excitation.

4. Among the three AIC control algorithms, the OCS control algorithm generally has the best control performance in terms of displacement and velocity response reduction. However, the OCS system also has a large number of attachment cycles. This problem can be partly alleviated by adding proper damping to the auxiliary structure. By connecting a fuse device with its maximum force being optimally tuned in series with the On/Off locking device, the TID system partly solves the problems with the OCS system while maintaining a comparable displacement response to the OCS system. Considering the impact problem and generally low performance of the AID system compared with the other AIC systems, the TID control algorithm is felt to have an advantage over the AID and OCS control algorithms in the future applications.

5. Large sampling periods and time delays may result in poor performance of the AIC control system. However, numerical simulation results show that the TID control algorithm is less sensitive than other algorithms to changes in sampling period and time delay.

6. For an N-story building, the number of configurations needed to examine in each sampling period is 2N for both Modal Control approach and Nodal Control approach since control decisions for one IE (interaction element) can be made independent of other IEs.

7. All of the AIC control algorithms, including the AID, OCS, and TID control algorithms, are capable of significantly reducing the inter-story drift values of the PS. Overall, the TID control algorithm exhibits better control performance and is thus more practical than the other AIC control algorithms. In the TID system, not only the inter-story drift, but also the absolute acceleration, number of attachments, control force level, AS displacement relative to its support floor, and AS absolute acceleration are greatly reduced.

8. An AS with a stiffness value comparable to the PS story stiffness and a natural period in the order of a few hundredths of a second is effective in reducing the displacement

response of the PS. The damping ratio for the AS is recommended to be of the order of 15-percent. The maximum control force level of the IE in the TID system can be tuned for optimal control performance.

5.3 Future Research Directions

The following topics are suggested for consideration in possible future research efforts:

1. Develop more realistic models for the interaction elements (IE) utilized in analysis and simulations. In the present study, the interaction element is modeled as being able to respond instantaneously to control signals. The actual behavior of interaction elements is much more complex than this simplistic IE model with only two operating states.

2. To verify the effectiveness of the proposed control approaches, experiments with small-scale or preferably full-scale structures equipped with the proposed control systems would be highly desired.

3. Artificial intelligence algorithms (e.g., neural network, fuzzy logic, etc.) may be used to determine the optimal control force limit for the fuse device. In the current study, this control force limit is obtained by numerical trials based on several earthquake ground motions. This approach is time-consuming and the control force limit determined in this way is generally not the optimal one over the whole parameter space.

4. In a real-world setting, uncertainties are expected to exist with structural models and excitations. The effect of incorporating these uncertainties in controlled structures needs to be examined.

5. Examine the performance of the proposed control approach with reduced state information.

6. Develop an automated capability for the control processor to identify and target dominant response modes in real time.

7. Develop a compensation scheme for time delays and response times associated with device operating state changes which would improve the response control effectiveness of the nominal-performance cases.

Bibliography

[1] Chopra, A. K., Dynamics of Structures: Theory and Application to Earthquake Engineering, Prentice-Hall (1995).

[2] Clough, R. W. and Penzien, J., Dynamics of Structures, McGraw-Hill (1993).

[3] Fujino, Y., Soong, T.T., and Spencer, B.F., Jr., "Structural Control: Basic Concepts and Applications," textslProceedings of the ASCE Structures Congress, Chicago, Illinois (1996).

[4] Gasparini, D. and Vanmarcke, E. H., "Simulated Earthquake Motions Compatible with Prescribed Response Spectra," *MIT, Department of Civil Engineering*, Report No. R76-4 (1976).

[5] Haruhiko, K. and Kobori, T., "Development and Modeling of Variable Damping Unit for Active Variable Damping System," *Proceedings of the Eleventh World Conference on Earthquake Engineering*, Acapulco, Mexico (1996).

[6] Hayen, J. C., "Response Control of Structural Systems Using Semi-Actively Controlled Interactions," *Ph. D. Thesis*, EERL Report 95-03, California Institute of Technology (1995).

[7] Hayen, J. C. and Iwan, W. D., "Realistic Model Studies of Active Interaction Control," *Report to Kajima Corporation*, EERL, California Institute of Technology (1999).

[8] Hayen, J. C. and Iwan, W. D., "Response Control of Structural Systems Using Active Interface Damping," *Proc. of the First World Conference on Structural Control*, V. 1, Los Angeles, California (1994).

[9] Housner, G. W., et al., "Special Issue on Structural Control: Past, Present, and Future," *Journal of Engineering Mechanics*, V. 123, No. 9 (1997).

[10] Housner, G. W. and Jennings, P. C., "Generation of Artificial Earthquakes," *Journal of the Engineering Mechanics Division, ASCE*, Vol. 90 (1964.)

[11] Inaudi J. A. and Kelly J. M., Nonlinear homogeneous dynamical systems, *UCB/EERC Report 93/11* (1995).

[12] Inaudi, J. A. and Kelly, J. M., "Variable-structure homogeneous control systems," *Proc. Int. Workshop Struct. Control* (1993).

[13] Inaudi, J. A. and De la Llera, J. C., "Dynamic Analysis of Nonlinear Structures Using State-Space Formulation and Partitioned Integration Schemes," *UCB/EERC Report 92/18* (1992).

[14] Iwan, W. D. and Wang, L.-J., "New Developments in Active Interaction Control," *Proc. 2nd Int. Workshop Struct. Control*, Hong Kong (1996).

[15] Iwan, W. D. and Wang, L.-J., "A Comparison of Control Algorithms for Active Interaction Control of Civil Structures," *Proc. of the Second World Conference on Structural Control*, V. 2, Kyoto, Japan (1998).

[16] Iyengar, R. N. and Iyengar, K. T., "Nonstationary Random Process Model for Earthquake Accelerograms," *Bulletin of the Seismological Society of America*, Vol. 59 (1969), pp. 1163-1188.

[17] Jennings, P. C., Housner, G. W. and Tsai, N. C., "Simulated Earthquake Motions," textslReport, Earthquake Engineering Research Laboratory, California Institute of Technology (1968).

[18] Kamagata, S. and Kobori, T., "Autonomous Adaptive Control of Active Variable Stiffness System for Seismic Ground Motion," *Proc. First World Conf. on Struct. Control*, Los Angeles, California (1994).

[19] Kanai, K., "Semi-Empirical Formula for the Seismic Characteristics of the Ground," *Bulletin of Earthquake Research Institute, University of Tokyo*, Vol. 35 (1957), pp. 309-325.

[20] King, A. C. Y. and Chen, C., "Artificial Earthquake Generation for Nuclear Power Plant Design," *Proc. 6th Conf. Earthquake Engineering*, Vol. III, New Dehli, India (1977).

[21] Kiureghian, A. D. and Crempien, J., "An Evolutionary Model for Earthquake Ground Motion," *Structural Safety*, Vol. 6 (1989) pp. 235-246.

[22] Kobori, T. and Takahashi, M., et al., "Shaking Table Experiment and Practical Application of Active Variable Stiffness (AVS) System," *Proceedings of the Second Conference on Tall Buildings in Seismic Regions 55th Regional Conference*, Los Angeles, California (1991), pp. 213-222.

[23] Kobori, T. and Kamagata, S., "Dynamic Intelligent Buildings - Active Seismic Response Control," *Intelligent structures - 2, Monitoring and Control*, Y. K. Wen (Editor), Elsevier Applied Science, London (1992).

[24] Kobori, T. and Takahashi, M., et al., "Seismic Response Controlled Structure with Active Variable Stiffness System," *Earthquake Engineering and Structural Dynamics*, V. 22 (1993), pp. 925-941.

[25] Kurata, N. and Kobori, T., et al., "Shaking Table Experiment of Active Variable Damping System," *Proceedings of the First World Conference on Structural Control*, Los Angeles, California (1994).

[26] Kurata, N. and Kobori, T., et al., "Forced Vibration Test of a Building with Semiactive Damper System," *Earthquake Engineering and Structural Dynamics*, V. 29 (1999), pp. 629-645.

[27] Leitmann, G., "Semiactive Control for Vibration Attenuation," *Journal of Intelligent Material Systems and Structures*, V. 5 (1994), pp. 841-846.

[28] MATLAB, *The Math Works Inc.*, Natick, Massachusetts (1998).

[29] Ohtori, Y., Christenson, R.E., and Spencer, B.F., Jr., "Benchmark Control Problems for Seismically Excited Nonlinear Buildings," *World Wide Web, http://www.nd.edu/ quake/benchmarks*, Date of access: Feb. 1, 2000.

[30] Polhemus, N. W. and Cakmak, A. S., "Simulation of Earthquake Ground Motions Using Autoregressive Moving Average (ARMA) Models," *Earthquake Engineering and Structural Dynamics*, Vol. 9 (1981), pp. 343-354.

[31] The SAC Steel Project, *World Wide Web, http://quiver.eerc.berkeley.edu:8080/*, Date of access: May 9, 2001.

[32] Saragoni, G. R. and Hart, G. C., "Simulation of Artificial Earthquakes," *Earthquake Engineering and Structural Dynamics*, Vol. 2 (1974), pp. 249-267.

[33] Slotine, J.-J. E. and Li, W., "Applied Nonlinear Control," *Prentice Hall*, Englewood Cliffs, New Jersey (1991).

[34] Soong, T. T. and Dargush, G. F., "Passive Energy Dissipation Systems in Structural Engineering," *John Wiley & Sons Ltd.* (1997).

[35] Spencer, B.F., Jr., and Sain, M.K., "Controlling Buildings: A New Frontier in Feedback," *IEEE Control Systems*, V. 17, No. 6 (1997), pp. 19-35.

[36] Spencer, B.F., Jr., and Soong, T.T., "New Application and Development of Active, Semi-Active and Hybrid Control Techniques for Seismic and Non-Seismic Vibration in the USA," *Proceedings of International Post-SMiRT Conference Seminar on Seismic Isolation, Passive Energy Dissipation and Active Control of Vibration of Structures*, Cheju, Korea (1999).

[37] Tajimi, H., "A Statistical Method of Determining the Maximum Response of a Building Structure During an Earthquake," *Proc. 2nd World Conf. Earthquake Engineering*, Tokyo and Kyoto, Vol. II (1960), pp. 781-798.

[38] Tsai, N.-C., "Spectrum-Compatible Motions for Design Purposes," *ASCE, Journal of Engineering Mechanics Division*, Vol. 98 (1972), pp. 345-355.

[39] Uang, C.-M. and Bertero, V. V., "Use of Energy as a Design Criterion in Earthquake-Resistant Design," *EERC Report No. UCB/EERC-88/18* (1988).

[40] International Council of Building Officials (ICBO), *Uniform Building Code*, Whittier, California (1997).

[41] Wang, L.-J., "Active Interaction Control for Civil Structures," *Ph. D. Thesis*, EERL 97-04, California Institute of Technology, Pasadena, California (1997).

[42] Watabe, M., Masao, T. and Tohdo, M., "Synthesized Earthquake Ground Motions for Earthquake Resistant Design," *Proc. 5th Canadian Conf. Earthquake Engineering*, Ottawa (1987), pp. 675-684.

[43] Yamada, K. and Kobori, T., "Control Algorithm for Estimating Future Responses of Active Variable Stiffness Structure," *Earthquake Engineering and Structural Dynamics*, V. 24 (1995), pp. 1085-1099.

[44] Yang, J. N., Li, Z., and Liu, S. C., "Stable Controllers for Instantaneous Optimal Control," *Journal of Engineering Mechanics*, V. 118, No. 8 (1992), pp. 1612-1630.

[45] Yao, J.T.P., "Concept of Structural Control," *Journal of the Structural Division*, V. 98, No. ST7 (1972), pp. 1567-1573.

Appendix A Partitioned Predictor-Corrector Method

This appendix provides a derivation of the results given in Chapter 2. Reference [13] has been used extensively for this appendix.

Consider the equation of motion for the controlled structure,

$$\dot{X}(t) = AX(t) + B_u u(t) + B_w w(t) \tag{A.1}$$

and the control force vector can be determined by the current state variables as follows:

$$u(t) = G(X(t)) = G(\mathbf{x}(t), \dot{\mathbf{x}}(t)) \tag{A.2}$$

Because of the nonlinearity and history dependence of the control forces, a numerical scheme for integrating in discrete time has to be employed. Assume that the state of the system $X(t_k)$ at step t_k and the external disturbance is known (as we can measure these by sensors installed within the structure). The state variable $X(t_{k+1})$ at time t_{k+1} is given by the following convolution integral:

$$X(t_{k+1}) = e^{A\Delta t}X(t_k) + \int_{t_k}^{t_{k+1}} e^{A(t_{k+1}-\tau)}[B_u u(\tau) + B_w w(\tau)]\mathrm{d}\tau \tag{A.3}$$

where $\Delta t = t_{k+1} - t_k$. Making the change of variable $\xi = \tau - t_k$, we can write

$$X(t_{k+1}) = e^{A\Delta t}X(t_k) + e^{A\Delta t}\int_0^{\Delta t} e^{-A\xi}[B_u u(t_k + \xi) + B_w w(t_k + \xi)]\mathrm{d}\xi \tag{A.4}$$

During the interval $0 < \xi < \Delta t$, the value of $u(t_k + \xi)$ is not known because Eqn. A.2 needs to be solved to find its value. Let's assume that the control force has a linear variation within the interval $0 < \xi < \Delta t$, i.e.,

$$u(t_k + \xi) = u(t_k) + \frac{\hat{u}(t_{k+1}) - u(t_k)}{\Delta t}\xi \tag{A.5}$$

where $\hat{u}(t_{k+1})$ represents the estimate of the control force at time t_{k+1} using the following procedures.

First find the estimate of the state variable $\hat{X}(t_{k+1})$ at time t_{k+1} by assuming zero-order holder for both $u(t_k+\xi)$ and $w(t_k+\xi)$ during the interval $0<\xi<\Delta t$.

$$\begin{aligned}\hat{X}(t_{k+1}) &= e^{A\Delta t}X(t_k)+\int_0^{\Delta t} e^{A\sigma)}\mathrm{d}\sigma[B_u u(t_k)+B_w w(t_k)] \\ &= e^{A\Delta t}X(t_k)+A^{-1}(e^{A\Delta t}-I)[B_u u(t_k)+B_w w(t_k)] \end{aligned} \tag{A.6}$$

Then the estimate of the control force $\hat{u}(t_{k+1})$ at time t_{k+1} can be determined by

$$\hat{u}(t_{k+1}) = G(\hat{X}(t_{k+1})) \tag{A.7}$$

The external disturbance term is known at discrete time t_k, and a linear variation is also assumed during the interval $0<\xi<\Delta t$,

$$w(t_k+\xi) = w(t_k)+\frac{w(t_{k+1})-w(t_k)}{\Delta t}\xi \tag{A.8}$$

Substituting Eqns. (A.5) and (A.8) into Eqn. (A.4) yields

$$X(t_{k+1}) = \Phi X(t_k)+B_{u1}u(t_k)+B_{u2}\hat{u}(t_{k+1})+B_{w1}w(t_k)+B_{w2}w(t_{k+1})] \tag{A.9}$$

where

$$\begin{aligned}\Phi &= e^{A\Delta t} \\ B_{u1} &= A^{-1}[\Phi-\frac{A^{-1}(I-\Phi)}{\Delta t}]B_u \\ B_{u2} &= A^{-1}[\frac{A^{-1}(\Phi-I)}{\Delta t}-I]B_u \\ B_{w1} &= A^{-1}[\Phi-\frac{A^{-1}(I-\Phi)}{\Delta t}]B_w \\ B_{w2} &= A^{-1}[\frac{A^{-1}(\Phi-I)}{\Delta t}-I]B_w \end{aligned} \tag{A.10}$$

Appendix B Analysis of Two Simple Cases

In this appendix, we will show analytically how a SDOF AIC system behaves in two simple cases, i.e., free oscillation and harmonical excitation. It is helpful for us to get a comprehensive view of the dynamic behavior of an AIC system by first studying these two simple cases. For the AIC system considered here, only Type A IE and Type 1 configuration are considered.

For convenience, the OCS control algorithm is stated heuristically as follows:

$$\begin{cases} u(t)\cdot\dot{x}_1(t)\geq 0 \text{ and } \dot{x}_1(t)=\dot{x}_2(t) & \Rightarrow \text{ IE locked (Attached)} \\ \text{otherwise} & \Rightarrow \text{ IE unlock (Detached)} \end{cases}$$

where $u(t)$ is the control force developed reactively within the IE which has an expression

$$u(t)=\begin{cases} \dfrac{m_1k_2x_2(t)-m_2k_1x_1(t)}{m_1+m_2}+\dfrac{m_1c_2-m_2c_1}{m_1+m_2}\dot{x}_1(t) & : \text{ IE locked} \\ 0 & : \text{ IE unlocked} \end{cases}$$

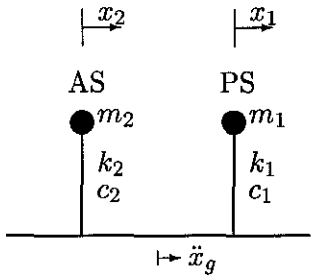

Figure B.1: A SDOF AIC Model

In Fig. B.1, the PS and AS in an AIC system are represented by two stick-mass models. The spring and dashpot are represented by the stick shown in the figure. We will use this way of representation to illustrate the dynamics of the PS and AS in various stages of interaction.

B.0.1 Free Oscillation

Case I: $c_1 = 0,\ c_2 = 0$

First, we will consider the simplest AIC system in which the PS and AS have no viscous damping ($c_1 = c_2 = 0$). As we will see later, this idealization will greatly simplify the formulation without losing the fundamental characteristics of an AIC system.

Assume that the PS is released from its initial position x_0 with zero velocity. The response of the AIC system at each critical time point are given as follows:

1. t=0 $x_1(0) = x_0,\ \dot{x}_1(0) = 0,\ x_2(0) = \dot{x}_2(0) = 0.$

At time $t = 0$, $\dot{x}_1 = \dot{x}_2 = 0$; therefore $u\dot{x}_1 = 0$. According to the control algorithms, the IE is locked and the AS is attached to the PS at time $t = 0^+$.

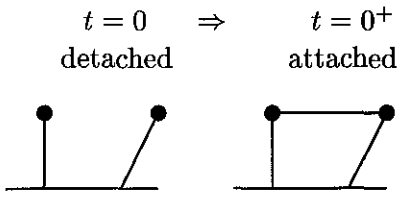

Figure B.2: Configuration of the AIC System at $t = 0$

The equations of motion of the PS and AS in the subsequent locked stage are expressed as

$$m_1\ddot{x}_1 + k_1 x_1 = -u \tag{B.1}$$

$$m_2\ddot{x}_2 + k_2 x_2 = u \tag{B.2}$$

with

$$\ddot{x}_2 = \ddot{x}_1, \quad x_2 = x_1 - x_0 \tag{B.3}$$

Adding Eqn. (B.1) and Eqn. (B.2), and considering Eqn. (B.3) yield

$$(m_1 + m_2)\ddot{x}_1 + (k_1 + k_2)x_1 = k_2 x_0 \tag{B.4}$$

For convenience, we will use the following notations:

$$\alpha = \frac{k_2}{k_1}, \quad \beta = \frac{m_2}{m_1}, \quad \omega_1 = \sqrt{\frac{k_1}{m_1}}, \quad \omega_2 = \sqrt{\frac{k_2}{m_2}},$$
$$\omega_3 = \sqrt{\frac{k_1+k_2}{m_1+m_2}} = \sqrt{\frac{1+\alpha}{1+\beta}}\omega_1 \tag{B.5}$$

With initial conditions of the PS given by $x_1(0) = x_0$, $\dot{x}_1(0) = 0$, the solution of Eqn. (B.4) is given by

$$x_1(t) = \frac{k_2 x_0}{k_1+k_2} + \frac{k_1 x_0}{k_1+k_2}\cos\omega_3 t = \frac{x_0}{1+\alpha}(\alpha + \cos\omega_3 t) \tag{B.6}$$

and

$$\begin{aligned} x_2(t) &= x_1(t) - x_0 = -\frac{k_1 x_0}{k_1+k_2} + \frac{k_1 x_0}{k_1+k_2}\cos\omega_3 t \\ &= \frac{x_0}{1+\alpha}(-1+\cos\omega_3 t) \end{aligned} \tag{B.7}$$

2. t=t_1 first detachment occurs since $t = 0^+$; $\dot{x}_1(t_1) = \dot{x}_2(t_1) = 0$.

At time $t = t_1$, $\dot{x}_1 = \dot{x}_2 = 0$, the velocity of the PS changes sign while the control force u does not change sign at this time instant. Therefore, $u\dot{x}_1$ undergoes a sign change. According to the OCS control algorithm, the AS is detached from the PS at time $t = t_1^+$.

The value of t_1 can be determined in the following way.

For $t \in (0, t_1)$,

$$\dot{x}_1(t) = \dot{x}_2(t) = -\frac{x_0}{1+\alpha}\omega_3 \sin\omega_3 t$$

Using the condition $\dot{x}_1 = 0$ yields

$$t_1 = \pi/\omega_3$$

and

$$x_1(t_1) = \frac{-1+\alpha}{1+\alpha}x_0$$
$$x_2(t_1) = -\frac{2}{1+\alpha}x_0$$

In Table B.1, values of $x_1(t_1)$ and $x_2(t_1)$ varying with α are listed.

Table B.1: Values of $x_1(t_1)$ and $x_2(t_1)$ varying with α

	α			
	0.5	1	1.5	2
$x_1(t_1)$ $(\times x_0)$	-1/3	0	0.2	1/3
$x_2(t_1)$ $(\times x_0)$	-4/3	-1	-0.8	-2/3

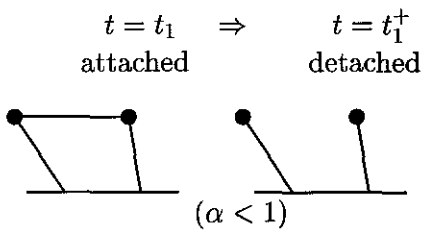

Figure B.3: Configuration of the AIC System at $t = t_1$

The PS and AS are in free oscillation motion until the next attachment occurs.

Denote $\tau = t - t_1$, the displacement and velocity of PS and AS in the subsequent detachment stage are given by

$$x_1(\tau) = \frac{-1+\alpha}{1+\alpha} x_0 \cos \omega_1 \tau \tag{B.8}$$

$$x_2(\tau) = -\frac{2}{1+\alpha} x_0 \cos \omega_2 \tau \tag{B.9}$$

$$\dot{x}_1(\tau) = \frac{1-\alpha}{1+\alpha} x_0 \omega_1 \sin \omega_1 \tau \tag{B.10}$$

$$\dot{x}_2(\tau) = \frac{2}{1+\alpha} x_0 \omega_2 \sin \omega_2 \tau \tag{B.11}$$

3. t=t_2 first attachment occurs following the last detachment at t_1; $\dot{x}_1(t_2) = \dot{x}_2(t_2)$, $u\dot{x}_1 \geq 0$.

At time $t = t_2$,

$$\dot{x}_1 = \dot{x}_2 \quad \Rightarrow \quad \frac{\sin \omega_1 \tau_2}{\sin \omega_2 \tau_2} = \frac{2\omega_2}{(1-\alpha)\omega_1} \tag{B.12}$$

where $\tau_2 = t_2 - t_1$ is the time interval between this attachment and last detachment.

One feature of the AIC system is that the AS functions as an actuator delivering the desired control force. Because the AS mass is typically much smaller than that of the PS (e.g., $m_2/m_1 = 0.02$ is used in the subsequent numerical calculations), the control force u

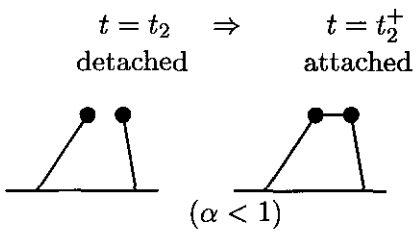

Figure B.4: Configuration of the AIC System at $t = t_2$ $(\alpha < 1)$

can be approximated as

$$u(t) \approx k_2 x_2(t)$$

Assume the PS's natural period T_1 is equal to 1 second, and $\beta = 0.02$, the values of τ_2 corresponding to various α values are calculated and listed in Table B.2.

Table B.2: Values of τ_2 Varying with α

α	$\frac{\omega_2}{\omega_1}$	T_2	$\frac{\sin\omega_1\tau_2}{\sin\omega_2\tau_2}$	τ_2 (sec.)
0.5	5	0.2	20	0.0991$\approx T_2/2$
1	7.071	0.1414	∞	0.0707$= T_2/2$
1.5	8.660	0.1155	-34.641	0.1151$\approx T_2$
2	10	0.1	-20	0.0995$\approx T_2$

It is observed that for $k_1 \geq k_2$, the time interval τ_2 between t_1 and t_2 is approximately equal to half of the AS's natural period T_2, while for $k_1 < k_2$, this time interval is close to the AS's natural period. Therefore, $k_1 = k_2$ or $\alpha = 1$ gives a bifurcation point. We will distinguish between these two cases in the following discussion.

▶ $\alpha \leq 1 \quad (t_2 - t_1 \approx T_2/2)$

The equations of motion of the PS and AS in the subsequent attachment stage until next detachment occurs are expressed as

$$m_1\ddot{x}_1 + k_1 x_1 = -u \tag{B.13}$$

$$m_2\ddot{x}_2 + k_2 x_2 = u \tag{B.14}$$

and

$$\ddot{x}_2 = \ddot{x}_1, \quad x_2 = x_1 - [x_1(t_2) - x_2(t_2)] \tag{B.15}$$

Adding Eqn. (B.13) and Eqn. (B.14), and considering Eqn. (B.15), yield

$$(m_1 + m_2)\ddot{x}_1 + (k_1 + k_2)x_1 = k_2[x_1(t_2) - x_2(t_2)] \tag{B.16}$$

Denote

$$\tau = t - t_2$$

With the initial condition of the PS given by $x_1(\tau = 0) = x_1(t_2)$, $\dot{x}_1(\tau = 0) = \dot{x}_1(t_2)$, the solution of Eqn. (B.16) is given by

$$\begin{aligned} x_1(\tau) &= x_1(t_2)\cos\omega_3\tau + \frac{\dot{x}_1(t_2)}{\omega_3}\sin\omega_3\tau + \frac{k_2[x_1(t_2) - x_2(t_2)]}{k_1 + k_2}(1 - \cos\omega_3\tau) \\ &= \frac{[k_1x_1(t_2) + k_2x_2(t_2)]}{k_1 + k_2}\cos\omega_3\tau + \frac{\dot{x}_1(t_2)}{\omega_3}\sin\omega_3\tau + \frac{k_2[x_1(t_2) - x_2(t_2)]}{k_1 + k_2} \\ &= \frac{[x_1(t_2) + \alpha x_2(t_2)]}{1 + \alpha}\cos\omega_3\tau + \frac{\dot{x}_1(t_2)}{\omega_3}\sin\omega_3\tau + \frac{\alpha[x_1(t_2) - x_2(t_2)]}{1 + \alpha} \end{aligned} \tag{B.17}$$

and

$$\begin{aligned} x_2(\tau) &= x_1(\tau) - (x_1(t_2) - x_2(t_2)) \\ &= \frac{[x_1(t_2) + \alpha x_2(t_2)]}{1 + \alpha}\cos\omega_3\tau + \frac{\dot{x}_1(t_2)}{\omega_3}\sin\omega_3\tau - \frac{[x_1(t_2) - x_2(t_2)]}{1 + \alpha} \end{aligned} \tag{B.18}$$

Taking derivative of $x_1(\tau)$ and $x_2(\tau)$ and considering the condition $\dot{x}_1(t_2) = \dot{x}_2(t_2)$ at time t_2 yield

$$\dot{x}_1(\tau) = \dot{x}_2(\tau) = -\frac{[x_1(t_2) + \alpha x_2(t_2)]}{1 + \alpha}\omega_3\sin\omega_3\tau + \dot{x}_1(t_2)\cos\omega_3\tau \tag{B.19}$$

▶ $\alpha > 1 \quad (t_2 - t_1 \approx T_2)$

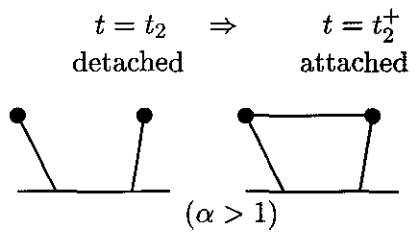

Figure B.5: Configuration of the AIC System at $t = t_2$ ($\alpha > 1$)

Similarly, denote

$$\tau = t - t_2$$

The equations describing the displacement and velocity of the PS and AS after t_2^+ till next detachment are the same as those for the $\alpha < 1$ case, i.e.,

$$x_1(\tau) = \frac{[x_1(t_2) + \alpha x_2(t_2)]}{1+\alpha}\cos\omega_3\tau + \frac{\dot{x}_1(t_2)}{\omega_3}\sin\omega_3\tau + \frac{\alpha[x_1(t_2) - x_2(t_2)]}{1+\alpha} \quad \text{(B.20)}$$

and

$$x_2(\tau) = \frac{[x_1(t_2) + \alpha x_2(t_2)]}{1+\alpha}\cos\omega_3\tau + \frac{\dot{x}_1(t_2)}{\omega_3}\sin\omega_3\tau - \frac{[x_1(t_2) - x_2(t_2)]}{1+\alpha} \quad \text{(B.21)}$$

Taking derivative of $x_1(\tau)$ and $x_1(\tau)$ yields

$$\dot{x}_1(\tau) = \dot{x}_2(\tau) = -\frac{[x_1(t_2) + \alpha x_2(t_2)]}{1+\alpha}\omega_3\sin\omega_3\tau + \dot{x}_1(t_2)\cos\omega_3\tau \quad \text{(B.22)}$$

4. t=t_3 first detachment occurs following the last attachment at t_2; $\dot{x}_1(t_3) = \dot{x}_2(t_3) = 0$, $u(t_3^+)\dot{x}_1(t_3^+) < 0$.

Denote $\tau_3 = t_3 - t_2$. At time t_3,

$$\begin{aligned}\dot{x}_1(t_3) = \dot{x}_2(t_3) = 0 \quad &\Rightarrow \quad -\frac{[x_1(t_2) + \alpha x_2(t_2)]}{1+\alpha}\omega_3\sin\omega_3\tau_3 + \dot{x}_1(t_2)\cos\omega_3\tau_3 = 0 \\ &\Rightarrow \quad \tan\omega_3\tau_3 = \frac{(1+\alpha)\dot{x}_1(t_2)}{\omega_3[x_1(t_2) + \alpha x_2(t_2)]} \end{aligned} \quad \text{(B.23)}$$

As before, we will distinguish between two cases: $\alpha \leq 1$ and $\alpha > 1$.

▶ $\alpha \leq 1$

Table B.3: Values of τ_3 Varying with α ($\alpha \leq 1$)

α	T_2 sec	τ_2 sec	$x_1(\tau_2)$	$x_2(\tau_2)$	$\dot{x}_1(\tau_2)$	T_3 sec	τ_3 sec	$x_1(t_3)$
1/8	0.4	0.1896	-0.2881	1.7541	4.5392	0.9522	0.2515	0.4637
1/4	0.2828	0.1378	-0.3888	1.5948	2.8713	0.9033	0.2231	0.0162
0.26	0.2774	0.1353	-0.3876	1.5827	2.7726	0.8997	0.2181	-0.0091
1/3	0.2450	0.1203	-0.3638	1.4977	2.1549	0.8746	0.1732	-0.1487
1/2	0.2	0.0991	-0.2708	1.3328	1.2215	0.8246	0.0717	-0.2259
3/4	0.1633	0.0814	-0.1246	1.1428	0.4393	0.7635	0.0154	-0.1212
7/8	0.1512	0.0755	-0.0593	1.0667	0.1913	0.7326	0.0057	-0.0588

To obtain an approximate solution of τ_3, the following assumptions are made:

$$\tau_2 = t_2 - t_1 \approx \frac{T_2}{2}, \quad x_1(t_2) \approx \frac{-1+\alpha}{1+\alpha} x_0,$$
$$x_2(t_2) \approx \frac{2}{1+\alpha} x_0, \quad \dot{x}_1(t_2) = +\epsilon \qquad (0 < \epsilon \ll 1)$$

Assume the PS's natural period T_1 is equal to 1 second, and $\beta = 0.02$. In Table B.3, values of τ_3 corresponding to various α values are listed.

By trial and error, another bifurcation point is determined as $\alpha = 0.26$ for the selected parameter values. If $\alpha > 0.26$, then $x_1(t_3) < 0$; otherwise, $x_1(t_3) \geq 0$. Fig. B.6 depicts the configuration of an AIC system at time $t = t_3$ for two different cases.

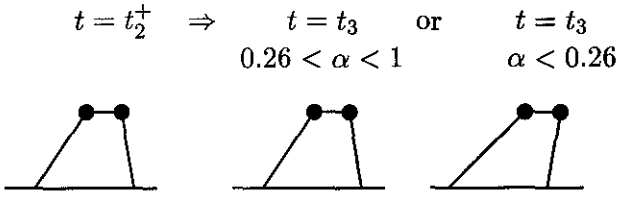

Figure B.6: Configuration of the AIC System at $t = t_3$ ($\alpha < 1$)

▶ $\alpha > 1$

Assume the natural period T_1 of PS equals 1 second, and $\beta = 0.02$, Table B.4 gives the values of τ_2 corresponding to changing α values.

Table B.4: Values of τ_3 Varying with α ($\alpha > 1$)

α	T_2 sec	τ_2 sec	$x_1(\tau_2)$	$x_2(\tau_2)$	$\dot{x}_1(\tau_2)$	T_3 sec	τ_3 sec	$x_1(t_3)$
1.5	0.1155	0.1151	0.1499	-0.7999	-0.8317	0.6387	0.0202	0.1415
2	0.1	0.0995	0.2702	-0.6664	-1.2261	0.5831	0.0288	0.2524
3	0.0816	0.0811	0.4364	-0.4996	-1.5330	0.5050	0.0349	0.4092
4	0.0707	0.0702	0.5426	-0.3996	-1.6095	0.4517	0.0360	0.5130

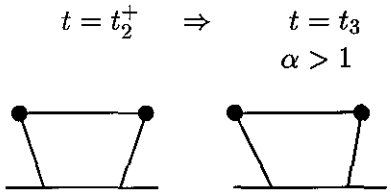

Figure B.7: Configuration of the AIC System at $t = t_3$ ($\alpha > 1$)

Case II: $c_1 = 0,\ c_2 > 0$

Now, let's consider a slightly complicated case in which the PS's damping factor is equal to zero while the AS has a nonzero viscous damping factor, i.e., $c_1 = 0$ but $c_2 > 0$.

Once again we assume a free oscillation is generated by releasing the PS from its initial position x_0 with zero initial velocity. The response of the AIC system at each critical time point are listed below.

1. t=0 $\quad x_1(0) = x_0,\ \dot{x}_1(0) = 0,\ x_2(0) = \dot{x}_2(0) = 0.$

At time $t = 0$, $\dot{x}_1 = \dot{x}_2 = 0$, and therefore $u\dot{x}_1 = 0$. According to the OCS control algorithm, the AS is attached to the PS at time $t = 0^+$.

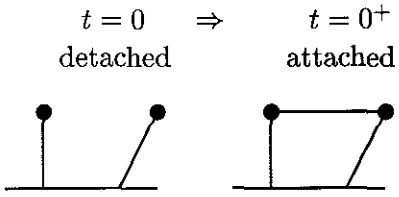

Figure B.8: Configuration of the AIC System at t=0

The equations of motion of the PS and AS in the subsequent locked stage are expressed

as

$$m_1\ddot{x}_1 + k_1 x_1 = -u \tag{B.24}$$

$$m_2\ddot{x}_2 + c_2\dot{x}_2 + k_2 x_2 = u \tag{B.25}$$

with

$$\ddot{x}_2 = \ddot{x}_1, \quad \dot{x}_2 = \dot{x}_1, \quad x_2 = x_1 - x_0 \tag{B.26}$$

Adding Eqn. (B.24) and Eqn. (B.25), and considering Eqn. (B.26) yield

$$(m_1 + m_2)\ddot{x}_1 + c_2\dot{x}_1 + (k_1 + k_2)x_1 = k_2 x_0 \tag{B.27}$$

For convenience, we will use the following notations:

$$\zeta = \frac{c_2}{2(m_1 + m_2)\omega_3}, \quad \omega_D = \omega_3\sqrt{1-\zeta^2}$$
$$\zeta_2 = \frac{c_2}{2m_2\omega_2} = \sqrt{\frac{(1+\alpha)(1+\beta)}{\alpha\beta}}\zeta \tag{B.28}$$

With the initial conditions of the PS given by $x_1(0) = x_0$, $\dot{x}_1(0) = 0$, the solution of Eqn. (B.27) is given by

$$\begin{aligned} x_1(t) &= \frac{k_2 x_0}{k_1 + k_2} + \frac{k_1 x_0}{k_1 + k_2} e^{-\zeta\omega_3 t}(\cos\omega_D t + \frac{\zeta}{\sqrt{1-\zeta^2}}\sin\omega_D t) \\ &= \frac{\alpha x_0}{1+\alpha} + \frac{x_0}{1+\alpha} e^{-\zeta\omega_3 t}(\cos\omega_D t + \frac{\zeta}{\sqrt{1-\zeta^2}}\sin\omega_D t) \qquad \text{(B.29)} \\ x_2(t) &= x_1(t) - x_0 \\ &= -\frac{x_0}{1+\alpha} + \frac{x_0}{1+\alpha} e^{-\zeta\omega_3 t}(\cos\omega_D t + \frac{\zeta}{\sqrt{1-\zeta^2}}\sin\omega_D t) \qquad \text{(B.30)} \end{aligned}$$

and

$$\dot{x}_1(t) = \dot{x}_2(t) = -\frac{x_0}{1+\alpha} e^{-\zeta\omega_3 t}\frac{\omega_3}{\sqrt{1-\zeta^2}}\sin\omega_D t \tag{B.31}$$

2. t=t_1 first detachment occurs since $t = 0^+$; $\dot{x}_1(t_1) = \dot{x}_2(t_1) = 0$.

At time $t = t_1$, $\dot{x}_1 = \dot{x}_2 = 0$, the velocity of the PS changes sign while the control force u does not change sign at this time instant. Therefore, $u\dot{x}_1$ undergoes a sign change. According to the OCS control algorithm, the AS is detached from the PS at time $t = t_1^+$.

Table B.5: Values of ζ_b Varying with α ($\alpha < 1$)

	α				
	1/8	1/4	1/2	3/4	7/8
ζ_b	28.7%	25.8%	18.1%	8.8%	4.2%

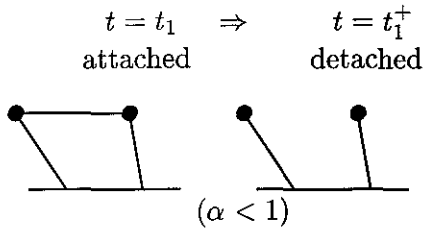

Figure B.9: Configuration of the AIC System at $t = t_1$

For $t \in (0, t_1)$,

$$\dot{x}_1(t) = \dot{x}_2(t) = -\frac{x_0}{1+\alpha} e^{-\zeta\omega_3 t} \frac{\omega_3}{\sqrt{1-\zeta^2}} \sin\omega_D t$$

Now solve for the value of t_1 using $\dot{x}_1(t_1) = 0$. This yields

$$t_1 = \pi/\omega_D$$

and

$$x_1(t_1) = \frac{x_0}{1+\alpha}(\alpha - e^{-\frac{\zeta\pi}{\sqrt{1-\zeta^2}}})$$

$$x_2(t_1) = -\frac{x_0}{1+\alpha}(1 + e^{-\frac{\zeta\pi}{\sqrt{1-\zeta^2}}})$$

It is observed that when $\alpha < 1$, a bifurcation value exists for ζ. When $\zeta < \zeta_b$, $x_1(t_1) < 0$; otherwise, $x_1(t_1) > 0$. ζ_b is solved as follows:

$$\alpha - e^{-\frac{\zeta_b\pi}{\sqrt{1-\zeta_b^2}}} = 0 \quad \Rightarrow \quad \zeta_b = \frac{|\ln\alpha|}{\pi\sqrt{1+\ln^2\alpha}}$$

Note that the above relationship is valid only for $\alpha < 1$.

Table B.5 gives the values of ζ_b corresponding to various α values. Table B.6 gives the values of $x_1(t_1)$ and $x_2(t_1)$ varying with α and ζ_2.

The PS and AS are in free oscillation motion until the next attachment occurs.

Denote $\tau = t - t_1$, the displacement and velocity of PS and AS in the subsequent

Table B.6: Values of $x_1(t_1)$ and $x_2(t_1)$ Varying with α and ζ_2

ζ_2	$\times x_0$	α				
		0.5	0.75	1	1.5	2
10%	$x_1(t_1)$	-0.317	-0.127	0.015	0.213	0.345
	$x_2(t_1)$	-1.317	-1.127	-0.985	-0.787	-0.655
20%	$x_1(t_1)$	-0.300	-0.111	0.030	0.226	0.356
	$x_2(t_1)$	-1.300	-1.111	-0.970	-0.774	-0.644
30%	$x_1(t_1)$	-0.284	-0.096	0.045	0.239	0.367
	$x_2(t_1)$	-1.284	-1.096	-0.955	-0.761	-0.633
40%	$x_1(t_1)$	-0.269	-0.081	0.059	0.251	0.378
	$x_2(t_1)$	-1.269	-1.081	-0.941	-0.749	-0.622
50%	$x_1(t_1)$	-0.254	-0.066	0.072	0.263	0.388
	$x_2(t_1)$	-1.254	-1.066	-0.928	-0.737	-0.612

detachment stage are given by

$$x_1(\tau) = x_1(t_1)\cos\omega_1\tau) \tag{B.32}$$

$$x_2(\tau) = x_2(t_1)e^{-\zeta_2\omega_2\tau}(\cos\omega_{2D}\tau + \frac{\zeta_2}{\sqrt{1-\zeta_2^2}}\sin\omega_{2D}t) \tag{B.33}$$

and

$$\dot{x}_1(\tau) = -x_1(t_1)\omega_1\sin\omega_1\tau \tag{B.34}$$

$$\dot{x}_2(\tau) = -\frac{e^{-\zeta_2\omega_2\tau}}{\sqrt{1-\zeta_2^2}}x_2(t_1)\omega_2\sin\omega_{2D}\tau \tag{B.35}$$

3. t=t_2 first attachment occurs following the last detachment at t_1; $\dot{x}_1(t_2) = \dot{x}_2(t_2)$, $u\dot{x}_1 \geq 0$.

At time $t = t_2$,

$$\dot{x}_1 = \dot{x}_2 \Rightarrow \frac{e^{-\zeta_2\omega_2\tau_2}\sin\omega_{2D}\tau_2}{\sin\omega_1\tau_2} = \frac{x_1(t_1)2\omega_1\sqrt{1-\zeta_2^2}}{x_2(t_1)\omega_2} \tag{B.36}$$

where $\tau_2 = t_2 - t_1$ is the time interval between this attachment and last detachment.

One feature of the AIC system is that the AS functions as an actuator delivering the desired control force. Because the AS mass is typically much smaller than that of the PS (e.g., $m_2/m_1 = 0.02$ is used in the subsequent numerical calculations), the control force u

in this case can be approximated as

$$u \approx k_2 x_2 + c_2 \dot{x}_1$$

Assume the PS's natural period T_1 is equal to 1 second, and $\beta = 0.02$, the values of τ_2 corresponding to various α values are calculated and listed in Table B.7.

It is observed that for $k_1 \geq k_2$, the time interval τ_2 between t_1 and t_2 is approximately equal to half of the AS's natural period T_2, while for $k_1 < k_2$, this time interval is close to the AS's natural period. The bifurcation point also depends on ζ_2 here. We will distinguish between these two cases in the following discussion.

▶ $\alpha < 1 \quad (t_2 - t_1 \approx T_2/2)$

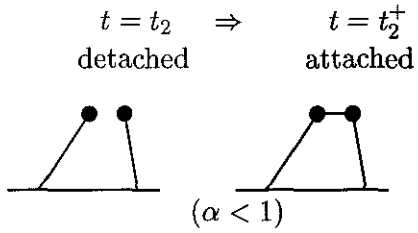

Figure B.10: Configuration of the AIC System at $t = t_2$ ($\alpha < 1$)

The equations of motion of the PS and AS in the subsequent attachment stage until next detachment occurs are expressed as

$$m_1 \ddot{x}_1 + k_1 x_1 = -u \tag{B.37}$$

$$m_2 \ddot{x}_2 + c_2 \dot{x}_2 + k_2 x_2 = u \tag{B.38}$$

and

$$\ddot{x}_2 = \ddot{x}_1, \quad \dot{x}_2 = \dot{x}_1, \quad x_2 = x_1 - (x_1(t_2) - x_2(t_2)) \tag{B.39}$$

Adding Eqn. (B.37) and Eqn. (B.38), and considering Eqn. (B.39), yield

$$(m_1 + m_2)\ddot{x}_1 + c_2 \dot{x}_1 + (k_1 + k_2) x_1 = k_2 (x_1(t_2) - x_2(t_2)) \tag{B.40}$$

Denote

$$\tau = t - t_2$$

Table B.7: Values of τ_2 Varying with α and ζ_2

ζ_2	α	T_{2D} sec	τ_2 sec	$x_1(\tau_2)$	$x_2(\tau_2)$	$\dot{x}_1(\tau_2)$
	0.5	0.2010	0.0993	-0.257	0.959	1.162
	0.75	0.1641	0.0817	-0.110	0.822	0.391
10%	1	0.1421	0.1421	0.010	-0.524	-0.075
	1.5	0.1161	0.1153	0.160	-0.418	-0.889
	2	0.1005	0.0996	0.280	-0.348	-1.270
	4	0.0711	0.0701	0.550	-0.208	-1.628
	0.5	0.2041	0.1004	-0.243	0.684	1.113
	0.75	0.1667	0.0829	-0.096	0.585	0.347
20%	1	0.1443	0.1441	0.019	-0.269	-0.149
	1.5	0.1179	0.1164	0.168	-0.214	-0.950
	2	0.1021	0.1002	0.288	-0.177	-1.319
	4	0.0722	0.0703	0.556	-0.105	-1.652
	0.5	0.2097	0.1026	-0.227	0.477	1.074
	0.75	0.1712	0.0851	-0.082	0.408	0.306
30%	1	0.1483	0.1474	0.027	-0.132	-0.224
	1.5	0.1210	0.1179	0.176	-0.104	-1.013
	2	0.1048	0.1011	0.296	-0.085	-1.370
	4	0.0741	0.0704	0.562	-0.049	-1.674
	0.5	0.2182	0.1059	-0.212	0.320	1.043
	0.75	0.1782	0.0884	-0.069	0.274	0.267
40%	1	0.1543	0.1519	0.034	-0.060	-0.300
	1.5	0.1260	0.1194	0.184	-0.045	-1.075
	2	0.1091	0.1015	0.304	-0.035	-1.414
	4	0.0772	0.0699	0.569	-0.018	-1.681
	0.5	0.2309	0.1108	-0.195	0.202	1.023
	0.75	0.1886	0.0934	-0.055	0.174	0.230
50%	1	0.1633	0.1566	0.040	-0.023	-0.377
	1.5	0.1333	0.1191	0.193	-0.012	-1.123
	2	0.1155	0.1000	0.314	-0.006	-1.434
	4	0.0826	0.0675	0.579	0.001	-1.644

With the initial condition of the PS given by $x_1(\tau = 0) = x_1(t_2)$, $\dot{x}_1(\tau = 0) = \dot{x}_1(t_2)$, the solution of Eqn. (B.40) is given by

$$\begin{aligned} x_1(\tau) &= x_1(t_2)e^{-\zeta\omega_3\tau}(\cos\omega_D\tau + \frac{\zeta}{\sqrt{1-\zeta^2}}\sin\omega_D\tau) + \dot{x}_1(t_2)\frac{e^{-\zeta\omega_3\tau}}{\omega_D}\sin\omega_D\tau \\ &\quad + \frac{k_2[x_1(t_2) - x_2(t_2)]}{k_1 + k_2}[1 - e^{-\zeta\omega_3\tau}(\cos\omega_D\tau + \frac{\zeta}{\sqrt{1-\zeta^2}}\sin\omega_D\tau)] \\ &= e^{-\zeta\omega_3\tau}\{\cos\omega_D\tau[x_1(t_2) - \frac{\alpha[x_1(t_2) - x_2(t_2)]}{1+\alpha}] + \sin\omega_D\tau[\frac{\zeta}{\sqrt{1-\zeta^2}}x_1(t_2) + \frac{\dot{x}_1(t_2)}{\omega_D} \\ &\quad - \frac{\zeta}{\sqrt{1-\zeta^2}}\frac{\alpha[x_1(t_2) - x_2(t_2)]}{1+\alpha}]\} + \frac{\alpha[x_1(t_2) - x_2(t_2)]}{1+\alpha} \end{aligned} \tag{B.41}$$

$$\begin{aligned} x_2(\tau) &= x_1(\tau) - (x_1(t_2) - x_2(t_2)) \\ &= e^{-\zeta\omega_3\tau}\{\cos\omega_D\tau[x_1(t_2) - \frac{\alpha[x_1(t_2) - x_2(t_2)]}{1+\alpha}] + \sin\omega_D\tau[\frac{\zeta}{\sqrt{1-\zeta^2}}x_1(t_2) + \frac{\dot{x}_1(t_2)}{\omega_D} \\ &\quad - \frac{\zeta}{\sqrt{1-\zeta^2}}\frac{\alpha[x_1(t_2) - x_2(t_2)]}{1+\alpha}]\} - \frac{[x_1(t_2) - x_2(t_2)]}{1+\alpha} \end{aligned} \tag{B.42}$$

Taking derivative of $x_1(\tau)$ and $x_2(\tau)$ yields

$$\begin{aligned} \dot{x}_1(\tau) &= \dot{x}_2(\tau) \\ &= e^{-\zeta\omega_3\tau}\{\dot{x}_1(t_2)\cos\omega_D\tau - \frac{\sin\omega_D\tau}{\sqrt{1-\zeta^2}}[\zeta\dot{x}_1(t_2) + \frac{\omega_3(x_1(t_2) + \alpha x_2(t_2))}{1+\alpha}]\} \end{aligned} \tag{B.43}$$

▶ $\alpha > 1 \quad (t_2 - t_1 \approx T_2)$

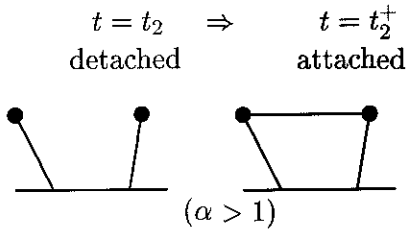

Figure B.11: Configuration of the AIC System at $t = t_2$ ($\alpha > 1$)

Similarly, denote

$$\tau = t - t_2$$

The equations describing the displacement and velocity of PS and AS after t_2^+ till next

detachment are the same as those for the $\alpha < 1$ case, i.e.,

$$\begin{aligned} x_1(\tau) &= x_1(t_2)e^{-\zeta\omega_3\tau}(\cos\omega_D\tau + \frac{\zeta}{\sqrt{1-\zeta^2}}\sin\omega_D\tau) + \dot{x}_1(t_2)\frac{e^{-\zeta\omega_3\tau}}{\omega_D}\sin\omega_D\tau \\ &\quad + \frac{k_2[x_1(t_2)-x_2(t_2)]}{k_1+k_2}[1 - e^{-\zeta\omega_3\tau}(\cos\omega_D\tau + \frac{\zeta}{\sqrt{1-\zeta^2}}\sin\omega_D\tau)] \\ &= e^{-\zeta\omega_3\tau}\{\cos\omega_D\tau[x_1(t_2) - \frac{\alpha[x_1(t_2)-x_2(t_2)]}{1+\alpha}] + \sin\omega_D\tau[\frac{\zeta}{\sqrt{1-\zeta^2}}x_1(t_2) + \frac{\dot{x}_1(t_2)}{\omega_D} \\ &\quad - \frac{\zeta}{\sqrt{1-\zeta^2}}\frac{\alpha[x_1(t_2)-x_2(t_2)]}{1+\alpha}]\} + \frac{\alpha[x_1(t_2)-x_2(t_2)]}{1+\alpha} \end{aligned} \tag{B.44}$$

$$\begin{aligned} x_2(\tau) &= x_1(\tau) - (x_1(t_2) - x_2(t_2)) \\ &= e^{-\zeta\omega_3\tau}\{\cos\omega_D\tau[x_1(t_2) - \frac{\alpha[x_1(t_2)-x_2(t_2)]}{1+\alpha}] + \sin\omega_D\tau[\frac{\zeta}{\sqrt{1-\zeta^2}}x_1(t_2) + \frac{\dot{x}_1(t_2)}{\omega_D} \\ &\quad - \frac{\zeta}{\sqrt{1-\zeta^2}}\frac{\alpha[x_1(t_2)-x_2(t_2)]}{1+\alpha}]\} - \frac{[x_1(t_2)-x_2(t_2)]}{1+\alpha} \end{aligned} \tag{B.45}$$

and

$$\begin{aligned} \dot{x}_1(\tau) &= \dot{x}_2(\tau) \\ &= e^{-\zeta\omega_3\tau}\{\dot{x}_1(t_2)\cos\omega_D\tau - \frac{\sin\omega_D\tau}{\sqrt{1-\zeta^2}}[\zeta\dot{x}_1(t_2) + \frac{\omega_3(x_1(t_2)+\alpha x_2(t_2))}{1+\alpha}]\} \end{aligned} \tag{B.46}$$

4. t=t_3 first detachment occurs following the last attachment at t_2; $\dot{x}_1(t_3) = \dot{x}_2(t_3) = 0$, $u\dot{x}_1(t_3^+) < 0$.

Denote $\tau_3 = t_3 - t_2$. At time t_3,

$$\begin{aligned} \dot{x}_1(t_3) = 0 \quad &\Rightarrow \quad \dot{x}_1(t_2)\cos\omega_D\tau_3 - \frac{\sin\omega_D\tau_3}{\sqrt{1-\zeta^2}}[\zeta\dot{x}_1(t_2) + \frac{\omega_3(x_1(t_2)+\alpha x_2(t_2))}{1+\alpha}] = 0 \\ &\Rightarrow \quad \tan\omega_D\tau_3 = \frac{(1+\alpha)\sqrt{1-\zeta^2}\dot{x}_1(t_2)}{(1+\alpha)\zeta\dot{x}_1(t_2) + \omega_3[x_1(t_2)+\alpha x_2(t_2)]} \end{aligned} \tag{B.47}$$

Assume the PS's natural period T_1 is equal to 1 second and $\beta = 0.02$. Table B.8 gives the values of τ_3 corresponding to various values of α and ζ_2.

As before, we will distinguish between two cases: $\alpha < 1$ and $\alpha > 1$.

▶ $\alpha < 1$

By trial and error, another bifurcation point is determined to be around $\alpha = 0.26$. If $\alpha > 0.26$, then $x_1(t_3) < 0$; otherwise, $x_1(t_3) \geq 0$. Fig. B.12 depicts the configuration of an

Table B.8: Values of τ_3 Varying with α and ζ_2

ζ_2		α					
		0.5	0.75	1	1.5	2	4
10%	T_{3D}	0.8246	0.7635	0.7142	0.6388	0.5831	0.4517
	τ_3	0.1043	0.0198	0.0038	0.0456	0.0650	0.0800
	$x_1(\tau_3)$	-0.193	-0.106	0.0095	0.139	0.237	0.477
20%	T_{3D}	0.8247	0.7636	0.7143	0.6389	0.5832	0.4518
	τ_3	0.1485	0.0257	0.0153	0.1009	0.1272	0.1273
	$x_1(\tau_3)$	-0.150	-0.092	0.017	0.117	0.189	0.4132
30%	T_{3D}	0.8249	0.7637	0.7145	0.6391	0.5834	0.4520
	τ_3	0.1961	0.0341	0.0504	0.1645	0.1725	0.1503
	$x_1(\tau_3)$	-0.099	-0.077	0.021	0.070	0.130	0.361
40%	T_{3D}	0.8251	0.7640	0.7147	0.6394	0.5837	0.4522
	τ_3	0.2344	0.0471	0.1327	0.1970	0.1925	0.1604
	$x_1(\tau_3)$	-0.045	-0.062	0.012	0.030	0.090	0.334
50%	T_{3D}	0.8253	0.7643	0.7150	0.6397	0.5841	0.4526
	τ_3	0.2591	0.0685	0.1949	0.2116	0.2028	0.1669
	$x_1(\tau_3)$	0.002	-0.047	-0.008	0.006	0.0704	0.324

AIC system at time $t = t_3$ for two different cases.

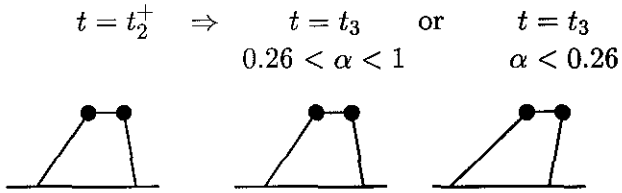

Figure B.12: Configuration of the AIC System at $t = t_3$ ($\alpha < 1$)

▶ $\alpha > 1$

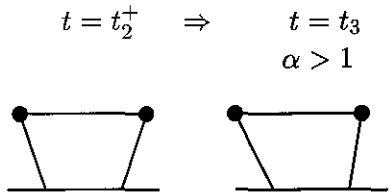

Figure B.13: Configuration of the AIC System at $t = t_3$ ($\alpha > 1$)

B.0.2 Harmonic Excitation

Case I: $c_1 = 0,\ c_2 = 0$

First, we will consider an AIC system in which the PS and AS have no viscous damping ($c_1 = c_2 = 0$). As we will see later, this idealization will greatly simplify the formulation without losing the fundamental characteristics of an AIC system.

Assume the following initial conditions and excitation.

$$x_1(0) = x_2(0) = 0, \quad \dot{x}_1(0) = \dot{x}_2(0) = 0, \quad \ddot{x}_g = A_g \sin \omega_g t$$

where ω_g is the forcing frequency.

The response of the AIC system at each critical time point are given as follows:

1. t=0 $x_1(0) = x_2(0) = 0,\ \dot{x}_1(0) = \dot{x}_2(0) = 0.$

At time $t = 0$, $\dot{x}_1 = \dot{x}_2 = 0$; therefore $u\dot{x}_1 = 0$. According to the control algorithms, the IE is locked and the AS is attached to the PS at time $t = 0^+$.

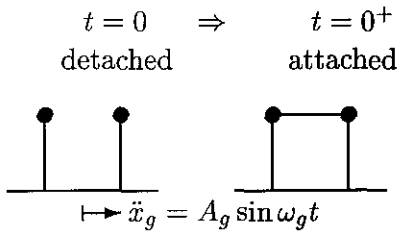

Figure B.14: Configuration of the AIC System at $t = 0$

The equations of motion of the PS and AS in the subsequent locked stage are expressed as

$$m_1\ddot{x}_1 + k_1 x_1 = -m_1\ddot{x}_g - u \tag{B.48}$$

$$m_2\ddot{x}_2 + k_2 x_2 = -m_2\ddot{x}_g + u \tag{B.49}$$

in attachment state

$$\ddot{x}_2 = \ddot{x}_1, \quad x_2 = x_1 \tag{B.50}$$

Adding Eqn. (B.48) and Eqn. (B.49), and considering Eqn. (B.50) yield

$$(m_1 + m_2)\ddot{x}_1 + (k_1 + k_2)x_1 = -(m_1 + m_2)\ddot{x}_g \tag{B.51}$$

For convenience, we will use the following notations:

$$\alpha = \frac{k_2}{k_1}, \quad \beta = \frac{m_2}{m_1}, \quad \omega_1 = \sqrt{\frac{k_1}{m_1}}, \quad \omega_2 = \sqrt{\frac{k_2}{m_2}},$$
$$\omega_3 = \sqrt{\frac{k_1 + k_2}{m_1 + m_2}} = \sqrt{\frac{1+\alpha}{1+\beta}}\omega_1 \tag{B.52}$$

With initial conditions of the PS given by $x_1(0) = 0$, $\dot{x}_1(0) = 0$, the solution of Eqn. (B.51) is given by

$$\begin{aligned} x_1(t) &= x_2(t) \\ &= \frac{A_g}{\omega_g^2 - \omega_3^2}(\sin\omega_g t - \frac{\omega_g}{\omega_3}\sin\omega_3 t) \qquad \text{(B.53)} \\ \dot{x}_1(t) &= \dot{x}_2(t) \\ &= \frac{\omega_g A_g}{\omega_g^2 - \omega_3^2}(\cos\omega_g t - \cos\omega_3 t) \qquad \text{(B.54)} \end{aligned}$$

2. t=t_1 first detachment occurs since $t = 0^+$; $\dot{x}_1(t_1) = \dot{x}_2(t_1) = 0$.

At time $t = t_1$, $\dot{x}_1 = \dot{x}_2 = 0$, the velocity of the PS changes sign while the control force u does not change sign at this time instant. Therefore, $u\dot{x}_1$ undergoes a sign change. According to the OCS control algorithm, the AS is detached from the PS at time $t = t_1^+$.

The value of t_1 can be determined as below.

$$\dot{x}_1(t_1) = \dot{x}_2(t_1) = 0 \quad \Rightarrow \quad \cos\omega_g t_1 = \cos\omega_3 t_1 \tag{B.55}$$

In Table B.9, values of $x_1(t_1)$ and $x_2(t_1)$ varying with α and ω_g are listed.

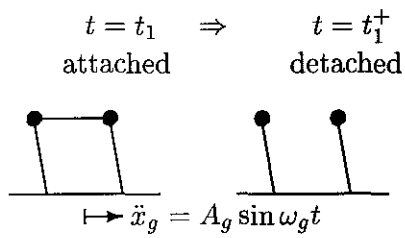

Figure B.15: Configuration of the AIC System at $t = t_1$

Table B.9: Values of $x_1(t_1)$ and $x_2(t_1)$ Varying with α and ω_g

ω_g/ω_3		α			
		0.5	1	2	4
1/4	t_1	0.6597	0.5713	0.4665	0.3613
	$x_1(t_1)$	-0.022	-0.016	-0.011	-0.007
1/2	t_1	0.5497	0.4761	0.3887	0.3011
	$x_1(t_1)$	-0.030	-0.022	-0.015	-0.009
2	t_1	0.2749	0.2380	0.1944	0.1506
	$x_1(t_1)$	-0.015	-0.011	-0.007	-0.004
4	t_1	0.1649	0.1428	0.1166	0.0903
	$x_1(t_1)$	-0.005	-0.004	-0.003	-0.002

Denote $\tau = t - t_1$, the displacement and velocity of PS and AS in the subsequent detachment stage are given by

$$x_1(\tau) = x_1(t_1)\cos\omega_1\tau - \frac{A_g}{\omega_g^2-\omega_1^2}\cdot\frac{\omega_g}{\omega_1}\sin\omega_1\tau + \frac{A_g}{\omega_g^2-\omega_1^2}\sin\omega_g\tau \quad \text{(B.56)}$$

$$x_2(\tau) = x_2(t_1)\cos\omega_2\tau - \frac{A_g}{\omega_g^2-\omega_2^2}\cdot\frac{\omega_g}{\omega_2}\sin\omega_2\tau + \frac{A_g}{\omega_g^2-\omega_2^2}\sin\omega_g\tau \quad \text{(B.57)}$$

$$\dot{x}_1(\tau) = -x_1(t_1)\omega_1\sin\omega_1\tau - \frac{A_g\omega_g}{\omega_g^2-\omega_1^2}\cos\omega_1\tau + \frac{A_g\omega_g}{\omega_g^2-\omega_1^2}\cos\omega_g\tau \quad \text{(B.58)}$$

$$\dot{x}_2(\tau) = -x_2(t_1)\omega_2\sin\omega_2\tau - \frac{A_g\omega_g}{\omega_g^2-\omega_2^2}\cos\omega_2\tau + \frac{A_g\omega_g}{\omega_g^2-\omega_2^2}\cos\omega_g\tau \quad \text{(B.59)}$$

3. t=t_2 first attachment occurs since the last detachment; $\dot{x}_1(t_2) = \dot{x}_2(t_2)$, $u\dot{x}_1 \geq 0$.

At time $t = t_2$,

$$\dot{x}_1 = \dot{x}_2 \Rightarrow -x_1(t_1)\omega_1\sin\omega_1\tau_2 - \frac{A_g\omega_g}{\omega_g^2-\omega_1^2}\cos\omega_1\tau_2 + \frac{A_g\omega_g}{\omega_g^2-\omega_1^2}\cos\omega_g\tau_2 =$$
$$-x_2(t_1)\omega_2\sin\omega_2\tau_2 - \frac{A_g\omega_g}{\omega_g^2-\omega_2^2}\cos\omega_2\tau_2 + \frac{A_g\omega_g}{\omega_g^2-\omega_2^2}\cos\omega_g\tau_2 \quad \text{(B.60)}$$

where $\tau_2 = t_2 - t_1$ is the time interval between this attachment and last detachment.

Assume the PS's natural period T_1 is equal to 1 second and $\beta = 0.02$. Table B.10 gives values of τ_2 corresponding to various α and ω_g values.

We will distinguish between the following two cases, i.e., $\omega_g/\omega_3 < 1$ and $\omega_g/\omega_3 > 1$.

▶ $\omega_g/\omega_3 < 1$

Table B.10: Values of τ_2 Varying with α and ω_g

ω_g/ω_3		α			
		0.5	1	2	4
1/4	τ_2	0.0966	0.0695	0.0496	0.0352
	$x_1(t_2)$	-0.0182	-0.0150	-0.0104	-0.0064
	$x_2(t_2)$	0.0215	0.0163	0.0109	0.0065
	$\dot{x}_1(t_2)$	0.0697	0.0383	0.0178	0.0069
1/2	τ_2	0.0967	0.0695	0.0496	0.0352
	$x_1(t_2)$	-0.0251	-0.0205	-0.0143	-0.0088
	$x_2(t_2)$	0.0293	0.0222	0.0148	0.0089
	$\dot{x}_1(t_2)$	0.0899	0.0491	0.0222	0.0081
2	τ_2	0.1962	0.1389	0.0983	0.0695
	$x_1(t_2)$	-0.0160	-0.0128	-0.0087	-0.0053
	$x_2(t_2)$	-0.0151	-0.0115	-0.0077	-0.0046
	$\dot{x}_1(t_2)$	-0.0160	-0.0379	-0.0406	-0.0359
4	τ_2	0.2304	0.1969	0.0947	0.0669
	$x_1(t_2)$	-0.0053	-0.0053	-0.0048	-0.0029
	$x_2(t_2)$	-0.0011	0.0031	-0.0023	-0.0015
	$\dot{x}_1(t_2)$	0.0552	0.0381	-0.0240	-0.0276

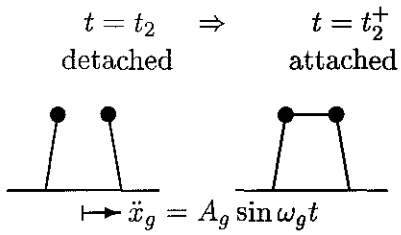

Figure B.16: Configuration of the AIC System at $t = t_2$ ($\omega_g/\omega_3 < 1$)

▶ $\omega_g/\omega_3 > 1$

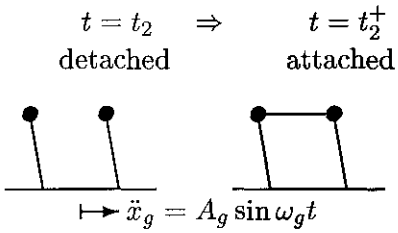

Figure B.17: Configuration of the AIC System $t = t_2$ ($\omega_g/\omega_3 > 1$)

The equations of motion of the PS and AS in the subsequent attachment stage until

next detachment occurs are expressed as

$$m_1\ddot{x}_1 + k_1 x_1 = -m_1\ddot{x}_g - u \tag{B.61}$$

$$m_2\ddot{x}_2 + k_2 x_2 = -m_2\ddot{x}_g + u \tag{B.62}$$

and

$$\ddot{x}_2 = \ddot{x}_1, \quad x_2 = x_1 - (x_1(t_2) - x_2(t_2)) \tag{B.63}$$

Adding Eqn. (B.61) and Eqn. (B.62), and considering Eqn. (B.63), yield

$$(m_1 + m_2)\ddot{x}_1 + (k_1 + k_2)x_1 = -(m_1 + m_2)\ddot{x}_g + k_2(x_1(t_2) - x_2(t_2)) \tag{B.64}$$

Denote

$$\tau = t - t_2.$$

With the initial condition of the PS given by $x_1(\tau = 0) = x_1(t_2)$, $\dot{x}_1(\tau = 0) = \dot{x}_1(t_2)$, the solution of Eqn. (B.63) is given by

$$\begin{aligned} x_1(\tau) &= x_1(t_2)\cos\omega_3\tau + \frac{\dot{x}_1(t_2)}{\omega_3}\sin\omega_3\tau + \frac{A_g}{\omega_g^2 - \omega_3^2}(\sin\omega_g\tau - \frac{\omega_g}{\omega_3}\sin\omega_3\tau) \\ &\quad + \frac{k_2[x_1(t_2) - x_2(t_2)]}{k_1 + k_2}(1 - \cos\omega_3\tau) \\ &= \frac{[x_1(t_2) + \alpha x_2(t_2)]}{1 + \alpha}\cos\omega_3\tau + \Big[\frac{\dot{x}_1(t_2)}{\omega_3} - \frac{A_g}{\omega_g^2 - \omega_3^2}\cdot\frac{\omega_g}{\omega_3}\Big]\sin\omega_3\tau \\ &\quad + \frac{A_g}{\omega_g^2 - \omega_3^2}\sin\omega_g\tau + \frac{\alpha[x_1(t_2) - x_2(t_2)]}{1 + \alpha} \end{aligned} \tag{B.65}$$

$$\begin{aligned} x_2(\tau) &= x_1(\tau) - (x_1(t_2) - x_2(t_2)) \\ &= \frac{[x_1(t_2) + \alpha x_2(t_2)]}{1 + \alpha}\cos\omega_3\tau + \Big[\frac{\dot{x}_1(t_2)}{\omega_3} - \frac{A_g}{\omega_g^2 - \omega_3^2}\cdot\frac{\omega_g}{\omega_3}\Big]\sin\omega_3\tau \\ &\quad + \frac{A_g}{\omega_g^2 - \omega_3^2}\sin\omega_g\tau - \frac{[x_1(t_2) - x_2(t_2)]}{1 + \alpha} \end{aligned} \tag{B.66}$$

Taking derivative of $x_1(\tau)$ and $x_2(\tau)$, and considering the condition $\dot{x}_1(t_2) = \dot{x}_2(t_2)$ at

Table B.11: Values of $x_1(t_1)$ and $x_2(t_1)$ Varying with α and ω_g

ω_g/ω_3		α			
		0.5	1	2	4
1/4	τ_3	0.2132	0.1191	0.0348	0.0088
	$x_1(t_3)$	-0.00653	-0.01211	-0.01013	-0.00639
1/2	τ_3	0.1980	0.1070	0.0314	0.0075
	$x_1(t_3)$	-0.01104	-0.01720	-0.01394	-0.00875
2	τ_3	0.021	0.1287	0.1156	0.0935
	$x_1(t_3)$	-0.01619	-0.01416	-0.01056	-0.00678
4	τ_3	0.2734	0.0557	0.1018	0.0821
	$x_1(t_3)$	0.00385	-0.00391	-0.00768	-0.00524

time t_2, yield

$$\begin{aligned}\dot{x}_1(\tau) &= \dot{x}_2(\tau) \\ &= -\frac{[x_1(t_2)+\alpha x_2(t_2)]}{1+\alpha}\omega_3 \sin\omega_3\tau + \left[\dot{x}_1(t_2) - \frac{A_g\omega_g}{\omega_g^2-\omega_3^2}\right]\cos\omega_3\tau \\ &\quad + \frac{A_g\omega_g}{\omega_g^2-\omega_3^2}\cos\omega_g\tau \end{aligned} \tag{B.67}$$

4. t=t_3 first detachment occurs since the last attachment at $t = t_2^+$; $\dot{x}_1(t_3) = \dot{x}_2(t_3) = 0$, and $u\dot{x}_1(t_3^+) < 0$.

Denote $\tau_3 = t_3 - t_2$. At time t_3,

$$\dot{x}_1(t_3) = \dot{x}_2(t_3) = 0 \quad \Rightarrow$$

$$-\frac{[x_1(t_2)+\alpha x_2(t_2)]}{1+\alpha}\omega_3 \sin\omega_3\tau_3 + \left[\dot{x}_1(t_2) - \frac{A_g\omega_g}{\omega_g^2-\omega_3^2}\right]\cos\omega_3\tau_3 + \frac{A_g\omega_g}{\omega_g^2-\omega_3^2}\cos\omega_g\tau_3 = 0 \tag{B.68}$$

Assume the PS's natural period T_1 is equal to 1 second and $\beta = 0.02$. Table B.11 gives the values of τ_2 corresponding to various values of α and ω_g.

Case II: $c_1 = 0$, $c_2 > 0$

Now, we consider an AIC system in which the PS has no damping but the AS have a nonzero damping factor, i.e., $c_1 = 0$, $c_2 > 0$.

Assume the following initial conditions and excitation.

$$x_1(0) = x_2(0) = 0, \quad \dot{x}_1(0) = \dot{x}_2(0) = 0, \quad \ddot{x}_g = A_g \sin \omega_g t$$

The dynamics of AIC system at every key time point are listed below.

1. t=0 $x_1(0) = x_2(0) = 0$, $\dot{x}_1(0) = \dot{x}_2(0) = 0$.

At time $t = 0$, $\dot{x}_1 = \dot{x}_2 = 0$; therefore $u\dot{x}_1 = 0$. According to the OCS control algorithm, the IE is locked and the AS is attached to the PS at time $t = 0^+$.

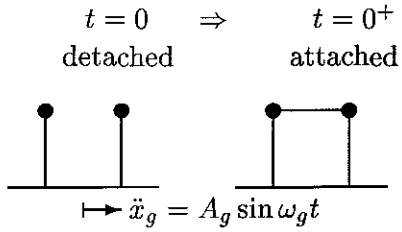

Figure B.18: Configuration of the AIC System at $t = 0$

The equations of motion of the PS and AS in the subsequent locked stage are expressed as

$$m_1\ddot{x}_1 + k_1 x_1 = -m_1\ddot{x}_g - u \tag{B.69}$$

$$m_2\ddot{x}_2 + c_2\dot{x}_2 + k_2 x_2 = -m_2\ddot{x}_g + u \tag{B.70}$$

with

$$\ddot{x}_2 = \ddot{x}_1, \quad \dot{x}_2 = \dot{x}_1, \quad x_2 = x_1 \tag{B.71}$$

Adding Eqn. (B.69) and Eqn. (B.70), and considering Eqn. (B.71), yield

$$(m_1 + m_2)\ddot{x}_1 + c_2\dot{x}_1 + (k_1 + k_2)x_1 = -(m_1 + m_2)\ddot{x}_g \tag{B.72}$$

For convenience, we will use the following notations:

$$\zeta = \frac{c_2}{2(m_1 + m_2)\omega_3}, \quad \omega_D = \omega_3\sqrt{1 - \zeta^2} \tag{B.73}$$

$$\zeta_2 = \frac{c_2}{2m_2\omega_2} = \sqrt{\frac{(1+\alpha)(1+\beta)}{\alpha\beta}}\zeta \tag{B.74}$$

With initial conditions of the PS given by $x_1(0) = 0$, $\dot{x}_1(0) = 0$, the solution of Eqn. (B.72) is given by

$$\begin{aligned} x_1(t) &= x_2(t) \\ &= e^{-\zeta\omega_3 t}(A\cos\omega_D t + B\sin\omega_D t) + C\sin\omega_g t + D\cos\omega_g t \qquad \text{(B.75)} \\ \dot{x}_1(t) &= \dot{x}_2(t) \\ &= e^{-\zeta\omega_3 t}[(-\zeta\omega_3 A + \omega_D B)\cos\omega_D t - (\zeta\omega_3 B + A\omega_D)\sin\omega_D t] \\ &\quad + C\omega_g\cos\omega_g t - D\omega_g\sin\omega_g t \qquad \text{(B.76)} \end{aligned}$$

where

$$C = \frac{(\omega_g^2 - \omega_3^2)A_g}{(\omega_g^2 - \omega_3^2)^2 + (2\zeta\omega_g\omega_3)^2} \quad , \quad D = \frac{2\zeta\omega_g\omega_3 A_g}{(\omega_g^2 - \omega_3^2)^2 + (2\zeta\omega_g\omega_3)^2}$$
$$A = -\frac{2\zeta\omega_g\omega_3 A_g}{(\omega_g^2 - \omega_3^2)^2 + (2\zeta\omega_g\omega_3)^2} \quad , \quad B = \frac{\zeta\omega_3 A - C\omega_g}{\omega_D}$$

2. t=t_1 first detachment occurs since $t = 0^+$; $\dot{x}_1(t_1) = \dot{x}_2(t_1) = 0$.

At time $t = t_1$, $\dot{x}_1 = \dot{x}_2 = 0$, the velocity of the PS changes sign while the control force u does not change sign at this time instant. Therefore, $u\dot{x}_1$ undergoes a sign change. According to the OCS control algorithm, the AS is detached from the PS at time $t = t_1^+$.

Solve for the value of t_1 using the condition

$$\dot{x}_1(t_1) = \dot{x}_2(t_1) = 0$$

Table B.12 gives the values of $x_1(t_1)$ and $x_2(t_1)$ varying with α, ω_g and ζ_2.

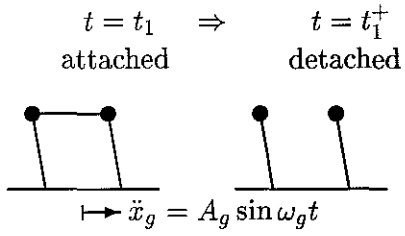

Figure B.19: Configuration of the AIC System at $t = t_1$

Denote $\tau = t - t_1$ and $\omega_{2D} = \omega_2\sqrt{1-\zeta_2^2}$, the displacement and velocity of PS and AS

Table B.12: Values of $x_1(t_1)$ and $x_2(t_1)$ Varying with α, ω_g and ζ_2

ζ_2	ω_g/ω_3		α			
			0.5	1	2	4
15%	1/2	t_1	0.5504	0.4768	0.3894	0.3017
		$x_1(t_1)$	-0.02934	-0.02192	-0.01457	-0.00872
	2	t_1	0.2739	0.2371	0.1934	0.1498
		$x_1(t_1)$	-0.01467	-0.01096	-0.00728	-0.00436
50%	1/2	t_1	0.5520	0.4786	0.3911	0.3032
		$x_1(t_1)$	-0.02825	-0.02094	-0.01383	-0.00824
	2	t_1	0.2718	0.2348	0.1914	0.1480
		$x_1(t_1)$	-0.01412	-0.01046	-0.00690	-0.00411

in the subsequent detachment stage are given by

$$x_1(\tau) = x_1(t_1)\cos\omega_1\tau - \frac{A_g}{\omega_g^2-\omega_1^2}\cdot\frac{\omega_g}{\omega_1}\sin\omega_1\tau + \frac{A_g}{\omega_g^2-\omega_1^2}\sin\omega_g\tau \tag{B.77}$$

$$x_2(\tau) = e^{-\zeta_2\omega_2\tau}(A\cos\omega_{2D}\tau + B\sin\omega_{2D}\tau) + C\sin\omega_g\tau + D\cos\omega_g\tau \tag{B.78}$$

$$\dot{x}_1(\tau) = -x_1(t_1)\omega_1\sin\omega_1\tau - \frac{A_g\omega_g}{\omega_g^2-\omega_1^2}\cos\omega_1\tau + \frac{A_g\omega_g}{\omega_g^2-\omega_1^2}\cos\omega_g\tau \tag{B.79}$$

$$\begin{aligned}\dot{x}_2(\tau) = {} & e^{-\zeta_2\omega_2\tau}[(-\zeta_2\omega_2 A + \omega_{2D}B)\cos\omega_{2D}\tau - (\zeta_2\omega_2 B + A\omega_{2D})\sin\omega_{2D}\tau] \\ & + C\omega_g\cos\omega_g\tau - D\omega_g\sin\omega_g\tau\end{aligned} \tag{B.80}$$

where

$$C = \frac{(\omega_g^2-\omega_2^2)A_g}{(\omega_g^2-\omega_2^2)^2+(2\zeta_2\omega_g\omega_2)^2}, \quad D = \frac{2\zeta_2\omega_g\omega_2 A_g}{(\omega_g^2-\omega_2^2)^2+(2\zeta_2\omega_g\omega_2)^2}$$

$$A = x_2(t_1) - D, \quad B = \frac{\zeta_2\omega_2 A - C\omega_g}{\omega_{2D}}$$

3. t=t_2 first attachment occurs since last detachment at t_1; $\dot{x}_1(t_2) = \dot{x}_2(t_2)$, $u\dot{x}_1 \geq 0$.

At time $t = t_2$,

$$\dot{x}_1(\tau_2) = \dot{x}_2(\tau_2) \quad \Rightarrow$$

$$\begin{aligned}-x_1(t_1)\omega_1\sin\omega_1\tau_2 - \frac{A_g\omega_g}{\omega_g^2-\omega_1^2}\cos\omega_1\tau_2 + \frac{A_g\omega_g}{\omega_g^2-\omega_1^2}\cos\omega_g\tau_2 = {} \\ e^{-\zeta_2\omega_2\tau_2}[(-\zeta_2\omega_2 A + \omega_{2D}B)\cos\omega_{2D}\tau_2 - (\zeta_2\omega_2 B + A\omega_{2D})\sin\omega_{2D}\tau_2] \\ + C\omega_g\cos\omega_g\tau_2 - D\omega_g\sin\omega_g\tau_2\end{aligned} \tag{B.81}$$

Table B.13: Values of τ_2 Varying with α, ω_g and ζ_2

ζ_2	ω_g/ω_3		α			
			0.5	1	2	4
15%	1/2	τ_2	0.0960	0.0696	0.0499	0.0355
		$x_1(t_2)$	-0.02471	-0.02010	-0.01397	-0.00856
		$x_2(t_2)$	0.01768	0.01343	0.00898	0.00539
		$\dot{x}_1(t_2)$	0.08773	0.04793	0.02162	0.00778
	2	τ_2	0.1946	0.1373	0.0972	0.0687
		$x_1(t_2)$	-0.01592	-0.01255	-0.00856	-0.00520
		$x_2(t_2)$	-0.00610	-0.00459	-0.00300	-0.00177
		$\dot{x}_1(t_2)$	-0.01817	-0.03878	-0.04067	-0.03559
50%	1/2	τ_2	0.0995	0.0751	0.0553	0.0401
		$x_1(t_2)$	-0.02352	-0.01896	-0.01315	-0.00805
		$x_2(t_2)$	0.00370	0.00315	0.00218	0.00132
		$\dot{x}_1(t_2)$	0.08586	0.04775	0.02149	0.00738
	2	τ_2	0.1716	0.1205	0.0855	0.0604
		$x_1(t_2)$	-0.01516	-0.01157	-0.00779	-0.00470
		$x_2(t_2)$	-0.00041	-0.00008	0.00003	0.00005
		$\dot{x}_1(t_2)$	-0.02759	-0.03622	-0.03499	-0.02975

where $\tau_2 = t_2 - t_1$ is the time interval between this attachment and the last detachment.

Assume the PS's natural period T_1 is equal to 1 second, and $\beta = 0.02$, the values of τ_2 corresponding to various α, ω_g and ζ_2 values are calculated and listed in Table B.13.

The equations of motion of the PS and AS in the subsequent attachment stage until next detachment occurs are expressed as

$$m_1\ddot{x}_1 + k_1x_1 = -m_1\ddot{x}_g - u \tag{B.82}$$

$$m_2\ddot{x}_2 + c_2\dot{x}_2 + k_2x_2 = -m_2\ddot{x}_g + u \tag{B.83}$$

and

$$\ddot{x}_2 = \ddot{x}_1, \quad \dot{x}_2 = \dot{x}_1, \quad x_2 = x_1 - (x_1(t_2) - x_2(t_2)) \tag{B.84}$$

Adding Eqn. (B.82) and Eqn. (B.83), and considering Eqn. (B.84), yield

$$(m_1 + m_2)\ddot{x}_1 + c_2\dot{x}_1 + (k_1 + k_2)x_1 = -(m_1 + m_2)\ddot{x}_g + k_2(x_1(t_2) - x_2(t_2)) \tag{B.85}$$

Denote

$$\tau = t - t_2$$

With the initial condition of the PS given by $x_1(\tau = 0) = x_1(t_2)$, $\dot{x}_1(\tau = 0) = \dot{x}_1(t_2)$, the solution of Eqn. (B.85) is given by

$$\begin{aligned} x_1(\tau) &= e^{-\zeta\omega_3\tau}(A\cos\omega_D\tau + B\sin\omega_D\tau) + C\sin\omega_g\tau + D\cos\omega_g\tau \\ &\quad + F[1 - e^{-\zeta\omega_3\tau}(\cos\omega_D\tau + \frac{\zeta}{\sqrt{1-\zeta^2}}\sin\omega_D\tau)] \\ &= e^{-\zeta\omega_3\tau}[(A-F)\cos\omega_D\tau + (B - \frac{\zeta F}{\sqrt{1-\zeta^2}})\sin\omega_D\tau] + C\sin\omega_g\tau \\ &\quad + D\cos\omega_g\tau + F \qquad \text{(B.86)} \\ x_2(\tau) &= x_1(\tau) - (x_1(t_2) - x_2(t_2)) \qquad \text{(B.87)} \end{aligned}$$

where

$$C = \frac{(\omega_g^2 - \omega_3^2)A_g}{(\omega_g^2 - \omega_3^2)^2 + (2\zeta\omega_g\omega_3)^2}, \quad D = \frac{2\zeta\omega_g\omega_3 A_g}{(\omega_g^2 - \omega_3^2)^2 + (2\zeta\omega_g\omega_3)^2}$$
$$A = x_1(t_2) - D, \quad B = \frac{\dot{x}_1(t_2) + \zeta\omega_3 A - C\omega_g}{\omega_D}, \quad F = \frac{\alpha[x_1(t_2) - x_2(t_2)]}{1+\alpha}$$

Taking derivative of $x_1(\tau)$ and $x_2(\tau)$ and considering the condition $\dot{x}_1(t_2) = \dot{x}_2(t_2)$ at time t_2, yield

$$\begin{aligned} \dot{x}_1(\tau) &= \dot{x}_2(\tau) \\ &= e^{-\zeta\omega_3\tau}[(-\zeta\omega_3 A + \omega_D B)\cos\omega_D\tau + (-\zeta\omega_3 B - \omega_D A + \frac{\omega_3 F}{\sqrt{1-\zeta^2}})\sin\omega_D\tau] \\ &\quad + C\omega_g\cos\omega_g\tau - D\omega_g\sin\omega_g\tau \qquad \text{(B.88)} \end{aligned}$$

4. t=t_3 first detachment occurs since last attachment at t_2; $\dot{x}_1(t_3) = \dot{x}_2(t_3) = 0$, and $u\dot{x}_1(t_3^+) < 0$.

Denote $\tau_3 = t_3 - t_2$. At time t_3,

$$\dot{x}_1(t_3) = \dot{x}_2(t_3) = 0 \qquad \Rightarrow$$

Table B.14: Values of $x_1(t_1)$ and $x_2(t_1)$ Varying with α, ω_g and ζ_2

ζ_2	ω_g/ω_3		α			
			0.5	1	2	4
15%	1/2	τ_3	0.3313	0.3101	0.2646	0.2098
		$x_1(t_3)$	-0.01439	-0.02491	-0.02547	-0.01937
	2	τ_3	0.0185	0.0393	0.0367	0.0291
		$x_1(t_3)$	-0.01615	-0.01370	-0.00980	-0.00611
50%	1/2	τ_3	0.3164	0.2979	0.2564	0.2046
		$x_1(t_3)$	-0.00604	-0.01450	-0.01586	-0.01231
	2	τ_3	0.0283	0.0329	0.0273	0.0209
		$x_1(t_3)$	-0.01574	-0.01259	-0.00868	-0.00531

$$e^{-\zeta\omega_3\tau_3}[(-\zeta\omega_3 A+\omega_D B)\cos\omega_D\tau_3+(-\zeta\omega_3 B-\omega_D A+\frac{\omega_3 F}{\sqrt{1-\zeta^2}})\sin\omega_D\tau_3]$$
$$+C\omega_g\cos\omega_g\tau_3-D\omega_g\sin\omega_g\tau_3=0 \qquad \text{(B.89)}$$

Assume the PS's natural period T_1 is equal to 1 second and $\beta = 0.02$. Table B.14 gives the values of τ_2 corresponding to various values of α, ω_g and ζ_2.

Appendix C Finite Element Models of the 9- and 20-story Buildings

The numerical models of the 9- and 20-story buildings discussed in Chapter 3 are derived in this appendix by using finite element method (FEM). The FEM code is developed in MATLAB [28]. The main part of this program is downloaded from Ref. [29] with slight modification made by the author for static condensation.

```
%-----------------------------------------------------------------------
%|*********************************************************************
%|*          Structural Data of the 9 Story 5 Bay Building
%|*
%|*                  University of Notre Dame
%|*                       November, 1999
%|*
%|*               Coded by      Y.Ohtori
%|*                             R.E.Christenson
%|*               Supervised by B.F.Spencer, Jr.
%|*
%|*               Modified by Yunfeng Zhang, EERL, Caltech, March 2000
%|*********************************************************************
%-----------------------------------------------------------------------

% ------------------------------------
% --- Set Data for Nodal Coordinate ---
% ------------------------------------
    Num_story = 9+1;                        % Number of stories + basement
    Num_bay   = 5;                          % Number of Bays
    Num_MRF   = 2;                          % Number of Moment Resisting Frame
    Num_node  = (Num_bay+1)*(Num_story+1);  % Number of Node
    Num_DOF   = 3*Num_node;                 % Number of Degree of Freedoms

    height = [ 3.6576 5.4864 3.9624 3.9624 3.9624 3.9624 ...
               3.9624 3.9624 3.9624 3.9624 ];
```

```
    width  = [ 9.1440 9.1440 9.1440 9.1440 9.1440 ];

% ------------------------------------------
% --- Define Material Table (left to right) ---
% ------------------------------------------
    Num_beam  = Num_bay*Num_story;              % Number of Beams
    Num_col   = (Num_bay+1)*Num_story;          % Number of Columns
    Num_elem  = Num_beam + Num_col;             % Number of Elements

    element_tbl = zeros(Num_elem,4);

%  - Column -

  for i=1:Num_col
    element_tbl(i,1) = i;
    element_tbl(i,2) = i + (Num_bay+1);
    element_tbl(i,4) = 1;
  end

 element_tbl(1:Num_col,3) = [
                      1    2    2    2    2    1  ...   %  basement
                      1    2    2    2    2    1  ...   %  1st floor
                      1   12   12   12   12    1  ...   %  2nd floor
                      1    3    3    3    3    1  ...   %  3rd floor
                     13   14   14   14   14   13  ...   %  4th floor
                      4    1    1    1    1    4  ...   %  5th floor
                     15   13   13   13   13   15 ...    %  6th floor
                      5    4    4    4    4    5 ...    %  7th floor
                     16   15   15   15   15   16 ...    %  8th floor
                      6    5    5    5    5    6 ...    %  9th floor
                                                  ]';

%  - Beam   -

  elem_no = Num_col;
  for i = 1:Num_story
    for j = 1:Num_bay
        elem_no = elem_no + 1;
        element_tbl(elem_no,1) = i*(Num_bay+1) + j;
```

```
        element_tbl(elem_no,2) = element_tbl(elem_no,1) + 1;
        element_tbl(elem_no,4) = 2;
      end
    end

  element_tbl(Num_col+1:Num_col+Num_beam,3) = [
                        7     7     7     7    7 ...   %  1st floor
                        7     7     7     7    7 ...   %  2nd floor
                        7     7     7     7    7 ...   %  3rd floor
                        8     8     8     8    8 ...   %  4th floor
                        8     8     8     8    8 ...   %  5th floor
                        8     8     8     8    8 ...   %  6th floor
                        8     8     8     8    8 ...   %  7th floor
                        9     9     9     9    9 ...   %  8th floor
                       10    10    10    10    10 ...   %  9th floor
                       11    11    11    11    11 ...   %  roof
                                                 ]';

  element_tbl(Num_col+[5 10 15 20 25 30 35 40 45 50],4) = 5;

% ----------------------------------
% --- Define Master - Slave Nodes ---
% ----------------------------------
  slv_tbl = [
%   Master  Dir  Num_slv  Slv_1  Slv_2  Slv_3  Slv_4
     15      1     5       13     14      16     17     18   %  2nd floor
     21      1     5       19     20      22     23     24   %  3rd floor
     27      1     5       25     26      28     29     30   %  4th floor
     33      1     5       31     32      34     35     36   %  5th floor
     39      1     5       37     38      40     41     42   %  6th floor
     45      1     5       43     44      46     47     48   %  7th floor
     51      1     5       49     50      52     53     54   %  8th floor
     57      1     5       55     56      58     59     60   %  9th floor
     63      1     5       61     62      64     65     66   %  roof
      ];
  Num_mst = length(slv_tbl(:,1));                  % Number of Master Nodes

% -------------------------
% --- Define Fixed Nodes ---
```

```
% -------------------------
%                       Fix: 1 , Free: 0
%              Node_no  Hor.   Vert.   Rot.
  Fix_node = [    1        1      1      0 ;
                  2        1      1      0 ;
                  3        1      1      0 ;
                  4        1      1      0 ;
                  5        1      1      0 ;
                  6        1      1      0 ;
                  7        1      0      0 ;
                  8        1      0      0 ;
                  9        1      0      0 ;
                  10       1      0      0 ;
                  11       1      0      0 ;
                  12       1      0      0 ;
                  ];
  Num_BND    = length(Fix_node(:,1));          % Number of Fixed Nodes

% --------------------------
% --- Define Element mass ---
% --------------------------
  seismic_mass1 = 4.8159e+05;
  seismic_mass2 = 5.0349e+05;
  seismic_mass3 = 4.9473e+05;
  seismic_mass4 = 5.3414e+05;

  Element_mass = [
   zeros(1,Num_col)...
   seismic_mass1*(1/(Num_bay))*ones(1,Num_bay)...   %  1st floor
   seismic_mass2*(1/(Num_bay))*ones(1,Num_bay)...   %  2nd floor
   seismic_mass3*(1/(Num_bay))*ones(1,Num_bay)...   %  3rd floor
   seismic_mass3*(1/(Num_bay))*ones(1,Num_bay)...   %  4th floor
   seismic_mass3*(1/(Num_bay))*ones(1,Num_bay)...   %  5th floor
   seismic_mass3*(1/(Num_bay))*ones(1,Num_bay)...   %  6th floor
   seismic_mass3*(1/(Num_bay))*ones(1,Num_bay)...   %  7th floor
   seismic_mass3*(1/(Num_bay))*ones(1,Num_bay)...   %  8th floor
   seismic_mass3*(1/(Num_bay))*ones(1,Num_bay)...   %  9th floor
   seismic_mass4*(1/(Num_bay))*ones(1,Num_bay)...   %  roof
                   ]';
```

```
% ----------------------------
% --- Define Material Table ---
% ----------------------------
% Type = 0: Spread Plasticity Model
%        1: Concentrated Plasticity Model

  mat_tbl = [
%Mat_no  EI1        EI2        EI3        EA         GA         d1         d2     type
1 4.5272e+08 4.0971e+08 1.3582e+07 1.4060e+10 8.8960e+15 1.0051e-02 1.0580e-02 1
2 6.8324e+08 6.1831e+08 2.0497e+07 1.8962e+10 8.8960e+15 9.5008e-03 1.0001e-02 1
3 5.9836e+08 5.4151e+08 1.7951e+07 1.7285e+10 8.8960e+15 9.6708e-03 1.0180e-02 1
4 3.1957e+08 2.8920e+08 9.5870e+06 1.0745e+10 8.8960e+15 1.0485e-02 1.1037e-02 1
5 2.8295e+08 2.5607e+08 8.4885e+06 9.7518e+09 8.8960e+15 1.0641e-02 1.1201e-02 1
6 2.5049e+08 2.2211e+08 7.5148e+06 8.8360e+09 8.8960e+15 1.0761e-02 1.1339e-02 1
7 8.1140e+08 6.8151e+08 2.4342e+07 6.0629e+09 8.8960e+15 4.0610e-03 4.2913e-03 1
8 6.4912e+08 5.5829e+08 1.9474e+07 5.1212e+09 8.8960e+15 4.1408e-03 4.3701e-03 1
9 3.3205e+08 2.8596e+08 9.9615e+06 3.7539e+09 8.8960e+15 4.9618e-03 5.2362e-03 1
10 2.3718e+08 2.2226e+08 7.1154e+06 3.1992e+09 8.8960e+15 5.4325e-03 5.7087e-03 1
11 1.5229e+08 1.3940e+08 4.5688e+06 2.5929e+09 8.8960e+15 6.1373e-03 6.4567e-03 1
                ];
% Add splice elements
  mat_tbl = [mat_tbl
12          (6/13)*mat_tbl(2,2:8)+(7/13)*mat_tbl(3,2:8)                          1
13          (6/13)*mat_tbl(1,2:8)+(7/13)*mat_tbl(4,2:8)                          1
14          (6/13)*mat_tbl(3,2:8)+(7/13)*mat_tbl(1,2:8)                          1
15          (6/13)*mat_tbl(4,2:8)+(7/13)*mat_tbl(5,2:8)                          1
16          (6/13)*mat_tbl(5,2:8)+(7/13)*mat_tbl(6,2:8)                          1
                ];

%---------------------------------------
% --- Define Building Characteristics ---
%---------------------------------------
 Idx_linear = 1; % 1:Linear 0:Nonlinear
 Damp_type  = 4; % 1:Mass, 2:Stiffness, 3:Rayleigh 4:Assigned modal damping
 Idx_Band   = 1; % Solver  1:Banded, 0: Symmetric

% ----------------------------
% Calculate the nodal coordinates
% ----------------------------
```

```
    EPS = 1.0E-14;

    y0 = 0.0;
    i  = 0;
    for no_story=1:Num_story+1
       x0 = 0.0;
       for no_bay=1:Num_bay+1
          i  = i + 1;
          x(i) =  x0;
          y(i) =  y0;
          if no_bay<=Num_bay
             x0 = x0 + width(no_bay);
          end
       end
       if no_story<=Num_story
          y0 = y0 + height(no_story);
       end
    end

% ----------------------------
% Set Node Numbers of Elements
% ------------------------------------------------------------------
%   element_tbl(:,1) = Node_a
%   element_tbl(:,2) = Node_b
%   element_tbl(:,3) = Material Table Number
%   element_tbl(:,4) = Type of Element (1: Column, 2: Beam, 3:Brace)
% ------------------------------------------------------------------
%  Judge Linear or Nonlinear Analysis
% ------------------------------------
  if Idx_linear == 1
     mat_tbl(:,7) = 10*mat_tbl(:,7);
     mat_tbl(:,8) = 10*mat_tbl(:,8);
  end
% ------------------------------------
% ---------------------
% Set Element Properties
% ---------------------

   for i=1:Num_elem
```

```
    na = element_tbl(i,1);
    nb = element_tbl(i,2);
    elem_prop(i,1) = sqrt((x(na)-x(nb))^2 + (y(na)-y(nb))^2);    % Length
    elem_prop(i,2) = mat_tbl(element_tbl(i,3),2);                % EI1
    elem_prop(i,3) = mat_tbl(element_tbl(i,3),3);                % EI2
    elem_prop(i,4) = mat_tbl(element_tbl(i,3),4);                % EI3
    elem_prop(i,5) = mat_tbl(element_tbl(i,3),5);                % EA
    elem_prop(i,6) = mat_tbl(element_tbl(i,3),6);                % GA
    elem_prop(i,7) = mat_tbl(element_tbl(i,3),7);                % d1
    elem_prop(i,8) = mat_tbl(element_tbl(i,3),8);                % d2
    elem_prop(i,9) = mat_tbl(element_tbl(i,3),9);                % Type
  end

% ------------------------------------
% Assemble Global Matricies [M] & [K]
% ------------------------------------

  MM = zeros(Num_DOF);
  KK = zeros(Num_DOF);
  CC = zeros(Num_DOF);

% --- Stiffness Matrix Fixed Fixed [K] ---

  for i=1:Num_elem
   na = element_tbl(i,1);
   nb = element_tbl(i,2);
   Ia = 3*(na-1)+[1 2 3];
   Ib = 3*(nb-1)+[1 2 3];
   EI = elem_prop(i,2);
   EA = elem_prop(i,5);
   invL=1.0/elem_prop(i,1);
   T=diag(ones(6,1));
   c(i)=(x(nb)-x(na))*invL;
   s(i)=(y(nb)-y(na))*invL;
   a=[1;2];
   b=a+3;
   T(a,a)=[c(i)  s(i);-s(i) c(i)];
   T(b,b)=[c(i)  s(i);-s(i) c(i)];
```

```
  if element_tbl(i,4)<=2 %      |-----|
    g=EA/EI;
    k1=[g;0;0;-g;0;0];
    k2=[0;12*invL*invL;6*invL;0;-12*invL*invL;6*invL];
    k3=[0;6*invL;4;0;-6*invL;2];
    k6=[0;6*invL;2;0;-6*invL;4];
    khat=(EI*invL)*[k1 k2 k3 -k1 -k2 k6];
    km=T'*khat*T;

  elseif element_tbl(i,4)==3 %      o-----o
    khat=zeros(6);
    k1=(EA*invL)*[1 -1;-1 1];
    khat([1 4],[1 4])=k1;
    km=T'*khat*T;

  elseif element_tbl(i,4)==4 %      o-----|
    khat=zeros(6);
    k1=(EA*invL)*[1 -1;-1 1];
    k2=(3*EI*invL)*[1*invL*invL -1*invL*invL 1*invL;-1*invL*invL ...
                    1*invL*invL -1*invL;1*invL -1*invL 1];
    khat([1 4],[1 4])=k1;
    khat([2 5 6],[2 5 6])=k2;
    km=T'*khat*T;

  elseif element_tbl(i,4)==5 %      |-----o
    khat=zeros(6);
    k1=(EA*invL)*[1 -1;-1 1];
    k2=(3*EI*invL)*[1*invL*invL 1*invL -1*invL*invL;1*invL 1 -1*invL; ...
                    -1*invL*invL -1*invL 1*invL*invL];
    khat([1 4],[1 4])=k1;
    khat([2 3 5],[2 3 5])=k2;
    km=T'*khat*T;
  end

    KK([Ia Ib],[Ia Ib]) = KK([Ia Ib],[Ia Ib])+km;

  end

% --- Lumped Mass Matrix [M] ---
```

```
% only the beam elements have mass associated with them

    alpha = 1e-06;

   for i=1:Num_elem
    na = element_tbl(i,1);
    nb = element_tbl(i,2);
    Ia = 3*(na-1)+[1 2 3];
    Ib = 3*(nb-1)+[1 2 3];
    mi = Element_mass(i)/2*diag([1 1 alpha*(elem_prop(i,1)^2)/210 ...
                                 1 1 alpha*(elem_prop(i,1)^2)/210]);
    MM([Ia Ib],[Ia Ib]) = MM([Ia Ib],[Ia Ib])+mi;
   end

% --- Place an arbitrary rotational mass on the basement pinned locations ---

   pinned_base=(Fix_node(:,1)<=Num_bay+1).*(1-Fix_node(:,4));

   for i = 1:length(pinned_base)
    if pinned_base(i)==1
     MM(Fix_node(i,1)*3,Fix_node(i,1)*3) = ...
     MM(Fix_node(i,1)*3+(Num_bay+1)*3,Fix_node(i,1)*3+(Num_bay+1)*3);
    end
   end

% ----------------------------------
% Eliminate Boundary Condition DOFs
% ----------------------------------

    Ref_BND = zeros(1,Num_DOF);

  for i=1:Num_BND
    Ref_BND(3*(Fix_node(i,1)-1) + [1 2 3]) = Fix_node(i,1+[1 2 3]);
  end

% eliminate the vertical DOFs
%  for i=1:Num_node
%    Ref_BND(3*(i-1) + 2) = 1;
%  end
```

```
    Order = 1:Num_DOF;

    free_vec = Order(Ref_BND==0);

% --- Eliminate the Fixed Boundary DOF ---

    M_free  = MM(free_vec,free_vec);
    K_free  = KK(free_vec,free_vec);

    Ord_vec = [Order(Ref_BND==0) Order(Ref_BND==1)];
    Out_idx(Ord_vec) = Order;
    Num_free = length(free_vec);

% ------------------------------------
% Eliminate Slave Nodes
% ------------------------------------

   T_rigid = eye(Num_DOF);

   for i=1:Num_mst
     i_mst = 3*(slv_tbl(i,1)-1) + slv_tbl(i,2);
     for j=1:slv_tbl(i,3)
         i_slv = 3*(slv_tbl(i,3+j)-1) + slv_tbl(i,2);
         T_rigid(i_slv,i_slv) = 0;
         T_rigid(i_slv,i_mst) = 1;
     end
   end

   Num_slv = max(slv_tbl(:,3));      % Max Number of Slave Nodes

   Tr_rigid = T_rigid(free_vec,free_vec);

   act_vec = find(diag(Tr_rigid));

   Tr2_rigid = Tr_rigid(:,act_vec);                    % Num_free * Num_act

   Num_act = length(act_vec);
```

```
   diagT = cumsum(diag(Tr_rigid));
   for i=1:Num_mst
     i_mst = 3*(slv_tbl(i,1)-1) + slv_tbl(i,2);
     for j=1:slv_tbl(i,3)
         i_slv = 3*(slv_tbl(i,3+j)-1) + slv_tbl(i,2);
         diagT(Out_idx(i_slv)) = diagT(Out_idx(i_mst));
     end
   end

% --- Remove Rigid Body -----------------

    M = Tr2_rigid' * M_free * Tr2_rigid;
    K = Tr2_rigid' * K_free * Tr2_rigid;

% --- Static Condensation/ignore and remove all verical and rotational inertia

 posit_vec=free_vec(act_vec);
 posit_mst=zeros(1,Num_mst);
 for i=1:Num_mst
    i_mst=3*(slv_tbl(i,1)-1)+slv_tbl(i,2);
    for j=1:length(posit_vec)
       if i_mst == posit_vec(j)
          posit_mst(i)=j;
          break;
       end
    end
 end

 ref_posit=zeros(1,length(posit_vec));
 for i=1:Num_mst
    ref_posit(posit_mst(i))=1;
 end
 order_posit=1:length(posit_vec);
 posit_slv=order_posit(ref_posit==0);

 Maa=M(posit_mst,posit_mst);
 Mab=M(posit_mst,posit_slv);
 Mba=M(posit_slv,posit_mst);
 Mbb=M(posit_slv,posit_slv);
```

```
Kaa=K(posit_mst,posit_mst);
Kab=K(posit_mst,posit_slv);
Kba=K(posit_slv,posit_mst);
Kbb=K(posit_slv,posit_slv);

M_red=Maa;
K_red=Kaa-Kab*inv(Kbb)*Kba;

M1=M_red([Num_mst:-1:1],[Num_mst:-1:1]);
K1=K_red([Num_mst:-1:1],[Num_mst:-1:1]);

save model9 Num_mst M1 K1 Kaa Kab Kbb;

%-------------------------------------------------------------------
%|*****************************************************************
%|*           Structural Data of the 20 Story 5 Bay Building
%|*
%|*                  University of Notre Dame
%|*                       November, 1999
%|*
%|*               Coded by      Y.Ohtori
%|*                             R.E.Christenson
%|*               Supervised by B.F.Spencer, Jr.
%|*
%|*               Modified by Yunfeng Zhang, EERL, Caltech, March 2000
%|*****************************************************************
%-------------------------------------------------------------------

% UNITS: N - m

% ------------------------------------------
% --- Define Initial Data for Calculations ---
% ------------------------------------------
    T_str   = 0.0;                    % Start time of the Response Analysis
    T_end   = 100.0;                  % End time of the Response Analysis
    dt_cal  = 0.01;                  % Calculation Interval Delta_t
    dt_out  = 0.01;                  % Output Interval for file
```

```
    beta_val  = 1.0/4.0;              % beta  value for Newmark-beta Method
    gamma_val = 1.0/2.0;              % gamma value for Newmark-beta Method

% ----------------------
% --- Define Damping ---
% ----------------------
    zeta_cr   = 0.02;                 % Critical Damping
    h_max     = 0.02;                 % Maximum Damping for Type 2
    nCutOff   = 5;                    % Number of mode for cutting off

clear

% -------------------------------------
% --- Set Data for Nodal Coordinate ---
% -------------------------------------
    Num_story = 20+2;                       % Number of stories + basements
    Num_bay   = 5;                          % Number of Bays
    Num_MRF   = 2;                          % Number of Moment Resisting Frame
    Num_node  = (Num_bay+1)*(Num_story+1);  % Number of Nodes
    Num_DOF   = 3*Num_node;                 % Number of Degree of Freedoms

    height = [ 3.6576 3.6576 5.4864 3.9624 3.9624 3.9624 3.9624 ...
               3.9624 3.9624 3.9624 3.9624 3.9624 3.9624 3.9624 ...
               3.9624 3.9624 3.9624 3.9624 3.9624 3.9624 3.9624 3.9624 ];

    width  = [ 6.0960 6.0960 6.0960 6.0960 6.0960 ];

% -----------------------------------------
% --- Define Material Table (left to right) ---
% -----------------------------------------
    Num_beam  = Num_bay*Num_story;          % Number of Beams
    Num_col   = (Num_bay+1)*Num_story;      % Number of Coloms
    Num_elem  = Num_beam + Num_col;         % Number of Elements

    element_tbl = zeros(Num_elem,4);

%  - Column -

   for i=1:Num_col
```

```
    element_tbl(i,1) = i;
    element_tbl(i,2) = i + (Num_bay+1);
    element_tbl(i,4) = 1;
  end

element_tbl(1:Num_col,3) = [
                      1    2    2    2    2    1  ...  % 1st basement
                      1    2    2    2    2    1  ...  % 2nd basement
                      1    2    2    2    2    1  ...  % 1st floor
                     17    2    2    2    2   17  ...  % 2nd floor
                      3    2    2    2    2    3  ...  % 3rd floor
                      3    2    2    2    2    3  ...  % 4th floor
                     18   19   19   19   19   18  ...  % 5th floor
                      4    5    5    5    5    4  ...  % 6th floor
                      4    5    5    5    5    4  ...  % 7th floor
                      4    5    5    5    5    4  ...  % 8th floor
                      4    5    5    5    5    4  ...  % 9th floor
                      4    5    5    5    5    4  ...  % 10th floor
                      4   20   20   20   20    4  ...  % 11th floor
                      4    6    6    6    6    4  ...  % 12th floor
                      4    6    6    6    6    4  ...  % 13th floor
                     21   22   22   22   22   21  ...  % 14th floor
                      7    8    8    8    8    7  ...  % 15th floor
                      7    8    8    8    8    7  ...  % 16th floor
                      7   23   23   23   23    7  ...  % 17th floor
                      7    9    9    9    9    7  ...  % 18th floor
                     24   25   25   25   25   24  ...  % 19th floor
                     10   11   11   11   11   10  ...  % 20th floor
                                                  ]';

%  - Beam   -

  elem_no = Num_col;
  for i = 1:Num_story
    for j = 1:Num_bay
        elem_no = elem_no + 1;
        element_tbl(elem_no,1) = i*(Num_bay+1) + j;
        element_tbl(elem_no,2) = element_tbl(elem_no,1) + 1;
        element_tbl(elem_no,4) = 2;
```

```
    end
  end

  element_tbl(Num_col+1:Num_col+Num_beam,3) = [
                        12    12    12    12    12  ...   %  1st basement
                        12    12    12    12    12  ...   %  1st floor
                        12    12    12    12    12  ...   %  2nd floor
                        12    12    12    12    12  ...   %  3rd floor
                        12    12    12    12    12  ...   %  4th floor
                        12    12    12    12    12  ...   %  5th floor
                        13    13    13    13    13  ...   %  6th floor
                        13    13    13    13    13  ...   %  7th floor
                        13    13    13    13    13  ...   %  8th floor
                        13    13    13    13    13  ...   %  9th floor
                        13    13    13    13    13  ...   %  10th floor
                        13    13    13    13    13  ...   %  11th floor
                        12    12    12    12    12  ...   %  12th floor
                        12    12    12    12    12  ...   %  13th floor
                        12    12    12    12    12  ...   %  14th floor
                         8     8     8     8     8  ...   %  15th floor
                         8     8     8     8     8  ...   %  16th floor
                         8     8     8     8     8  ...   %  17th floor
                        14    14    14    14    14  ...   %  18th floor
                        14    14    14    14    14  ...   %  19th floor
                        15    15    15    15    15  ...   %  20th floor
                        16    16    16    16    16  ...   %  roof
                              ]';

  element_tbl(Num_col+[1 2 3 4 5],4) = 3;

% ----------------------------------
% --- Define Master - Slave Nodes ---
% ----------------------------------
  slv_tbl = [
%   Master  Dir  Num_slv  Slv_1  Slv_2  Slv_3  Slv_4  Slv_5
      9      1     5        7      8      10     11     12    %  1st basement
     21      1     5       19     20      22     23     24    %  2nd floor
     27      1     5       25     26      28     29     30    %  3rd floor
     33      1     5       31     32      34     35     36    %  4th floor
```

```
    39      1     5      37     38      40      41      42   %  5th floor
    45      1     5      43     44      46      47      48   %  6th floor
    51      1     5      49     50      52      53      54   %  7th floor
    57      1     5      55     56      58      59      60   %  8th floor
    63      1     5      61     62      64      65      66   %  9th floor
    69      1     5      67     68      70      71      72   %  10th floor
    75      1     5      73     74      76      77      78   %  11th floor
    81      1     5      79     80      82      83      84   %  12th floor
    87      1     5      85     86      88      89      90   %  13th floor
    93      1     5      91     92      94      95      96   %  14th floor
    99      1     5      97     98     100     101     102   %  15th floor
   105      1     5     103    104     106     107     108   %  16th floor
   111      1     5     109    110     112     113     114   %  17th floor
   117      1     5     115    116     118     119     120   %  18th floor
   123      1     5     121    122     124     125     126   %  19th floor
   129      1     5     127    128     130     131     132   %  20th floor
   135      1     5     133    134     136     137     138   %  roof
        ];
  Num_mst = length(slv_tbl(:,1));                    % Number of Master Nodes

% -------------------------
% --- Define Fixed Nodes ---
% -------------------------
%                       Fix: 1 , Free: 0
%              Node_no  Hor.  Vert.  Rot.
  Fix_node = [    1       1     1      0 ;
                  2       1     1      0 ;
                  3       1     1      0 ;
                  4       1     1      0 ;
                  5       1     1      0 ;
                  6       1     1      0 ;
                 13       1     0      0 ;
                 14       1     0      0 ;
                 15       1     0      0 ;
                 16       1     0      0 ;
                 17       1     0      0 ;
                 18       1     0      0 ;
                  ];
  Num_BND    = length(Fix_node(:,1));          % Number of Fixed Nodes
```

```
% --------------------------
% --- Define Element mass ---
% --------------------------
  seismic_mass1 = 2.6561e5;
  seismic_mass2 = 2.8166e5;
  seismic_mass3 = 2.7582e5;
  seismic_mass4 = 2.9188e5;

  Element_mass = [
   zeros(1,Num_col)...
   seismic_mass1*(1/(Num_bay))*ones(1,Num_bay)...   %  1st basement
   seismic_mass1*(1/(Num_bay))*ones(1,Num_bay)...   %  1st floor
   seismic_mass2*(1/(Num_bay))*ones(1,Num_bay)...   %  2nd floor
   seismic_mass3*(1/(Num_bay))*ones(1,Num_bay)...   %  3rd floor
   seismic_mass3*(1/(Num_bay))*ones(1,Num_bay)...   %  4th floor
   seismic_mass3*(1/(Num_bay))*ones(1,Num_bay)...   %  5th floor
   seismic_mass3*(1/(Num_bay))*ones(1,Num_bay)...   %  6th floor
   seismic_mass3*(1/(Num_bay))*ones(1,Num_bay)...   %  7th floor
   seismic_mass3*(1/(Num_bay))*ones(1,Num_bay)...   %  8th floor
   seismic_mass3*(1/(Num_bay))*ones(1,Num_bay)...   %  9th floor
   seismic_mass3*(1/(Num_bay))*ones(1,Num_bay)...   %  10th floor
   seismic_mass3*(1/(Num_bay))*ones(1,Num_bay)...   %  11th floor
   seismic_mass3*(1/(Num_bay))*ones(1,Num_bay)...   %  12th floor
   seismic_mass3*(1/(Num_bay))*ones(1,Num_bay)...   %  13th floor
   seismic_mass3*(1/(Num_bay))*ones(1,Num_bay)...   %  14th floor
   seismic_mass3*(1/(Num_bay))*ones(1,Num_bay)...   %  15th floor
   seismic_mass3*(1/(Num_bay))*ones(1,Num_bay)...   %  16th floor
   seismic_mass3*(1/(Num_bay))*ones(1,Num_bay)...   %  17th floor
   seismic_mass3*(1/(Num_bay))*ones(1,Num_bay)...   %  18th floor
   seismic_mass3*(1/(Num_bay))*ones(1,Num_bay)...   %  19th floor
   seismic_mass3*(1/(Num_bay))*ones(1,Num_bay)...   %  20th floor
   seismic_mass4*(1/(Num_bay))*ones(1,Num_bay)...   %  roof
                   ]';

% ----------------------------
% --- Define Material Table ---
% ----------------------------
% Type = 0: Spread Plasticity Model
```

```
%        1: Concentrated Plasticity Model
  mat_tbl = [
%Mat_no  EI1        EI2        EI3        EA         GA         d1         d2    type mod.
 1  2.4959e+08 2.2584e+08 7.4866e+06 1.3416e+10 8.8960e+15 1.2659e-02 1.3325e-02  1
 2  9.9037e+08 8.9628e+08 2.9710e+07 1.2693e+10 8.8960e+15 6.3675e-03 6.7026e-03  1
 3  1.8176e+08 1.6450e+08 5.4532e+06 8.8686e+09 8.8960e+15 1.2090e-02 1.2726e-02  1
 4  1.5305e+08 1.3847e+08 4.5904e+06 7.2239e+09 8.8960e+15 1.1899e-02 1.2525e-02  1
 5  6.3667e+08 5.7617e+08 1.9099e+07 8.6687e+09 8.8960e+15 6.5645e-03 6.9100e-03  1
 6  5.2099e+08 4.7145e+08 1.5629e+07 7.2626e+09 8.8960e+15 6.6336e-03 6.9828e-03  1
 7  1.2076e+08 1.0927e+08 3.6222e+06 5.5147e+09 8.8960e+15 1.1708e-02 1.2324e-02  1
 8  3.3456e+08 3.0277e+08 1.0036e+07 4.9664e+09 8.8960e+15 6.8374e-03 7.1972e-03  1
 9  2.9462e+08 2.6660e+08 8.8380e+06 4.4375e+09 8.8960e+15 6.8621e-03 7.2233e-03  1
 10 8.4639e+07 7.6629e+07 2.5401e+06 3.7410e+09 8.8960e+15 1.1518e-02 1.2124e-02  1
 11 1.9724e+08 1.7849e+08 5.9170e+06 3.1863e+09 8.8960e+15 7.0212e-03 7.3908e-03  1
 12 3.3207e+08 2.8596e+08 9.9615e+06 3.7539e+09 8.8960e+15 4.9618e-03 5.2362e-03  1
 13 3.7201e+08 3.5399e+08 1.1160e+07 4.0892e+09 8.8960e+15 4.9116e-03 5.1575e-03  1
 14 2.3719e+08 2.2226e+08 7.1154e+06 3.1992e+09 8.8960e+15 5.4325e-03 5.7087e-03  1
 15 1.2900e+08 1.2362e+08 3.8698e+06 2.3478e+09 8.8960e+15 6.2635e-03 6.5748e-03  1
 16 8.1893e+07 7.1509e+07 2.4567e+06 1.8963e+09 8.8960e+15 7.0934e-03 7.4803e-03  1
                ];
% Add splice elements
  mat_tbl = [mat_tbl
17          (6/13)*mat_tbl(1,2:8)+(7/13)*mat_tbl(3,2:8)                          1
18          (6/13)*mat_tbl(3,2:8)+(7/13)*mat_tbl(4,2:8)                          1
19          (6/13)*mat_tbl(2,2:8)+(7/13)*mat_tbl(5,2:8)                          1
20          (6/13)*mat_tbl(5,2:8)+(7/13)*mat_tbl(6,2:8)                          1
21          (6/13)*mat_tbl(4,2:8)+(7/13)*mat_tbl(7,2:8)                          1
22          (6/13)*mat_tbl(6,2:8)+(7/13)*mat_tbl(8,2:8)                          1
23          (6/13)*mat_tbl(8,2:8)+(7/13)*mat_tbl(9,2:8)                          1
24          (6/13)*mat_tbl(7,2:8)+(7/13)*mat_tbl(10,2:8)                         1
25          (6/13)*mat_tbl(9,2:8)+(7/13)*mat_tbl(11,2:8)                         1
               ];

%---------------------------------------
% --- Define Building Characteristics ---
%---------------------------------------
 Idx_linear = 1; % 1:Linear 0:Nonlinear
 Damp_type  = 4; % 1:Mass, 2:Stiffness, 3:Rayleigh 4:Assigned modal damping
 Idx_Band   = 1; % Solver  1:Banded, 0: Symmetric
```

```
% ------------------------------
% Calculate the nodal coordinates
% ------------------------------
     EPS = 1.0E-14;

     y0 = 0.0;
     i  = 0;
     for no_story=1:Num_story+1
        x0 = 0.0;
        for no_bay=1:Num_bay+1
           i  = i + 1;
           x(i) =  x0;
           y(i) =  y0;
           if no_bay<=Num_bay
              x0 = x0 + width(no_bay);
           end
        end
        if no_story<=Num_story
           y0 = y0 + height(no_story);
        end
     end

% ---------------------------
% Set Node Numbers of Elements
% ---------------------------------------------------------------------
%   element_tbl(:,1) = Node_a
%   element_tbl(:,2) = Node_b
%   element_tbl(:,3) = Material Table Number
%   element_tbl(:,4) = Type of Element (1: Column, 2: Beam, 3:Brace)
% ---------------------------------------------------------------------
%  Judge Linear or Nonlinear Analysis
% ----------------------------------
  if Idx_linear == 1
     mat_tbl(:,7) = 10*mat_tbl(:,7);
     mat_tbl(:,8) = 10*mat_tbl(:,8);
  end
% ----------------------------------
% ----------------------
```

```
% Set Element Properties
% ----------------------

   for i=1:Num_elem
     na = element_tbl(i,1);
     nb = element_tbl(i,2);
     elem_prop(i,1) = sqrt((x(na)-x(nb))^2 + (y(na)-y(nb))^2);    % Length
     elem_prop(i,2) = mat_tbl(element_tbl(i,3),2);                % EI1
     elem_prop(i,3) = mat_tbl(element_tbl(i,3),3);                % EI2
     elem_prop(i,4) = mat_tbl(element_tbl(i,3),4);                % EI3
     elem_prop(i,5) = mat_tbl(element_tbl(i,3),5);                % EA
     elem_prop(i,6) = mat_tbl(element_tbl(i,3),6);                % GA
     elem_prop(i,7) = mat_tbl(element_tbl(i,3),7);                % d1
     elem_prop(i,8) = mat_tbl(element_tbl(i,3),8);                % d2
     elem_prop(i,9) = mat_tbl(element_tbl(i,3),9);                % Type
   end

% ------------------------------------
% Assemble Global Matricies [M] & [K]
% ------------------------------------

   MM = zeros(Num_DOF);
   KK = zeros(Num_DOF);
   CC = zeros(Num_DOF);

% --- Stiffness Matrix Fixed Fixed [K] ---

   for i=1:Num_elem
    na = element_tbl(i,1);
    nb = element_tbl(i,2);
    Ia = 3*(na-1)+[1 2 3];
    Ib = 3*(nb-1)+[1 2 3];
    EI = elem_prop(i,2);
    EA = elem_prop(i,5);
    invL=1.0/elem_prop(i,1);
    T=diag(ones(6,1));
    c(i)=(x(nb)-x(na))*invL;
    s(i)=(y(nb)-y(na))*invL;
    a=[1;2];
```

```
   b=a+3;
   T(a,a)=[c(i)  s(i);-s(i) c(i)];
   T(b,b)=[c(i)  s(i);-s(i) c(i)];

 if element_tbl(i,4)<=2 %      |-----|
   g=EA/EI;
   k1=[g;0;0;-g;0;0];
   k2=[0;12*invL*invL;6*invL;0;-12*invL*invL;6*invL];
   k3=[0;6*invL;4;0;-6*invL;2];
   k6=[0;6*invL;2;0;-6*invL;4];
   khat=(EI*invL)*[k1 k2 k3 -k1 -k2 k6];
   km=T'*khat*T;

 elseif element_tbl(i,4)==3 %      o-----o
   khat=zeros(6);
   k1=(EA*invL)*[1 -1;-1 1];
   khat([1 4],[1 4])=k1;
   km=T'*khat*T;

 elseif element_tbl(i,4)==4 %      o-----|
   khat=zeros(6);
   k1=(EA*invL)*[1 -1;-1 1];
   k2=(3*EI*invL)*[1*invL*invL -1*invL*invL 1*invL;-1*invL*invL ...
                   1*invL*invL -1*invL;1*invL -1*invL 1];
   khat([1 4],[1 4])=k1;
   khat([2 5 6],[2 5 6])=k2;
   km=T'*khat*T;

 elseif element_tbl(i,4)==5 %      |-----o
   khat=zeros(6);
   k1=(EA*invL)*[1 -1;-1 1];
   k2=(3*EI*invL)*[1*invL*invL 1*invL -1*invL*invL;1*invL 1 -1*invL; ...
                   -1*invL*invL -1*invL 1*invL*invL];
   khat([1 4],[1 4])=k1;
   khat([2 3 5],[2 3 5])=k2;
   km=T'*khat*T;
 end

   KK([Ia Ib],[Ia Ib]) = KK([Ia Ib],[Ia Ib])+km;
```

```
  end

% --- Lumped Mass Matrix [M] ---
% only the beam elements have mass associated with them

    alpha = 1e-06;

   for i=1:Num_elem
    na = element_tbl(i,1);
    nb = element_tbl(i,2);
    Ia = 3*(na-1)+[1 2 3];
    Ib = 3*(nb-1)+[1 2 3];
    mi = Element_mass(i)/2*diag([1 1 alpha*(elem_prop(i,1)^2)/210 ...
                                 1 1 alpha*(elem_prop(i,1)^2)/210]);
    MM([Ia Ib],[Ia Ib]) = MM([Ia Ib],[Ia Ib])+mi;
   end

% --- Place an arbitrary rotational mass on the basement pinned locations ---

   pinned_base=(Fix_node(:,1)<=Num_bay+1).*(1-Fix_node(:,4));

   for i = 1:length(pinned_base)
    if pinned_base(i)==1
     MM(Fix_node(i,1)*3,Fix_node(i,1)*3) = ...
     MM(Fix_node(i,1)*3+(Num_bay+1)*3,Fix_node(i,1)*3+(Num_bay+1)*3);
    end
   end

% ------------------------------------
% Eliminate Boundary Condition DOFs
% ------------------------------------

    Ref_BND = zeros(1,Num_DOF);

  for i=1:Num_BND
    Ref_BND(3*(Fix_node(i,1)-1) + [1 2 3]) = Fix_node(i,1+[1 2 3]);
  end
```

```
% eliminate the vertical DOFs
%  for i=1:Num_node
%    Ref_BND(3*(i-1) + 2) = 1;
%  end

    Order = 1:Num_DOF;

    free_vec = Order(Ref_BND==0);

% --- Eliminate the Fixed Boundary DOF ---

    M_free  = MM(free_vec,free_vec);
    K_free  = KK(free_vec,free_vec);

    Ord_vec = [Order(Ref_BND==0) Order(Ref_BND==1)];
    Out_idx(Ord_vec) = Order;
    Num_free = length(free_vec);

% ------------------------------------
% Eliminate Slave Nodes
% ------------------------------------

   T_rigid = eye(Num_DOF);

   for i=1:Num_mst
     i_mst = 3*(slv_tbl(i,1)-1) + slv_tbl(i,2);
     for j=1:slv_tbl(i,3)
         i_slv = 3*(slv_tbl(i,3+j)-1) + slv_tbl(i,2);
         T_rigid(i_slv,i_slv) = 0;
         T_rigid(i_slv,i_mst) = 1;
     end
   end

   Num_slv = max(slv_tbl(:,3));     % Max Number of Slave Nodes

   Tr_rigid = T_rigid(free_vec,free_vec);

   act_vec = find(diag(Tr_rigid));
```

```
   Tr2_rigid = Tr_rigid(:,act_vec);                    % Num_free * Num_act

   Num_act = length(act_vec);

   diagT = cumsum(diag(Tr_rigid));
   for i=1:Num_mst
     i_mst = 3*(slv_tbl(i,1)-1) + slv_tbl(i,2);
     for j=1:slv_tbl(i,3)
         i_slv = 3*(slv_tbl(i,3+j)-1) + slv_tbl(i,2);
         diagT(Out_idx(i_slv)) = diagT(Out_idx(i_mst));
     end
   end

 save tmp20 Tr2_rigid  M_free K_free free_vec act_vec Num_mst slv_tbl ;

 clear;

 load tmp20;

% --- Remove Rigid Body -----------------

    M = Tr2_rigid' * M_free * Tr2_rigid;
    K = Tr2_rigid' * K_free * Tr2_rigid;

% --- Static Condensation/ignore and remove all verical and rotational inertia

 posit_vec=free_vec(act_vec);
 posit_mst=zeros(1,Num_mst);
 for i=1:Num_mst
    i_mst=3*(slv_tbl(i,1)-1)+slv_tbl(i,2);
    for j=1:length(posit_vec)
       if i_mst == posit_vec(j)
          posit_mst(i)=j;
          break;
       end
    end
 end

 ref_posit=zeros(1,length(posit_vec));
```

```
for i=1:Num_mst
   ref_posit(posit_mst(i))=1;
end
order_posit=1:length(posit_vec);
posit_slv=order_posit(ref_posit==0);

Maa=M(posit_mst,posit_mst);
Mab=M(posit_mst,posit_slv);
Mba=M(posit_slv,posit_mst);
Mbb=M(posit_slv,posit_slv);

Kaa=K(posit_mst,posit_mst);
Kab=K(posit_mst,posit_slv);
Kba=K(posit_slv,posit_mst);
Kbb=K(posit_slv,posit_slv);

M_red=Maa;
K_red=Kaa-Kab*inv(Kbb)*Kba;

M1=M_red([Num_mst:-1:1],[Num_mst:-1:1]);
K1=K_red([Num_mst:-1:1],[Num_mst:-1:1]);

save model20 Num_mst M1 K1;
```